INFRARED POLARIZATION STUDIES OF PROTOSTARS

Carol J. Lonsdale

Doctor of Philosophy
University of Edinburgh
1980

I declare that this thesis is composed entirely by me, and that the work is entirely my own, except where reference is made to others.

Jan 4th 1980

LIST OF CONTENTS

ACKNOWLEDGMENT

I am indebted to many people for their kindness and encouragement during the time that I was occupied in the research which comprises this thesis. I would like to thank my supervisor Ray Wolstencroft for his continual efforts on my behalf, and for his patience. I am very grateful to Terry Lee for finding much time to help me, when he had not much to spare. Mel Dyck invited me to the University of Hawaii to obtain the data at Mauna Kea Observatory, and assisted and encouraged me greatly in my efforts to do so, for which I would like to express special thanks.

Many other folk have refreshed me from time to time by a kind encouragement. I would like to especially thank Chris Impey, Gareth Wynn-Williams, Charlie Telesco, Ian Gatley and Jeanne Koch for their concern.

My mother, Margaret Lonsdale, expended much time and effort typing a first draft, for which I wish to thank her enormously. Jeanne Koch made an excellent job of typing the final draft in a very short time. To Barbara Schaefer I say a special thank you for drawing some of the figures so well.

Finally, I owe the greatest thanks to Eric Becklin, who instilled in me self-confidence, the single most important determining factor in the success of this research. I therefore dedicate this thesis to him.

ABSTRACT

The thesis to be proved is that the mechanism of optical interstellar polarization, preferential extinction by magnetically aligned aspherical grains, can be extrapolated successfully to explain the large infrared polarizations observed in molecular cloud protostellar sources. Observations of the linear polarization of 13 sources between 1.65 μm and 4.8 μm and of the circular polarization of 9 sources at 2.2 μm have been obtained. Analogously to the optical interstellar case, the data have been modelled using the Rayleigh approximation to calculate extinction and phase-lag efficiencies for a number of grain models. The models successfully account for the high infrared ellipticities (ratio of linear to circular polarization) observed in the molecular clouds, with twists in the grain alignment of about 40°; smaller than those required to explain optical interstellar circular polarization. A shortcoming in the model linear polarization at $\lambda < 3$ μm is attributable to a failure in the Rayleigh approximation. A dissimilarity in the polarization through the ice band between two of the protostellar sources can be understood by differing grain compositions. A correlation between the position angles of polarization of the protostars and the nearby interstellar field stars can be interpreted by saying that the Galactic magnetic field permeates the dense molecular clouds. There are indications that the polarization mechanism even operates in the enhanced density regions of the clouds; then a more efficient alignment mechanism than paramagnetic relaxation is required. It is suggested that this may be "pinwheeling," possibly accompanied by super-paramagnetism of the grains. The twists in the magnetic field lines implied by the model may arise in the collapse process of the rotating, magnetized clouds.

CHAPTER I

INTRODUCTION

Infrared polarization was first observed in a protostar in 1973 when Breger and Hardorp (1973), Loer et al (1973) and Dyck et al (1973) detected large amounts of linear polarization between 1.6 μm and 11 μm in the Becklin-Neugebauer (BN) object in the Orion Nebula. In the same year circular polarization was observed at 3.5 μm in BN (Serkowski and Rieke 1973). At this time there was some controversy over whether BN was in fact a protostar or a heavily reddened evolved star. Therefore, polarization by preferential extinction by aligned elongated or flattened grains foreground to the source was suggested to explain the wavelength dependence of polarization observed in BN, especially the behaviour in the 10 μm "silicate" feature. This is the same mechanism as is used to explain interstellar optical polarization. Little attention was paid to the circular polarization, beyond pointing out that it could arise by linear birefringence in the medium of aligned grains.

A theory of interstellar circular polarization has been developed for optical and ultraviolet wavelengths by Kemp and Wolstencroft (1972), Martin (1974 and references therein) and Shapiro (1975) in which linear birefringence is created in the interstellar medium by a twist in the orientation of alignment of the grains along the line-of-sight. This converts some of the linear polarization into circular. However, at optical wavelengths perfect twists of greater than 80° would be required to produce ellipticities (ratio

of circular to linear polarization) as large as that observed at 3.5 μm in BN (9%) by such a model (hereafter referred to as an IS (for *interstellar*) model). Such a twist is not unrealistic between discrete interstellar clouds, but seems unreasonable for the relatively short pathlengths through the presumably continuous molecular cloud medium.

A survey of linear polarization between 1 μm and 3.5 μm undertaken in 1977-1978 (Dyck and Capps 1978, Dyck 1978) of a number of BN-like compact infrared sources in molecular clouds and H II regions, revealed that the majority of these sources, many of which may be protostars, are also highly polarized, so much so, in fact, that it appears that large infrared polarization may be considered a characteristic of young objects which are still buried within their natal clouds. In this case it is clear that an understanding of the origin of the polarization could be very important to theories of star formation and for our knowledge of the physical environment of protostars. For example, if an IS model is ruled out because the large twist angles required to produce the circular polarization are considered untenable, or for some other reason, then a model involving scattering off grains in an asymmetric circumstellar shell may be invoked. In this case, a specialised geometry involving an optically thick equatorial disk would be required to reproduce the wavelength dependence of linear polarization observed in the 10 μm feature of BN, which would be very popular with proponents of pre-planetary disks. It is important to know if it is necessary to invoke such geometries.

Various models for the polarization of BN have been developed, and observations to discriminate among the models suggested. (Dyck and Beichman 1974, Dennison 1977, Elsässer and Staude 1978). However, each of these suffers from drawbacks, and none has made any attempt to account for the circular polarization, although, as illustrated above, it can provide important constraints upon the models.

This dissertation reports observations of circular polarization at 2.2 μm of eight protostellar sources with moderate-to-high levels of linear polarization, which were made to remedy the deficiency described above. In Chapter II a brief review is given of recent progress in the field of star formation, resulting in a description of the characteristics of protostars and their environment. A description and discussion of the various models for the polarization is also given and it is shown that an IS model is the more appropriate. The observations and results are described in Chapter III.

In Chapter IV the theory of interstellar circular polarization is investigated, resulting in an IS model which accounts well for the infrared linear and circular polarization of the molecular cloud sources, using twists in the orientation of grain alignment of the order of only ~40°, depending on the model grain composition.

Also presented in Chapter III are observations of the linear polarization of a number of sources, including the wavelength dependence of polarization in the 3.1 μm "ice" feature of GL 2591, a BN-

like object, which were made to provide additional information on the polarization mechanism. The "ice" feature data illustrate an interesting contrast between GL 2591 and BN, the only other object for which "ice" band polarimetry exists. These results are discussed in Chapter V.

In Chapter VI is presented an analysis of the broad-band data. Together with the survey mentioned above these observations bring the total number of molecular cloud sources observed to 30-40. The data presented here comprises ~30% of this sample, which now represents a large proportion of all known molecular cloud sources which are accessible from the northern hemisphere, and which are bright enough to be observed for polarization. The characteristics of the various sources are discussed in some detail. A statistical analysis of the position angles of the infrared sources compared to the mean optical position angle of nearby field stars is shown to reveal a correlation which has important implications for the influence of the galactic magnetic field on star formation.

The results of the different pieces of work are drawn together and discussed in Chapter VII.

CHAPTER II

THE RELEVANCE OF POLARIZATION TO STAR FORMATION.

(1) Star Formation in the Galaxy.

The Becklin-Neugebauer object is now commonly termed a "protostar" in the literature. It is a compact, bright source of 2 - 20 μm radiation which lies at the peak of a dense molecular cloud associated with the well-studied Orion Nebula. In this section the characteristics which indicate that BN, and other sources like it may be newly formed stars are reviewed, and a brief description of protostars and regions of star formation from both observational and theoretical viewpoints is presented. In the next section polarization studies of protostars and related objects are reviewed, and their bearing on the problems of star formation in the context of models which attempt to explain the polarization are discussed.

The use of the term "protostar" is somewhat loose and is not agreed by everyone to be correct in application to a set of sources of uncertain evolutionary status, such as the obscured, infrared sources described here. A protostar may be thought of as an object which is still in the process of accreting matter and which has not yet started nuclear burning, however it is convenient to apply one word to the description of a set of objects which are undoubtedly young and closely related. In any case theories of star formation and observational studies of young stars have not yet evolved so far that it is understood at what stage accretion stops, or whether mass infall or outflow is occurring in particular sources, or indeed how

these two processes may co-exist. In addition, the Kelvin-Helmholtz timescale of massive stars is expected to be shorter than the accretion timescale, in other words, stars that have already reached the main sequence may still be accreting matter. The sources studied in this research are therefore termed loosely "protostars" or "protostellar sources" for convenience, unless they are known to possess well-developed H II regions, as a way of describing sources with similar extrinsic properties.

It has in fact not always been accepted that BN is a young object, but rather that it might be an obscured luminous ordinary star (Penston et al 1971) or an evolved star with a hot dust shell (Becklin et al 1973). Statistical arguments concerning the number of similar compact infrared sources that have now been discovered, singly or in clusters, closely associated with other signposts of recent star formation (e.g. bright H II regions, dense molecular cloud peaks, OH and H_2O masers) now make these alternatives highly implausible. Even so, independent evidence exists that the sources are young. In the case of BN it is clear that the object does not lie by chance behind the molecular cloud since it is a member of a cluster of compact sources (Rieke et al 1973) which are enveloped in an extended region of 10 and 20 μm emission, (Kleinmann and Low 1967) the KL nebula. Absence of CO absorption lines in the near infrared spectrum of BN implies that the star is of type G or earlier. An F star would need to be behind approximately 80 magnitudes of visual extinction to match the observed continuum flux (Penston et al 1971). Such a star would possess more luminosity than the entire KL nebula

(Rieke et al 1973). Therefore the near infrared flux must be dust emission, not reddened photospheric emission from a normal star. The detection of Br α emission from the source determined unambiguously that it must be a young object (Grasdalen 1976), and not an evolved star with a circumstellar dust shell.

This research is principally concerned with the study of massive star formation. It is generally held that the star formation process for stars of low mass ($\leq$ 3 $M_\odot$) differs from that for massive stars (> 3 $M_\odot$). Low mass stars may form anywhere in a molecular cloud or less dense cloud, but the conditions required for massive star formation are probably more stringent. Possibly low mass stars can also form under these same conditions, in which case some of the less luminous objects considered here may in fact be not very massive. Selection effects operate heavily in favour of massive stars in the search for protostars, however. Most compact, infrared protostellar candidates have been found by searching suspected star forming areas, such as dense molecular cloud peaks with nearby H II regions and associated masers. Less massive stars are more likely to form inconspicuously within less dense clouds, and to be observable first as T Tauri stars or Herbig-Haro objects when they have emerged from the enveloping dust. As less luminous infrared sources they would be observable only out to about 1 kpc (Evans 1978).

It is clear that massive star formation is progressing at the present time in the Galaxy because there exist many massive stars which have lifetimes much shorter than the lifetime of the Galaxy.

Theories of star formation face several difficulties; however it is possible to sketch a scenario from current theoretical and observational studies which illustrates the background for the polarization studies to be described. This scenario may not be a universally acceptable one but is sufficient for the purposes of this work.

Massive stars form in giant molecular clouds which are found mainly in the spiral arms, or at least in a ring between 4 - 8 kpc from the Galactic Centre (Burton 1976), and in the Galactic Centre itself. The sizes and masses of such clouds are not agreed upon, indeed they may even be a continuous entity, but a typical size may be of the order of $\lesssim$ 100 pc, a mass of $\sim 10^5$ $M_\odot$ or more and a lifetime of $\lesssim 10^7$ years (Stark and Blitz 1978). To begin to collapse, the gravitational force of the cloud must overcome the resistance of internal gas pressure and any other restraining force such as turbulence, angular momentum and magnetic fields, perhaps with the assistance of external pressure such as supernova shock waves or the Galactic density wave shock. Calculations of the Jeans mass tend to indicate that the clouds are easily massive enough to begin to collapse, and large molecular line widths have been interpreted as indicating that the clouds are in fact in a state of free-fall collapse (Goldreich and Kwan 1974). Therefore at first sight it would appear that star formation is easy. It turns out that if these interpretations are correct then it would be *too* easy; many more OB stars than are observed would be formed if the clouds collapsed in this manner. Therefore one or more of the restraining mechanisms mentioned above must be invoked to slow the collapse. It

is generally agreed that turbulence cannot cope (e.g. Lequeux 1977); therefore angular momentum and magnetic fields are commonly appealed to. Direct measurement of either of these phenomena is unfortunately fraught with difficulty. Interpretation of molecular line velocity profiles can be very ambiguous (e.g. Field 1978) and measurements of magnetic fields are not at all straightforward (see later). Therefore some of the fundamental problems of star formation are tied to the existence and nature of magnetic fields and angular momentum in molecular clouds, and the interaction of the two. Fragmentation appears to play a major role, but theories which attempt to overcome the problem involved are complex and would benefit greatly from observational information. Measurement of polarization is one tool that can conceivably aid in establishing the presence of magnetic fields in star forming clouds, measuring their strength, and mapping the field lines. The aspects of the present research which are relevant to this problem are returned to in Chapter VII, where the status of theoretical models is discussed in more detail. Taking the easy route for the moment therefore, this problem can be avoided by noting that stars do indeed form, and the sketch of the scenario of star formation in the Galaxy can be continued, to establish the expected appearance and morphology of protostars and protostellar clusters.

Evidence that fragmentation is indeed important comes from various observations. It appears that new associations of stars are localised, and are seen close to the edges of molecular clouds, not at the centre. The fragments will typically have a size of ~1 pc,

masses of 10^3 - 10^4 M_o and lifetimes ~10^6 years, the time required to form a massive star.

Collapse of the fragments is probably assisted by external pressure, though probably of a more local nature than the Galactic density wave shock usually invoked to collapse the massive clouds. This may be shocks from supernova remnants, expanding H II regions or stellar winds. A very attractive theory that has developed is the theory of sequential star formation, in which star formation progresses steadily into a molecular cloud, driven by previous bouts of star formation (Elmegreen and Lada 1977). Sequences such as this have been identified observationally, the best known being in Orion where a massive elongated molecular cloud complex extends 45 pc with the Orion OB association at its head. Next to the OB association lies the Trapezium cluster of 4 massive young OB stars in their bright H II region, the Orion nebula. Beside them, in the molecular cloud is the infrared cluster of protostars, including BN. According to this model, the sequence is as follows: A fragment collapses at the edge of a molecular cloud to produce a cluster of stars (the Trapezium). As these evolve to the main sequence they form an H II region (M42). The ionization front expands into the molecular cloud, preceded by a shock front which initiates compression of another fragment, which in turn collapses to produce a new cluster of protostars (the infrared cluster).

At the earliest stage of their evolution the protostars are therefore expected to be heavily enshrouded still in the dust cloud,

and to be observable, if at all, only as infrared sources as the hot new objects heat the surrounding dust which radiates in the infrared. They will lie at peaks in the density distributions of the molecular clouds, as mapped in molecular lines, and probably close to, but not necessarily coincident with, radio emission from H II regions associated with earlier bursts of star formation. This is exactly the situation that was anticipated in Orion. Infrared searches for a protostar indeed discovered the BN object (Becklin and Neugebauer 1967) bright at 3 μm, displaced from Orion A and later found to be located at the peak of a dense molecular cloud. Many more protostars in similar situations have since been discovered at infrared wavelengths, guided by molecular line and radio observations.

Models of the final stages of evolution of protostars indicate that an opaque dust cocoon will form (Davidson and Harwit 1967, Kahn 1974) Continued accretion will eventually be retarded and reversed by radiation pressure. A second cooler shell may then form. An H II region may begin to form inside the first cocoon, expanding and becoming visible as the optical depth of the cocoon to UV radiation reduces (Yorke 1977, Yorke and Krügel 1977). There are several possible observable stages. If it is not completely obscured the protostar will first appear as a very cool infrared source, when the cocoon is still thick to near infrared photons as well as optical and UV. As the optical depth falls it will be observable at shorter wavelengths with a size of the order of $\sim 10^{15}$ cm, depending on the mass. There will be far infrared flux from the surrounding cooler dust. At later stages an ultracompact, then a compact H II region

will be observed. Whether it is accompanied by an infrared source will depend on whether the surrounding dust is optically thick to infrared flux. Sources which may be interpreted as being at various stages of such a model have been observed. W3/IRS 5 is a very compact, highly obscured near infrared source with no indication of an H II region. Brackett line observations have revealed very faint, ultracompact H II regions in several sources including BN. Recent VLA observations (Beichman et al 1979), 15 to 90 times more sensitive than the Brackett line studies, show extremely faint radio emission in some objects. NGC 7538/IRS 1 is an example of a young star with a stronger, but still ultracompact H II region. W3/IRS 1 is a more evolved H II region. Many compact H II regions with no associated infrared emission are also known.

The spectrum of BN and KL is shown in Figure II.1. It resembles the second stage of the cocoon model described above, though the precise interpretation of the spectrum is complicated by various effects (see later). The absorption features at 3.1 μm and 9.7 μm are usually attributed to absorption by cool ice and silicate grains respectively. It is not universally agreed that this attribution is correct (see section 3), but it will be adopted here for convenience.

The cocoon model described above deals with the collapse of a symmetric cloud. If instead the collapse is axially symmetric in a rotating cloud, calculations show that a disc may form rather than a symmetric shell (Bertout and Yorke 1978), though the outcome depends

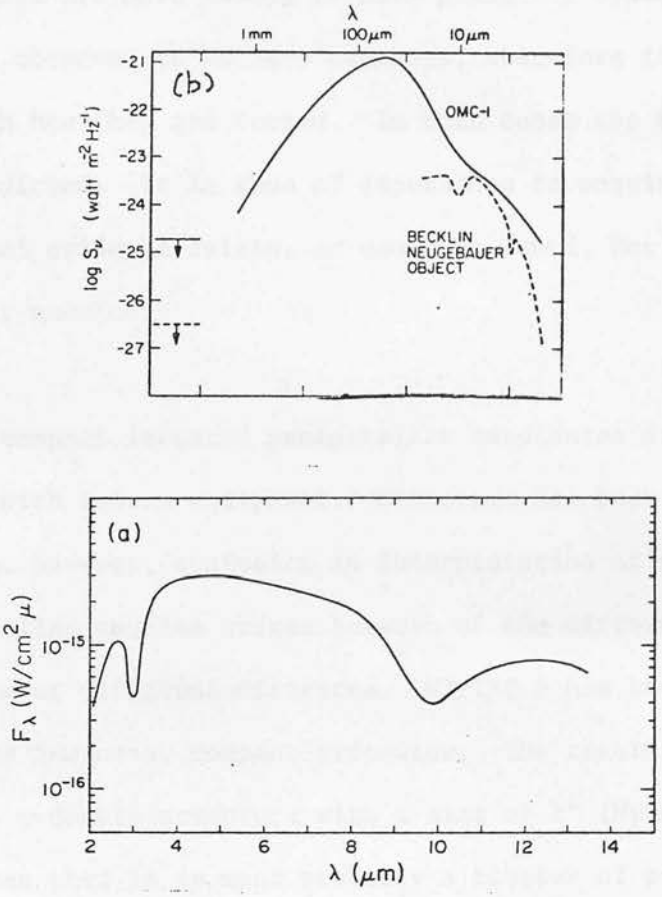

Figure II.1 Spectra of BN (a), and of OMC 1 (Werner et al 1977, and references therein).

on the effect of the magnetic field, which was not considered by these authors. If a disc or torus does form then it is possible that a binary system, a multiple star system or a planetary system may form (Larson 1978). Gehrels (1978) expects that a star of any mass may form planets, although it is usually believed that solar-type low mass stars are more likely to have planetary systems. Binary systems are observed to be very numerous, therefore it is desirable to establish how they are formed. In both cases the existence of a disc is predicted. It is thus of importance to enquire whether observational evidence exists, or could be found, for such discs in protostellar nebulae.

Most compact infrared protostellar candidates are in fact unresolved with modern equipment. Structure has been observed in a few of them, however, confusion in interpretation of observations of the protostellar sources arises because of the different scale size of complexes at different distances. W3/IRS 5 has been considered to be a very luminous, compact protostar. The resolution of the object into a double structure with a size of 1" (Wynn-Williams 1977) now indicates that it is most probably a cluster of protostars of absolute size similar to the KL nebula in Orion. Six times closer to us than W3, KL is a 20 μm nebula which encompasses the Orion infrared cluster. Even at the proximity of KL (~500 pc) it is very hard to resolve and map the contribution to radiation from KL from the various cluster members, and to deduce the contribution from the extended molecular cloud. Much less is this possible in W3/IRS 5. The result is that the mass distribution of dust and gas in the vicinity of protostars is generally poorly understood.

On a larger scale, far infrared and submillimetre observations of regions of star formation are of interest because the emission is usually optically thin, therefore information is obtained on both the temperature and the dust column density, although the best resolution available is about 20" arc. It is becoming evident that most of the far infrared flux is radiation from grains in the molecular clouds outside the H II regions (e.g. Gatley et al 1979). The observations support the "blister" model of formation of H II regions on the edges of molecular clouds (Israel 1978). The dust density increases beyond the ionisation front into the molecular cloud, as the dust temperature falls. The dust is heated by nebular radiation or by infrared re-radiated flux from dust grains close to the ionisation front. In turn the dust heats the molecular gas (Goldreich and Kwan 1974) which is very similar in spatial appearance, as mapped in molecular lines, to the far infrared emission. Measurements of the mass column density show that the dust is concentrated towards the peak of the molecular cloud and falls away with an $r^{-\alpha}$ law, where α is between 1 and 2 (e.g. Smith et al 1979). If a new star cluster has already formed at the molecular cloud peak, it will form a new heating source for the gas and dust.

The far infrared emitting dust must be the same as the dust responsible for the visual extinction, since variations in the optical extinction (A_v) and the far infrared optical depth (τ_{FIR}) appear to correspond closely, even though the optical properties of grains in the far infrared, and the far infrared optical depths, are not well known. Therefore, much of the extinction to the protostars

probably originates in the dense cores of the cloud fragments, as indicated by the submillimetre maps.

Unfortunately, however, these studies no not help immediately with the problem of the detailed mass distribution in the protostellar vicinity, because the beams are large, and it cannot be determined how much extinction is associated locally with each source, even if the optical extinctions obtained by extrapolation of the submillimetre optical depths were totally reliable. Direct measurements of near infrared extinction are seriously complicated by uncertainty of the nature of the underlying source, and by dust re-emission. It is usually assumed that re-emission is only important for wavelengths greater than about 5 μm, but Brackett line intensities and widths indicate that it may be a problem at shorter wavelengths also (e.g. Wynn-Williams et al 1978).

Probably on a larger scale than expected to be relevant to pre-planetary discs but still on a smaller scale than normally observable at longer infrared wavelengths at which the dust distribution could be probed, indirect evidence exists that non-symmetric geometries may exist around certain protostars. Members of a cluster of sources can have different properties that cannot be entirely attributed to differing intervening extinction, but to some extent must be due to intrinsic differences (Beichman et al 1979). An example is NGC 7538/IRS 9, which is best understood by a higher extinction in the line of sight than perpendicular to it (Werner et al 1979).

In the next section the relevance of polarization studies to these various aspects of protostars and star formation is explored.

(2) Polarization in Molecular Clouds.

Approximately 18% of the flux from BN at 2 μm has a preferential orientation of the electric vector. The understanding of the cause of such a high level of polarization from this enigmatic object, and others like it, clearly has the potential of revealing much about star formation. In particular, the study of the polarization from protostars could conceivably clarify the mass distribution problem alluded to above, and the role of magnetic fields in star formation as noted earlier. Assuming that the polarization production is associated with the dust which obscures BN, since polarization is observed to be correlated with the ice and silicate absorption features, the two most likely polarizing mechanisms are scattering in an asymmetric shell (which would give information about the mass distribution) and preferential extinction in a medium of aligned grains (which would have implications for the magnetic field).

Besides BN, many other protostellar sources have large infrared polarizations (Dyck and Capps 1978 (DC), Dyck 1978). The sources selected for observation were chosen as being most likely to be protostellar. Objects with stellar photospheric features (e.g. first-overtone bands of CO) were excluded. The sources tend to be situated close to compact H II regions, maser sources and molecular clouds,

and most show one or both of the 3.1 μm and 9.7 μm absorption features. Dyck and Capps' (1978) table of results is reproduced in Table II.1. The objects range in nature from protostars to fairly well-developed H II regions. DC noted a correlation between source size (an indication of youth) and degree of polarization which can be interpreted as indicating that the polarizing dust is closely associated with the youngest objects, and as they evolve it either is dissipated or loses its polarizing properties. This is an important result in the context of the dust location and geometry. However, observations of additional molecular cloud sources (Dyck 1978, unpublished) have revealed several objects which cast doubt on the size/polarization correlation. Because of the importance of such a correlation the survey begun by Dyck and Capps was extended to broaden the data base. In particular, emphasis was put on observing multiple sources within a cluster for direct comparison of their polarization properties. These observations are presented in Chapter III and discussed in detail in Chapter VI. The interpretation of the results is not straightforward. It is therefore not anticipated here, beyond noting that a correlation is found between the position angles of the multiple sources, and between the angle of the infrared sources and the nearby optical interstellar polarization. This indicates a similar origin for the polarization in most of the sources, whatever the nature, and has implications for the magnetic fields in molecular clouds. Exceptions to this result are discussed in Chapter VI. The main result of the broad band survey of importance at this point is that the size/polarization correlation is not supported by the new data, therefore they do not

Table II.1

Source	Distance (kpc)	IR Size (arcsec)	Diameter (cm)	Radio Continuum	$\tau_{9.7\,\mu m}$	$P_H \pm \epsilon$(%)	θ_H	$P_K \pm \epsilon$(%)	θ_K	$P_L \pm \epsilon$(%)	θ_L
W3/IRS 5.....	3.1	1.2	6×10^{16}	No	7.6	...	...	...	...	10.1±0.2	84°
BN.....	0.5	≤0.7	$\leq5\times10^{15}$	No	3.3	38±2	117°	17.1±0.2	113°	5.9±0.3	102
W33/IRS 3.....	4.6/14.9	11	$0.7\text{–}2.1\times10^{18}$	Yes	4.8	...	...	1±1	...	...	...
W33 A.....	...	...	...	No	7	...	...	16±1	67	...	...
G29.9−0.0.....	7.1/10	12	$1.2\text{–}1.8\times10^{18}$	Yes	2.5	...	...	0.8±0.4	...	...	...
G45.1+0.1.....	5/10	≤3	$2.4\text{–}4.5\times10^{17}$	Yes	2.7	...	...	3.0±0.4	174	2.1±0.8	73
W51/IRS 2.....	6.5	5	5×10^{17}	Yes	2.8	6±1	134	4.7±0.3	130	2.3±0.3	113
K3-50 IRS.....	8	1.2	1.4×10^{17}	Yes	2.8	...	...	1.9±0.2	67	4.0±0.6	64
S88 B.....	2.0/7.5	30	$0.9\text{–}3.4\times10^{18}$	Yes	3.6	...	...	0.7±0.9	...	...	...
S106/Source 3.....	2.3	≤4	$\leq1.4\times10^{17}$	No	3.2	4.0±0.5	58	3.5±0.4	51	...	...
CRL 2591.....	1.5	0.5	1×10^{16}	No	3.5	10.9±0.8	171	12.7±0.1	172	3.8±0.4	171
W75/IRS 1.....	...	...	...	...	≥2	...	...	2.5±0.6	120	...	...
S140.....	0.9	...	...	No	3.0	16.0±0.3	80	12.0±0.1	68	3.2±0.3	61
NGC 7538/IRS 1..	4.9	<1	$<7\times10^{16}$	Yes	6.4	3.2±0.8	73	11.2±0.1	72	5.7±0.2	72
NGC 7538 E.....	4.9	<1	$<7\times10^{16}$	No	3.5	...	...	13±2	157	1.2±0.3	11

From Dyck and Capps (1978).

bear directly on solution of the polarization production problem. Therefore, discussion of the survey is deferred till later. It is more appropriate here to consider the more detailed information available for BN and KL, to enquire after the possibility of solving the problem of the origin of the polarization. The conclusion of Chapter VI anticipated here, that a similar mechanism operates for most of the protostellar sources, justifies the neglect of the other objects for the moment.

Infrared studies have determined that BN is no larger than 10^{15} cm in diameter (Werner et al 1977, Foy et al 1979) which is very comparable to the predicted size of a newly formed cocoon. Therefore it is likely that BN is a single, newly formed massive star. Detection of the Brackett lines indicates that it could be a very newly formed star with an extremely young H II region, still optically thick in the radio, which is confined behind the very small, dense cocoon. No asymmetry has been detected to 10^{15} cm, but this is not to say that it does not exist, therefore it is very important to determine whether the polarization observations require an asymmetric scattering geometry in interpretation.

Some contribution to the flux, in the 8" and 10" beams used to measure the polarization of BN, may be scattered from the surrounding medium (Becklin and Neugebauer 1967) but the majority of the 2 - 5 μm infrared flux originates from the compact core with no contamination from other discrete sources or background flux from KL (at these wavelengths) in the beam at a significant level. The spectrum and

wavelength dependence of linear polarization of BN are shown in Figure II.2 (Dyck and Beichman 1974, Capps 1976). In addition there also exists a measurement of circular polarization q = 0.85% at 3.45 μm (Serkowski and Rieke 1973) and observations of linear polarization at 11.1 μm and 19.6 μm at various points in KL (Dyck and Beichman 1974, Knacke and Capps 1979). Polarization is seen to be positively correlated with optical depth in both the ice and the silicate bands.

Although it has not always been accepted that BN is a protostar it is obvious that it is a highly obscured object. The infrared and radio spectra are thermal, therefore non-thermal polarization mechanisms can be rejected immediately. The presence of absorption features attributed to ice and silicate at 3.1 μm and 9.7 μm, and the correlation of polarization and absorption in these features establishes beyond doubt that the polarization is due to dust. In this case the polarization may be due to scattering in an asymmetric circumstellar shell or a reflection nebula, or by extinction in a medium of asymmetric aligned grains. Dyck and Beichman (DB) rejected the scattering mechanism because the spatial agreement in position angle of the 11.1 μm observations in KL find a natural explanation in a common foreground medium of aligned grains. Also the wavelength dependence of polarization in the absorption bands is easily explained in such a model. Simple scattering models predict the opposite behaviour in the bands: the polarization would decrease with increasing absorption. Therefore DB adopted a model of extinction by foreground aligned grains, which is an extension of the

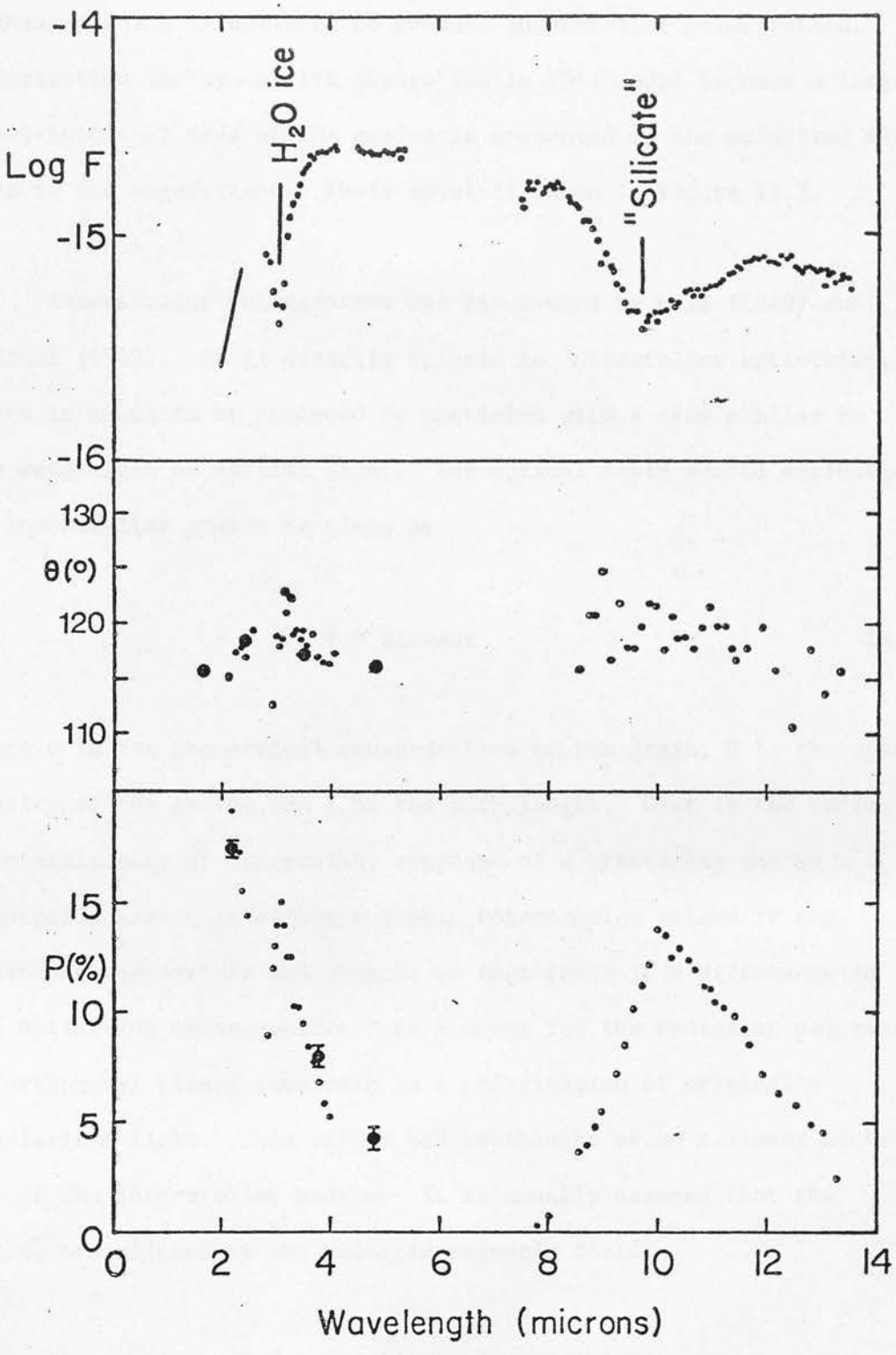

Figure II.2 Observed spectrum and polarization of BN (Capps 1976).

mechanism which is believed to produce interstellar polarization. Polarization increases with absorption in this model because a larger cross-sectional area of the grains is presented to the polarized flux than to the unpolarized. Their model is shown in Figure II.3.

Interstellar polarization was discovered by Hall (1949) and Hiltner (1949). It is directly related to interstellar extinction, which is known to be produced by particles with a size similar to the wavelength of optical light. The optical depth due to extinction by interstellar grains is given by

$$\tau = Nl\sigma Qext \qquad II.1$$

where σ is the geometrical cross-section of the grain, N is the space density of the grains and l is the path length. Qext is the extinction efficiency of the grains, composed of a scattering and an absorption part Qext = Qsca + Qabs. Polarization arises if the grains are asymmetric and aligned so that there is a difference in the extinction cross-section Cext = σQext for the radiation polarized in orthogonal planes resulting in a polarization of originally unpolarized light. This effect can be thought of as a linear dichroism of the interstellar medium. It is usually assumed that the grains are aligned by the Galactic magnetic field.

Observations of interstellar infrared polarization do not extrapolate exactly from the empirical relationship for optical interstellar polarization, $P/Pmax = \exp(-1.15\ln^2(\lambda max/\lambda))$, derived

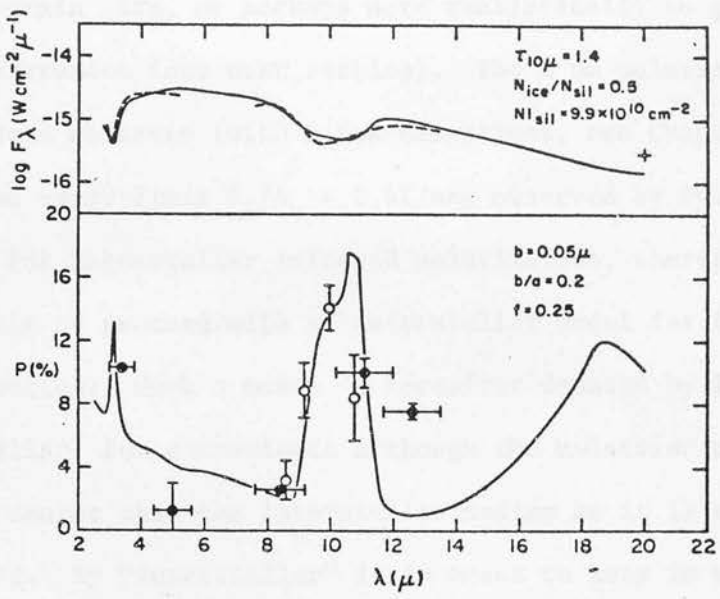

Figure II.3 Dyck and Beichman's (1974) model fit to the observed polarization of BN (Dyck et al 1973, Dyck and Beichman 1974) and the observed flux spectrum (dashed line: Gillett and Forrest 1973). The model is described in the text.

by Serkowski (1971) but the differences can be attributed quite well to grain size, or perhaps more realistically to grain composition differences (see next section). The 2 μm polarization P_K of all the sources observed (with a few exceptions, see Chapter VI) falls below the upper limit $P_K/A_v < 0.6\%/\text{mag}$ observed by Dyck and Jones (1978)[1] for interstellar infrared polarization, therefore it is reasonable to proceed with an interstellar model for the molecular cloud sources. Such a model is hereafter denoted by IS (for interstellar) for convenience although the molecular cloud medium is much denser than the interstellar medium as it is usually envisaged. By "interstellar" it is meant to keep in mind the similarity of this polarization to normal interstellar polarization although it might arise quite close to the source.

DB used a combination of prolate ice and silicate grains of a single size in a picket fence alignment (non-spinning) perpendicular to the line-of-sight to model the polarization of BN-KL between 3 and 20 μm assuming a cool, overlying absorbing dust dayer. They also derived the flux spectrum by assuming a black body spectrum for the source. DB used the Rayleigh theory to calculate cross-sections for extinction, and hence optical depths, according to equation II.1. Defining a cross-section appropriate to two orthogonal directions on the sky, x, y, the polarization is given by

$$p = \frac{e^{-\tau x} - e^{-\tau y}}{e^{-\tau x} + e^{-\tau y}}$$

1 This is true even if the A_v's estimated for the IR sources are in error to some extent (see Chapter VI).

(see Chapter IV for details). The fit to the flux spectrum is quite good, although it is crude compared to more recent, sophisticated models that consider radiative transfer effects (e.g. Kwan and Scoville 1976) in which the absorption features can arise in the shell without the need for a foreground absorbing layer. Depending on the optical depth one can see further into the shell at different wavelengths; therefore seeing less far into the shell as optical depth in a feature increases, the feature may appear in absorption as cooler layers contribute to the flux. The approximation of the spectrum and polarization by a hot emitting source and a cooler foreground absorbing layer is justified as follows. A good fit to the spectrum of a number of compact H II regions was obtained by Gillett et al (1975a) assuming an underlying silicate emission spectrum similar to the one observed in the Trapezium H II region (Gerhz et al 1975) and a cooler absorbing layer. Such a model naturally fits the optically thin H II regions, however they also managed to successfully model the optically thick BN, although radiative transfer effects may be important. In fact, as noted by Gillett et al their model is a simplication of what may be a quite complicated physical situation, however the good fit to the data implies that it is sufficient to say that such a situation can be successfully approximated by a reversing layer model.

Observations at longer wavelengths in fact indicate that the reversing layer model may be quite realistic in the case of BN. 16 - 40 μm spectroscopy of the KL nebula with a 25" beam (Forrest, Houck and Reed 1976) indicates dust at the centre of the nebula with

a black body temperature of ~80°K. That much of this dust is silicate is evidenced by the small 20 μm absorption feature also attributed to silicates, and the strong peak in 10 μm silicate absorption at BN-KL in the maps of Gehrz et al (1975). Dust at 80°K emits very little at 10 μm therefore it is reasonable to assume that radiative transfer effects are likely to be unimportant at 10 μm, even at the centre of the nebula.

The polarization spectrum is reproduced fairly well by the DB model, although in detail there are discrepancies. These do not compromise the applicability of models of this type (see Chapter IV) and may be due to observational errors in the polarimetry or the optical constants of the minerals. The assumption of a single grain size instead of a size distribution has no consequence in the Rayleigh domain. Also the assumption of picket fence alignment is not realistic, but use of a more realistic spinning oblique alignment will only affect the degree of alignment required, not the qualitative results.[1]

Extrapolation of the DB model to shorter wavelengths reveals that it falls below the observed polarization. This could be due to a failure of the Rayleigh approximation; however the steep slope of the polarization at $\lambda < 4$ μm is indicative of a contribution by Rayleigh scattering, which has a λ^{-4} dependence compared to the λ^{-1} dependence in the Mie domain. In fact DB did not use grains large

[1] Note that this exacerbates an already strained problem in producing sufficient alignment given magnetic field strengths expected to exist in molecular clouds. This problem is addressed later.

enough to scatter appreciably at $\lambda < 4$ μm: if the ratio of the scattering to absorption efficiencies, $Q_{sca}/Q_{abs} \propto (2\pi a/\lambda)^3$ is to be significant, the grain size a must be not much less than ~0.6 μm. DB adopted a size of 0.25 μm which produces albedos of the order of 10^{-3} or less. The poor fit of the model at short wavelengths is therefore a deficiency that remains to be corrected.

Because they felt that scattering was not adequately treated by DB, Elsässer and Staude (1979) (ES) developed a model for BN and KL with a specialised circumstellar geometry to account for the polarization by scattering using Mie theory. Another major thrust of ES's work was the problem in aligning the grains adequately in the DB model. The most viable alignment process presently known is by paramagnetic relaxation by a magnetic field (Davis-Greenstein alignment). Using this mechanism DB were forced to adopt an unreasonably low temperature of 6°K for the grains, and a magnetic field strength of 7 milligauss. Dennison (1977) reduced the temperature problem, but not the field strength one by using the value of τ_{10} μm adopted by Gillett et al (1975a) of 3.3 instead of 1.3 used by DB. (The larger value applies to an underlying spectrum of silicate emission instead of a black body continuum). One of the conclusions of an IS model is therefore that a more efficient alignment process than Davis-Greenstein (DG) may be required. This is not an unreasonable result, considering that the magnetic fields required to produce the ordinary interstellar polarization by DG alignment are too large also, by a factor of > 10 compared to measurements of the Galactic magnetic field by Zeeman splitting of 21 cm lines and depolarization of extra-

galactic radio sources and pulsars, yet the production of interstellar polarization by aligned grains is not questioned. More efficient aligning mechanisms do exist, though the theory is young. The question of the alignment mechanism and magnetic fields in molecular clouds is discussed in more detail later.

These considerations aside, the reservations of Elsässer and Staude are valid ones. Their model for BN-KL consists of a thick equatorial disc surrounded by a more tenuous shell or polar lobes, similar to the bipolar nebulae envisaged by Ney et al (1975). Jones and Dyck (1978) have observed large infrared polarizations in three bipolar nebulae. The important aspect in the case of BN-KL is a steep density gradient which is necessary to produce the sense of the correlation of polarization and absorption in the absorption bands. In a simple, non-structured scattering shell, the scattered polarized flux travels further in the shell than the direct unpolarized flux, therefore polarization decreases with increasing optical depth. In the ES model the direct, unpolarized flux is attenuated more in the thick disc than the scattered polarized flux from the lobes as optical depth increases. ES attributed the spatial correspondence of position angles of the polarization in KL to the reflection nebula mechanism, thus interpreting the flux from KL as mainly scattered radiation from BN. All the extinction observed to BN arises in the disc.

There are a number of problems with such a model. Although some evidence exists that reflection nebulosities occur at short

infrared wavelengths (2 and 3 μm) it is hard to imagine them at 10 μm. As much as 6% of the 2 μm flux in a 10" aperture from BN may be due to an extended scattered contribution. (This is an upper limit to the scattered flux, depending on the relative contribution from free-free emission from the foreground H II region (Becklin and Neugebauer 1967, Becklin et al 1976)). If this were 100% polarized the resulting observed linear polarization at 2 μm in a 10" aperture would be ~6%. This is considerably lower than observed but not unacceptable if it is postulated that more scattering occurs closer to BN. However, at 10 μm calculated albedos for a variety of grain compositions and sizes are found to be at least a factor of 200 lower than at 2 μm, for both Mie and Rayleigh theory (this research, Bertout and Yorke 1978, Kunkle 1979), yet the ES model predicts similar degrees of polarization at these two wavelengths although the optical depths are very similar (see later discussions). The distribution of grain sizes used by ES does not seem to be large enough to produce appreciable albedos at 10 μm compared to 2 μm. It is possible that the observed extended 10 μm emission from KL is scattered flux from BN but it is more likely that it is emission from faint sources or extended thermal dust emission from KL, absorbed by the overlying cooler dust which produces the black body-like spectrum with a temperature of ~80°K (Forrest et al 1976) with possibly some contribution from the foreground H II region.

A second possible shortcoming of the ES model is that at wavelengths where the total optical depth is small (5 - 8 μm) scattering in the equatorial disc may become greater than in the lobes in which

case the position angle would be perpendicular to that observed at other wavelengths.

The most serious drawback to the ES model is the predicted polarization at 20 μm. Here the contribution to the flux by scattering must be minimal, since the grain albedos are much lower even than at 10 μm. Knacke and Capps (1979) have observed in BN a polarization of 6.3% near 20 μm, which cannot be attributed to the scattering model (Staude 1979, private communication).

Knacke and Capps also observed polarization at 11.1 and 19.6 μm from a few locations in KL. They found that the position angles agree closely both spatially and with wavelength, thus corroborating the earlier 11.1 μm observations of DB. Therefore these polarizations should be attributed to the same mechanism: transfer of radiation through a medium of aligned grains.

It is likely that radiative transfer effects are more important at 20 μm than at 10 μm, indeed the small depth of the 20 μm feature in KL compared to the 10 μm one was attributed to such effects by Forrest and Soifer (1976). A small emission component is admitted by the data of Knacke and Capps (1979): as long as the source is optically thick the absorption polarization will dominate the emission. However, Knacke and Capps consider that their data is most consistent with a pure absorbing cloud, and that the 20 μm absorption feature could be reduced by contamination in the 25" beam of Forrest and Soifer (1976) by KL. This interpretation does not necessarily

require that the 20 μm polarization occurs in cooler dust foreground to the 80°K KL dust because the apertures used by Knacke and Capps overlap and include the discrete cluster members IRc 2 - 5 (Rieke and Low 1973, Rieke et al 1973), which could be the emitting sources. The importance of radiative transfer effects at 20 μm is therefore not directly relevant to this work. The 10 to 20 μm data are consistent with polarization at all wavelengths by a medium of commonly aligned grains which may be closely confined to KL (~10^{17} cm) or may stretch along the whole pathlength through the cloud (~10^{18} cm, Zuckerman and Palmer 1975, Zuckerman 1977). Given the far infrared and submillimetre observations which indicate that the dust density peaks strongly towards the central regions (Harper 1974, Thronson et al 1979, Smith et al 1979) and the observations of Harris et al (1978) that the ice feature, which is polarized, is only seen in the densest central cloud regions (see next section), it is likely that most of the polarization occurs in the central regions of the cloud.

A test of the DB model is to search at longer wavelengths for polarization in emission from the same aligned grains that polarize by absorption at 2 to 20 μm. Such searches have so far been unsuccessful (Dennison 1977, Gull et al 1978), although the instrumental errors of these experiments are large enough that it may be hard to detect the polarization.

It is natural to attribute the shorter wavelength polarization to the same mechanism required for the long wavelength data, especially since there is no significant rotation of position angle with

wavelength (see Figure II.2). The deficiency in the DB model at short wavelengths remains however, and it is possible that a scattering shell at a smaller scale than envisaged by ES may exist, which enhances the short wavelength polarization, or that the scattering properties of the aligned grains have been underestimated. Also, no attempt has been made to account for the circular polarization. The question that must be addressed is whether a circumstellar scattering shell is required in BN and sources like it, or whether an IS model can be found which can match the linear polarization better than the DB model, and which can also account for the circular polarization.

Circular polarization can arise by multiple scattering, or by single scattering off aligned grains, in a circumstellar shell. Multiple scattering requires a considerable optical thickness to scattering thereby limiting the linear polarization produced to about 10% (Chandrasekhar 1946), and requiring high albedos. Circular polarization has been observed at 1 and 2 μm in VY CMa (Serkowski 1973), an object in which the linear polarization is attributed to scattering in a shell of dielectric particles (Dyck, Forbes and Shawl 1971). Serkowski ascribed the circular polarization to multiple scattering from these grains. As expected, the circular polarization peaks where the linear polarization is a minimum. The observations show that where the polarization p is small, the ellipticity e can be significant, but where p is large the ellipticity is 2% or less. By comparison, if the polarization of BN arose in a multiple scattering nebula, it is unlikely that the ellipticity could

be as high as 9% when the linear polarization is 18%, as observed. The linear polarization produced in this way could be enhanced by transfer through the aligned grain material that polarizes the longer wavelength flux, but the position angles would have to coincide. Possibly the same magnetic field that aligns the grains could govern the geometry of the source. Flattening produced by faster collapse along the field lines than perpendicular to them would result in an asymmetric shell which would produce polarization *perpendicular* to interstellar polarization (unless reverse Davis-Greenstein alignment operates, see next section).

Also, for circular polarization to be produced in a multiple scattering circumstellar shell, the shell must be considerably more asymmetric than required to produce linear polarization: to avoid cancellation of opposite handedness from opposite sides of the shell, the geometry must also be skewed in some way (Wolstencroft 1979, private communication). This latter comment applies to circular polarization produced by single scattering off aligned grains in a circumstellar shell also. In this latter case the linear polarization is also *perpendicular* to that produced by dichroism of aligned grains, therefore the total polarization will be reduced rather than enhanced.

All these considerations lead to the conclusion that scattering geometries are not very helpful in solving the problem of the polarization. The natural next step is to ask whether BN is an exception in being circularly polarized, or whether other molecular

cloud sources are also. In other words, is it necessary to worry about specialised, asymmetric geometries as a characteristic of protostars? To answer this question, observations of the circular polarization of 8 molecular cloud sources were obtained and are presented in Chapter III.

The next step is to enquire whether the DB model can be improved, and whether it can account for the circular polarization. In the next section the characteristics of dust grains in molecular clouds are considered, with a view to improving the model composition. Circular polarization has been detected at optical wavelengths from several stars which have interstellar linear polarization. Following a suggestion by van de Hulst (1957) models invoking linear birefringence to accompany the linear dichroism of the interstellar medium have been developed in the literature. The birefringence results from a change in the orientation of grain alignment along the line-of-sight and produces a phase retardation of one orientation of polarization with respect to the orthogonal one.

In Figure II.4 are reproduced the measures of linear dichroism and birefringence for representative refractive indices calculated for infinite cylinders by Martin (1974) (adapted from his Figure 2) and for prolate spheroids by Rogers and Martin (1979) (adapted from their Figure 1) using Mie theory. The representation of dichroism and birefringence in the two papers is different, but equivalent, as described in Chapter IV. The ordinates are arbitrarily normalised to $\lambda max = 1$ for easy comparison. The abscissae depend on the size

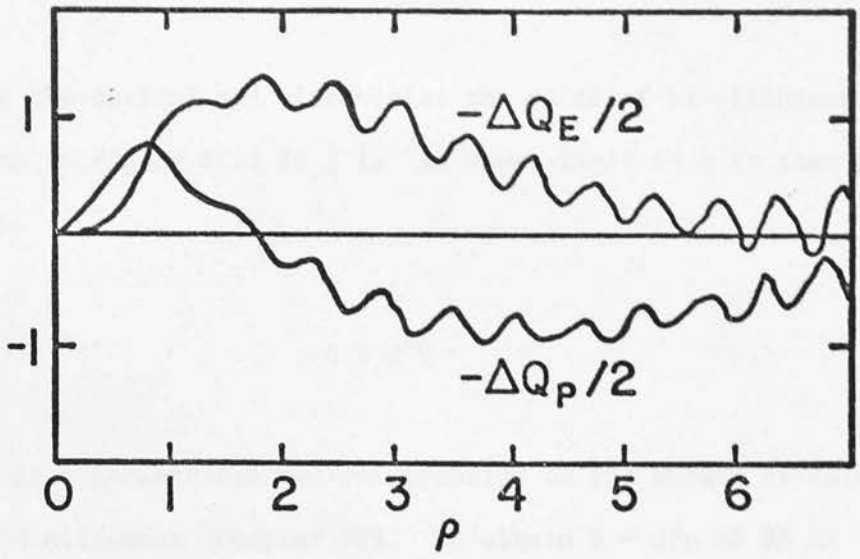

II.4.a

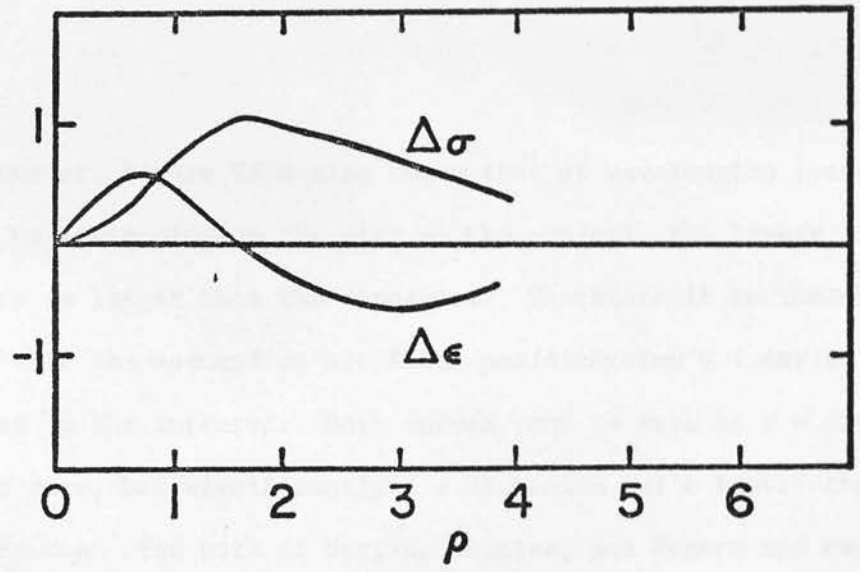

II.4.b

Figure II.4.a Birefringence ΔQ_p and dichroism ΔQ_E as a function of $\rho = 4\pi a(m - 1)/\lambda$ for prolate grains with m = 1.33 (Rogers and Martin (1979)).

b Same for circular cylinders with m = 1.5 (Martin 1974). The representations of birefringence and dichroism are explained in the text.

distributions chosen for the grain models. The two sets of curves exhibit very similar behaviour. The curves calculated for magnetite by Shapiro (1975) are similar.

In the optical and ultraviolet the ratio of birefringence to dichroism in Figure II.4 is $\lesssim 1$. An upper limit to q is then given by

$$q \lesssim p^2 G \qquad \text{II.2}$$

where G is a geometrical factor depending on the amount of twist in the grain alignment (Chapter IV). To obtain $e = q/p$ of 9% as observed at 3.45 μm in BN would require $\phi \gtrsim 80°$, which is a rather large value to expect for a perfect twist in a dense molecular cloud.[1]

However, Figure II.4 also shows that at wavelengths longer than about 1 μm (depending on the size of the grains), the linear birefringence is larger than the dichroism. Therefore it is immediately evident that the assumption birefringence/dichroism $\lesssim 1$ may be incorrect in the infrared. Both curves tend to zero as $\rho = 4\pi a/\lambda$ tends to zero, but significantly the dichroism falls faster than the birefringence. The work of Martin, Shapiro, and Rogers and Martin,

[1] Larger values of ϕ are quoted in the literature to fit interstellar optical circular polarizations, however these apply to the angle between two or more discrete clouds along a long line-of-sight. The pathlengths through the aligned grains to the infrared sources in molecular clouds are much shorter, also discrete slab models are not very appropriate.

however, is not adequate for application to infrared observations. The calculations have not been carried out in sufficient detail at wavelengths of interest, in which case it is not possible to tell whether ϕ could be reduced to a low enough value to make an IS model for the polarization plausible. In any case it may not be necessary to deal with the rigorous and cumbersome Mie theory in the infrared. where the Rayleigh approximation is likely to be valid (e.g. see Figure II.2 and relevant text). In spite of the generalisation of the Mie solution to arbitrarily shaped spheroids (Asano and Yamamoto 1975) the Rayleigh theory remains much more flexible. In view of the fact that the shapes, sizes and compositions of interstellar grains are really not well known within certain limits, this flexibility is very desirable. These points alone make a study of the situation at infrared wavelengths using Rayleigh theory very attractive. In addition, the most important defect of the published work as regards application to the infrared is the fact that the refractive indices used for the grain materials have not been allowed to vary with wavelength. This approximation may not have much importance at optical wavelengths, but in the infrared it is a serious oversimplification of the physical situation. In Figure II.5 is illustrated the behaviour of the complex index of refraction $\tilde{m} = \tilde{n}' - i\tilde{n}''$ at the wavelengths of interest for some commonly adopted grain materials.

In view of these considerations, and the earlier discussion of the applicability of an IS model to the linear data it seems that an IS model with a twisting grain alignment may be well suited to

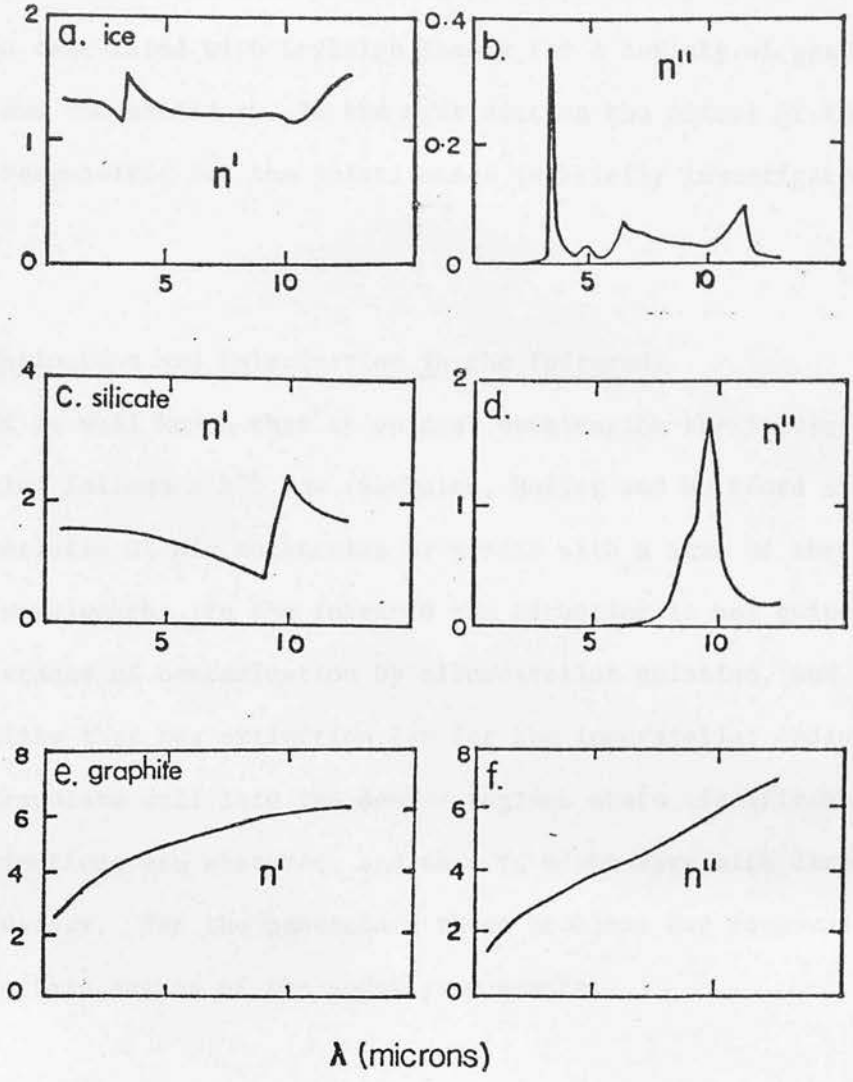

Figure II.5 Dependence of the refractive index m = n' - in" with wavelength for,

a. and b.: ice (Irvine and Pollack 1968),
c. and d.: obsidian (Pollack et al 1973) and
e. and f.: graphite (Bergeat et al 1976).

fitting the data. Such a model is therefore developed and used in Chapter IV to fit the data presented in Chapter III, using cross-sections calculated with Rayleigh theory for a variety of grain shapes and compositions. In the next section the nature of the dust grains responsible for the polarization is briefly investigated.

(3) Extinction and Polarization in the Infrared.

It is well known that at optical wavelengths the interstellar extinction follows a λ^{-1} law (Stebbins, Huffer and Whitford 1940) characteristic of Mie scattering by grains with a size of the order of the wavelength. In the infrared the situation is not quite so clear because of contamination by circumstellar emission, and the possibility that the extinction law for the interstellar medium does not extrapolate well into the denser regions where significant infrared extinctions are observed, and that it might vary with direction in the Galaxy. For the protostars these problems are compounded by the uncertain nature of the underlying source.

An empirical relationship has also been found for the wavelength dependence of interstellar optical polarization (Serkowski 1971). It is given by

$$P/P_{max} = \exp[-k \ln^2(\lambda_{max}/\lambda)] \qquad \text{II.3}$$

where k is a constant equal to 1.15.

It has long been thought that there are variations in $R = A_v/E_{B-V}$, the ratio of total to selective extinction in different regions of the Galaxy (e.g. Johnson 1968), which were attributed to variations in the grain sizes, since larger grains are relatively more efficient absorbers and scatterers at longer wavelengths. λ_{max} is also seen to vary (Serkowski, Mathewson and Ford 1975, Gehrels et al 1974). This has also been attributed to a size effect, since polarization at optical wavelengths is basically a scattering effect, which is controlled by the phase lag term in the difference in the extinction cross-sections for radiation polarized in orthogonal planes,

$$\Delta\phi = \frac{4\pi a(n' - 1)}{\lambda} \qquad \text{II.4}$$

Therefore $\lambda_{max} \alpha \langle a(n' - 1) \rangle$ where a is the grain size and n' the real part of the refractive index, and the angular brackets denote an average over the line-of-sight.

Some of the variations in R have been found to be spurious, but variations in R and λ_{max} still exist, especially in the local dark clouds (Carrasco, Strom and Strom 1973, Coyne et al 1974, Serkowski et al 1975, Breger 1977, McMillan 1977). Here R and λ_{max} appear to be larger than normal, thereby possibly indicating larger grains in denser regions. A fairly constant value of the ratio $R/\lambda_{max} = 5.6$ has been inferred by Whittet and van Breda (1978). A representative extinction curve is illustrated in Figure II.6 (Savage and Mathis 1979).

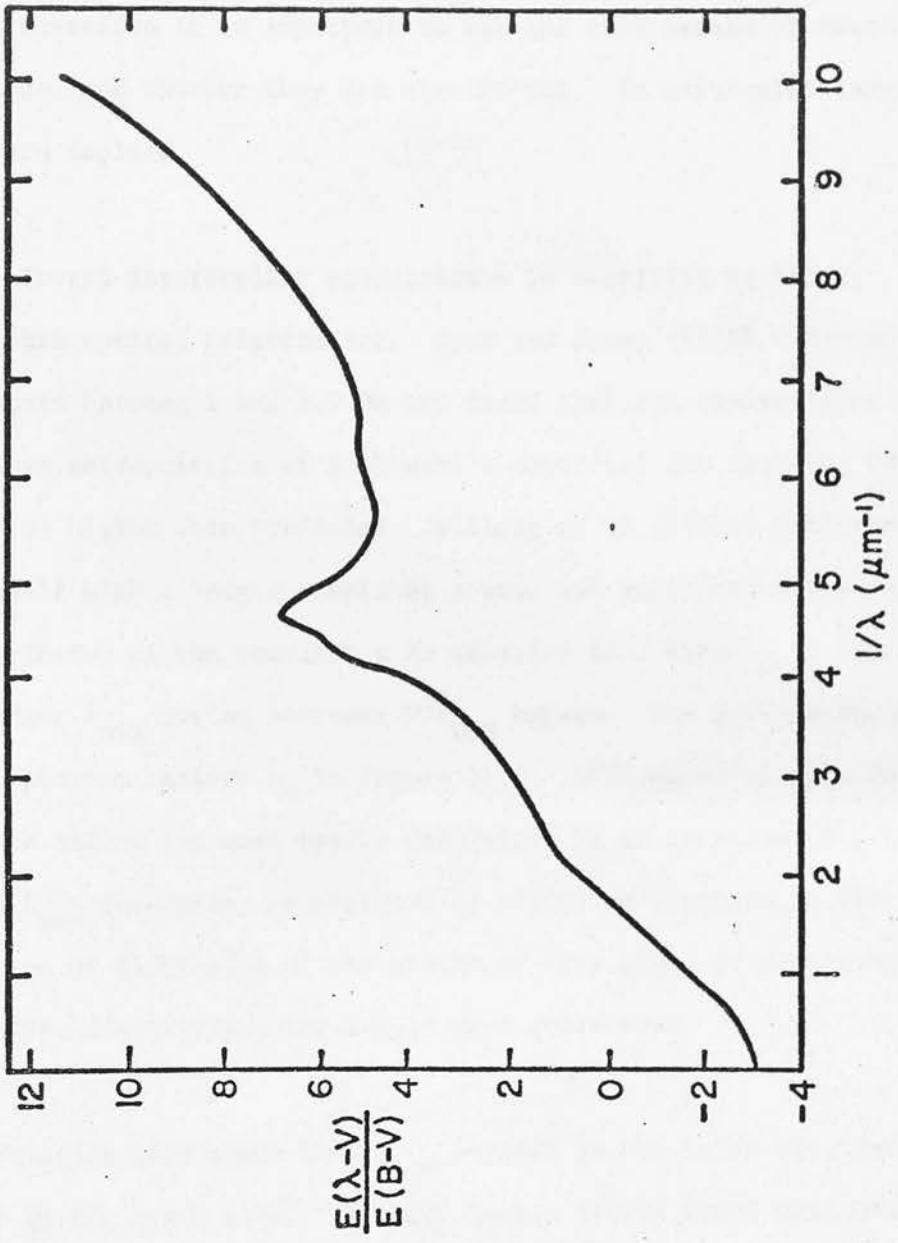

Figure II.6 An average interstellar extinction curve (Savage and Mathis 1979).

Variations are seen to occur in the R and λ_{max} in the dark clouds so it is very likely that conditions can be appreciably different in the still denser, central regions of the molecular clouds, therefore it is important to ask the true nature of these variations, and whether they are significant. In particular larger grains are implied.

Infrared interstellar polarization is sensitive to larger grains than optical polarization. Dyck and Jones (1978) observed seven stars between 1 and 2.2 μm and found that the observations do not fit an extrapolation of Serkowski's empirical law exactly, but tend to be higher than predicted. Wilking et al (1979b) confirmed this result with a larger sample of stars, and interpreted the change as a variation of the constant k in equation II.3 with λ_{max}; stars with larger λ_{max} having narrower P/P_{max} curves. The polarization data is plotted against A_v in Figure II.8. Wilking et al considered that this effect was most easily understood by an increase in grain size as λ_{max} increases, accompanied by either an increase in the elongation or flattening of the grains as they grow, or a narrowing of the size distribution for larger mean grain size.

Equation II.4 shows that λ_{max} depends on the refractive index as well as the grain size. In fact, Kunkle (1979) found that his four component model (Figure II.7), derived to fit the interstellar extinction could not fit the observed R/λ_{max} relationship with a simple change in grain size, contrary to the prediction of Wilking et al, or by a change in refractive index. The relationship is

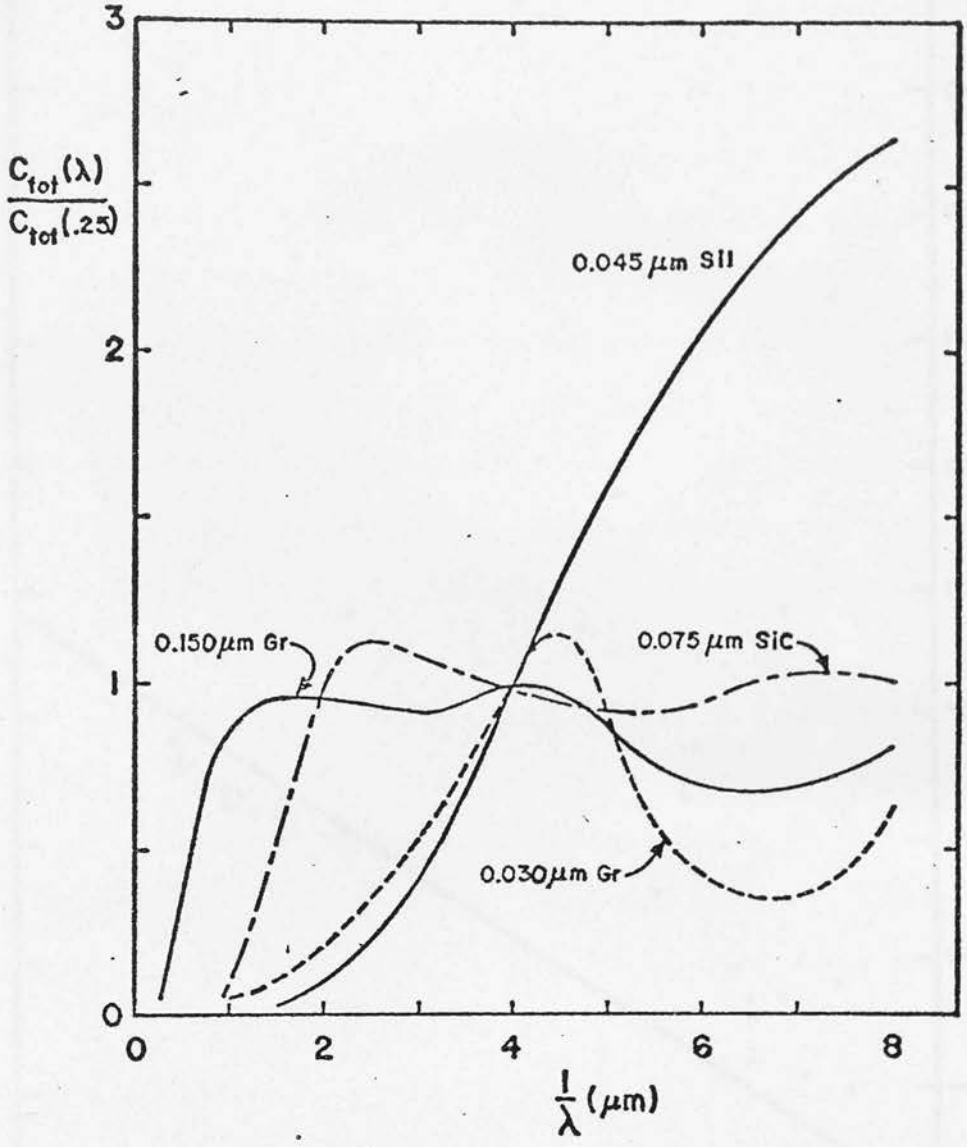

Figure II.7 Normalised extinction efficiencies for the grains comprising the four-component interstellar model of Kunkle (1979).

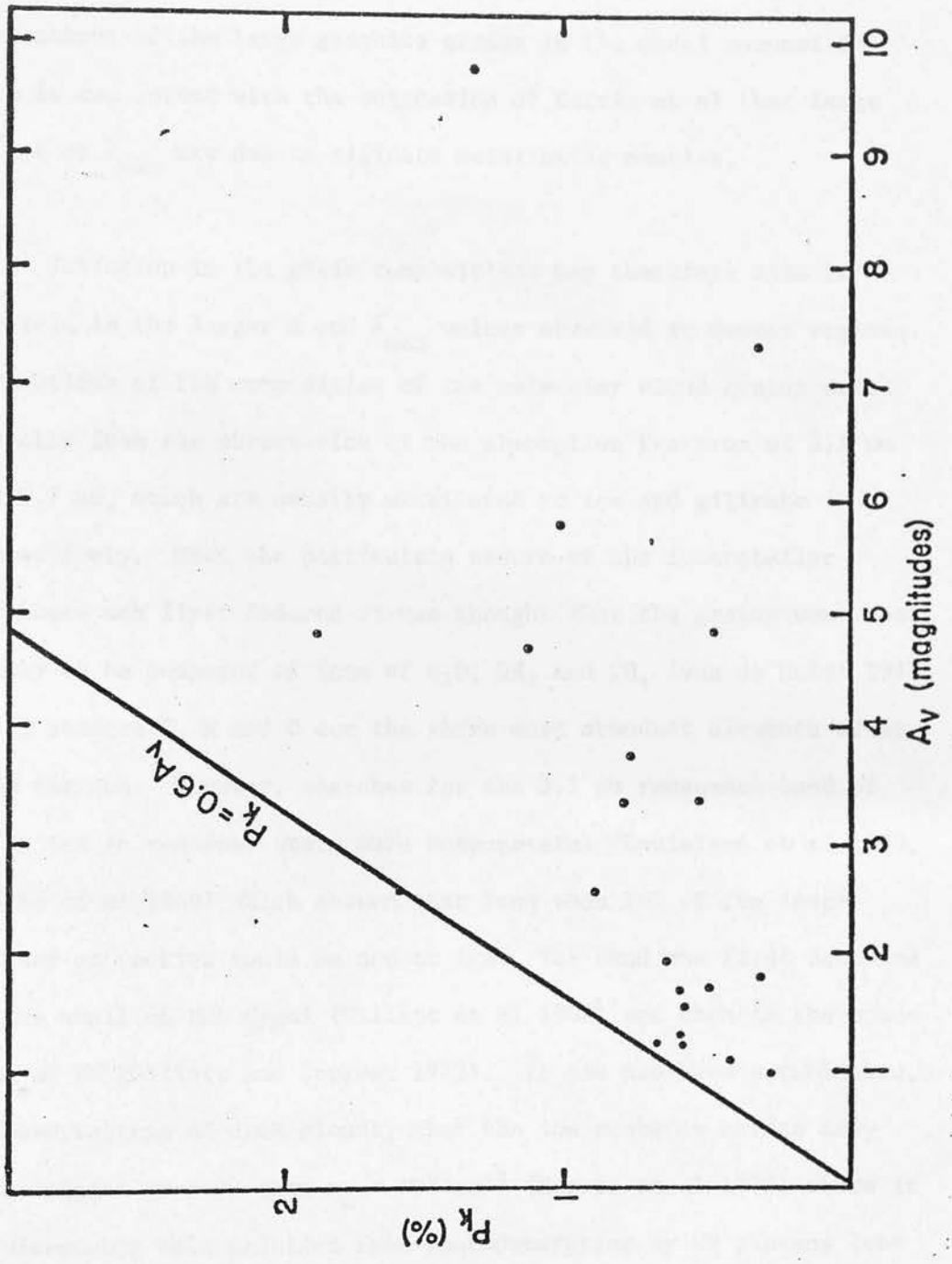

Figure II.8 Infrared interstellar polarization data plotted against optical extinction. The data are from Dyck and Jones (1978) and Wilking et al (1979b).

fitted well instead, by increasing a and n *simultaneously* (i.e. by the addition of an absorbing grain mantle) and by altering the relative amount of the large graphite grains in the model composition. This is consistent with the suggestion of Harris et al that large values of λ_{max} are due to silicate metal oxide mantles.

Variation in the grain compositions may therefore also be implicit in the larger R and λ_{max} values observed in denser regions. Indications of the composition of the molecular cloud grains comes directly from the observation of the absorption features at 3.1 μm and 9.7 μm, which are usually attributed to ice and silicate respectively. When the particulate nature of the interstellar absorbers was first deduced it was thought that the grains were most likely to be composed of ices of H_2O, NH_3 and CH_4 (van de Hulst 1946, 1949) because C, N and O are the three most abundant elements after H in the sun. However, searches for the 3.1 μm resonance band of water ice in reddened stars were unsuccessful (Danielson et al 1965, Knacke et al 1969) which showed that less than 10% of the interstellar extinction could be due to ice. The band was first detected in the shell of NML Cygni (Gillett et al 1968) and then in the spectrum of BN (Gillett and Forrest 1973). It has now been established, by observations of dark clouds, that the ice probably exists only at densities greater than $n_H \simeq 10^5$ cm^{-3} (Harris et al 1978) where it is presumably well shielded from photodesorption by UV photons (the interstellar medium being *cold* enough for it to exist). Also, it makes no contribution to near infrared extinction (Harris et al 1978) and has no effect on the values of R and λ_{max} (McMillan 1979). Therefore

it is not accretion of ice mantles onto refractory grains that causes these high values in dark clouds, in agreement with Kunkle's (1979) conclusion that mantles consist of an absorbing material.

Evidence for a substantial component of some other material than ice in the grains comes from UV observations of depletions in the gas phase, which indicate that the heavier elements Mg, Si and Fe are strongly depleted and therefore probably condensed into grains, (Field 1974, 1975, Spitzer and Jenkins 1975, Morton 1975, Snow 1976). The theory of grain formation in the atmospheres of oxygen rich stars predicts the formation of silicates but modelling of the 9.7 μm feature, which is remarkably similar in shape in both emission and absorption throughout the Galaxy, using crystalline, hydrated or amorphous terrestrial, lunar and metoritic silicates is not successful in detail (e.g. Knacke 1978). However, most people agree that the feature is due to some kind of silicate and that cosmic abundances of Si, Mg, etc. are sufficient to account for the observed optical depths.

Silicates, however, cannot account at all well for the 2200 Å bump (Figure II.6), also Kunkle (1979) has shown that they cannot account well for the near infrared extinction (Figure II.7). In addition it is likely that silicates cannot account for the entire optical extinction. Gillett et al (1975b) derived a value of 1×10^{-4} to 7×10^{-4} gm cm^{-2} for the mass column density of silicates to BN, depending on the adopted 10 μm optical depth, and found that silicates could only account for ~50% of the extinction to

VI Cyg no. 12 unless the peak bandstrength of the interstellar silicates is lower than that of terrestrial and lunar silicates. Some evidence in support of this comes from the polarization observations in the silicate band (Martin 1975, Capps 1976, Capps and Knacke 1976). The ratio of polarization to absorption across the band is sensitive to the bandstrength. Laboratory observations of amorphous silicates indicate that they have such low bandstrengths (Day 1976b), and may be able to account for all of the observed extinction. Experiments also show that amorphous silicates are more likely to condense than crystalline ones (Day and Donn 1978).

Graphite and silicon carbide are predicted to form in the atmospheres of carbon stars. There is theoretical evidence that SiC might improve the model fits of the long wavelength side of the 9.7 μm band (Gilra 1971, Kunkle 1979). There is no direct evidence for graphite in the interstellar medium, but carbon is very abundant. Small graphite grains can best explain the 2200 Å "knee" in the interstellar extinction curve (Figure II.6) (e.g. Aannestad and Purcell 1973), while large ones have been employed successfully for the near infrared curve (Kunkle 1979).

Simultaneous attempts to match the observed wavelength dependence of extinction and polarization in detail with combinations of these grain materials face numerous problems. The major one is that Mie theory applies only to spheres, which cannot polarize unless the grain material is not isotropic; therefore the treatments are not always self-consistent. Also, the models are not at all unique,

there being too many free parameters available. The most recent, sophisticated models available are those of Mathis et al (1977), Mathis (1979) and Kunkle (1979).

For the purposes of the present work it is necessary only to consider the aspects of such models which are relevant to the dense molecular cloud situations. The important points to note are that silicates can probably not account for all the extinction, including the near infrared, that the ice does not affect the near infrared extinction, and that the inclusion of relatively large grains of a material such as graphite is important to the near infrared extinction, and can help to explain the larger values of λ_{max} observed in denser regions. The possibility that the grains are also larger than in the interstellar medium is unimportant, because the absolute grain size is basically neglected by the Rayleigh theory (see Chapter IV). It therefore seems reasonable to improve the DB model using relatively large graphite grains (after Kunkle 1979)) in addition to the silicates and ice to increase the short wavelength linear polarization. Such an improvement is attempted in Chapter IV, and the resulting models are used to fit the circular polarization.

Determinations of the magnetic field strength in the Galaxy are somewhat indirect. The methods employed include the measurement of the Faraday rotation of extragalactic radio sources and of pulsars, and Zeeman splitting of the 21 cm absorption line of hydrogen. The results from these two methods do not always agree, but a general

picture seems to emerge of a longitudinal field directed towards $l^{II} = 90°$ (Mathewson and Nicholls 1968), with large and small scale fluctuating components. The longitudinal field appears to have a strength on the order of 1 - 3 microgauss (Heiles 1976, Manchester 1974). Optical polarization maps (Mathewson and Ford 1970, Axon and Ellis 1976) show vectors aligned with the plane, and great arches above the plane. Observations of filamentary structure and maps of dark clouds show polarization vectors aligned with the streamers, strongly indicating the influence of the magnetic field in the cloud morphology (Elvius and Hall 1965, Schlosser and Schmidt-Kaler 1974, Vrba et al 1976).

In the dark clouds and the dense molecular clouds, determinations of the magnetic field strength are even harder. Where neutral hydrogen exists the splitting of the 21 cm line may be observed. Elmegreen (1978) has suggested that such observations might be successful even in the dense clouds but so far none has been attempted. In any case the 21 cm line may become self-absorbed in dense clouds. Most measurements come from observations of the splitting of molecular lines and type I OH masers. Interpretation of the suspected Zeeman patterns is hard because complete patterns never seem to be observed: the linearly polarized components are often missing. Also, the left and right circularly polarized components cannot always be spatially correlated. In addition the masers arise in dense localised regions where the magnetic field is probably not at all representative of the general molecular cloud fields. Field strengths of the order of 10^{-3} gauss are commonly

quoted for the dense maser regions ($n_{H_2} \sim 10^6$ cm^{-3} or more) (Moran et al 1978, Heiles 1976).

The origin of the maser emission in regions of star formation is not well understood, also the relationship of the H_2O and OH masers is not clear. The general opinion, however, is that they form in dense, small sites closely associated with a protostar or compact H II region in an expanding shell or an accretion front (Genzel et al 1979) and in shocked layers near an expanding ionisation front (Gatley et al 1979, Moran et al 1978). Genzel et al (1979), using VLBI observations have resolved H_2O masers on a milliarcsecond scale, and have found a cluster of sites at W51 M which are best interpreted as originating in the 10^{15} cm disc or shell of a single object, which, in this case, is expanding. It seems clear from such observations that observations of magnetic field strengths from Zeeman patterns of masers do not assist much with interpretation of the infrared polarization observations.

Dyck and Beichman (1974) interpreted their polarimetry of BN-KL in terms of the Davis-Greenstein alignment mechanism (Davis and Greenstein 1951). This mechanism is based on the idea that a magnetic torque acts on grains with paramagnetic impurities, causing the rotation along axes perpendicular to the field direction of a randomly rotating grain to be damped. The torque depends on χ'', the imaginary part of the magnetic susceptibility, and on B, the magnetic field strength, and if successful will align the grains with their angular momentum vectors parallel to B. Randomizing collisions with

the gas atoms can destroy the effect, therefore the success of the mechanism depends on the relative timescales for magnetic damping τ_{DG} and randomization τ_{gas}. τ_{DG} is given by

$$\tau_{DG} = \frac{\gamma I}{VB^2K} \qquad \text{II.5}$$

where γI is the moment of inertia of the grain about the axis transverse to the symmetry axis, V is the volume and K is given by $K = \chi''/\omega = K'/T_d$. T_d is the temperature of the grain and ω is the rotational velocity. τ_{gas} is given by

$$\tau_{gas} = \frac{C\gamma I}{\langle v \rangle \rho_{gas} V^{3/4}} \qquad \text{II.6}$$

where C is a shape dependent parameter (Purcell and Spitzer 1971), $\langle v \rangle$ is the mean gas velocity and ρ_{gas} is the gas mass density. For alignment to occur $\delta = \tau_{gas}/\tau_{DG} > 1$.

Alignment depends on the relative gas and dust temperatures, T_g and T_d respectively. It can be shown that alignment can only occur if $T_g \neq T_d$ since a relationship exists between the polarization reduction factor $R(\xi)$ (Greenberg 1968), which is twice the degree of alignment f, such that

$$\xi^2 = \frac{1 + \delta(T_d/T_g)}{1 + \delta} \qquad \text{II.7}$$

$R \to 1$ as $\xi \to 0$, and $R \to 0$ as $\xi \to 1$.

If $T_g > T_d$, "normal" DG operates, and prolate grains will align with their symmetry axes perpendicular to the field, and oblate ones with their axes parallel to the field. This produces the same sense of polarization, parallel to B. In reverse alignment the opposite will be true, the polarization will be perpendicular to B. Reverse alignment occurs when $T_g < T_d$. Since it is normally assumed that $T_g > T_d$ in the interstellar medium (Spitzer 1978) the polarization vectors should reflect the field lines of the Galactic magnetic field directly.

Field strengths normally required in the interstellar medium to explain the optical polarization by normal DG alignment are of the order of 20 to 30 microgauss (Aannestad and Purcell 1973) for optimum conditions where the field is transverse to the line-of-sight and does not vary in direction along the line-of-sight. These values are at least an order of magnitude greater than the observations of the magnetic field indicate. Knacke and Capps (1977) required a similarly large value to explain the polarization of the Galactic Centre sources in the near infrared by dust grains in the spiral arms.

In the molecular clouds larger field strengths are to be expected if the cloud collapses with a frozen-in magnetic field (see Chapter VII). However, DB required a field strength of 7 milligauss in a region where the dust is still cold and the densities are presumably not very high. Dennison (1977) used reverse DG alignment to relax the temperature problem, but required even larger field strengths to align the grains. Knacke and Capps (1977) also required

milligauss field strengths to explain the 11 μm polarization in the Galactic Centre.

It is not clear that flux-freezing cannot account for the increased field strengths required in the dense clouds, (this is discussed later), however DG alignment falls well short of explaining the interstellar polarization so that it is likely that a more efficient process is required, in any case. It turns out in fact, that the requirement that $T_g \neq T_d$ is difficult to meet in the dense clouds (see Chapters VI and VII).

The alignment may be improved either by altering the grain properties or by making the mechanism more efficient by some means. This is discussed later, but it should be noted here that changes in the composition of the grains in the model to be developed are not required. The silicate and ice grains must be aligned, therefore use of ferromagnetic grains cannot help. Super-paramagnetic properties induced in the silicates and ice by inclusions of magnetic materials will not affect the optical properties. Also anisotropy of conductivity of the graphite, or birefringence of crystalline silicate grains would have negligible effect (Aannestad and Purcell 1973), and are therefore ignored. Finally the value of χ'' might be expected to optimise for certain materials, but theoretical treatments indicate that it is remarkably constant giving $K \simeq 2 \times 10^{12}/T_d$ for all paramagnetic substances (Aannestad and Purcell 1973). Experimental determinations of χ'' do not yet exist.

CHAPTER III

OBSERVATIONS

(1) Instrumentation and Techniques

The observations for this thesis were made primarily on the 2.24m telescope of the University of Hawaii, situated on Mauna Kea.

The equipment is illustrated in Figure III.1. The detector is mounted on the side of the photometer, light being reflected into it by a dichroic mirror after passing through the polarimeter. Initially an eye piece was used at the optical focus. An integrating Quantex TV acquisition system was mounted there in April 1979. The polarimeter consists of an analyser which can be rotated continuously or in steps, and a stationary quartz Lyot depolarizer, which can be slid into the beam above the dichroic mirror.

Three analysers were used at different times. An HR polaroid for wavelengths shorter than 2.2μm, and two Cambridge Physical Sciences barium fluoride wire grids, which operate at all the wavelengths of concern in this research. The HR polaroid has a lower instrumental polarization than the wire grids, but was not used unless all the observations of a particular night were to be at 2.2μm or less, because it is a considerable waste of time to change analysers during observing. Also the efficiency of the HR is less than that of the grids at 2.2μm. However, the grids suffer from a large pseudo-instrumental polarization,

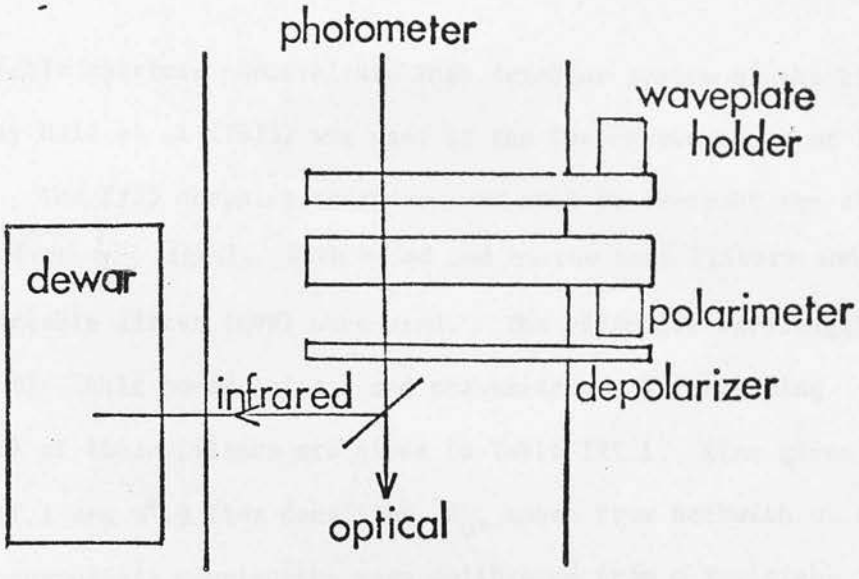

Figure III.1 Schematic representation of the equipment.

which varies over long timescales, which the depolarizer cannot eliminate because it is of a mechanical nature (see discussion of error analysis).

A variable aperture photovoltaic InSb detector system of the kind described by Hall et al (1975) was used at the Cassegrain focus of the telescope. The f/35 chopping secondary was used to subtract the sky background from the signal. Both broad and narrow band filters and a circular variable filter (CVF) were used. The effective wavelengths λ_o bandpasses $\Delta\lambda$ (half power points) and transmissions T (excluding atmospheric) of these filters are given in Table III.1. Also given in Table III.1 are $0^m.0$ flux densities, F_ν, taken from Beckwith et al (1976). Intermediate wavelengths were calibrated from a Rayleigh-Jeans interpolation. Also given are typical telluric extinction coefficients for Mauna Kea for the broad band filters.

The polarimeter is adapted to the measurement of circular polarization by the insertion of a quarter wave plate for the appropriate wavelength above the analyser. The wave plate is rotated by step, while the analyser rotates continuously. For this work a 2.2μm quarter wave plate made of mica between fused silica cover plates was used.

The simplest way to operate the linear polarimeter as presently implemented is to use a stepper motor and to rotate the analyser by 45^o at a time using a manual controller. An integration is made at each position of the analyser. The secondary chops at a frequency of

Table III.1

The Filters

Filter	λ_o (μm)	Δλ (μm)	T (%)	F_ν (Jy) ± 10%	Ext (mag/airmass)
H	1.65	1.52-1.80	85	980	0.06
K	2.22	1.99-2.41	80	620	0.10
-	2.91	2.81-3.01	63	400	-
-	3.05	3.00-3.10	65	370	-
-	3.23	3.08-3.38	70	340	-
-	3.51	3.41-3.61	78	300	-
L'	3.82	3.51-4.18	85	280	0.15
M	4.76	4.48-5.05	78	153	0.30

20Hz therefore the signal from the object results in a 20Hz AC signal at the preamplifier of the detector. This signal is fed to a lock-in amplifier tuned to this frequency. The amplifier output is then recorded directly on a strip chart recorder and a high-speed counter via a voltage to frequency converter. This method of operation was used for the nights of 6th through 10th May 1978 because problems were being experienced with the new LSI-11 data acquisition system installed at the computer in November 1978.

It is more efficient to spin the analyser continuously rather than step it, because a large amount of dead time can be wasted stepping the analyser, and stopping and starting the integrations. To spin the analyser a different motor is used. The speed is not controlled by the computer but by motor control electronics, and the position of the analyser is read by the computer at the 0^{o}, 90^{o}, 180^{o}, 270^{o} positions using a signal from an optical encoder. The polarimeter is illustrated in Figure III.2. The analyser spins at about 1Hz. The lock-in demodulated signal in this case is fed to the data acquisition computer, which was an IBM 1800 for the September 1978 run, and an LSI-11 for the other runs. The computer times the rotation of the analyser, and when an observation is started it integrates over the eight 45^{o} segments, storing the values in 4 channels. (Each half-cycle of the analyser should give identical data, therefore the 225^{o} data is stored in the 45^{o} channel, etc.) This procedure is repeated for a specified integration time (usually 20 secs). Several oscillations of the secondary mirror, which runs independently of the polarimeter, occur in each 45^{o} segment. When the integration is

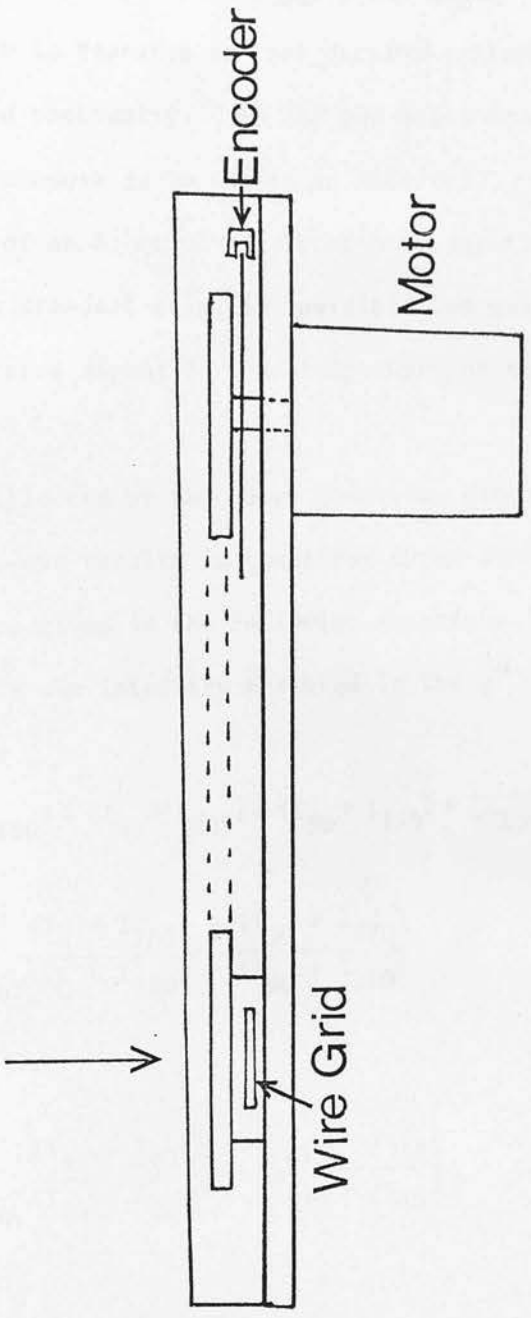

Figure III.2 The polarimeter.

finished the telescope is moved to place the object in the other beam and the procedure is repeated so that data are collected in the way of standard infrared photometry. If the two beams are termed A and B, the observing procedure is to obtain an ABBA set. Guiding is generally done at the end of an A, or of a pair of B integrations, since the object, unless a standard star, is invisible and guiding has to be done on the infrared signal on the strip chart or the lock-in amplifier.

The data collected by the above observing procedure is processed by the programme and results in the first three Stokes parameters I, Q and U. They are given in the following equations. (See data analysis section.) I_θ is the intensity measured in the θ^o to $\theta^o + 45^o$ segment of the analyser.

$$I = \tfrac{1}{2}[(I_0 + I_{180}) + (I_{45} + I_{225}) + (I_{90} + I_{270}) + (I_{135} + I_{315})] \qquad \text{III.1}$$

$$\frac{Q}{I} = \frac{1}{P_o} \frac{(I_0 + I_{180}) - (I_{90} + I_{270})}{(I_0 + I_{180}) + (I_{90} + I_{270})} \qquad \text{III.2}$$

$$\frac{U}{I} = \frac{1}{P_o} \frac{(I_{45} + I_{225}) - (I_{135} + I_{315})}{(I_{45} + I_{225}) + (I_{135} + I_{315})} \qquad \text{III.3}$$

The data have to be multiplied by the efficiency factor, $\frac{1}{P_o}$ which takes into account the fact that the polarimeter is not ideal. This is done for each filter and analyser by making a measurement of a star with an analyser of known efficiency in the beam above the

spinning analyser.

To obtain the fourth Stokes parameter V, the wave plate is inserted into the photometer and the above procedure is repeated for each of eight positions of the wave plate, (see next section).

Standard stars were observed to calibrate the polarimetry. Since the polarization is a ratio of intensities the photometry does not have to be absolute, therefore not many standard stars need to be observed, unless the photometry obtained at the same time is of value. The instrumental polarization at each wavelength is obtained by observation of supposedly unpolarized standard stars. The Stokes parameters for all the standards for a night are averaged and subtracted vectorially from the Stokes vectors of the programme objects. The calibration of the position angle of the polarization is obtained by observing an object of known polarization. The standard stars used are listed in Table III.2. The L magnitude has an effective wavelength of 3.45μm. To calibrate the 3.82μm photometry the L' magnitude of the standards was estimated by interpolation.

(2) Data Analysis

The analysis of polarization data has been described very well by Serkowski (1962). However, there are some small errors in some of his equations, therefore, the treatment will be given here briefly.

An attractive and simple way of treating the passage of polarized

Table III.2

Standard Stars Used to Calibrate the Photometry and Polarimetry

Star	RA (1975)	Dec. (1975)	V.	Spectral Type
α And	00 07 05.5	28 57 09	2.1	A0p
γ Peg	00 11 52.7	15 02 41	2.9	B2
χ' Ori	05 52 54.1	20 16 22	4.41	F8
β Vir	11 49 23.5	01 54 20	3.60	F8
η Vir	12 18 37.5	-00 31 41	3.90	A0
β CVn	12 32 33.5	41 29 35	4.3	G0
β Com	13 10 42.4	28 00 16	4.26	G0
α Boo	14 14 31.2	19 18 43	-0.05	K0
χ Her	15 51 48.6	42 31 15	4.62	G0
α Lyr	18 36 05.5	38 45 34	0.03	A0
111 Her	18 45 54.9	18 09 09	4.4	A3
α Aql	19 49 33.7	08 48 04	0.9	A5
β Aql	19 54 05.0	06 20 36	3.72	K0
VI Cyg No. 12	20 32 13	41 13 17	11.5	B8

light through an optical system can be given in terms of the Stokes vector (Stokes 1852) and Mueller matrix algebra (Mueller 1948). The polarization properties of a beam of light can be completely characterized by the four element Stokes column vector

$$S = \begin{bmatrix} I \\ Q \\ U \\ V \end{bmatrix}$$

The parameters are intensities, and the four parameters completely parameterise the polarization properties of the beam. I is the total intensity. The degree, p, and orientation, θ, of linear polarization are given by

$$p = [Q^2 + U^2]^{\frac{1}{2}}/I \ , \qquad \tan 2\theta = U/Q \qquad \text{III.4}$$

and the degree of circular polarization by

$$q = V/I \qquad \text{III.5}$$

Unpolarized light has $Q = U = V = 0$. A partially elliptically polarized beam has

$$I \geq Q + U + V, \qquad Q, U, V, \neq 0$$

The general polarization ellipse is illustrated in Figure III.3. The parameters of the ellipse are related to the Stokes parameters in the following way. If the components of the electric vector $\underset{\sim}{E}$ of the incident wave are given by

$$E_{\parallel} = E_{\parallel_o} \sin(\omega t - \varepsilon_{\parallel})$$

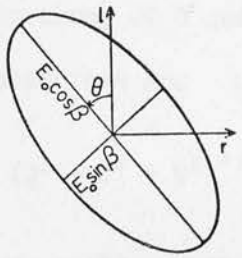

Figure III.3 The polarization ellipse which defines the parameters of a generally polarized beam. The l axis is parallel to the meridian and is directed north.

$$E_{\perp} = E_{\perp_o} \sin(\omega t - \varepsilon_{\perp})$$

parallel ($\|$) and perpendicular ($\perp$) to the plane of the meridian in the equatorial coordinate system, where ω is the angular frequency and $E_{\|_o}$, $E_{\perp_o}$, $\varepsilon_{\|}$ and $\varepsilon_{\perp}$ are constants, then the polarization ellipse is the outline of the $\underset{\sim}{E}$ vector in the plane of the sky, and the axes of the ellipse are given by $E_{\theta} = E_o \cos\beta \sin\omega t$, $E_{\theta+90} = E_o \sin\beta \cos\omega t$. $E_{\|_o}$ and $E_{\perp_o}$, and hence the intensities $I_{\|}$ and $I_{\perp}$, can then be found in terms of θ and β. The resulting equations for the Stokes parameters are

$$I = E_{\|_o}^2 + E_{\perp_o}^2 = (Q^2 + U^2 + V^2)^{1/2}$$

$$Q = E_{\|_o}^2 - E_{\perp_o}^2 = I \cos 2\beta \cos 2\theta$$

$$U = -2E_{\|_o} E_{\perp_o} \cos(\varepsilon_{\|} - \varepsilon_{\perp}) = I \cos 2\beta \sin 2\theta$$

$$V = 2E_{\|_o} E_{\perp_o} \sin(\varepsilon_{\|} - \varepsilon_{\perp}) = I \sin 2\beta$$

The sense of rotation of the polarization vector with increasing θ is determined by the sense of rotation of the analyser. The convention that θ increases counterclockwise from north on the sky is used here, because it is most commonly adopted in the literature. Both senses are actually used by different authors in the literature; in particular van de Hulst (1957) uses the opposite one to that adopted here.

The sense of circular polarization is defined to be $V > 0$ for right-handed circular polarization and $V < 0$ for left-handed polarization.

An optical element such as a polarizer or a waveplate can be represented by a 16 element Mueller matrix, M. Then the transfer of a polarized beam represented by vector S through the element described by M is given by the relation $S' = M S$. III.6

Consider the analysis of a linearly polarized beam. The analyser is not ideal. If k_1 and k_2 represent the principal transmittances for plane polarized light incident perpendicular and parallel respectively to the analyser axis, then the Mueller matrix for the analyser is given by (e.g. Shurcliff 1962).

$$N = \frac{1}{2}\begin{bmatrix} k_1 + k_2 & k_1 - k_2 & 0 & 0 \\ k_1 - k_2 & k_1 + k_2 & 0 & 0 \\ 0 & 0 & 2\sqrt{k_1 k_2} & 0 \\ 0 & 0 & 0 & 2\sqrt{k_1 k_2} \end{bmatrix} \qquad \text{III.7}$$

The axis of the analyser makes an arbitrary angle ϕ with the plane of polarization. If $R(\phi)$ is the rotation matrix then

$$\mathcal{S}' = R(-\phi)\, N(0)\, R(\phi)\, S \qquad \text{III.8}$$

or

$$S' = N(\phi)\, S \qquad \text{III.9}$$

$R(\phi)$ is given by

$$R(\phi) = \begin{bmatrix} 1 & 0 & 0 & 0 \\ 0 & C_{2\phi} & S_{2\phi} & 0 \\ 0 & -S_{2\phi} & C_{2\phi} & 0 \\ 0 & 0 & 0 & 1 \end{bmatrix} \qquad \text{III.10}$$

where we have used the convention

$$C^n_{k\alpha} = \cos^n k\alpha \qquad S^n_{k\alpha} = \sin^n k\alpha$$

then $N(\phi)$ =

$$1/2 \begin{bmatrix} k & \Delta k C_{2\phi} & \Delta k S_{2\phi} & 0 \\ \Delta k C_{2\phi} & k C_{2\phi}^2 + 2\sqrt{k_1 k_2} S_{2\phi}^2 & k C_{2\phi} S_{2\phi} - 2\sqrt{k_1 k_2} C_{2\phi} S_{2\phi} & 0 \\ \Delta k S_{2\phi} & k C_{2\phi} S_{2\phi} - 2\sqrt{k_1 k_2} C_{2\phi} S_{2\phi} & k S_{2\phi}^2 + 2\sqrt{k_1 k_2} C_{2\phi}^2 & 0 \\ 0 & 0 & 0 & 2\sqrt{k_1 k_2} \end{bmatrix}$$

where $k = k_1 + k_2$

$\Delta k = k_1 - k_2$ III.11

We are interested in the emergent intensity $I'(\phi)$.

Substituting III.11 into III.9 gives

$$I'(\phi) = \frac{1}{2}\{ (k_1 + k_2) I + (k_1 - k_2) \cos 2\phi\, Q + (k_1 - k_2) \sin 2\phi\, U \}$$

$$= \frac{1}{2} (k_1 + k_2) \{ I + P_o \cos 2\phi\, Q + P_o \sin 2\phi\, U \} \qquad \text{III.12}$$

where $P_o = \dfrac{k_1 - k_2}{k_1 + k_2}$,

Substitution of the position angles of the analyser for ϕ into equation III.12 shows that

$$\frac{Q}{I} = \frac{1}{P_o} \frac{I'(0^o) - I'(90^o)}{I'(0^o) + I'(90^o)}$$

and

$$\frac{U}{I} = \frac{1}{P_o} \frac{I'(45^o) - I'(135^o)}{I'(45^o) + I'(135^o)} \qquad \text{III.13}$$

Measuring the intensity at eight positions of the analyser instead of four, for better accuracy, results in equation III.2 and III.3. The position angle θ is then given by III.4.

This analysis can be easily extended to describe the measurement of circular polarization by including the matrix for a retarder in equation III.9. The matrix for a wave plate of retardence δ is given by

$$W(0,\delta) = \begin{bmatrix} 1 & 0 & 0 & 0 \\ 0 & 1 & 0 & 0 \\ 0 & 0 & C_\delta & S_\delta \\ 0 & 0 & -S_\delta & C_\delta \end{bmatrix}$$

Then for an arbitrary orientation of the wave plate $\times$

$$S' = R(-\phi)\, N(0)\, R(\phi)\, R(-\times)\, W(0,\delta)\, R(\times)\, S$$

or $$S' = T(\phi, \times, \delta)\, S \qquad \text{III.14}$$

The procedure of observation has been described above. For each angle $\times_i$ of the wave plate the intensity at the eight positions of the analyser is measured. We can therefore derive the quantities $A_{\times_i}$ and $B_{\times_i}$ in analogy to equation III.13.

$$A_{x_i} = \frac{I'_{x_i}(0) - I'_{x_i}(90) + I'_{x_i}(180) - I'_{x_i}(270)}{I'_{x_i}(0) + I'_{x_i}(90) + I'_{x_i}(180) + I'_{x_i}(270)}$$

III.15

$$B_{x_i} = \frac{I'_{x_i}(45) - I'_{x_i}(135) + I'_{x_i}(225) - I'_{x_i}(315)}{I'_{x_i}(45) + I'_{x_i}(135) + I'_{x_i}(225) + I'_{x_i}(315)}$$

Making the transformation $x_i = x + x_o$ and putting $x = 0\ (45)\ 315$, it can be shown that:

$$\frac{V}{I} = \frac{1}{4\ P_o\ S_\delta} \left[(-A_{o+x_o} + A_{90+x_o} - A_{180+x_o} + A_{270+x_o})^2\right] + \left[(-A_{45+x_o} + A_{135+x_o} - A_{225+x_o} + A_{315+x_o})^2\right]^{\frac{1}{2}} \qquad \text{III.16}$$

$$= \frac{1}{4\ P_o\ S_\delta} \left[(B_{o+x_o} - B_{90+x_o} + B_{180+x_o} - B_{270+x_o})^2\right] + \left[(-B_{45+x_o} + B_{135+x_o} - B_{225+x_o} + B_{315+x_o})^2\right]^{\frac{1}{2}}$$

δ is obtained from the linear polarimetry using

$$\sum_{x=o}^{315} A_{x+x_o} = 4P_o\ (1 + C_\delta)\ \frac{Q}{I}, \qquad \sum_{x=o}^{315} B_{x+x_o} = 4P_o\ (1 + C_\delta)\ \frac{U}{I}$$

The analysis described above deals with intensity measured at eight discrete positions of the analyser. However, the measurements were actually made over eight 45^o segments of a continuously rotating analyser. This results in only a small loss in efficiency compared to the time wasted in moving the analyser by step.

(3) Accuracy of the Techniques

The formal errors of a polarimetric observation follow the laws of photon statistics and are given by

$$\varepsilon_p = \left[\frac{U^2\varepsilon_U{}^2 + Q^2\varepsilon_Q{}^2}{p^2}\right]^{1/2}$$

$$\varepsilon_\theta = \frac{\varepsilon_p}{2p} \cdot 1 \text{ radian}$$

The accuracy of the polarization observations reported here, as measured by their repeatability, is poorer than indicated by these equations due to such effects as guiding errors, and systematic errors in determining the efficiency of the calibration analyser and the instrumental polarization. The errors quoted in Tables III.3-8 are therefore computed from the statistics of several independent measurements.

The instrumental polarization of the system can be quite large. Instrumental polarization can arise in any of the reflections encountered in the system (*i.e.* the primary mirror, the secondary mirror and the dichroic mirror), however the major instrumental polarization of the system probably arises in the non-homogenous analyser. As the analyser rotates the non-parallelism of the faces will cause the beam to sweep around on the small face of the infrared detector. Some of this effect can be reduced by using a Lyot depolarizer, and thereby ensuring that the light that falls on the detector is at least unpolarized. Operation of the system with the HR analyser and the depolarizer resulted in instrumental polarizations of the order of 0.4% at K.

The wire grids possess a much larger instrumental polarization, which varies over long periods of time. The exact nature of this polarization is unclear but observations of the amount of instrumental polarization in the 3 μm spectral region indicates that it may be a pseudo-polarization due to absorption of water by the substrate. The wavelength dependence of the instrumental polarization for one of the wire grids in the wavelength region is illustrated in Figure III.4. Since this polarization is due to variable extinction as the polarizer is rotated in the beam, it cannot be eliminated by the depolarizer, and must simply be measured accurately and subtracted vectorially from the observed polarization in the same way as normal instrumental polarization.

The performance of the system is illustrated in Figure III.5 which shows the 2.2 μm magnitude of an object being observed versus the accuracy of a polarization observation in percent obtainable in 80 seconds of integration at the 2.24-m telescope. These data were accumulated during 1977 and 1978 (Dyck 1979). The dashed line is the predicted performance of the system under detector noise limited operation, assuming a loss of about $1^{m}.5$ with the analyser in the beam. The observations of faint objects lie close to the theoretical limit. Brighter objects do not meet the limit due to "technique" noise, such as the finite speed of rotation of the analyser. Over the past year when the observations reported here were being obtained, the performance of the InSb detector was improved significantly, resulting in an increase of observing power of about one magnitude over that indicated in Figure III.5.

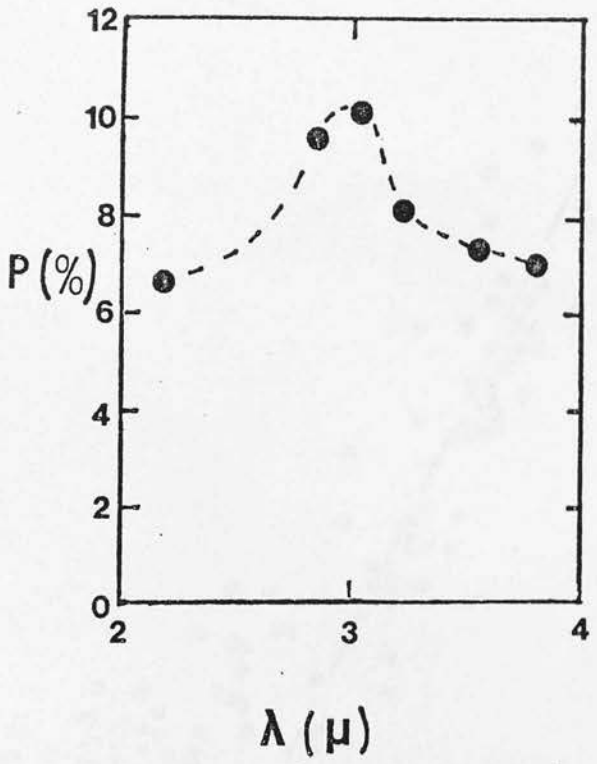

Figure III.4 Instrumental polarization of the BaFl #2 wire grid on the night of May 8, 1979 UT.

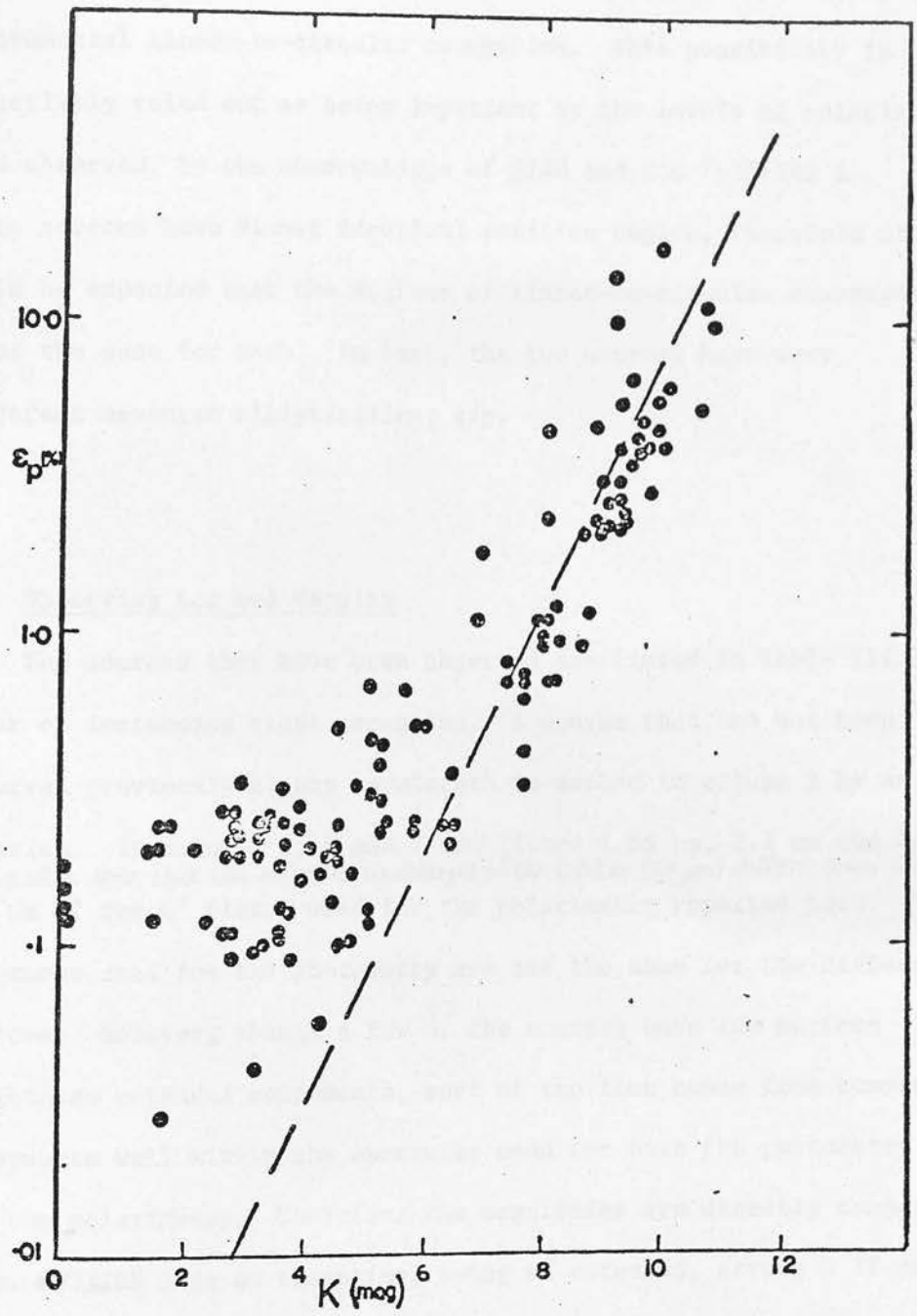

Figure III.5 Accuracy of a polarization observation for an integration of 80 seconds at the 2.24 m telescope.

The circular polarization observations could be affected by instrumental linear-to-circular conversion. This possibility is effectively ruled out as being important at the levels of polarization observed, by the observations of S140 and NGC 7538/IRS 1. These sources have almost identical position angles, therefore it would be expected that the degrees of linear-to-circular conversion to be the same for both. In fact, the two sources have very different measured ellipticities, q/p.

(4) Observing Log and Results

The sources that have been observed are listed in Table III.3 in order of increasing right ascension. A source that has not been observed previously at any wavelength is marked in column 1 by an asterisk. In columns 5, 6 and 7 are listed 1.65 μm, 2.2 μm and 3.5 μm magnitudes. Note that the effective wavelength of the L filter (3.5 μm) differs from the 3.8 μm of the L' filter used for the polarimetry reported here. The apertures used for the photometry are not the same for the different sources. However, though a few of the sources have low surface brightness extended components, most of the flux comes from compact components well within the apertures used for both the photometry and the polarimetry. Therefore the magnitudes are directly comparable. W3/IRS 1 is an exception, being an extended, strong H II region.

The broad band linear polarimetry, ice band circular variable filter (CVF) and narrow band (NB) polarimetry and photometry, and the circular polarimetry observations are described in Tables III.4, 5 and 6 respectively. Entries marked with an asterisk indicate that

Table III.3

The Sources Observed

Source	H	K	L'	Other Names
W3/IRS 1*	8.1	6.7	4.5	
W3/IRS 9*	10.7	8.9	6.8	
IC 1848 A/IRS 1*	9.0	7.0	5.5	GL 4029
GL 437 W*	10.8	9.8	8.1	
GL 437 N*	10.8	10.2	7.7	
GL 437 S*	10.8	9.4	7.2	
GL 490	7.8	5.2	3.1	U of A 1
S228*	>11.2	9.5	6.5	
OMC 1/IRS 1	9.6	5.1	2.1	BN
OMC 1/IRS 2	8.6	6.4	4.2	Hilgeman's Source
Mon R2/IRS 1*	10.9	8.6	6.6	Beckwith et al's (1976) terminology. Also known as VdB 67 and GL 877.
Mon R2/IRS 2	>12.3	7.9	3.7	
Mon R2/IRS 3	9.6	6.4	3.0	
ρ Oph No. 29	10.8	6.8	3.9	
GL 961*	-	7.4	4.4	Cohen's Source
W33 A	12.4	9.1	6.0	Kleinmann-Wright Source
M17/KW	-	6.8	4.4	
W51/IRS 2	9.8	7.5	4.0	
W40/IRS 1*	6.0	5.7	3.9	
W40/IRS 2*	7.1	5.7	4.5	
W40/IRS 3*	9.0	6.9	5.7	
S106	7.9	6.1	4.2	M1-19, GL 2584
GL 2591	9.0	5.3	1.7	U of A 27
S140	7.7	5.4	3.0	GL 2884
NGC 7538/IRS 1	-	8.0	4.1	
NGC 7538/IRS 4*	9.2	7.9	-	
NGC 7538/IRS 9	14.8	8.9	4.6	

Table III.4

Observing Log of Broad Band Polarimetry

Source	Date (UT)	Wavelength	Aperture	Instrumentation
GL 2591	15/9/78	1.65*,2.2*,3,8,4.8 μm	3 mm	BaF1 #1, Sp, 1800
IC 1848 A/IRS 1	15/9/78	2.2 μm	3 mm	BaF1 #1, Sp, 1800
GL 437 N	15&16/9/78	2.2 μm	3 mm	BaF1 #1, Sp, 1800
GL 437 S	15&16/9/78	2.2 μm	3 mm	BaF1 #1, Sp, 1800
GL 437 W	15&16/9/78	2.2 μm	3 mm	BaF1 #1, Sp. 1800
NGC 7538/IRS 9	15&16/9/78	2.2*μm	3 mm	BaF1 #1, Sp. 1800
W3/IRS 1	23/12/78	2.2 μm	3 mm	BaF1 #1, Sp, LSI 11
W3/IRS 9	23/12/78	2.2 μm	3 mm	BaF1 #1, Sp, LSI 11
S228	23/12/78	2.2 μm	3 mm	BaF1 #1, Sp, LSI 11
Mon R2/IRS 1	23/12/78	2.2 μm	3 mm	BaF1 #1, Sp, LSI 11
Mon R2/IRS 2	23/12/78	2.2*μm	3 mm	BaF1 #1, Sp, LSI 11
GL 961	19/1/79	2.2 μm	3 mm	BaF1 #1, Sp, LSI 11
W40/IRS 1	6/5/79	2.2 μm	3 mm	HR + Lyot, St
W40/IRS 2	6/5/79	2.2 μm	3 mm	HR + Lyot, St
W40/IRS 3	6/5/79	2.2 μm	3 mm	HR + Lyot, St
W51/IRS 2	6&7/5/79	2.2*μm	3 mm	HR + Lyot, St
ρ Oph No. 29	7/5/79	2.2*μm	3 mm	HR + Lyot, St
W33 A	8/5/79	2.2,3.8*μm	3 mm	BaF1 #2, St
M17/KW	10/5/79	3.8 μm	3 mm	BaF1 #2, St
GL 2591	10/5/79	3.8 μm	3 mm	BaF1 #2, St
GL 2591	13/6/79	3.8 μm	4 mm	BaF1 #2, Sp, LSI 11
GL 2591	14/6/79	3.8 μm	4 mm	BaF1 #2, Sp, LSI 11

Note: See text for explanation of instrumentation.

Table III.5

Observing Log of Ice Band Polarimetry and Photometry

Source	Date (UT)	Standard	Wavelength	Aperture	Polarimetry	Photometry
GL 2591	13&14/9/78	β Peg, α Lyr	CVF: 2.90-3.49 μm	3 mm	✓	✓
S140	14/9/78	α Lyr	CVF: 2.90-3.49 μm	3 mm	X	✓
Mon R2/IRS 2	18&19/1/79	β Vir	NB: 2.86-3.56 μm	4 mm	3.25, 3.56 μm	✓
Mon R2/IRS 3	18/1/79	χ' Ori	NB: 2.86-3.5 μm	4 mm	X	✓
W33 A	8/5/79	β Vir	NB: 3.56 μm*	3 mm	✓	✓
GL 2591	10/5/79	β Vir	NB: 3.25, 3.56 μm	3 mm	✓	✓
GL 2591	14/6/79	α Boo	NB: 2.86-3.56 μm	4 mm	✓	✓

Table III.6

Observing Log of Circular Polarimetry

Source	Date (UT)	Wavelength	Aperture
GL 2591	31/8/79	2.2 μm*	4 mm
S140	31/8/79	2.2 μm*	4 mm
OMC 1/IRS 1	31/8/79	2.2 μm	4 mm
V1 Cyg No. 12	1/9/79	2.2 μm	4 mm
NGC 7538/IRS 1	1,2&3/9/79	2.2 μm	4 mm
NGC 7538/IRS 4	1&2/9/79	2.2 μm	4 mm
OMC 1/IRS 2	2&3/9/79	2.2 μm	4 mm
GL 490	3/9/79	2.2 μm	4 mm
S106	3/9/79	2.2 μm*	4 mm

the source has been observed previously at these wavelengths. The plate scale of the 2.24-m telescope is 2.5 arcsec/mm so that a 3-mm aperture corresponds to about 8 arcseconds, and a 4-mm one to about 10 arcseconds. The fifth column of Table III.4 indicates the instrumentation used on each night. Which of the three analysers was used is first noted. Sp indicates that the analyser was used in spinning mode, and St that it was used in step mode (as explained in Section (1)). The use of the IBM 1800 or LSI 11 computers is also indicated. The instrumentation for the ice band observations is the same as for the broad band observations for September, May and June respectively. In January 1978 the BaFl No. 1 wire grid was used in spinning mode with the LSI 11 computer. For the circular polarimetry the HR polaroid was used with the Lyot depolarizer, the 2.2 μm quarter wave plate and the LSI 11.

The results of the observations are illustrated in Figures III.6 and 7 or are listed in Tables III.7 and 8. The broad band polarization for all the sources observed except GL 2591 are given in Table III.7. The broad band and ice band polarimetry of GL 2591 and Mon R2/IRS 2 is plotted in Figure III.6. For those sources which have been observed previously the new data agrees well with earlier data except in the case of ρ Oph No. 29. This source has been observed on several different occasions (Dyck 1979) and appears to vary. The observations of GL 961, W40 and M17/KW are non-detections, therefore θ is undefined.

The ice band photometry excluding that of W33 A is illustrated

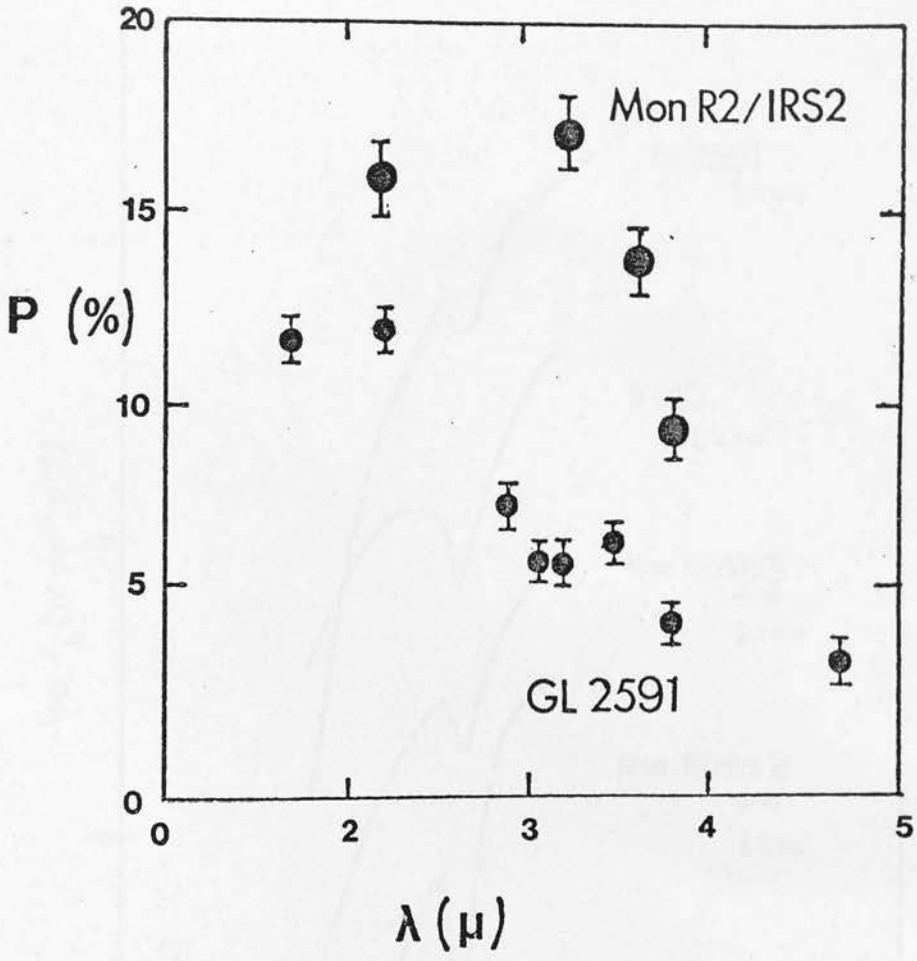

Figure III.6 Narrow-band polarization observations of Mon R2/IRS 2 and GL 2591. The CVF data for GL 2591 has been incorporated.

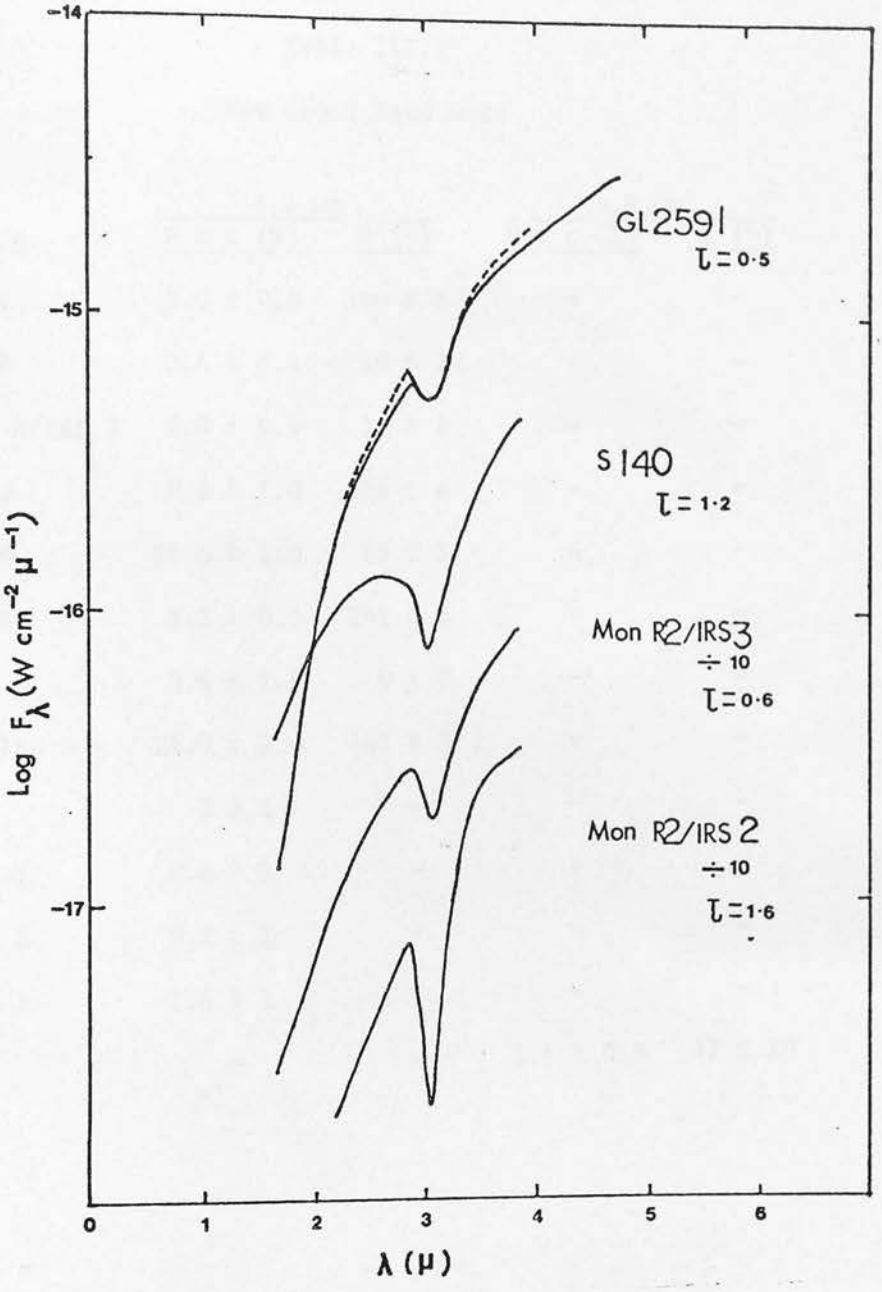

Figure III.7 Ice band photometry.

Table III.7

New Broad Band Data

Source	2.2 μm		3.8 μm	
	P ± ε (%)	θ (°)	P ± ε (%)	θ (°)
W3/IRS 1	5.0 ± 0.6	140 ± 3	-	-
W3/IRS 9	2.4 ± 0.6	90 ± 7	-	-
IC 1848 A/IRS 1	2.9 ± 0.4	11 ± 4	-	-
GL 437 W	8.0 ± 1.0	104 ± 4	-	-
GL 437 N	24.0 ± 1.0	89 ± 1	-	-
GL 437 S	3.2 ± 0.5	141 ± 4	-	-
S228	5.6 ± 1.8	6 ± 9	-	-
Mon R2/IRS 1	22.0 ± 2.0	161 ± 3	-	-
GL 961	2 ± 1	-	-	-
W40/IRS 1	0.4 ± 1	-	-	-
W40/IRS 2	0.2 ± 1	-	-	-
W40/IRS 3	1.8 ± 1	-	-	-
M17/IRS	-	-	1.4 ± 0.9	47 ± 18

in Figure III.7. This photometry is new, except in the case of GL 2591 which has been observed previously by Merrill et al (1976). Their spectrum is shown for comparison. The two spectra are very similar. The optical depths, τ_{ice}, in the bands as measured assuming a flat continuum are given in Figure III.7. Both the photometry and and polarimetry of W33 A agree well with that of Capps et al (1978), and no new information was obtained.

Finally the circular polarimetry is listed in Table III.8. The observations of VI Cygni No. 12, S106 and NGC 7538/IRS 1 and 4 are upper limits. VI Cygni No. 12 has a high interstellar infrared polarization (P_K = 1.22 ± 0.12%), and was observed to check that the technique was not giving rise to systematic instrumental circular polarizations, insufficiently corrected for in the data analysis. The upper limit to the ellipticity, e = q/p, of VI Cygni No. 12 is 4% at 2.2 μm; smaller than the values found in the molecular cloud sources.

Table III.8

Circular Polarization Data

Source	$q \pm \varepsilon$ (%)
GL 490	-0.43 ± 0.06
OMC 1/IRS 1	1.56 ± 0.18
OMC 1/IRS 2	0.66 ± 0.15
S106	0.20 ± 0.07
S140	-0.99 ± 0.23
GL 2591	-0.76 ± 0.20
NGC 7538/IRS 1	-0.20 ± 0.20
NGC 7538/IRS 4	-0.40 ± 0.30
VI Cyg No. 12	0.05 ± 0.03

CHAPTER IV

CIRCULAR POLARIMETRY

The observation of circular polarization in BN (Serkowski and Rieke 1973) has been confirmed, and of the seven new sources observed for circular polarization four have been found to possess ellipticities of a similar magnitude to BN. It has therefore been shown that BN is not an exception in being circularly polarized in the near infrared, and that the high degree of ellipticity observed in it is not unique.

(1) The Data.

The measurements listed in Table III.8 are the first infrared circular polarization data of any astronomical source to be published, besides the 3.45 μm observation of BN reported by Serkowski and Rieke (1973). The brightest, most highly linearly polarized sources from the linear polarization survey (Dyck and Capps 1978, Dyck 1978, and this work Chapter VI) were chosen for observation because they represent the most likely candidates for circular polarization (equation II.2). This unfortunately means that there is a large selection effect involved with the sample, however, current instrumentation available limits the selection severely. The total number of sources for which infrared circular polarimetry is possible is not much larger than the sample presented here. This assertion is verified as follows.

Ellipticities measured in astronomical sources at optical and ultraviolet wavelengths are lower than the values found here for the

protostellar sources, therefore a generous upper limit for any sources would be $e \lesssim 10\%$. For typical linear polarizations of the molecular cloud sources $p \simeq 10\%$, this means that to measure circular polarization to an accuracy of 10% requires the equivalent of 0.1% photometry, or a loss of observing power of 5 magnitudes compared to a photometric measurement of 10% accuracy. The University of Hawaii InSb detector is capable of a measurement of a source with a 2.2 μm magnitude of 14.1 to 10% accuracy in 240 seconds of integration (Becklin 1978), therefore, for an ideal system one would expect to be able to observe a 9th magnitude object with 10% linear polarization to an accuracy of 10% in circular polarization in 240 seconds. In fact, as described in Chapter III, the transmission and instrumental polarization of the polarimeter further reduce this figure. Figure III.5 shows that the linear system is typically capable of a 10% measurement of linear polarization of a 10th magnitude object in 80 seconds, which is equivalent to a circular polarization measurement of a $7^m.5$ object to the same accuracy in 240 seconds. Comparison with the value of $9^m.0$ derived above shows that about $1^m.5$ is lost due to inefficiencies of the polarimeter. A further loss may be expected due to the introduction of the rotating waveplate into the system. The accuracy can, of course, be increased by lengthening the observing time. These last two factors tend to balance each other so that an effective limiting magnitude for circular infrared polarimetry is about $8^m.0$ at 2.2 μm for a linear polarization of 10%. In spite of these limitations, 2.2 μm is the optimum wavelength for these observations because while at shorter wavelengths the degree of polarization is higher, there is less total

flux. At longer wavelengths the sources may be brighter but the degree of polarization has dropped. (See Figure II.2.)

The magnitudes of the programme sources are listed in Table III.3. The effect of the limiting magnitude is illustrated by NGC 7538/IRS 1 for which only a 2σ upper limit to the circular polarization could be obtained in an observing time of 1120 seconds, in spite of the fact that the linear polarization is high. S106 is relatively bright, but shows less than 3% linear polarization which also makes detection of a circular component hard. The characteristics of all the molecular cloud sources which have now been observed for linear polarization are listed in Tables VI.1 and VI.2. Of these, all, except GL 989, for which the combination of the observed flux and linear polarization are such that it is reasonable to expect detection of circular polarization according to the limitations of the system described above, have been observed on the programme.[1] Seven other sources are borderline cases, in the sense that if the ellipticities were high it may be possible to detect circular polarization with long enough integration times. These sources are W3/IRS 1, OMC 2/IRS 3, Mon R2/IRS 1, 2 and 3, ρ Oph No. 29 and M17/KW.

Dyck and Capps (1978, unpublished) have previously made

[1] The criterion used is the following. If the ellipticity were 10% then the observed degree of circular polarization would be $q = p/10$, for known p (%). The largest magnitude for which it would be feasible to detect q is then given by $K = 14 - [2.5 \log(1000/p) + 1]$.

observations at 2.2 μm of three of the sources listed in Table III.8, as noted in Table III.6. They also observed Galactic Centre source No. 7 and W33 A. The analysis of their data was not completed, therefore it is included here with their permission. A paper reporting the observations and some of the analysis presented here is in preparation for publication in the Astrophysical Journal in 1980 (Lonsdale, Dyck, Capps and Wolstencroft 1980). Table IV.1 lists the complete set of 2.2 μm circular polarization data. Also listed are linear polarizations p, and ellipticities e. Comparison with Table III.8 shows clearly that the 1978 data for GL 2591, S140 and S106 agree very closely with the 1979 data. The circular polarization of GC No. 7 and W33 A was not determined. In spite of the additional data the polarization of S106 also remains undetermined.

The circular polarization is plotted against linear polarization in Figure IV.1. It is not possible to determine whether a relationship exists between the two quantities from this data. Note that an obvious correlation does not exist between θ and the sign of q. This is not inconsistent with an IS model because it depends on the sense of rotation of the grain alignment.

Having shown that high circular polarizations exist in other protostars beside BN, an attempt is now made to establish a model to account for the data. As concluded in Chapter II, linear dichroism and birefringence of the molecular cloud medium is a promising mechanism.

Table IV.1

2.2 μm Circular and Linear Polarization Data

Source	$P \pm \varepsilon$ (%)	θ (°)	$q \pm \varepsilon$ (%)	$e \pm \varepsilon$ (%)
GL 490	7.2 ± 0.1	103	-0.43 ± 0.06	6 ± 1
OMC 1/IRS 1 (BN)	18.4 ± 0.6	115	1.56 ± 0.18	8 ± 1
OMC 1/IRS 2	10.8 ± 1.0	136	0.66 ± 0.15	6 ± 1
W33 A	15.4 ± 0.6	68	-1.4 ± 0.7	<9*
GL 2591	12.0 ± 0.4	171	-0.85 ± 0.08	7 ± 1
S106	2.3 ± 0.6	47	-0.1 ± 0.1	<9*
S140/IRS 1	13.7 ± 0.5	70	-0.93 ± 0.12	7 ± 1
NGC 7538/IRS 1	10.5 ± 0.8	69	-0.2 ± 0.2	<4*
NGC 7538/IRS 4	6.2 ± 0.4	68	-0.4 ± 0.3	<10*

*These are 2σ upper limits to e.

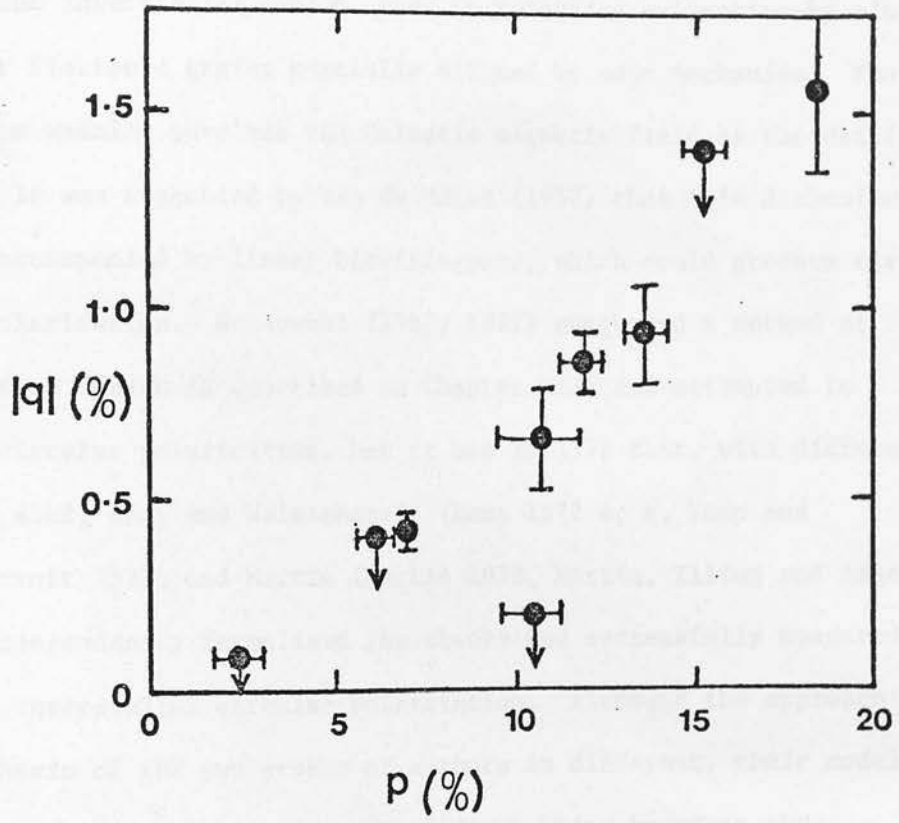

Figure IV.1 Observed linear and circular polarization at 2.2 μm.

(2) The Theory of Interstellar Circular Polarization.

The theory of interstellar linear polarization has been outlined in Chapter II: it is believed to be produced by linear dichroism of the interstellar medium, that is selective extinction by elongated or flattened grains partially aligned by some mechanism. The mechanism usually involves the Galactic magnetic field as the driving force. It was suggested by van de Hulst (1957) that this dichroism may be accompanied by linear birefringence, which could produce circular polarization. Serkowski (1962, 1971) suggested a method of observation (which is described in Chapter III) and attempted to detect circular polarization, but it was in 1972 that, with different aims in mind, Kemp and Wolstencroft (Kemp 1972 a, b, Kemp and Wolstencroft 1972) and Martin (Martin 1972, Martin, Illing and Angel 1972) independently formalised the theory and successfully measured optical interstellar circular polarization. Although the approach and emphasis of the two groups of authors is different, their models for the circular polarization are similar, being based on the suggestion of van de Hulst. The theory is described here.

The interstellar medium can be thought of as an "optical element" characterised by a complex refractive index $\tilde{m} = \tilde{n}' - i\tilde{n}''$. In an analogous way to the analysis of polarized light in Chapter III, the problem of interstellar polarization can then be treated as the passage of light characterised by the Stokes vector through this "optical element" using Mueller matrix algebra. Assuming initially unpolarized light it is desirable to model the observed Stokes vector, using the Mueller matrix which describes the interstellar medium, to derive the equation of transfer for the Stokes parameters.

Following van de Hulst (p. 33) the refractive index of the medium is denoted by $\tilde{m}$ to differentiate from the index of the grains themselves, m. Because the number density of grains is very small, $\tilde{m}$ is close to one.

An arbitrary optical element with polarization properties may possess any combination of the properties linear dichroism and birefringence, and circular dichroism and birefringence, in which case $\tilde{m}$ becomes a four element matrix $\tilde{M}$ instead of a scalar. Linear dichroism and birefringence have been defined in Chapter II. Circular dichroism and birefringence are defined analogously, i.e. different extinction (dichroism) and different phase velocities (birefringence) for circularly polarized light of opposite handedness. The linear effects are usually found together, as are the circular ones, though this is not always so.

The theory of extinction in a medium containing many scattering particles, such as the dust grains in the interstellar medium, leads to an expression for the refractive index of the medium in terms of the complex forward scattering amplitude function of the particles, S(0), and the number density of particles N

$$\tilde{M} = 1 - i\, S(0) \cdot 2\pi N k^{-3} \qquad \text{IV.1}$$

where k is the wave number, $k = 2\pi/\lambda$ (van de Hulst 1957).

In the interstellar medium circular dichroism and birefringence

can be neglected, therefore the matrix $\tilde{M}$ never has the full complement of four elements. There remain, therefore, two elements, which refer to two perpendicular directions in the medium, l and r[1], parallel and perpendicular to the major axis of the aligned grains. The dichroism[2] is related to the difference in the imaginary parts, $\tilde{n}_l'' - \tilde{n}_r''$, of the two indices, which describes an extinction. The expectation of accompanying birefringence[2] follows analogously from the possibility of the existence of a difference in the real parts, $\tilde{n}_l' - \tilde{n}_r'$, which would describe a phase lag.

From equation IV.1 it follows that the real and imaginary parts of $\tilde{m} = \tilde{n}' - i\tilde{n}''$ are related to those of S(0) by

$$\tilde{n}'_{l,r} - 1 = \mathrm{Im}[S_{l,r}(0)] \cdot 2\pi N k^{-3}$$

$$\tilde{n}''_{l,r} = \mathrm{Re}[S_{l,r}(0)] \cdot 2\pi N k^{-3} \qquad \text{IV.2}$$

Therefore, to find the dichroism and birefringence of the interstellar medium the amplitude functions of the particles must be determined. Equation IV.2 is the link between the treatment of the medium as a "macroscopic" element and the "microscopic" properties of the dust grains. The elements of the 16 element transfer matrix are found from linear combinations of sums, differences and products of the elements (and their complex conjugates) of the

1 For parallel and perpendicular.

2 The word "linear" is hereafter dropped because circular dichroism and birefringence are not dealt with.

4 element matrix which describes the transfer of the two components of the electric field of the incident wave,

$$\begin{bmatrix} E_l \\ E_r \end{bmatrix} = \begin{bmatrix} 1 - qS_r(0) & 0 \\ 0 & 1 - qS_l(0) \end{bmatrix} \begin{bmatrix} E_{lo} \\ E_{ro} \end{bmatrix} \qquad \text{IV.3}$$

where $q = 2\pi N l k^{-2}$ and l is the thickness of the medium (van de Hulst p. 34). The sixteen element matrix can either be written directly in terms of the properties of the dust grains, or in terms of $\tilde{m}_{l,r}$ using equation IV.2. Martin (1974) defined the quantities $\sigma_{l,r}$ and $\varepsilon_{l,r}$ such that

$$\tilde{m}_{l,r} = 1 + (\varepsilon_{l,r} - i\sigma_{l,r}) \frac{\lambda}{2\pi}$$

to describe the extinction and phase change per unit path length dl respectively. It is preferable to use the cross-sections Cext,[1] defined in Chapter II, and Cp, defined analogously, to avoid confusion. Recall that the optical depth is given by

$$\tau_{l,r} = N l C e_{l,r}$$

Also, $\tau_{l,r}$ is defined as

$$\tau_{l,r} = \frac{4\pi}{\lambda} l \tilde{n}''_{l,r}$$

1 Not to be confused with the abbreviation $C^n_{k\alpha} = \cos^n k\alpha$. Cext is replaced by Ce for convenience.

by anology a cross-section for phase lag can be defined

$$Cp_{l,r} = \frac{4\pi}{N\lambda} (\tilde{n}'_{l,r} - 1)$$

Thus, neglecting terms in dl^2, we have the transfer matrix

$$F = \frac{N}{2} dl \begin{bmatrix} (2/Ndl)-\delta & \Delta Ce & 0 & 0 \\ \Delta Ce & (2/Ndl)-\delta & 0 & 0 \\ 0 & 0 & (2/Ndl)-\delta & -\Delta Cp \\ 0 & 0 & \Delta Cp & (2/Ndl)-\delta \end{bmatrix}$$

where $\delta = Ce_l + Ce_r$, $\Delta Ce = Ce_l - Ce_r$, $\Delta Cp = Cp_l - Cp_r$. If S is the Stokes vector, the transfer through an element of the medium of thickness dl is given by

$$S' = FS$$

To integrate along the line-of-sight, let

$$\frac{dS}{dl} = \frac{S' - S}{dl}$$

Then writing $F = I + dlF'$ where I is the identity matrix, it follows that

$$\frac{dS}{dl} = F'S$$

F' is given by

$$F' = \frac{N}{2}\begin{bmatrix} -\delta & \Delta Ce & 0 & 0 \\ \Delta Ce & -\delta & 0 & 0 \\ 0 & 0 & -\delta & -\Delta Cp \\ 0 & 0 & \Delta Cp & -\delta \end{bmatrix}$$

So far the analysis has been carried out in a coordinate system fixed to the grain. To transform to a more general coordinate system in the plane of the sky as illustrated in Figure IV.2 the rotation matrix $R(\psi)$ is used, in the same way as in Chapter III, to give

$$\frac{dS(\psi)}{dl} = R(-\psi)F'R(\psi)S$$

i.e.

$$\frac{dS(\psi)}{dl} = \frac{N}{2}\begin{bmatrix} -\delta & \Delta Ce\cos 2\psi & \Delta Ce\cos 2\psi & 0 \\ \Delta Ce\cos 2\psi & -\delta & 0 & \Delta Cp\sin 2\psi \\ \Delta Ce\sin 2\psi & 0 & -\delta & -\Delta Cp\cos 2\psi \\ 0 & -\Delta Cp\sin 2\psi & \Delta Cp\cos 2\psi & -\delta \end{bmatrix} \qquad \text{IV.4}$$

The quantities that are measured by the procedure described in Chapter III are I, Q/I, U/I and V/I rather than I,Q,U,V therefore we require to calculate $\frac{d(S/I)}{dl}$ [1]

$$\frac{d(S/I)}{dl} = I^{-1}\frac{dS}{dl} - \frac{S}{I}I^{-1}\frac{dI}{dl}$$

[1] We replace $S(\psi)$ by S for convenience.

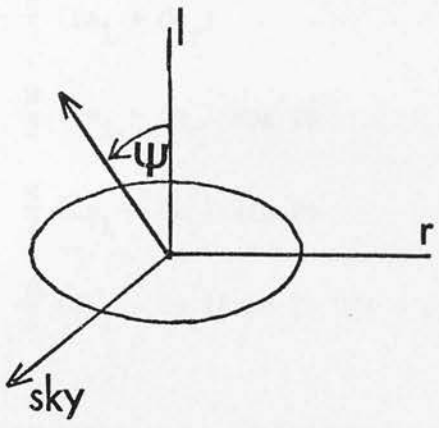

Figure VI.2 The rotation through the angle ψ from the grain coordinate system to a system in the plane of the sky, illustrated for a prolate grain.

therefore from IV.4 we have (assuming $(Q/I)^2$, $(U/I)^2$, $(Q/I)(U/I)$, (V/I) are all small)

$$
\begin{aligned}
I^{-1}\, dI/dl &= -\frac{N}{2}\,(Ce_l + Ce_r) \\
d(Q/I)/dl &= \frac{N}{2}\,(Ce_l - Ce_r)\cos 2\psi \\
d(U/I)/dl &= \frac{N}{2}\,(Ce_l - Ce_r)\sin 2\psi \\
d(V/I)/dl &= \frac{N}{2}\,(Cp_l - Cp_r)[\cos 2\psi\ U/I - \sin 2\psi\ Q/I]
\end{aligned}
\qquad \text{IV.5}
$$

These are the transfer equations. It is immediately obvious that circular polarization only results if linear polarization is incident upon birefringent grains at some angle ψ other than 0° or 90° to their major axes. In other words, assuming that the flux from the source is intrinsically unpolarized, there must be some variation in the direction of grain alignment along the line-of-sight.

A model with a continuous twist $\phi = K1$ in the grain alignment is adopted as being more physically reasonable for a molecular cloud than a multiple slab model, and equations IV.5 are integrated. The linear polarization is given by

$$Q/I = \frac{1}{2}\,N1\,\Delta Ce\,\sin 2\phi/\phi$$

$$U/I = \frac{1}{2}\,N1\,\Delta Ce\,\sin^2\phi/\phi$$

$$p = [(Q/I)^2 + (U/I)^2]^{1/2} = \frac{1}{2}\,N1\,\Delta Ce\,\sin\phi/\phi \qquad \text{IV.6}$$

$$\theta = \frac{1}{2}\tan^{-1}(U/Q) = \phi/2 \qquad \text{IV.7}$$

As expected, the linear polarization is given by the dichroism represented by the difference in extinction cross-section for the perpendicular axes of a single grain, multiplied by the column density of grains, N1.

The circular polarization is then

$$V/I = -\frac{1}{4} N^2 l^2 \Delta Ce \Delta Cp \left[\frac{2\phi - \sin 2\phi}{(2\phi)^2}\right] \qquad \text{IV.8}$$

Thus the wavelength dependence of q = V/I follows that of the product of the dichroism and the birefringence. This form for q is not very illustrative, since the column density is generally unknown. Therefore, on an arbitrary scale, the birefringence accompanying a given amount of dichroism is calculated. This is equivalent to calculating the amount of circular polarization expected to accompany the linear polarization for a given twist ϕ, as desired. To eliminate N1 from equation IV.6 note that as $K \to 0$, $Q/I \to \frac{1}{2} N1\Delta Ce$, which may be called p_o, the polarization that would be observed if there were no twist.[1] Then

$$p = p_o \sin \phi/\phi \qquad \text{IV.9}$$

and

1 Note that $U/I \to 0$ as $K \to 0$ so that if there is no twist all the polarization is in the Q parameter, as expected from the definition of the coordinate system in Figure IV.2.

$$V/I = -\frac{\Delta Cp}{\Delta Ce} p^2 \left[\frac{2\phi - \sin 2\phi}{4 \sin^2\phi}\right] \qquad \text{IV.10}$$

$(2\phi - \sin 2\phi)/(4 \sin^2\phi)$ is the quantity G in equation II.2.

(3) The Models.

Equation IV.10 forms the basis of the models for the circular polarization. It has been pointed out in Chapter II that at optical wavelengths $\Delta Cp/\Delta Ce \lesssim 1$, therefore, unless ϕ becomes unrealistically large ellipticities of the same size as measured at 3.45 μm in BN (9%) cannot be accounted for. However, there is an indication in Figure II.4 that $\Delta Cp/\Delta Ce$ may be larger than 1 in the infrared. The models described here involve calculations of this ratio for a variety of grain sizes, shapes and compositions, using Rayleigh theory and wavelength dependent optical constants, in an attempt to match the observed ellipticities.

The models are based upon the linear polarization model of BN of Dyck and Beichman (1974) which is described in Chapter II. This model assumes prolate ice and silicate grains of constant size in a picket-fence alignment (static alignment with long axes perpendicular to the line-of-sight). The computer code used by DB was rewritten to include calculation of the phase-lag cross-sections, $Cp_{l,r}$. It was also generalised to allow mixtures of up to four different grain species with different shapes and sizes. It is shown below that the assumption of constant grain size, instead of a more realistic size distribution, has no effect in the Rayleigh domain, unless a shape distribution is also used. The picket-fence alignment (PF) was used initially in order to optimise the ratio $\Delta Cp/\Delta Ce$ to determine whether

a fit to the ellipticities was feasible with this kind of model. It was later generalised to a more realistic Davis-Greenstein alignment (DG). In DG alignment the grains spin about their short axes at some oblique angle to the line-of-sight. The University of Hawaii Institute for Astronomy IBM 1130 was used to calculate the models.

A best fit to the linear polarization is first found, because, since the circular polarization is produced by a conversion of some of the linear, there is no point in a model for the circular which is not a good fit to the linear also. A depolarization will occur in the linear polarization due to the twist in the grain alignment. The magnitude of the depolarization is given by $\sin \phi/\phi$ (equation IV.9), which is a weak function of ϕ for $0 < \phi < \pi/2$, and unity for small ϕ.

The best silicate-ice model of DB provides a reasonable fit to p between 3 μm and 12 μm but is inadequate at 2.2 μm (Figure II.3). The fit at 2.2 μm can be improved by increasing the alignment or the axial ratio, but this has the effect of worsening the fit at the other wavelengths, by making p too large. DB used optical constants for lunar silicates (Perry et al 1972), extrapolating to wavelengths shorter than 6 μm where the data of Perry et al stop. This procedure is not very accurate; however terrestrial silicates have much lower continuum imaginary refractive indices n" than the lunar silicates, therefore they produce much lower polarization, even, than the moon-rocks. Increasing the amount of ice, even if it were not constrained by the optical depth of the ice feature, only increases p (2.2 μm) marginally. Also, ice is observed to have no effect on near infrared

extinction (Harris et al 1978). Therefore a third grain component with a high continuous opacity is a possible way to improve the fit to the short wavelength polarization. Recall (Chapter II) that the existence of such a component is also desirable to fit optical interstellar extinction and polarization and near infrared extinction (Mathis et al 1977, Mathis 1979, Kunkle 1979). Graphite was chosen as the additional grain component because these authors were able to obtain good fits using it. Oblate grains were used because it is normally assumed that graphite particles exist as flakes. This assumption is not critical.

The relationship used by Dyck and Beichman for the optical thickness in two perpendicular directions, as illustrated for a prolate grain in Figure IV.2 is given by

$$\tau_{x,y} = [NaQ_{l,r} + \frac{1}{2}(Q_{l,r} + Q_{r,l})Nu]\sigma l$$

$$= \frac{1}{2}[(1 + f)Q_{l,r} + (1 - f)Q_{r,l}]\sigma Nl \qquad \text{IV.11}$$

where Na, Nu are the number of totally aligned and randomly aligned particles respectively, N = Na + Nu, f = Na/N is the fractional alignment, l is the path length in the medium, $Q_{l,r}$ are the extinction efficiencies parallel and perpendicular to the grain size of symmetry and σ is the effective geometrical cross-section of the grain, such that $C_{l,r} = \sigma Q_{l,r}$. The polarization is given by

$$p = \frac{e^{-\tau x} - e^{-\tau y}}{e^{-\tau x} + e^{-\tau y}} \qquad \text{IV.12}$$

These equations reduce exactly to equations IV.6 as follows. Writing $\tau = \frac{1}{2}(\tau_x + \tau_y)$, $\Delta\tau = \tau_x - \tau_y$ it can be seen that $\tau = \frac{1}{2}(Qe_l + Qe_r)\sigma N l$ and the polarization is given by

$$p = \tanh(\Delta\tau/2) \simeq \frac{\Delta\tau}{2}$$

for $p <$ about 20%. Therefore,

$$p = \frac{1}{2} f(Qe_l - Qe_r)\sigma N l \qquad \text{IV.13}$$

This is equivalent to equation IV.6 with $f = 1$ for $\phi \to 0$. The exact solution IV.12 is in fact used in the calculations.

The calculation is normalised to a standard optical depth at 10 μm. DB used $\tau_{10\ \mu m} = 1.3$; however current opinion favours a value of $\tau_{10\ \mu m} = 3.3$ (Chapter II) therefore this value is adopted. f can then be reduced from 0.25 to 0.10. The mass column density of silicate grains is fixed by this procedure, independently of grain size, to 1.4×10^{-3} gm cm^{-2}. This value is slightly higher than that found by Gillett et al (1975b) (Chapter II) because lunar silicates have a weaker 9.7 μm bandstrength than terrestrial ones (Zaikowski and Knacke 1975).

The amount of the other grain materials is then specified by mass relative to silicate. Initially the mass ratio adopted was the DB ice to silicate ratio, and the Kunkle (1979) silicate to graphite ratio. Thus $A_{ice} : A_{silicate} : A_{graphite} = 0.10 : 0.62 : 0.29$.

These values are consistent with mass column densities estimated by other authors and with cosmic abundancies.

The programme calls on a subroutine for each grain material to obtain the optical constants at each wavelength. The ice data is taken from Irvine and Pollack (1968) and the graphite from Bergeat et al (1976). The programme then calls on a subroutine which uses Rayleigh theory to calculate absorption and scattering efficiencies for the two axes of each grain species. Then $\tau_{l,r}$, and hence p are calculated as a function of wavelength, using the normalised mass ratios A_i.

$$Ce_{l,r}(\lambda) = \sum_i \sigma_i A_i (Qe_{l,r})_i$$

$$\tau_{l,r}(\lambda) = \tau_{l,r}(\lambda_{STD}) \frac{Ce_{l,r}(\lambda)}{Ce_{l,r}(\lambda_{STD})} A_{STD} \qquad \text{IV.14}$$

$$\tau_{x,y}(\lambda) = \frac{1}{2}[(1 + f)\tau_{l,r} + (1 - f)\tau_{r,l}]$$

Also calculated is the albedo, and the spectrum assuming a temperature for the underlying source and a black body subroutine.

Given the linear polarization, the circular polarization is found as follows. The subroutine Rayleigh spheroid was adapted to calculate the phase lag efficiencies for the two perpendicular axes of the grains, as well as the extinction efficiencies.[1] The

1 The expression for the phase-lag efficiency according to Rayleigh theory is derived in Appendix A.

efficiencies for the different species are combined in the same way as the extinction efficiencies.

$$Cp_{l,r}(\lambda) = \sum_i \sigma_i A_i (Qp_{l,r})_i$$

The ratio $(Cp_l - Cp_r)/(Ce_l - Ce_r) = \Delta Cp/\Delta Ce$ of equation IV.10 can then be calculated directly. Substitution for the observed polarization into IV.10 gives the amount of twist in the grain alignment required ϕ.

Two models for the linear polarization are shown in Figure IV.3. Model 1 is identical to the best fit model of DB, and is shown for comparison to the models which include graphite. The input parameters are $\tau_{10\ \mu m} = 3.3$, f = 0.10, semi-minor axis b = 0.022 μm and the axial ratio r = b/a = 0.2. (For prolate grains a > b = c.) These grains are a factor of 10 smaller in volume than the grains used by DB.[1] The same volume ratio of graphite to silicate grains derived by Kunkle was used. Model 8 illustrated in Figure IV.3 includes oblate graphite grains (a < b = c) of this size, i.e. b = 0.215 μm, r = 5.

It was stated earlier that is is unnecessary to use a size distribution instead of a single grain size in the Rayleigh approximation. This can be seen directly by study of the expressions for the cross-sections. They are

1 The difference in size does not affect the model - see later discussion.

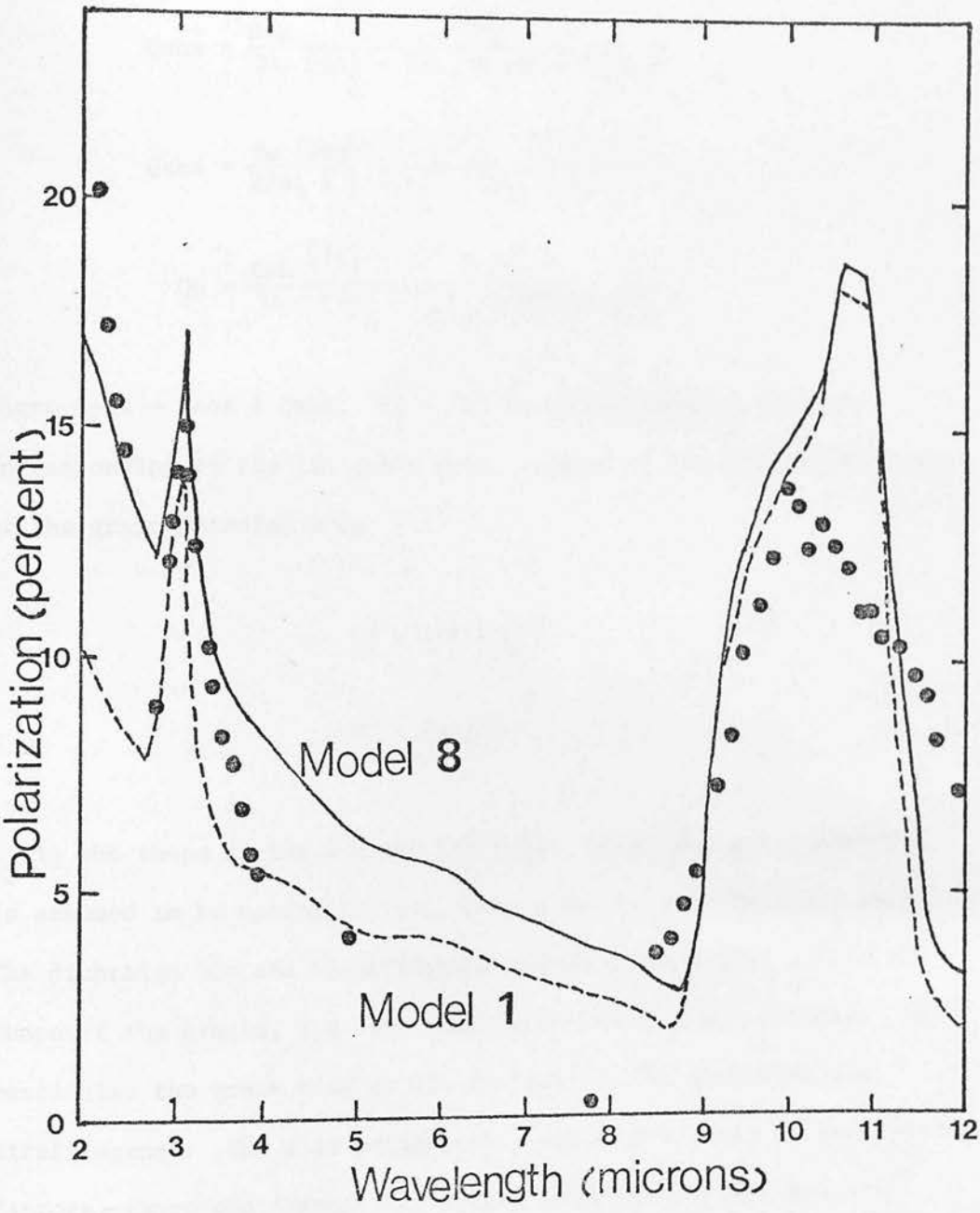

Figure IV.3 Linear polarization predicted by the DB model (model 1) and by a model identical to the DB model except that it also includes 0.215 μm oblate graphite grains.

$$Qabs = \frac{8\pi b}{3\lambda} \frac{\varepsilon_j''}{[(\varepsilon_j' - 1)L_j + 1]^2 + \varepsilon_j''^2 L_j^2}$$

$$Qsca = \frac{8a}{27b}\left(\frac{2\pi b}{\lambda}\right)^4 \frac{(\varepsilon_j' - 1)^2 + \varepsilon_j''^2}{[(\varepsilon_j' - 1)L_j + 1]^2 + \varepsilon_j''^2 L_j^2}$$

$$Qp = \frac{8\pi b}{3\lambda} \frac{[(\varepsilon_j' - 1)^2 + \varepsilon_j''^2]L_j + \varepsilon_j' - 1}{[(\varepsilon_j' - 1)L_j + 1]^2 + \varepsilon_j''^2 L_j^2}$$

where Qext = Qsca + Qabs. $\varepsilon_j' - i\varepsilon_j''$ is the dielectric constant corresponding to the jth grain axis, related to the refractive index of the grain material m by

$$\varepsilon' = n'^2 - n''^2$$

$$\varepsilon'' = 2n'n''$$

L_j is the shape factor for the jth axis. Since the grain material is assumed to be optically isotropic, ε is the same for each axis. The dichroism ΔQe and birefringence ΔQp then arise purely from the shape of the grains, i.e. the difference in the shape factors. In particular the grain size is not explicit in the dichroism and birefringence. The size parameters a and b enter only as multiplying factors, therefore introducing a size distribution just has the effect of changing these parameters to effective sizes for the mean grain of the size distribution. In fact the as and bs used here correspond to the mean grains of Kunkle's size distribution, which is an Oort-van de Hulst distribution.

The size of the grains in fact cancels out completely in

equations IV.14 for models in which each grain species has the same size or size ratio, and the albedo is small. This is the reason that Model 1 is independent of size. The relative size of different grain species *is* of importance, and is one of the free parameters used to obtain the best fit to the observations.

There are two situations in which the above arguments concerning the grain sizes are not valid. If a shape distribution were assumed for any or all of the grain species then the size parameters could not be simply considered as multiplying factors in the expressions for the efficiencies. Although there undoubtedly exists a distribution of grain shapes it is undesirable to introduce one into the calculations. The effect of a shape distribution would be to change the degree of alignment required somewhat, without disturbing the polarization or spectrum at all, at the expense of the clarity of the interpretation of the models, and therefore of their practicality.

The second caution about the grain sizes is that the relative contributions of scattering and absorption to the extinction and polarization depend on size, in the sense that scattering becomes relatively more important for larger grains at a given wavelength. At the wavelengths of interest here scattering generally plays a much less important role than absorption. In other words, the albedos are low, therefore this effect is small, though observable in the trial models. It was noted in Chapter II that evidence in fact exists for the importance of scattering in the infrared

in certain situations.[1] This may be entirely due to abnormal grain conditions, however it is argued below that more adequate consideration of scattering may improve the model fits found in this research.

Finally, the models can be generalised from the static PF alignment to spinning DG alignment at oblique incidence as follows. Greenberg (1968, pp. 319) has shown that for DG alignment the factor $\cos^2\psi$ should be incorporated into equation IV.13 where ψ is the angle between the magnetic field direction and the plane of the sky. In addition we must account for the fact that oblate grains are two times more efficient as polarizers than prolate grains, because, spinning around their short axes, prolate grains will not present their maximum cross-section to the incident radiation all the time. For prolate grains with axes $a > b = c$, the effective cross-sections Ce_l and Cp_l must then be replaced by $\frac{1}{2}(C_l + C_r)$, while C_r remains unchanged. For oblate grains, $a < b = c$, both cross-sections are unchanged. Equation IV.13 for prolate grains then becomes

$$p = \frac{1}{4}\cos^2\psi\, f(Ce_l - Ce_r)Nl$$

The optical depth is also altered, because the effective cross-section $C = \frac{1}{2}(Cx + Cy)$ must be replaced by $C = 0.25(C_l + 3C_r)$. This affects the column density little.

Equations IV.14 were altered to incorporate this generalisation

1 Also see Chapter VI for a discussion of anomalous objects whose polarization may be due to scattering.

into the models. The net effect is that f must be increased by a factor of 2 $\cos^2\psi$ to make up for the reduced efficiency of the prolate grains. The axial ratio or column density of the oblate graphite grains must then be reduced to offset this increase in alignment, which applies to them also.[1] Table IV.2 compares the parameters required for models 1 and 8 assuming DG alignment instead of PF with $\psi = 0$. The effect on f of non-zero values of ψ is shown in Figure IV.4.

(4) Results and Discussion.

Some representative models are shown in Figure IV.5 and 6. Their characteristic parameters are listed in Table IV.2. The model predicted spectrum is not shown, even for the best fit model, 14, because the models were basically developed to match the polarization and do not compare in sophistication to recent models for the spectrum of protostars and H II regions (e.g. Kwan and Scoville 1976, Yorke and Krugel 1977, Finn and Simon 1977). $\tau_{10} = 3.3$ assumes a silicate emission spectrum beneath, therefore a blackbody routine is inappropriate. The circular polarization in the models is forced to match the observed polarization q_{obs} (2.2 μm) by suitable choice of ϕ. For those models for which the calculated linear polarization

1 Note that this is an artificial computational procedure. Oblate grains are harder to align than prolate grains; also larger grains are harder to align. Therefore it is strictly the magnetic field strength which should be kept the same for both grain types, not the degree of alignment. In reality f will be smaller for the graphite, which can be offset by considering them to be flatter than predicted by the models.

Table IV.2

Characteristic Parameters of the Models for BN

Model Number	Type of Alignment	Input Parameters: sil/ice (μ) a	sil/ice (μ) b/a	graphite (μ) a	graphite (μ) b/a	Relative Mass (ice : sil : graph)	Predicted Parameters: Ml_{sil} ($g\ cm^{-2}$)	P (%) 2.0 μ	P (%) 3.1 μ	P (%) 8.0 μ	P (%) 10.5 μ	Optical Depth 2.0 μ	Optical Depth 3.1 μ	Optical Depth 10.5 μ	Albedo 2.0 μ	Albedo 10.5 μ	ΔCp/ΔCe 2.2 μ
1	PF	0.02	0.5	0	0	0.16 : 1.0 : 0.0	1.4×10^{-3}	10.6	13.4	2.6	16.9	3.4	5.0	3.3	1.0×10^{-3}	5.7×10^{-6}	2.02
1	DG	0.02	0.5	0	0	0.16 : 1.0 : 0.0	1.86×10^{-3}	7.0	8.8	1.7	11.0	3.7	5.7	3.3	1.4×10^{-3}	7.9×10^{-6}	1.96
1	DG	0.02	0.5	0	0	0.16 : 1.0 : 0.0	1.83×10^{-3}	10.9	13.8	2.7	17.3	3.6	5.6	3.2	1.4×10^{-3}	7.9×10^{-6}	1.96
8	PF	0.02	0.5	0.215	5	0.16 : 1.0 : 0.5	1.42×10^{-3}	17.4	17.2	3.5	17.4	4.1	5.4	3.4	1.2×10^{-3}	8.0×10^{-6}	2.28
8	DG	0.02	0.5	0.215	5	0.16 : 1.0 : 0.5	1.83×10^{-3}	24.5	21.5	4.5	18.4	4.6	6.1	3.3	1.2×10^{-3}	7.9×10^{-6}	2.34
8	DG	0.02	0.5	0.215	2.5	0.16 : 1.0 : 0.5	1.83×10^{-3}	16.2	16.6	3.3	17.7	4.1	5.8	3.2	1.4×10^{-3}	8.0×10^{-6}	2.55
11	PF	0.02	0.5	0.11	5	0.16 : 1.0 : 0.5	1.42×10^{-3}	23.4	20.7	4.3	17.9	4.8	5.8	3.5	1.1×10^{-3}	8.0×10^{-6}	2.33
12	PF	0.02	0.5	0.15	5	0.16 : 1.0 : 0.5	1.42×10^{-3}	20.2	18.9	3.9	17.6	4.4	5.6	3.4	1.2×10^{-3}	8.0×10^{-6}	2.35
14	PF	0.02	0.5	0.15	5	0.16 : 1.0 : 0.5	1.43×10^{-3}	16.4	15.3	3.1	14.3	4.5	5.7	3.5	1.2×10^{-3}	8.0×10^{-6}	2.36
15	PF	0.02	0.5	0.15	5	0.2 : 1.0 : 1.0	1.42×10^{-3}	13.7	17.0	3.1	17.2	3.7	6.0	3.4	1.4×10^{-3}	7.9×10^{-6}	2.22

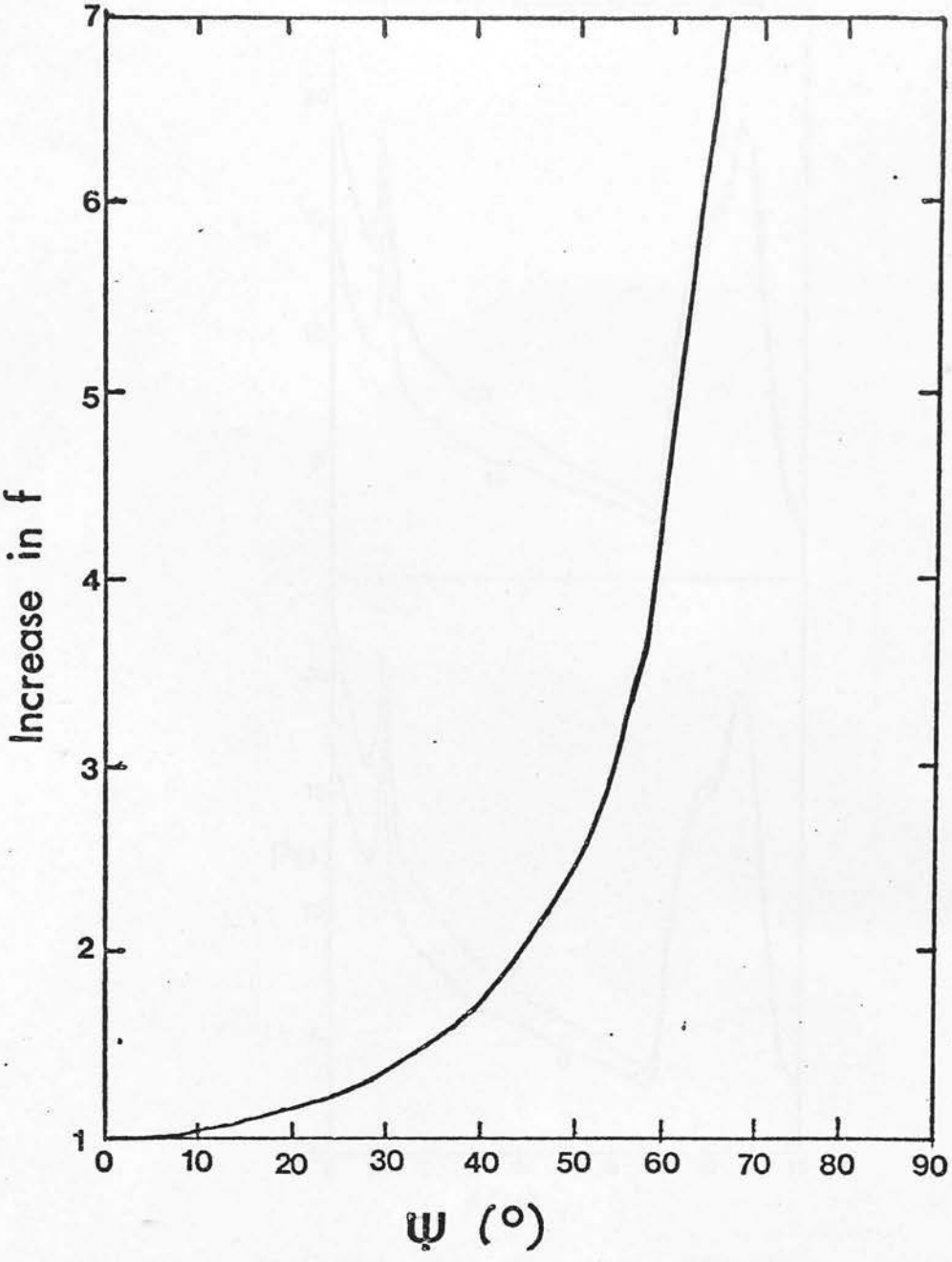

Figure IV.4 Increase in alignment f required by the models to offset non-zero values of the angle between the magnetic field and the plane of the sky, ψ.

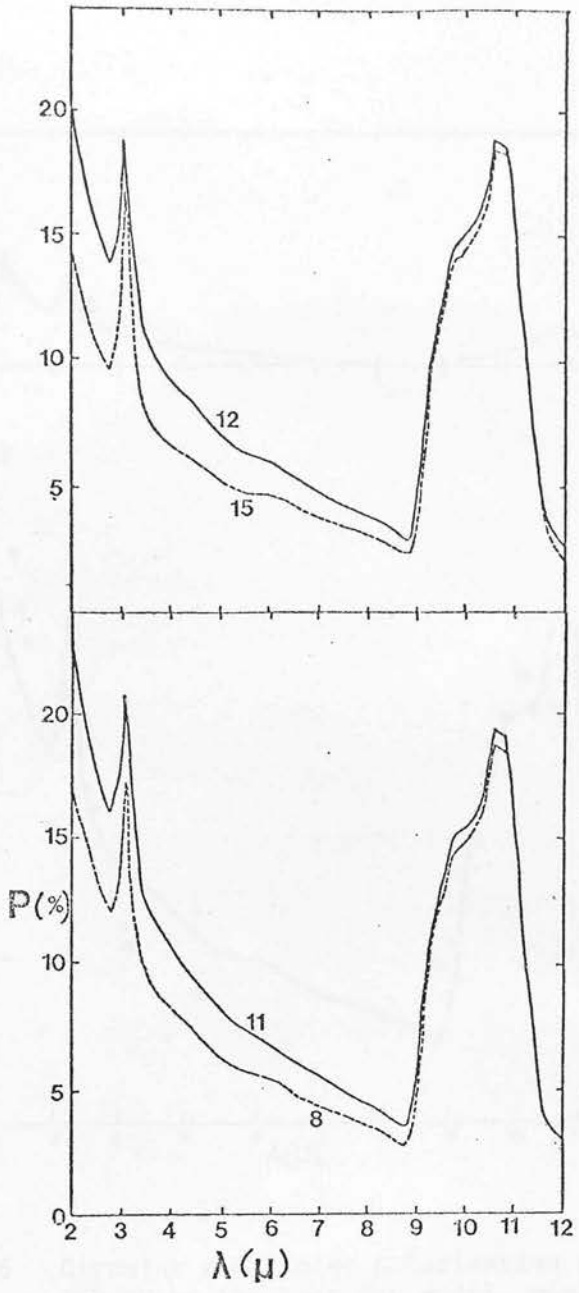

Figure IV.5 Linear polarization predicted by models 8, 11, 12 and 15.

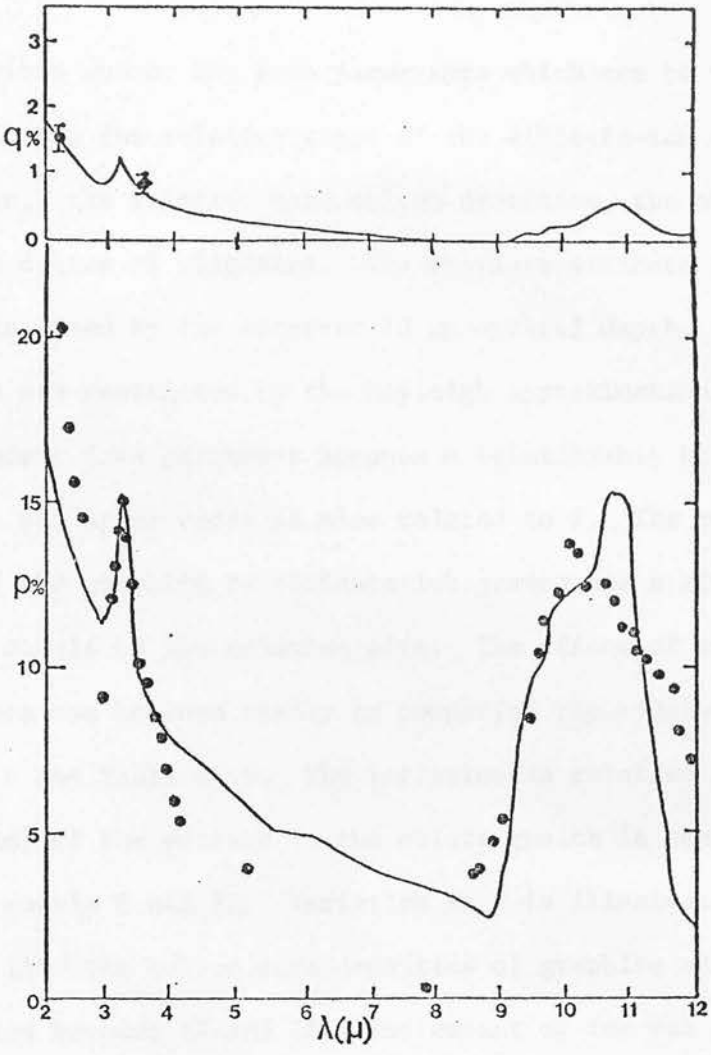

Figure IV.6 Circular and linear polarization predicted for BN by the best fit model, number 14, compared to the observations. The diamond symbol is the observation of Serkowski and Rieke (1973).

p_{calc} (2.2 μm) does not agree very well with the observed p_{obs} (2.2 μm), ϕ is obviously approximate.

As described above, the free parameters which can be varied to improve the fit are the relative sizes of the silicate-ice and the graphite grains,[1] the relative mass column densities, the axial ratios and the degree of alignment. The absolute silicate column mass density is fixed by the observed 10 μm optical depth, and the absolute sizes are restricted by the Rayleigh approximation. ψ is not an independent free parameter because a relationship between ψ and f exists. The axial ratio is also related to f. The relative axial ratio of the graphite to silicate-ice grains has a similar effect on the models as the relative size. The effect of varying these parameters can be seen easily by comparing the models in Figures IV.5, 6 and Table IV.2. The variation in relative size (or axial ratio) of the prolate to the oblate grains is seen in comparison of models 8 and 11. Variation in f is illustrated by models 12 and 14. The column mass densities of graphite and silicate were varied between 12 and 15. The amount of ice was also changed in model 15, to compensate for the decrease in the continuum level caused by the reduction in graphite.

Another grain material was tried in an attempt to improve the models. A terrestrial silicate (Obsidian, Pollack et al 1973) was

[1] There is no point in varying the ice to silicate size ratio because the ice makes only a small contribution to the continuum extinction and polarization (this work, and Harris et al 1979).

used instead of the moonrock. As expected, the level of polarization was very low. A similar mass column density as for the moonrock was required. Note that the optical constants of the various moonrock samples are not identical (sample number 12002 was used for these models), therefore use of a different sample would result in a different mass column density. This would affect the relative shapes, which must therefore be considered to be determined only within broad limits.

The best fit model 14 was obtained by reducing the degree of alignment of model 12, which was artifically high in the DB model to force a fit to the short wavelength polarization using only dielectric grains. f has been reduced by 10% from the value used in model 12, and by 40% from the DB model. The silicate feature polarization is much improved, and the ice feature and continuum fits are quite good also. A remaining defect is that the slope of the polarization spectrum at $\lambda < 8$ μm is still too shallow. It is possible that this defect could be eliminated by more adequate treatment of scattering. The steep slope of the polarization spectrum at $\lambda < 4$ μm is indicative of the increasing importance of scattering: for Rayleigh grains $Qsca/Qabs \alpha \left(\frac{2\pi a}{\lambda}\right)^3$. However, even for the largest grains used in this research the calculated albedos are low, (10^{-3}), because a is smaller than required to make $Qsca/Qabs \simeq 1$, as in the DB model. Increasing the size further to increase the scattering contribution will violate the Rayleigh criterion, yet in the Mie domain the polarization spectrum might not be expected to be so steep. In any case, the assumptions made in the derivation of the

transfer equations have the consequence that scattering is not well treated by this theory. This can be seen directly from equations IV.5: there are no cross terms between the Stokes parameters. In fact, the amplitude function for forward scattering is adopted, by definition of an IS model; therefore the polarization properties of light scattered into the beam are explicitly ignored. In addition the models derived here predict 2 μm optical depths of 3 to 4 (which are in good agreement with current opinion for the optical extinction to BN, and the extrapolation of the interstellar extinction law to the infrared (Chapters II and VI)). Therefore the optical depth in scattering could be appreciable, resulting in multiple scattering, which is impossible to treat well without knowledge of the size, shape and composition distributions of the dust as a function of distance from the source. (Note that ES did not consider multiple scattering.) Model 14 therefore represents the best fit to data that can be achieved at this time, though it should be kept in mind that the effect of large scattering optical depths on the circular polarization is unpredictable.

The model has not been extended to 20 μm, in an attempt to match the polarization observed by Knacke and Capps (1979), because of the possibility that radiative transfer effects play an important role at these wavelengths (see Chapter II). In fact a degree of polarization of about 12% is predicted in the 20 μm band by model 14. The observed value is lower (6.3%) but consistent with the range of values expected for typical silicates in a pure absorbing cloud (Knacke and Capps 1979), such as modelled here. The disagreement in

observed and calculated values could be due to radiative transfer effects, incorrect choice of absorbing silicates or temperature effects which can alter the ratio of the 10 and 20 μm band strengths in the interstellar medium from those measured in the laboratory (Day 1976a).

For this model of BN a value of $\phi = 33°$ is required for the total twist, to match the observed circular polarization. This value is lower than those required in interstellar optical circular polarization models (e.g. Martin 1974), which is due to the relatively large birefringence in the infrared. The predicted circular polarization at 3.45 μm is consistent with the observation of Serkowski and Rieke (1975). The models predict a wavelength dependence of circular polarization which may be observable with current instrumentation, especially in the absorption features.

The other sources with circular polarization are not so easily modelled as BN because there exists less information about the wavelength dependence of linear polarization. In particular, little information exists in the silicate band. That data which does exist is illustrated in Figure VI.1. It is at least clear that it would be possible to find some model similar to the ones described above that could reasonably fit the polarization spectra. Unfortunately, although a column density of silicates can be estimated from the observed $\tau_{10\ \mu m}$, there is no way to tell their polarizing properties, and hence no indication of the relative polarizing contribution of silicates and graphite at 2 μm, which is the main determinant of ϕ.

However, an estimate of ϕ can be found by assuming that the values of $\Delta Cp/\Delta Ce$ calculated for models 1 and 14 may not be significantly different from the values corresponding to the actual grain compositions near these sources. Values of ϕ required to obtain the observed ellipticities using a DB model are given in Table IV.3. Also given are values calculated for model 14. These are the twist angles that would be required if a similar proportion of graphite to silicates contributes to the polarization as in BN. Comparison of Figures IV.5, 6 and VI.1 indicates that model 14 is more appropriate than model 1. However, it is possible that grain compositions vary from source to source. (Chapter V illustrates an example where the grain composition may differ from that in BN in the sense that relatively more graphite may contribute to the continuum polarization.) In this case the values of ϕ would vary from those listed in Table IV.3, because the different grain compositions would have different values of $\Delta Cp/\Delta Ce$. Also, the values of ϕ for the two models are not directly comparable because there is a 33% difference between the linear polarizations predicted: for a particular source for which the observed polarization could be predicted well by each model, the values of $\Delta Cp/\Delta Ce$ obtained and therefore of ϕ, would differ from those given by models 1 and 14. The result would be that there would be a larger difference between the twists predicted by the two models, with the smaller values corresponding to the models containing graphite. It therefore seems possible to successfully model all the sources for which q has been determined by transfer of radiation through a medium of aligned grains with a twist in the alignment along the line-of-sight through the molecular

Table IV.3

Derived Values of the Twist Angle
for Models Described in the Text

Source	Total Twist Angle ϕ (°) Model 1	Model 14
GL 490	61	53
OMC 1/IRS 1	37	33
OMC 1/IRS 2	45	38
W33A	<46	<40
GL 2591	46	40
S106	<125	120
S140	42	35
NGC 7538/IRS 1	<30	<25
NGC 7538/IRS 4	<90	<83
	$\langle\phi\rangle = 44 \pm 10°$	$\langle\phi\rangle = 38 \pm 9°$[1]

[1] The upper limits to ϕ for S106 and NGC 7538/IRS 1 have been excluded from the calculations of the average twist.

cloud of $\phi \lesssim 50°$.[1] These values are considerably lower than those encountered in the interstellar medium, owing to the relatively large values of $\Delta Cp/\Delta Ce$.

The suggestion that the infrared polarization of many protostars could be attributed to a physically acceptable IS model has therefore been verified. An important conclusion is that it is unnecessary to invoke specialised scattering geometries to account for the polarization of the five sources for which detected circular polarization has been detected. In Chapter VI it is shown that this conclusion probably extends to the majority of protostellar sources also. Some exceptions, for which scattering may be important, are also discussed in Chapter VI. The consequences of the model derived here as regards the origin of the twists and the role of magnetic fields in star forming molecular clouds are discussed in Chapter VII.

It is also important to note that although the models may be deficient somewhat in fitting the short wavelength linear polarization, the circular polarization can arise by conversion of some of the polarization that *is* predicted by the models without greatly increasing the twist required (ϕ would need to be 47° for model 14 of BN, and less for the other sources).

[1] Note that no rotation of the position angle of polarization with wavelength is predicted by this model (see equation IV.7) unless there is a wavelength dependence of ϕ, introduced, for example, by a radial composition dependence of the grains. Also, for small values of ϕ the depolarization factor $\sin \phi/\phi$ is small.

Finally, it has been suggested that scattering by larger aligned grains may enhance the short wavelength linear polarization. The circular polarization from such scattering is unpredictable. The possible importance of such grains versus the influence of graphite polarization is discussed in the context of GL 2591 in the next chapter.

CHAPTER V

ICE BAND POLARIMETRY

The polarization observations in the vicinity of the 3.1 μm ice feature of GL 2591 and Mon R2/IRS 2 are shown in Figure III.6. The earlier observations of BN (Capps 1976) are shown in Figure II.2 and of W33 A (Capps et al 1978) in Figure V.1. These are the only sources for which ice band polarimetry exists.

W33 A is a compact luminous source with very similar characteristics to BN (except that it coincides with an OH source) which suggests that it is a massive protostar. It has exceptionally deep ice and silicate features (Capps et al). The polarization behaviour in the ice band is not established owing to the faintness of the source and the depth of the feature, but it appears to behave in the same way as BN. The polarization observations of BN have been attributed to aligned grains in the line-of-sight (Chapters II and IV), particularly to explain the increase in polarization with optical depth in the silicate band and the circular polarization. The ice feature data therefore show that the ice is also aligned near BN, whether as grain mantles or entire grains.

Observations of the polarization of the ice band of GL 2591 and Mon R2/IRS 2 were made as a test of the dichroic absorption model for other sources besides BN. As described in Chapter II the positive polarization/optical depth correlation observed in BN is not a conclusive test of the model, but discovery of a *negative* correlation

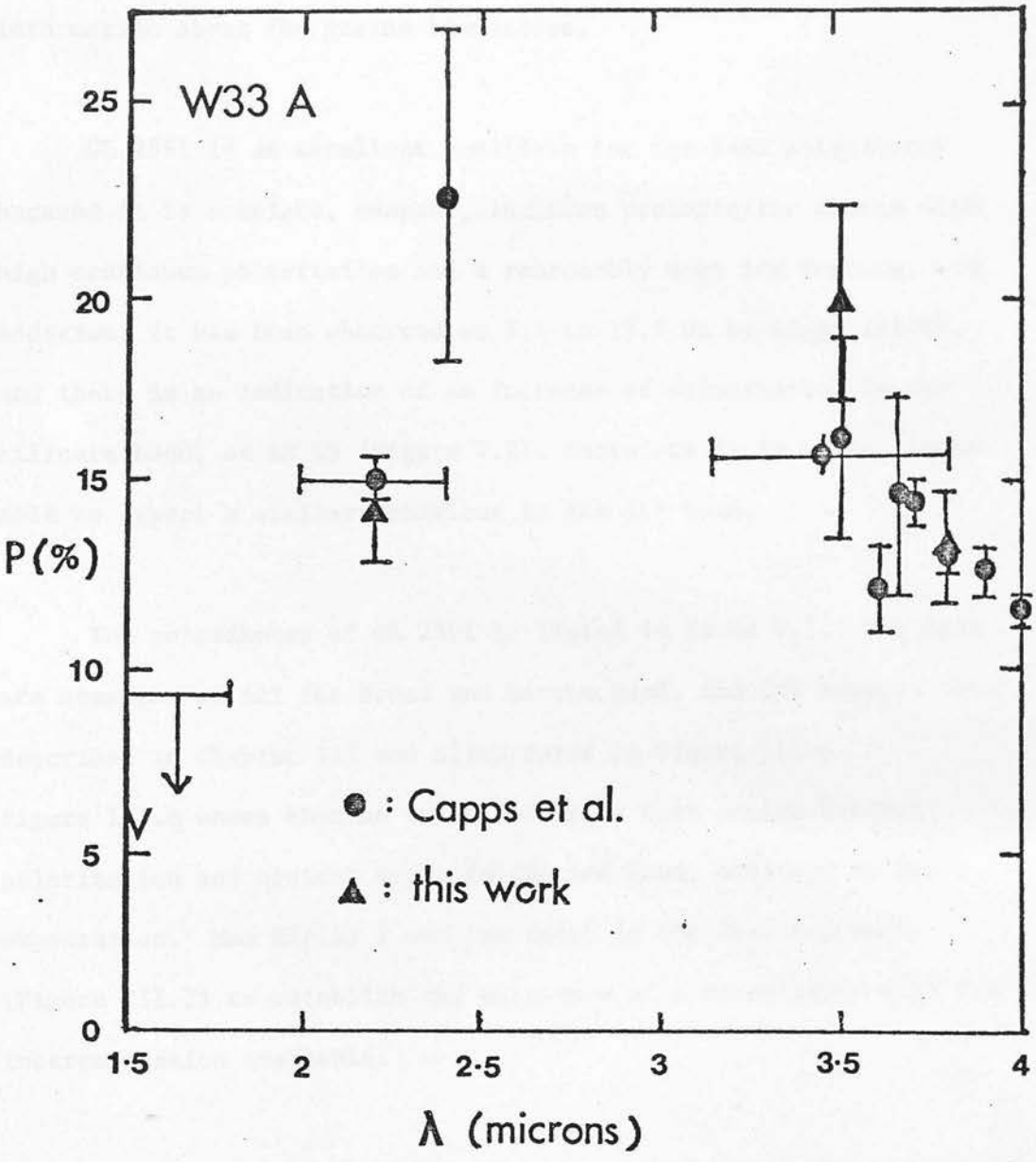

Figure V.1 Polarimetry of W33 A in the vicinity of the ice band.

(polarization *decreasing* with increasing optical depth) would certainly pose problems for it. Also ice band polarimetry can reveal information about the grains themselves.

GL 2591 is an excellent candidate for ice band polarimetry because it is a bright, compact, luminous protostellar source with high continuum polarization and a reasonably deep ice feature. In addition, it has been observed at 8.4 to 12.6 μm by Capps (1976), and there is an indication of an increase of polarization in the silicate band, as in BN (Figure V.2), therefore it is quite reasonable to expect a similar behaviour in the ice band.

The polarimetry of GL 2591 is listed in Table V.1. The data are averages of all the broad and narrow band, and CVF observations described in Chapter III and illustrated in Figure III.6. Figure III.6 shows that no relationship in fact occurs between polarization and optical depth in the ice band, contrary to the expectation. Mon R2/IRS 2 was too faint in the deep ice band (Figure III.7) to establish the existence of a correlation with the instrumentation available.

The fact that a *negative* polarization/optical depth correlation is not observed in GL 2591 means that no conflict with the interpretation of the polarization as due to absorption by aligned grains has been discovered. This is pleasing, since GL 2591 resembles BN closely in two aspects which have led to the adoption of the IS model: the degree of 2 μm ellipticity and the increase of

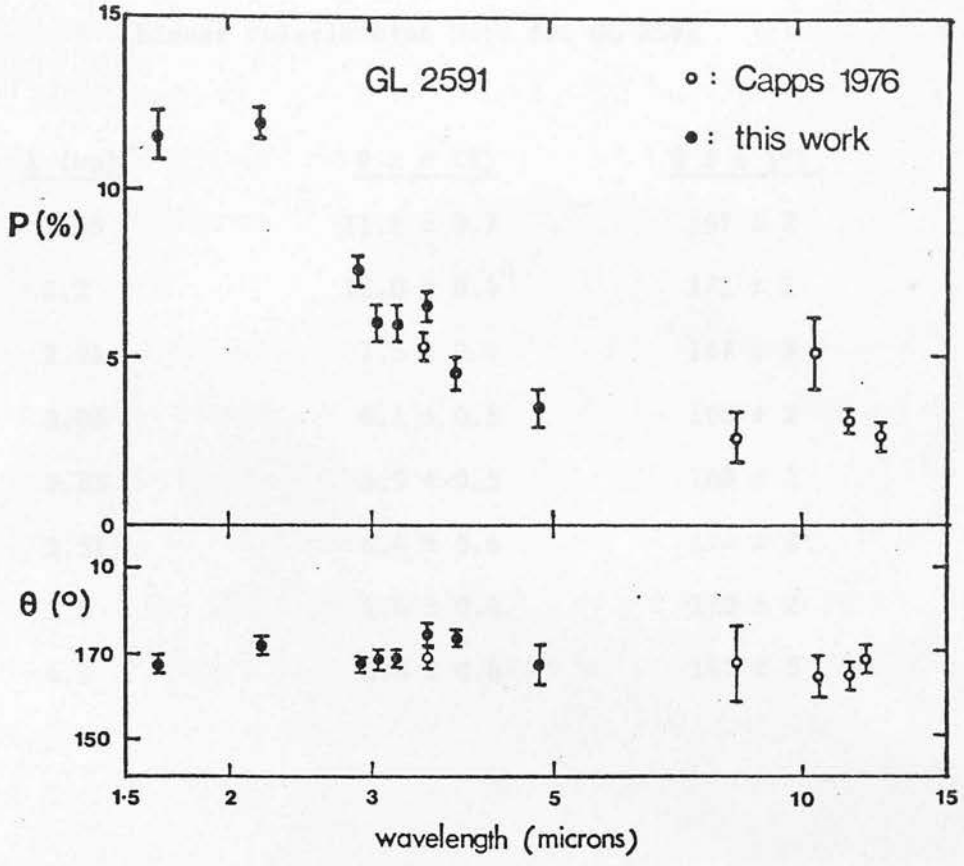

Figure V.2 Complete linear polarization data set available for GL 2591.

Table V.1

Linear Polarization Data for GL 2591

λ (μm)	P $\pm$ ε (%)	θ $\pm$ ε (°)
1.65	11.6 ± 0.7	167 ± 2
2.2	12.0 ± 0.4	171 ± 1
2.91	7.5 ± 0.4	167 ± 2
3.05	6.1 ± 0.5	168 ± 2
3.23	5.9 ± 0.5	168 ± 2
3.51	6.4 ± 0.4	174 ± 2
3.8	4.6 ± 0.4	173 ± 2
4.8	3.6 ± 0.6	167 ± 5

polarization in the silicate band. This very similarity, however, makes the lack of a *positive* ice band correlation very surprising. It might be interpreted as indicating that the ice grains or ice-coated grains are spherical or unaligned near GL 2591, which is a peculiar conclusion when the ice component near BN is clearly aspherical and aligned.

It should be noted here that GL 2591 does *not* resemble BN in another obvious aspect. This is that the polarization does not continue to rise towards the shortest wavelength observed but flattens out at 2 μm. Such behaviour is in fact also observed in W33 A, Mon R2/IRS 2, NGC 7538/IRS 1 and K3-50. In the first three of these at least, there is strong evidence that the turnover is due to contamination by an unpolarized source in the beam, either a normal star, or in the case of Mon R2/IRS 2 and NGC 7538/IRS 1, nearby extended, more evolved infrared/H II region sources (Beckwith et al 1976, also see Chapter VI). No such diluting source is known in the case of GL 2591, but no scans have been made at $\lambda \leq 2$ μm. An alternative explanation is that the turnover is due to the onset of the influence of scattering over absorption by relatively large grains, either in a shell or in the line-of-sight aligned grain extinction. The latter scattering effect is the more likely of the two since GL 2591 is observed to be very compact (Foy et al 1979).

Returning to the ice band problem, an indication that it may not be necessary to conclude that the GL 2591 ice grains are not aligned comes from another, less obvious difference between the BN

and GL 2591 polarization spectra. This is the ratio of 10 μm to 2.2 μm polarization, which is twice as large in BN as in GL 2591 although the peak silicate optical depth is larger in GL 2591 than in BN. Using this fact, the following analysis leads to a model for GL 2591 which does not require non-polarizing ice grains.

Polarization produced by dichroism of aligned grains is proportional to the extinction τ

$$P = f\left(\frac{Ce_l - Ce_r}{\overline{C}}\right)\tau$$

where $\overline{C}$ is the mean cross-section of the grain. This equation follows from equation IV.13 and the relation for τ immediately preceding. Therefore the polarization of GL 2591 can be expressed in terms of the relative degree of alignment of GL 2591 and BN $\alpha = f_{2591}/f_{BN}$ and the polarization of BN, for identical grain properties

$$P^{2591} = \alpha\left(\frac{\tau^{2591}}{\tau^{BN}}\right)P^{BN} \qquad \text{V.1}$$

Then if it is assumed in an ad hoc fashion that the polarization at any wavelength is due to a contribution from each of a silicate, an ice, and also a continuum component such that

$$P = P_{ICE} + P_{SIL} + P_{CONT} \qquad \text{V.2}$$

then

$$P^{2591}(\lambda) = \alpha\left[\left(\frac{\tau^{2591}}{\tau^{BN}}\right)_{ICE} P^{BN}_{ICE}(\lambda) + \left(\frac{\tau^{2591}}{\tau^{BN}}\right)_{SIL} P^{BN}_{SIL}(\lambda) + \left(\frac{\tau^{2591}}{\tau^{BN}}\right)_{CONT} P^{BN}_{CONT}(\lambda)\right] \qquad V.3$$

The ratios of the ice and silicate optical depths are known from the observations of the absorption features, and the infrared continuum optical depth ratio, β, is a parameter to be determined. The three components of the polarization of BN (equation V.2) can be found by drawing a smooth continuum through the polarization spectrum, and by making the following assumptions:

$$P^{BN}_{CONT} = 18\% \qquad \lambda = 2.2\ \mu m$$

$$= 0 \qquad \lambda \gtrsim 8\ \mu m$$

$$P^{BN}_{ICE} = 0 \qquad \lambda \lesssim 2.9\ \mu m, \text{ and}$$

$$\lambda \gtrsim 4\ \mu m$$

$$P^{BN}_{SIL} = 0 \qquad \lambda \lesssim 8\ \mu m$$

The decomposition of the polarization spectrum is illustrated in Figure V.3.

α is found from the observed polarizations at 10.5 μm from equation V.1:

$$\alpha = \left(\frac{P^{2591}}{P^{BN}}\right)_{10.5\ \mu m}\left(\frac{\tau^{BN}}{\tau^{2591}}\right)_{SIL} = 0.22$$

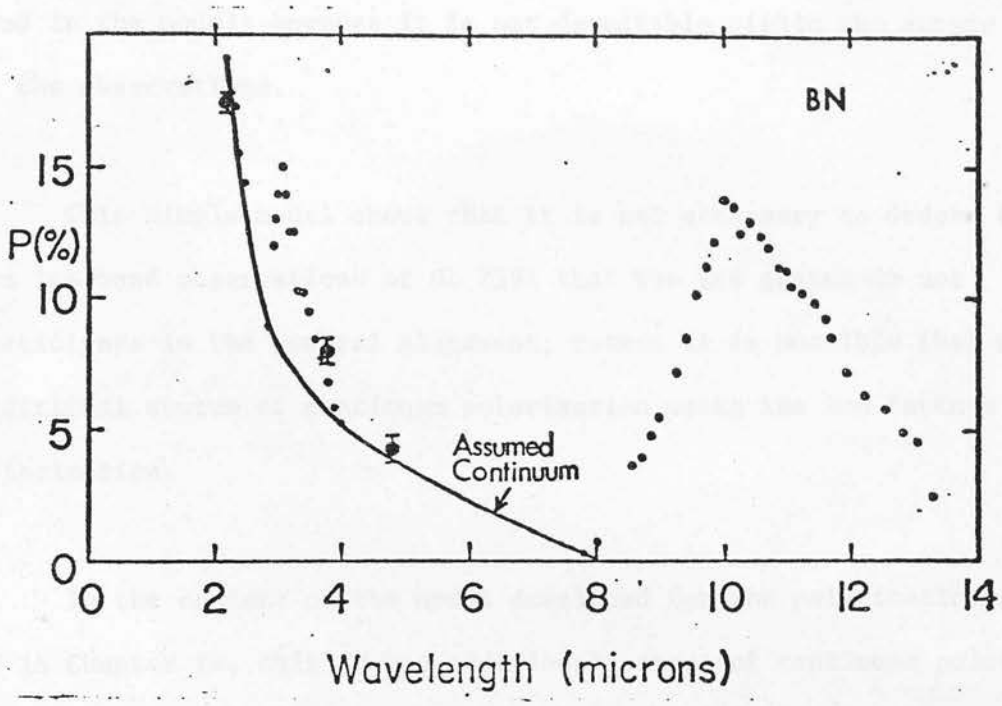

Figure V.3 The polarization spectrum of BN showing the continuum component assumed in the decomposition process.

Taking β as a free parameter, the best fit to the polarization spectrum of GL 2591 was found for $\beta = 3.3$. This fit is illustrated in Figure V.4. There is a small reversal in polarization at the ice band in the model; however it is not detectable within the errors of the observations.

This simple model shows that it is not necessary to deduce from the ice band observations of GL 2591 that the ice grains do not participate in the general alignment; rather it is possible that an additional source of continuum polarization masks the ice feature polarization.

In the context of the model developed for the polarization of BN in Chapter IV, this ad hoc additional source of continuum polarization could be due to the graphite grains. In this case there would be approximately three times as many metallic grains relative to dielectric ones near GL 2591 as near BN. Alternatively, a larger species of (non-ice) grains than found near BN could enhance the aligned grain polarization by scattering light out of the beam, rather than by pure absorption. Such a situation was suggested above as a possible explanation for the turnover in the polarization spectrum of GL 2591 at $\lambda < 2$ μm. To test these ideas the model developed in Chapter IV was adapted to fit the polarization spectrum of GL 2591, using the parameters described above as a starting point; *i.e.* $\tau_{9.7} = 1.8\ \tau_{9.7}^{BN} = 5.9$, $\tau_{3.1} = 0.6\ \tau_{3.1}^{BN} = 0.84$, $f = 0.22\ f_{BN} = 0.018$, and $\beta = 3.3$. The resulting fit is shown in Figure V.5. The continuum polarization is a little high in this model. The best fit

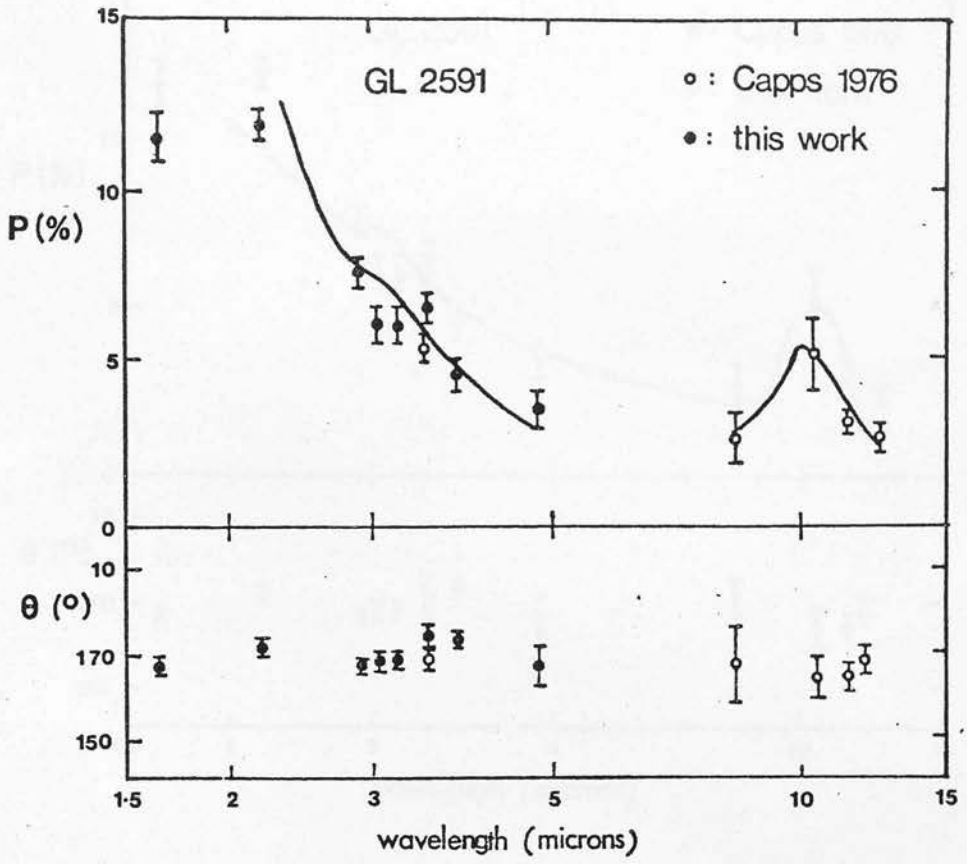

Figure V.4 The simple three-component model described in the text superimposed on the observational data.

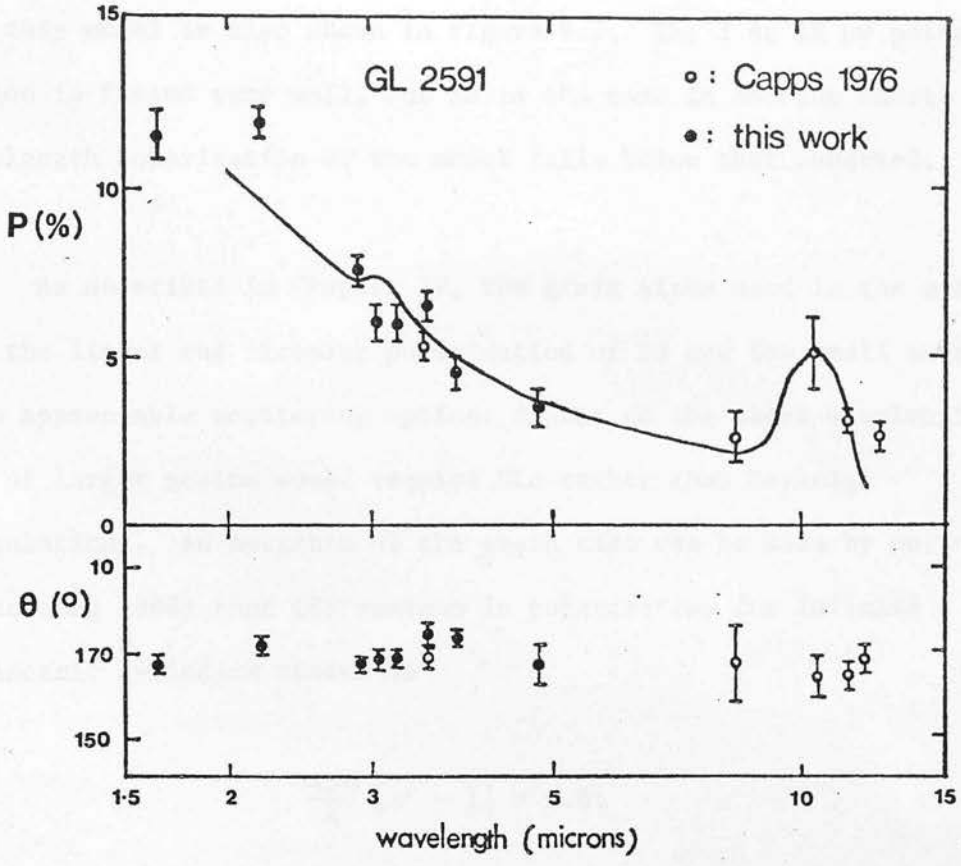

Figure V .5 The model of Chapter IV applied to GL 2591 as described in the text. The optical depth used is $\tau_{10} = 4.5$, and the degree of alignment is $f = 0.18$.

was obtained by reducing the silicate optical depth by about 15%, and this model is also shown in Figure V.5. The 3 to 12 μm polarization is fitted very well, but as is the case in BN, the short wavelength polarization of the model falls below that observed.

As described in Chapter IV, the grain sizes used in the models for the linear and circular polarization of BN are too small to produce appreciable scattering optical depths at the short wavelengths. Use of larger grains would require Mie rather than Rayleigh calculations. An estimate of the grain size can be made by noting (Greenberg 1968) that the maximum in polarization for infinite dielectric cylinders scales as

$$\frac{4\pi a}{\lambda} |n' - 1| \simeq 1.6 \qquad \text{V.4}$$

For the interstellar medium $\lambda_{max} \simeq 0.56$ μm (Serkowski et al 1975). For silicates with a typical refractive index $n' \simeq 1.5$, the grain size is approximately $a \simeq 0.14$ μm. If the intrinsic polarization spectrum of GL 2591 turns over at 2 μm owing to the scattering characteristics of large silicate grains, these grains would have to be of the order of $a = 0.5$ μm in size, according to equation V.4, or about four times larger than the typical interstellar grains.

To explain the circular polarization at 3 μm of GL 2591 by the best fit model in Figure V.5 would require a twist in the grain alignment of 40°.

CHAPTER VI

LINEAR POLARIZATION SURVEY

(1) The Data

The near infrared linear polarization data of protostars that had been obtained prior to winter of 1977 has been published by Dyck and Capps (1978) and by Kobayashi et al (1978). A total of 19 sources had been observed at this time, 15 of them by Dyck and Capps. These data have been reproduced in Table II. 1. The new observations bring the total number now measured up to 41. The sources are listed in order of increasing RA in Table VI. 1. The polarization is shown in Table VI. 2. This data now represents a significant fraction of protostellar sources observable for polarization. Of the additional 22 new sources, 13 were observed on this programme. The remaining 9 were observed by Dyck in late 1977 and 1978. Several of the sources that had already been observed were re-observed on this programme, or were observed at different wavelengths in addition, as noted in Table III. 5. This is the reason that some of the values are not the same as in Table II. 1. The original data obtained by Kobayashi et al. is indicated by an asterisk. The uncertainty in the position angle is about 10° or less in all cases. The notes and references apply to both tables, and the optical depths are estimated for a flat continuum, for easy intercomparison. The values of A_V given in Table VI. 1 have been derived by a number of methods, as described later. Br in column 5

Table VI.1

Source	Distance (kpc)	Av	Right Ascension	Declination	References	Notes
W3/IRS 1	3.1	19	2 21 56.0	61 52 45	1,2,3,4,5,6,7,8,9 10,11,12,48	
W3/IRS 5	3.1	100	2 21 53.2	61 52 21		
W3/IRS 9	3.1	25	2 23 21.4	61 39 10		
IC 1848 A/IRS 1	1.7	20	2 57 37.8	60 17 28	13,14,15	
GL 437 W	3.0	10	3 03 31.3	58 19 19	16,17,18,19	
GL 437 N	3.0	26	3 03 32.1	58 19 23		
GL 437 S	3.0	14	3 03 32.2	58 19 14		
GL 490	1.4	14	3 23 38.8	58 36 39	20,21,22,47,48	
S228	1.0	17	5 10 00.4	37 23 41	23,24,25,26	1
OMC 1/IRS 1 (BN)	0.5	44	5 32 46.6	-05 24 17	6,27,28,29,30	
OMC 1/IRS 2	0.5	30	5 32 46.3	-05 23 55		
OMC 2/IRS 3	0.5	30	5 32 59.1	-05 12 10	31	
NGC 2024 No. 2	0.45	30-50	5 39 14.3	-01 55 59	22,32,33	
Mon R2/IRS 1	0.95	27	6 05 20.0	-06 22 37	34,35	
Mon R2/IRS 2	0.95	37	6 05 19.4	-06 22 23		
Mon R2/IRS 3	0.95	34	6 05 21.7	-06 22 25	36,48	
S255/IRS 1	1.0	22	6 09 58.5	18 00 11	96,37,38,48	1
GL 961	1.4		6 31 59.0	04 15 09	39	
GL 989	0.8	35	6 38 24.9	09 32 29	22,24,40,41,42,43,44,48	
ρ Oph No. 29	0.2	40	16 24 07.7	-24 30 40	45,46	
NGC 6334/IRS 1	0.7		17 17 32.5	-35 44 07	49,50,51,52,53	
IR 12.4 + 0.5	1.8	14	18 07 55.8	-17 56 32	14,54	1
W33/IRS 3	4.6		18 11 18.1	-17 56 38	4,55	1
W33 A	4.4	70	18 11 44.2	-17 52 59	4,44,48,56,57,58,59	1
M17/KW IRS	1.8	36	18 17 26.5	-16 14 54	60,61,62,63,64,65,66,67	1
W40/IRS 1	0.7		18 28 51.7	-02 07 33	68	
W40/IRS 2	0.7		18 28 47.7	-02 07 41		
W40/IRS 3	0.7		18 28 47.6	-02 06 19		
G29.9 - 0.0	7.1	15	18 43 27.8	-02 42 48	69	1
G45.1 + 0.1	5.0	14	19 11 06.4	10 48 24	48,70,71	1
W51/IRS 2	6.5	33	19 21 22.4	14 25 12	12,48,72,73,74,75,76,81	
S88 B	2.0	19	19 44 41.8	25 05 18	77	1
K 3-50/IRS	8.0	31	19 59 50.1	33 24 19	12,74,75,78,79,80,81	
S106/IRS 3	2.3	28	20 25 33.8	37 12 52	82,83,84,85,86,87	
GL 2591	1.5	33	20 27 36.5	40 01 21	21,22,48,88,89,90,91,92	1
W75/IRS 1	1.5	23	20 37 10.1	42 12 08	2,4,72,93,94	1
S140/IRS 1	0.9	22	22 17 41.3	63 03 40	36,37,48,95,96,97,98	
NGC 7538/IRS 1	4.9	44	23 11 36.8	61 11 49	12 48,72,74,99,100 101,102	
NGC 7538/IRS 4	4.9		23 11 24.1	61 12 43		
NGC 7538/IRS 5	4.9		23 11 21.7	61 13 50		
NGC 7538/IRS 9	4.9	79	23 11 52.8	61 10 59		

Notes: 1. Distance uncertain.

Table VI.2

Source	Diameter (cm)	$\tau_{9.7}$	$\tau_{3.1}$	GHz free-free (Jy)	$P_H \pm \epsilon$ (%)	θ_H	$P_K \pm \epsilon$ (%)	θ_K	$P_L \pm \epsilon$ (%)	θ_L
W3/IRS 1	1.8×10^{18}	0.9		yes			5.0 ± 0.6	140		
W3/IRS 5	4.5×10^{16}	4.0		<0.012					10.1 ± 0.2	84
W3/IRS 9	$<4.5 \times 10^{17}$						2.4 ± 0.6	90		
IC 1848 A/IRS 1	$<7.6 \times 10^{16}$	1.4		<0.008			2.9 ± 0.4	11		
GL 437 W		0.6		yes			8 ± 1	104		
GL 437 N		1.7					24 ± 1	89		
GL 437 S		1.1			2.9 ± 2.2	-	3.2 ± 0.5	141		
GL 490		0.8	0.3	Br			4.2 ± 0.1	103		
S228	$<2.7 \times 10^{17}$			<0.012			5.6 ± 1.8	6		
OMC 1/IRS 1 (BN)	$<\sim 10^{15}$	1.3	1.4	Br	34 ± 1	116	18.4 ± 0.6	115	6.8 ± 0.2	107
OMC 1/IRS 2					14 ± 1	137	10.8 ± 1.0	136	2 ± 1	-
OMC 2/IRS 3		0		<0.25	12 ± 1	125	3.8 ± 0.3	124	2 ± 1	-
NGC 2024 No. 2		0.8	0.9	?			1 ± 1*	-		
Mon R2/IRS 1	1.4×10^{17}	<0.3		yes			22 ± 2	161		
Mon R2/IRS 2	$<3 \times 10^{15}$	1.0	1.6				16 ± 1	160	9.6 ± 0.6	158
Mon R2/IRS 3	5×10^{15}	2.0	0.6	<0.0016	5.1 ± 0.6	161	1.5 ± 0.2	116	1 ± 1	-
S255/IRS 1	3.7×10^{15}	2.3	0.9	<0.0016			14.6 ± 0.9	150	2 ± 1	-
GL 961							2 ± 1	-		
GL 989	$<6 \times 10^{16}$	0.5	1.3	Br			3.7 ± 0.9*	117		
ρ Oph No. 29	3×10^{14}	1.5					6.4 ± 1.6	28		
NGC 6334/IRS 1	$<1 \times 10^{16}$			yes			8.6 ± 1.3	105		
IR 12.4 + 0.5	1.2×10^{17}	0		<0.010			3.6 ± 0.7	106		
W33/IRS 3	1×10^{18}	1.1		yes			1 ± 1	-		
W33 A	$<4.6 \times 10^{16}$	3.8	>7	<0.015			15.4 ± 0.6	68	13.3 ± 1.4	70
M17/KW IRS	2×10^{16}		0.2	Br			4.5 ± 0.3	32	1.4 ± 0.9	47
W40/IRS 1	ext			?			0.4 ± 1	-		
W40/IRS 2				?			0.2 ± 1	-		
W40/IRS 3				?			1.8 ± 1	-		
G29.9 - 0.0	2×10^{18}	0.9		yes			0.8 ± 0.4	-		
G45.1 + 0.1	$<5 \times 10^{17}$	0.2		yes			3.0 ± 0.4	174	2 ± 1	-
W51/IRS 2	$<1.9 \times 10^{17}$	0.8	0.8	yes	6 ± 1	135	4.7 ± 0.3	130	2.3 ± 0.3	113
S88 B	9×10^{17}	1.7		yes			1 ± 1	-		
K 3-50/IRS	1.2×10^{17}	1.2	0.2	yes			1.9 ± 0.2	67	4.0 ± 0.6	64
S106/IRS 3	$<1 \times 10^{17}$	0.4	0	yes	4.0 ± 0.5	58	2.3 ± 0.6	47		
GL 2591	1×10^{16}	1.7	0.5	<0.005	11.6 ± 0.5	167	12.0 ± 0.4	171	4.2 ± 0.2	172
W75/IRS 1		<1.5		<0.15			2.5 ± 0.6	120		
S140/IRS 1	8×10^{15}	1.6	1.2	0.006	16.0 ± 0.3	80	13.7 ± 0.5	70	3.2 ± 0.3	61
NGC 7538/IRS 1	$<5.2 \times 10^{16}$	3.2	1.0	yes	3.2 ± 0.8	73	10.5 ± 0.8	69	5.7 ± 0.2	72
NGC 7538/IRS 4							6.2 ± 0.4	68		
NGC 7538/IRS 5							1 ± 1	-		
NGC 7538/IRS 9	$<5.2 \times 10^{16}$	1.8		<0.010			11.1 ± 1.0	161	1.2 ± 0.3	11

References to Tables VI.1 and VI.2

1. Wynn-Williams et al. 1972
2. Wynn-Williams 1971
3. Hackwell et al. 1978
4. Dyck and Simon 1977
5. Harvey et al. 1977a
6. Werner et al. 1977
7. Harris and Wynn-Williams 1976
8. Westbrook et al. 1976
9. Willner 1977
10. Aitken and Jones 1973
11. Lada et al. 1978
12. Thronson and Harper 1979
13. Loren and Wootten 1978
14. Beichman 1979
15. Osterbrock 1956
16. Schneps et al. 1978
17. Kleinmann et al. 1977
18. Cohen and Kuhi 1977
19. Wynn-Williams 1978
20. Harvey et al. 1979a
21. Thompson and Tokunaga 1979b
22. Merrill and Stein 1976
23. Frogel and Persson 1973
24. Harris 1976
25. Terzian 1970
26. Churchwell and Walmsley 1973
27. Becklin et al. 1973
28. Gillett et al. 1975a
29. Wynn-Williams and Becklin 1974
30. Martin and Gull 1976
31. Gatley et al. 1974
32. Grasdalen 1974
33. Hudson and Soifer 1976
34. Loren 1977
35. Beckwith et al. 1976
36. Thompson and Tokunaga 1979a
37. Blair et al. 1975
38. Evans et al. 1977
39. Cohen 1973
40. Allen 1972
41. Thompson and Tokunaga 1978
42. Harvey et al. 1977b
43. Crutcher et al. 1978
44. Walker 1956
45. Myers et al. 1978
46. Elias 1978
47. Morris et al. 1974
48. Simon, Simon and Joyce 1979
49. Cheung et al. 1978
50. Dickel et al. 1977
51. McBreen et al. 1979
52. Emerson et al. 1973
53. Becklin and Neugebauer 1974
54. Wright et al. 1979
55. Balick 1972
56. Habing et al. 1974
57. Gardner and Whiteoak 1972
58. Capps et al. 1978
59. Soifer et al. 1979
60. Kleinmann and Wright 1973
61. Lada et al. 1974
62. Wilson et al. 1979
63. Harper et al. 1976
64. Lada 1978
65. Tokunaga and Thompson 1979a
66. Elmegreen et al. 1979
67. Gatley et al. 1979
68. Zeilik and Lada 1978
64. Soifer and Pipher 1975
70. Zeilik et al. 1975
71. Matthews et al. 1977
72. Wynn-Williams et al. 1974
73. Martin 1972
74. Soifer et al. 1976
75. Puetter et al. 1979
76. Mufson and Liszt 1979
77. Pipher et al. 1977
78. Persson and Frogel 1974
79. Lester et al. 1979
80. Wynn-Williams et al. 1977b
81. Thompson and Tokunaga 1979c
82. Pipher et al. 1976
83. Sibille et al. 1975
84. Israel and Felli 1978
85. Lucas et al. 1979
86. Eiroa et al. 1979
87. Tokunaga and Thompson 1979b
88. Wynn-Williams et al. 1977a
89. Foy et al. 1979
90. Merrill and Soifer 1974
91. Wendker and Baars 1974
92. Merrill and Stein 1976
93. Werner et al. 1975
94. Dickel et al. 1978
95. Beichman et al. 1979
96. Harvey et al. 1978
97. Tokunaga et al. 1978
98. Dinerstein et al. 1979
99. Downes and Wilson 1974
100. Willner 1976
101. Werner et al. 1979
102. Israel et al. 1975

of Table VI. 2 indicates that Brackett line observations reveal an H II region. Capps (1976) has observed some of the sources listed in Table VI. 1 at 3.5 μm and longer. The data for all the sources for which wavelength information exists are plotted in Figure VI. 1, except those which are illustrated earlier; BN (Figure II. 2), GL 2591 and Mon R2/IRS 2 (Figure III. 6) and W33 A (Figure V. 1). The 2 μm observation of Mon R2/IRS 3 is most likely a non-detection (Dyck (1979), the small error being fortuitous, therefore these data are not plotted.

The general appearance of the data is not dissimilar to that of BN. In most cases the polarization falls with varying degrees of steepness as λ increases, up to 8 μm. There are indications of structure in the silicate band in all three sources with measurements beyond 8 μm, but it is not clear if it is real or whether polarization increases or decreases with optical depth.

Nine sources are unpolarized to the accuracy of the measurements. These are NGC 2024 No. 2, W33/IRS 3, G29.9 - 0.0, S88 B, GL 961, NGC 7538/IRS 5 and the W40 sources. Zeilik and Lada (1978) reported detection of three infrared sources coincident with radio emission from H II region W40, which probably lies at the front surface of the molecular cloud. Whilst observing these sources it was possible to see optical images on the Quantex TV screen, therefore they are most probably the exciting stars of the optically visible H II region, or foreground stars. In any case it is unlikely that

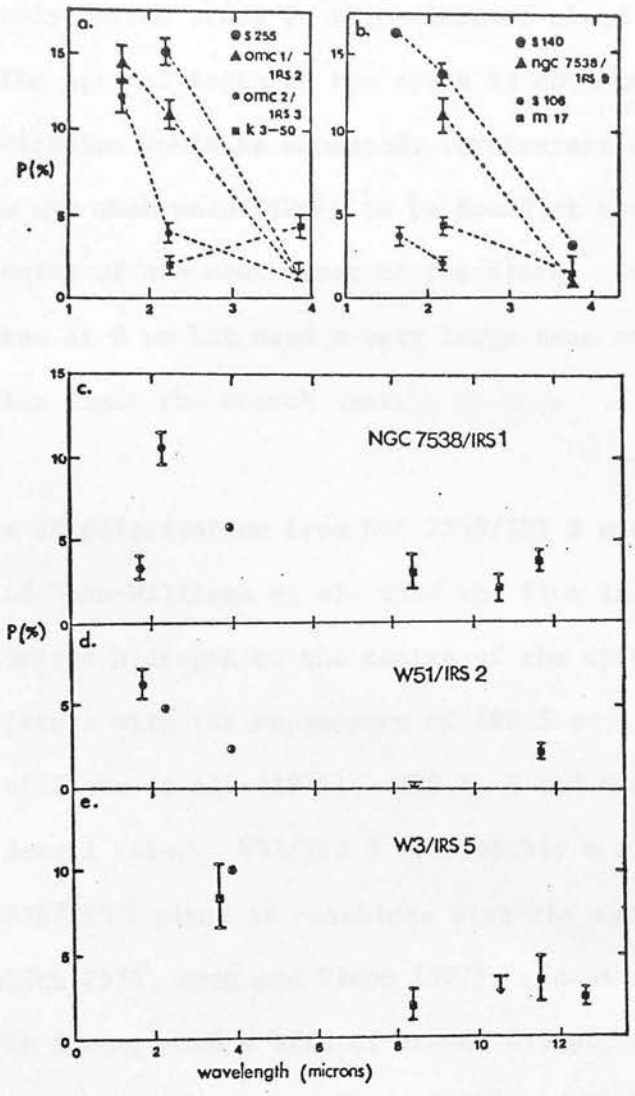

Figure VI.1 The wavelength dependence of polarization for several sources. Square symbols on Figures VI.1.c, d, and e are data from Capps (1976).

they could be newly formed stars in the molecular cloud behind W40. In either case the optical depth to the stars is obviously small, and little polarization would be expected. Protostars and obscured infrared sources are much more likely to be found at the molecular cloud peak 3 minutes of arc south west of the stars. Zeilik searched this area at 2 μm but used a very large beam and does not state to what flux limit the search went.

The absence of polarization from NGC 7538/IRS 5 supports the interpretation of Wynn-Williams et al. that the flux is thermal emission from ionised hydrogen at the centre of the optical nebula. It is also consistent with the appearence of IRS 5 as a star on the 0.9 μm picture of Beetz et al. (1976). IRS 1, 4 and 9 are discussed in more detail below. W33/IRS 3 is probably a similar source to NGC 7538/IRS 5 since it coincides with the radio source G12.8 - 0.2 (Balick 1972, Dyck and Simon 1977). Scans have revealed that W33/IRS 3 is large, with a size of around 0.3 pc, although the distance of W33 is uncertain (Dyck and Simon 1977). G29.9 - 0.0 is a compact H II region with an infrared source of size ~ 2×10^{18} cm (Soifer and Pipher 1975), with an extinction of probably not much more than A_v = 15 magnitudes, although there is a 10 μm absorption feature. This extinction is not greater than expected from general interstellar extinction, A_v = 2mag kpc^{-1} (Salpeter 1977).

NGC 2024 No. 2, also known as Grasdalen's source, was discovered in a search for the exciting star of NGC 2024 (Grasdalen

1974). It has a spectrum which is very similar to that of BN, and Hudson and Soifer (1976) suggested that it is the power source of the associated molecular clouds rather than of the H II region, although it does not lie at the peak of the molecular emission. In either case large extinctions are implied for the source, therefore the lack of polarization may help distinguish between the models. GL 961 is Cohen's source, probably associated with the Rossette fan-shaped cometary nebula. Finally S88 B (GL 2444) is a bright Hα knot (Sharpless 1959) with an associated H II region G61.5 + 0.1. The geometry of the sources are not clear but Pipher et al. (1977) have suggested a model in which the infrared source is associated with a compact H II region on the surface of a molecular cloud behind the Hα knot.

(2) Interpretation

Having developed successfully an IS model to interpret the linear and circular polarization of BN and 4 other sources, it is very important to enquire whether the other characteristics of the data sample are consistent with such a model, and if so, whether they can shed any more light on the situation.

Dyck and Capps (1978) discovered evidence for a correlation between the size and the degree of polarization of the 15 sources for which they possessed data, which has important implications for star formation. The new data presented here provides a larger sample to check this correlation. Size is plotted against P_K in

Figure VI. 2. The fact that the distance to several of the sources is not well known complicates the interpretation somewhat, however, the correlation observed by Dyck and Capps is not so marked when the new data are included. The two sources which are most ambiguous are the luminous H II regions W3/IRS 1 and Mon R2/IRS 1. The other sources may be consistent with a relationship such as the dashed line in the Figure, but this is not clear since so many of them are unresolved. There is evidence that some may be clusters of protostars, e.g. W3/IRS 5 (Wynn-Williams 1977). Therefore it is possible that the polarization is associated with only one of these sources, (which would move the plotted point towards the right and downwards on the diagram, since the other sources would dilute the polarization) or each source is equally polarized (which would just bring the point down). Little more can be said at this time, until the sources are mapped and individual objects resolved, therefore it should simply be noted that this diagram by itself is consistent with *either* an intrinsic or an extrinsic origin for the polarization. No conclusions can be drawn about the evolution of a polarization mechanism associated with the newly formed stars. Individual sources will be discussed in more detail later.

If the polarization is produced by a dichroic dust medium it is possible, although not necessary, that a relationship between P and one or all of $\tau_{9.7}$, $\tau_{3.1}$ and A_v would exist, since the polarization is related directly to the extinction (equation II. 1 and accompanying text). In the hope of finding supporting evidence for

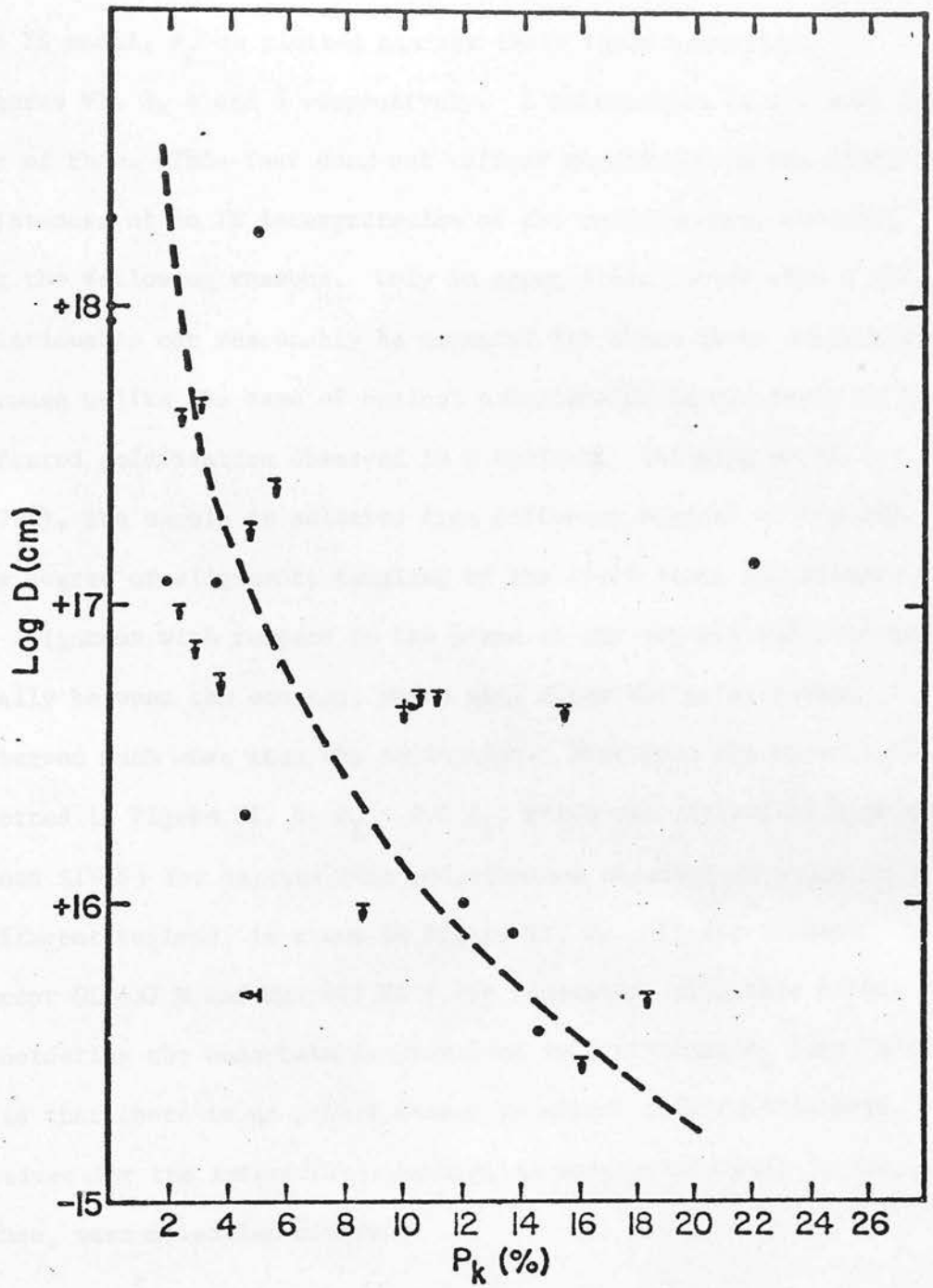

Figure VI.2 Plot of infrared source size against polarization.

the IS model, P_K is plotted against these three quantities in Figures VI. 3, 4 and 5 respectively. A correlation is not seen for any of them. This fact does not reflect negatively on the appropriateness of an IS interpretation of the polarization, however, for the following reasons. Only an upper limit rather than a firm relationship can reasonably be expected for these three comparisons, because unlike the case of optical polarization in clusters, or the infrared polarization observed in ρ Ophiuchi (Wilking et al. 1979a), the sample is selected from different regions of the sky. The degree of alignment, tangling of the field lines and orientation of alignment with respect to the plane of the sky can vary substantially between the sources, which will alter the polarization observed much more than the extinction. Therefore the upper limit plotted in Figure II. 8, $P_K < 0.6\ A_v$, which was derived by Dyck and Jones (1978) for interstellar polarization observed in stars in different regions, is shown in Figure VI. 5. All the sources except GL 437 N and Mon R2/IRS 1 are consistent with this limit, considering the uncertainties involved in estimating A_v (see below). Note that there is no priori reason to expect this relationship, derived for the interstellar medium, to extrapolate well to the dense, warm molecular clouds.

In addition to the randomization effect of observing sources in very different regions described above, $\tau_{9.7}$ and $\tau_{3.1}$ present other difficulties in interpretation. The 9.7 μm feature may be filled in somewhat by emission (Kwan and Scoville 1976, also see

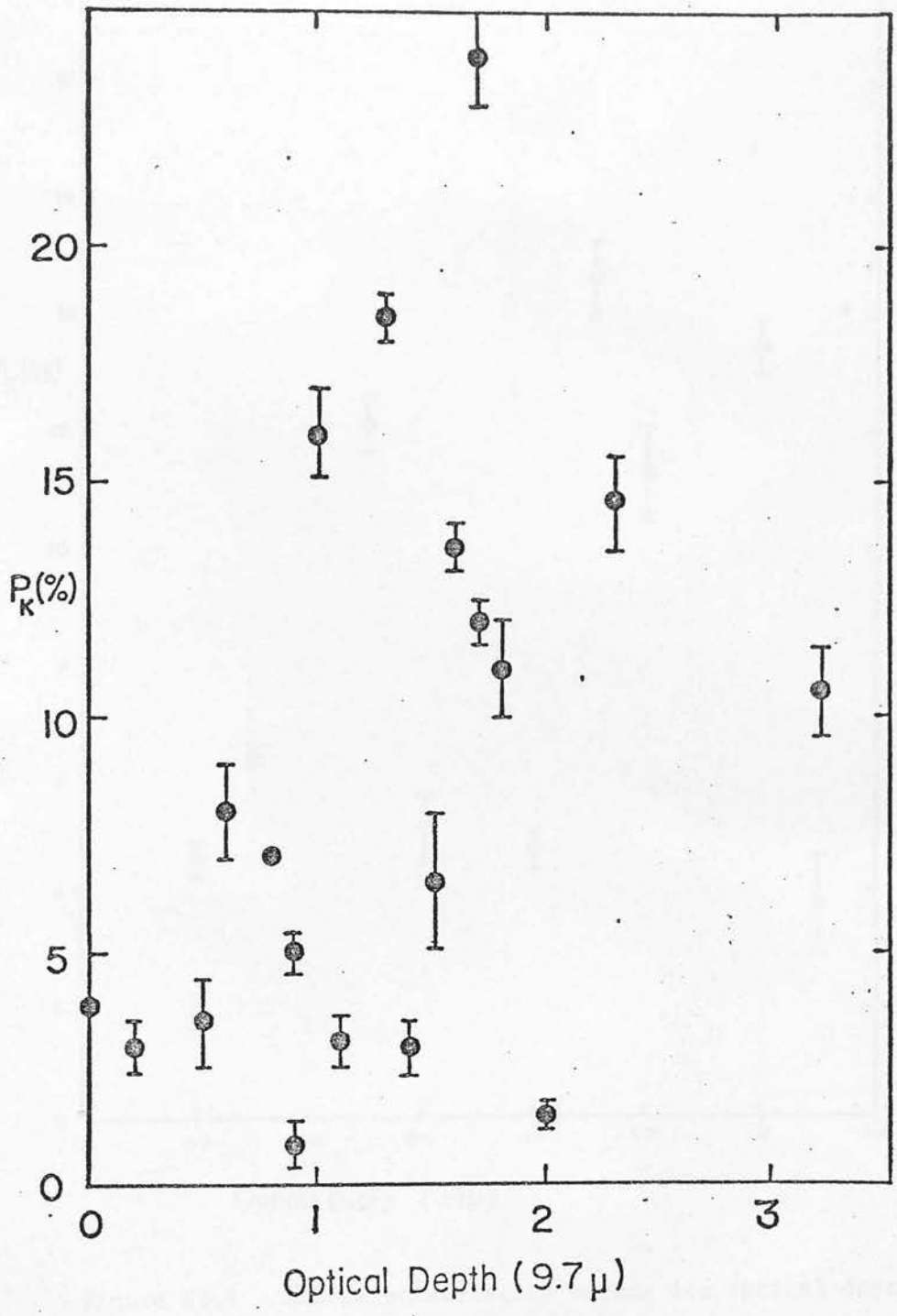

Figure VI.3 2.2 μm polarization versus silicate optical depth.

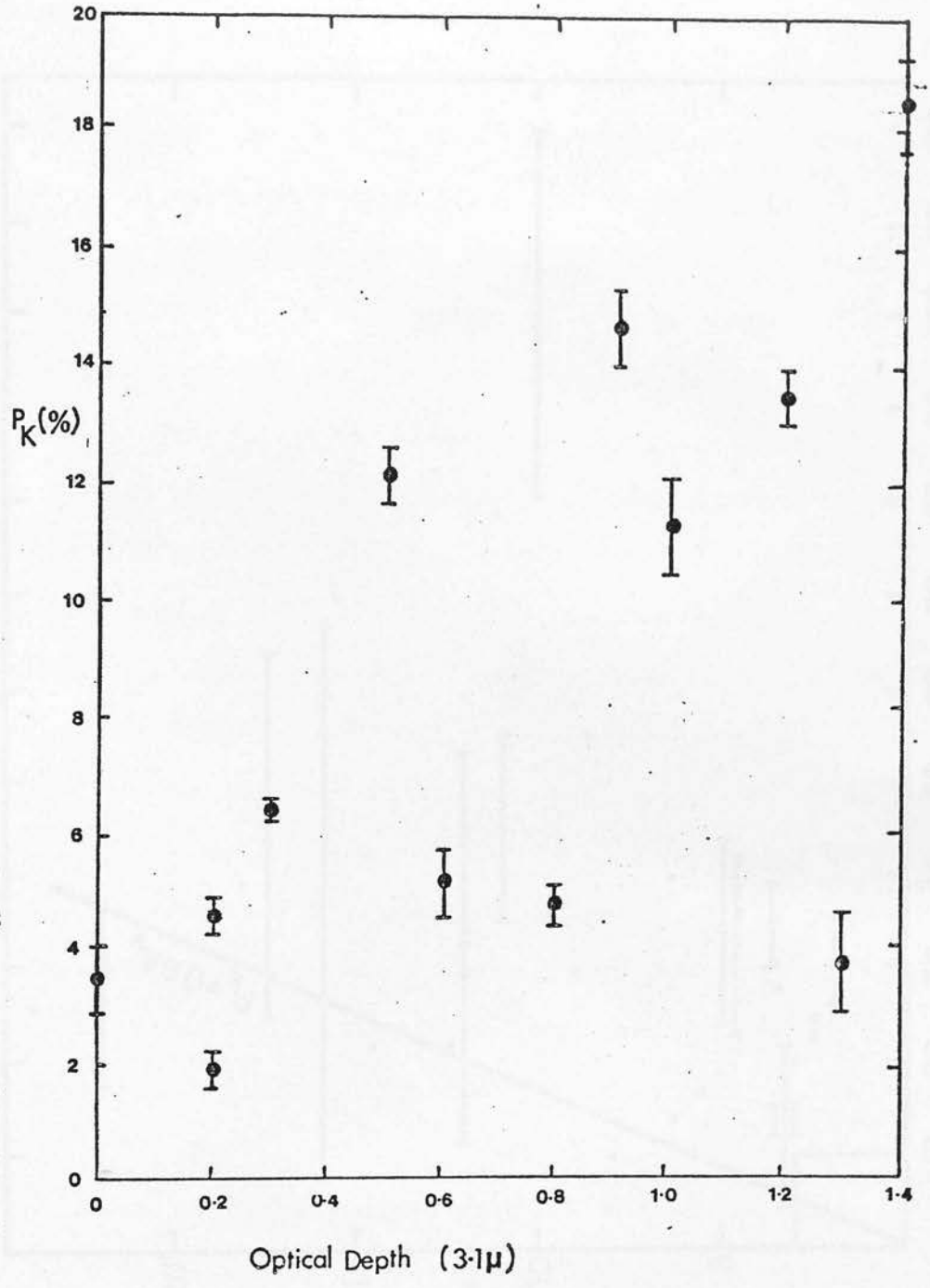

Figure VI.4 2.2 μm polarization versus ice optical depth.

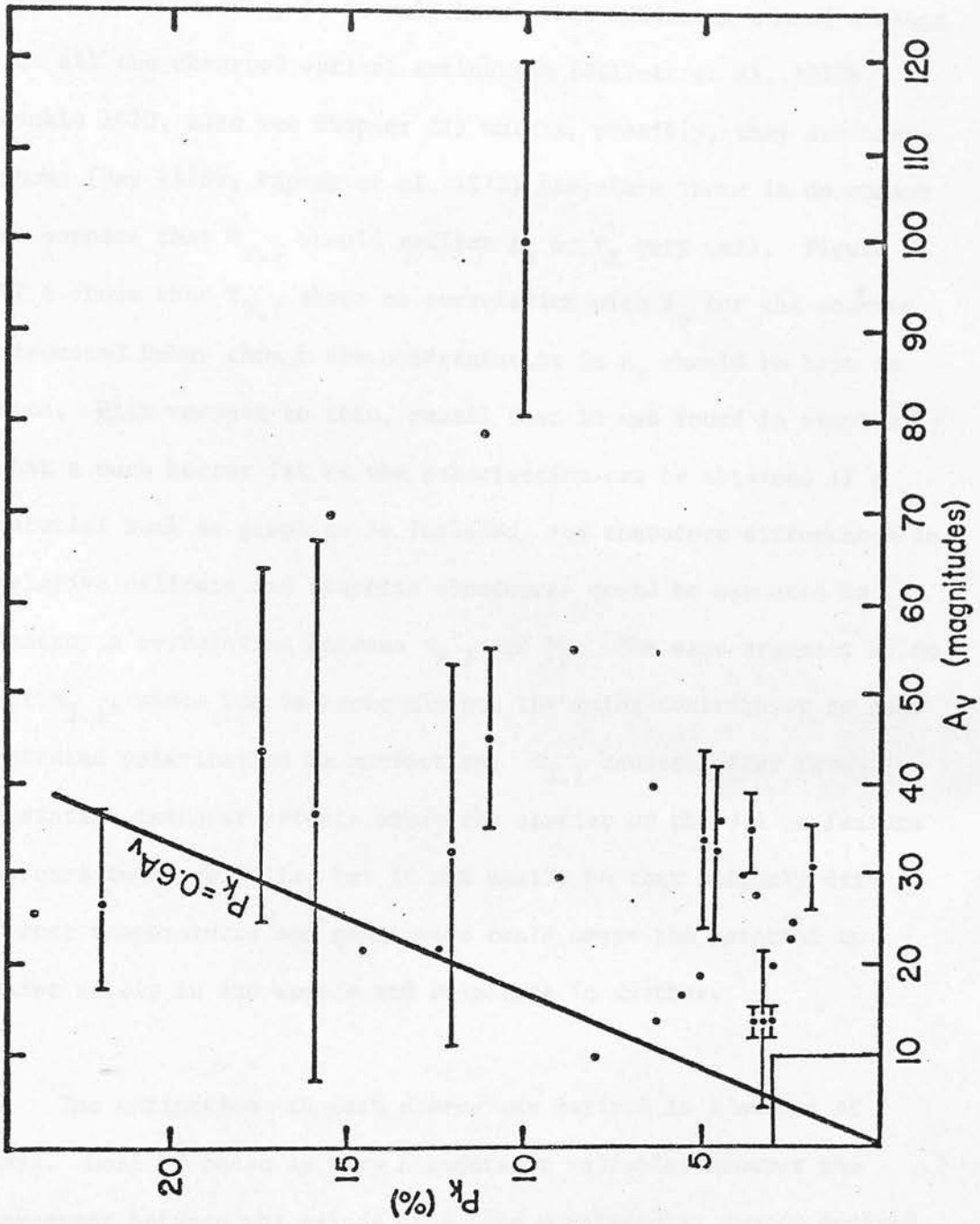

Figure VI.5 Extrapolation of the infrared interstellar polarization upper limit (Figure II.8) to the molecular cloud sources. The area corresponding to Figure II.8 is indicated by the small box on the bottom left.

Chapter II) so that $\tau_{9.7}$ may not be very representative of extinction. Besides this, it is well known that silicates cannot account for all the observed optical extinction (Gillett et al. 1975b, Kunkle 1979, also see Chapter II) unless, possibly, they are amorphous (Day 1976b, Pipher et al. 1978) therefore there is no reason to suppose that $\tau_{9.7}$ should reflect A_v or P_K very well. Figure VI.6 shows that $\tau_{9.7}$ shows no correlation with A_v for the sources discussed here, though the uncertainties in A_v should be kept in mind. With respect to this, recall that it was found in Chapter IV that a much better fit to the polarization can be obtained if a material such as graphite is included, and therefore differences in relative silicate and graphite abundances would be expected to destroy a correlation between $\tau_{9.7}$ and P_K. The same argument holds for $\tau_{3.1}$, since ice is certainly not the major contributor to near infrared polarization or extinction. $\tau_{3.1}$ cannot suffer from radiative transfer effects since the carrier of the 3.1 μm feature appears to be volatile, but it may easily be that slightly different temperatures and geometries could cause the material to exist safely in one source and evaporate in another.

The extinction to each source was derived in a number of ways. None of these is very accurate or reliable; however the agreement between the values of A_v for a particular source derived by different methods lends credence to them. The range of errors shown in Figure VI. 5 indicates the range of these different estimates. Since the nature of the underlying sources is usually

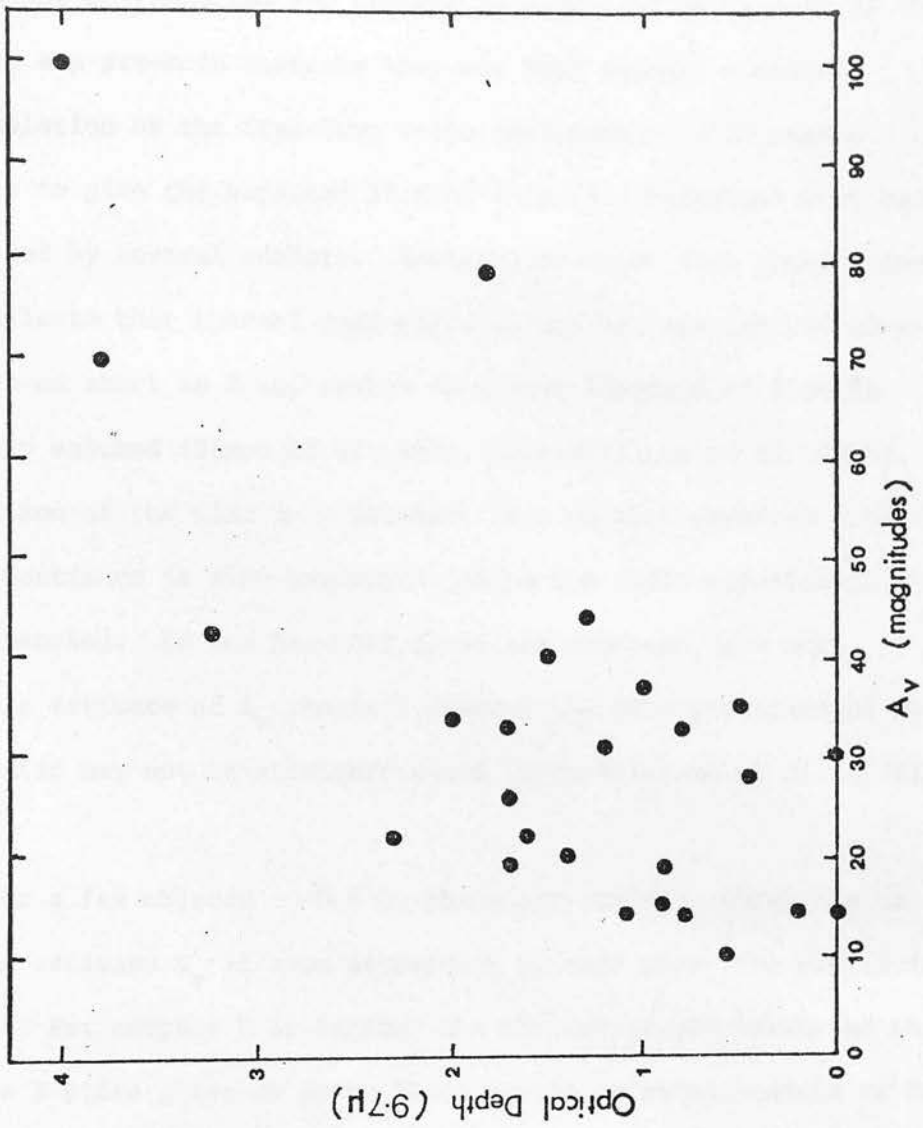

Figure VI.6 Direct comparison of the measured silicate optical depths of the molecular cloud sources with their estimated optical extinctions. The error bars have been omitted for clarity. The range of uncertainty in each quantity can be seen in Figures VI.3 and VI.5.

not known, de-reddening the spectra is hard. In particular if the sources are pre-main sequence they may have unusual spectra. Extrapolation of the free-free radio continuum of H II region sources to give the expected flux at 2 μm is a technique that has been used by several authors. However, Brackett line observations now indicate that thermal dust emission may be important at wavelengths as short as 2 μm, rather than just longward of 5 μm as normally assumed (Simon et al. 1979, Wynn-Williams et al. 1978). Comparison of the flux in a Brackett line to that expected from the radio continuum is also hazardous, since the radio emission may be self-absorbed. If two Brackett lines are observed, the most reliable estimate of A_v results; however the interpretation of even this ratio may not be straightforward (Wynn-Williams et al. 1978).

For a few objects 0.9 μm photometry exists, which can be used to estimate A_v if some assumption is made about the underlying source. For compact H II regions the absence of nebulosity on the Palomar E plate gives an upper limit to the emission measure of H which can be compared to the radio flux. This suffers from the possibility of self-absorption in the radio also and does not give a very stringent limit to A_v. The simplest way to estimate A_v is from the H-K colours of the sources, which are steeper than Rayleigh-Jeans curves. If it is assumed that the intrinsic spectra of the underlying sources are unlikely to be steeper than a Rayleigh-Jeans curve, then an interstellar extinction curve (e.g. the one derived by Becklin et al. 1978) can be used to de-redden the observed

spectrum. Extinctions derived in this way are upper limits, because the presence of dust emission would tend to redden the H-K colour, and also because the underlying objects may be cooler than the 5000°K of an object with an H-K colour of zero.

So far, the linear polarization data has been found to be consistent with the IS model developed in Chapter IV, but no positive supportive evidence for such a model has been forthcoming. Also no evidence to help in placing the relative location of the polarizing dust with respect to the source has emerged. As anticipated prior to making the observations (Chapter II), it is the study of circular polarization that has been most definitive in distinguishing between polarization models.

It was also anticipated that comparison of the linear polarization properties of different sources in a single complex may prove very informative. Five complexes in which more than one source has been detected appear in Table VI. 1 and 2. These sources, and also some of the single ones are discussed in more detail later; however some simple observations should be noted here first. The degrees of polarization observed in separate cluster members can vary quite a lot, as can the silicate optical depth and the visual extinction derived by the methods described above. However, it does not appear that even within clusters these quantities always vary together. In other words, not only the polarization but the polarization efficiency may not necessarily be constant

within a single complex. On the other hand, the position angles of the the sources tend to be *very similar* for objects in the same complex, with some exceptions (see later). Clearly it must be concluded that the manner in which the polarization is produced is strongly related in the multiple sources[1], even though the efficiency may be variable.

(3) The Galactic Magnetic Field as the Aligning Mechanism.

The most obvious mechanism to invoke to align the grains similarly throughout the sources is the Galactic magnetic field which is evidenced by optical interstellar polarization. In this case a similarity might be expected between the polarization of the infrared molecular cloud sources and nearby field stars. Kobayashi et al. (1978) looked for a correlation in the position angles of GL 490, GL 989, BN and GL 2591, and neighbouring field stars under the assumption that the molecular cloud field will inherit the same orientation as the interstellar field, as the cloud collapses. They found that the infrared position angles do indeed reflect the nearby interstellar field.

With the much larger polarization data set of molecular cloud sources now available, it is possible to look much more generally

1 This of itself is consistent with both an IS model and a model whereby scattering shells have a common orientation of asymmetry, left over from some pattern of their evolution.

at this correlation between the molecular clouds and the Galactic magnetic field. Therefore the analysis of Kobayashi et al has been repeated for the 19 regions with measurable polarizations, which are close enough to the sun for interstellar polarization data to be available. The optical polarization vectors of the field are illustrated for comparison to the molecular cloud sources in Figures VI.8-12. There exists a marked, statistically significant correlation between the infrared vector and the mean interstellar vector. This work has been published (Dyck and Lonsdale 1979) and the paper is attached at the back of the dissertation. Since publication, one additional source, NGC 7538/IRS 4, has been observed, and a few of the other sources were re-observed. The correlation is strengthened by the new data, and the new table of results is shown in Table VI.3. The correlation is shown in Figure VI.7. The description of each field remains the same as given in Dyck and Lonsdale (1979), therefore is not repeated in the text here. A larger sample of field stars expected to bracket the distance to the infrared sources than used by Kobayashi et al (1978) is plotted, by use of the extensive Hall (1958) catalogue, which was presumably not available to the Japanese authors. It was also possible to restrict the sample to stars with reasonably large optical polarization, for which position angles are more reliable than some of the stars with small polarizations used by Kobayashi et al. Polarimetry of field stars was also taken from Breger (1976), Vrba, Strom and Strom (1976), Mathewson and Ford (1970), Klare and Neckel (1977) and Hoag and van P. Smith (1959). All field stars within the adopted distance and polarization ranges which lie within the fields shown in Figures VI.8-12 have been plotted.

Table VI.3

Polarization data for infrared sources and nearby stars. Unless noted P_{IR} and θ_{IR} are 2.2 μm data.

Source	d(kpc)	$P_{IR}\pm\varepsilon$(%)	θ_{IR}(°)	θ^{G}_{IR}(°)	$\theta_{*}\pm$ rms(°)	$\theta_{IR}-\theta_{*}$(°)	$d_{min}-d_{max}$	P^{min}_{visual}(%)	Notes
W3/IRS 1	3.1	5.0±0.6	140	118	109±8	31	2.5-3.8	2.8	
W3/IRS 5	3.1	10.1±0.2	84	62	109±8	-25	2.5-3.8	2.8	1
W3/IRS 9	3.1	2.4±0.6	90	66	109±8	-19	2.5-3.8	2.8	
IC 1848A/IRS 1	1.7	2.9±0.4	11	162	116±5	75	1.2-2.2	2.2	
GL 437 W	3.0	8±1	104	72	118±3	-14	2.3-3.6	3.1	
GL 437 N	3.0	24±1	89	57	118±3	-29	2.3-3.6	3.1	
GL 437 S	3.0	3.2±0.5	141	109	118±3	23	2.3-3.6	3.1	
GL 490	1.4	6.3±0.9	115	80	116±7	- 1	0.9-1.9	3.0	2
S 228	1.0	5.6±1.8	6	131	160±17	28	0.5-1.7	1.0	
OMC 1/IRS 1	0.5	18.4±0.6	115	55	109±22	6	?	2.1	
OMC 1/IRS 2	0.5	10.8±1.0	136	76	109±22	27	?	2.1	
OMC 2/IRS 3	0.5	3.8±0.3	124	62	109±22	15	?	2.1	
Mon R2/IRS 1	0.95	22±2	161	98	170±20	- 9	0.5-1.5	1.0	
Mon R2/IRS 2	0.95	16.0±1	160	97	170±20	-10	0.5-1.5	1.0	
Mon R2/IRS 3	0.95	5.1±0.6	161	98	170±20	- 9	0.5-1.5	1.0	3
S 255/IRS 1	1.0	14.6±0.9	150	89	171±6	-21	0.5-1.5	2.1	
GL 989	0.8	3.7±0.9	117	55	172±19	-55	0.3-1.3	1.0	2
ρ Oph #29	0.2	6.4±1.6	28	77	37±16	- 9	0.2	2.2	
NGC 6334/IRS 1	0.7	8.6±1.3	105	160	180±17	-75	0.4-1.2	2.0	
IR 12.4+0.5	1.8	3.6±0.7	106	171	116±31	-10	1.2-2.4	2.0	
W 33(A)	4.4	15.6±0.8	68	129	84±19	-16	3.2-4.9	1.2	
M 17/KW IRS	1.8	4.5±0.3	32	93	176±8	36	1.8	2.0	
G 45.1+0.1	5	3.0±0.4	174	54	-	-	-	-	
W 51/IRS 2	6.5	4.7±0.3	130	10	-	-	-	-	
K 3-50/IRS	8	1.9±0.2	67	123	-	-	-	-	
S 106/Source 3	2.3	2.3±0.6	47	99	58±9	-11	1.8-2.8	1.9	
GL 2591	1.5	12.0±0.4	171	43	40±31	-49	1.0-2.0	2.0	
W 75/IRS 1	1.5	2.5±0.6	120	170	43±27	77	1.0-2.0	2.0	
S 140/IRS 1	0.9	13.7±0.5	70	102	86±17	-16	0.5-1.5	2.0	
NGC 7538/IRS 1	4.9	10.5±0.8	69	89	60±15	- 9	4.2-5.6	1.8	
NGC 7538/IRS 9	4.9	11.1±1.0	161	1	60±15	-80	4.2-5.6	1.8	
NGC 7538/IRS 4	4.9	6.2±0.4	68	88	60±15	- 8			

Notes: 1. Infrared P and θ are 3.8 μm data. 2. Infrared polarimetry from Kobayashi et al. (1978).
3. Infrared P and θ are 1.65 μm data.

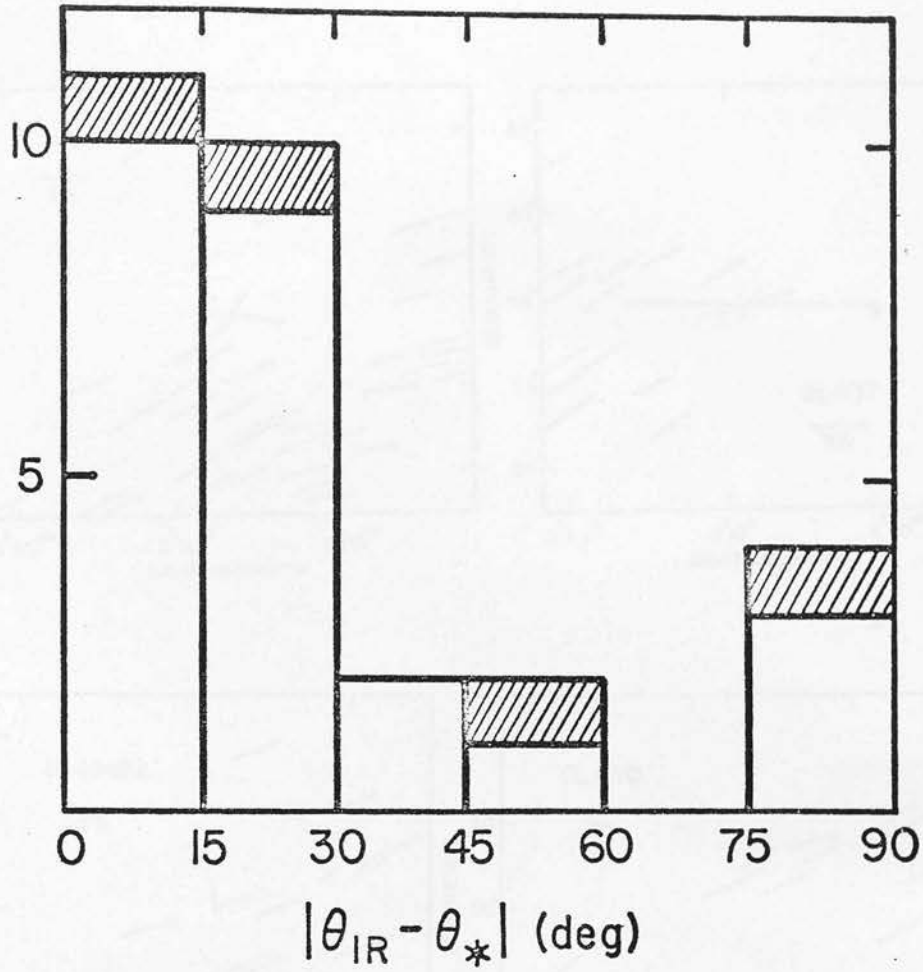

Figure VI.7 Correlation between the position angles of polarization of the infrared sources and optical interstellar polarization. The shaded areas represent fields in which the polarization direction is poorly determined.

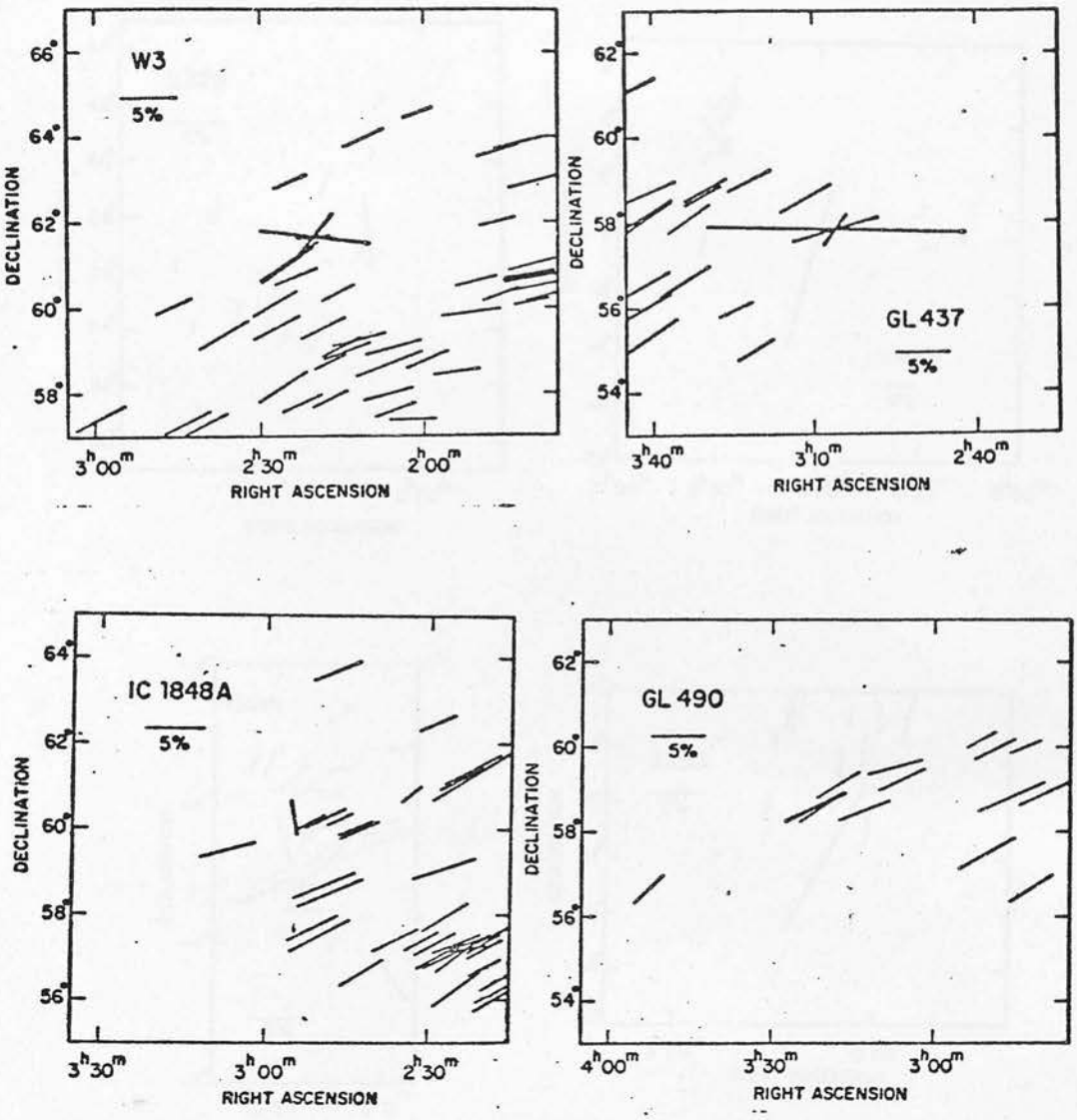

Figure VI.8 Infrared polarization measurements of sources in W3, GL 437, IC 1848 A and GL 490 (heavy lines) compared with nearby optical interstellar polarization. The length of the line is proportional to the percent polarization, and the orientation is that of the electric vector on the sky.

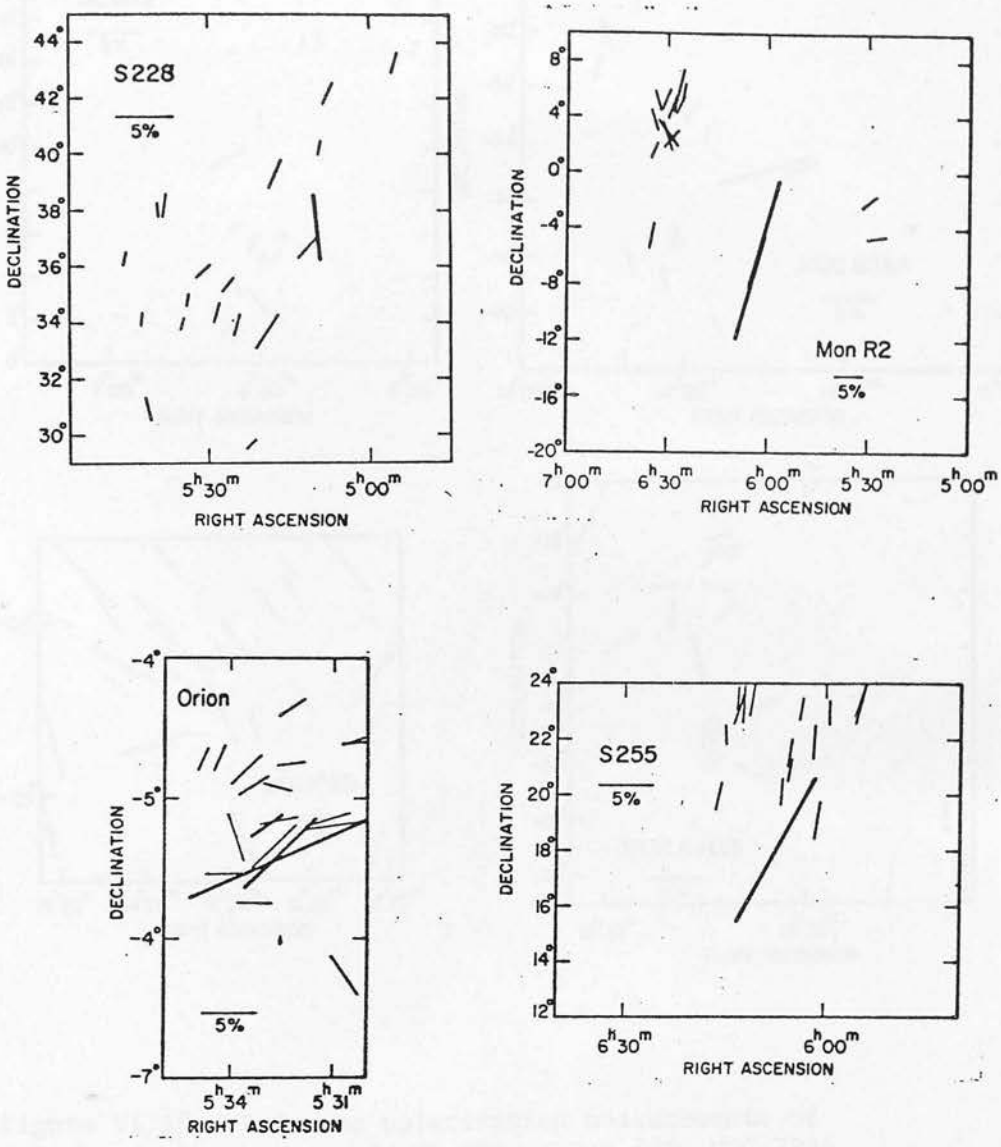

Figure VI.9 Infrared polarization measurements of sources in S228, Orion, Mon R2 and S255 (heavy lines) compared with nearby optical interstellar polarization. The length of the line is proportional to the percent polarization, and the orientation is that of the electric vector on the sky.

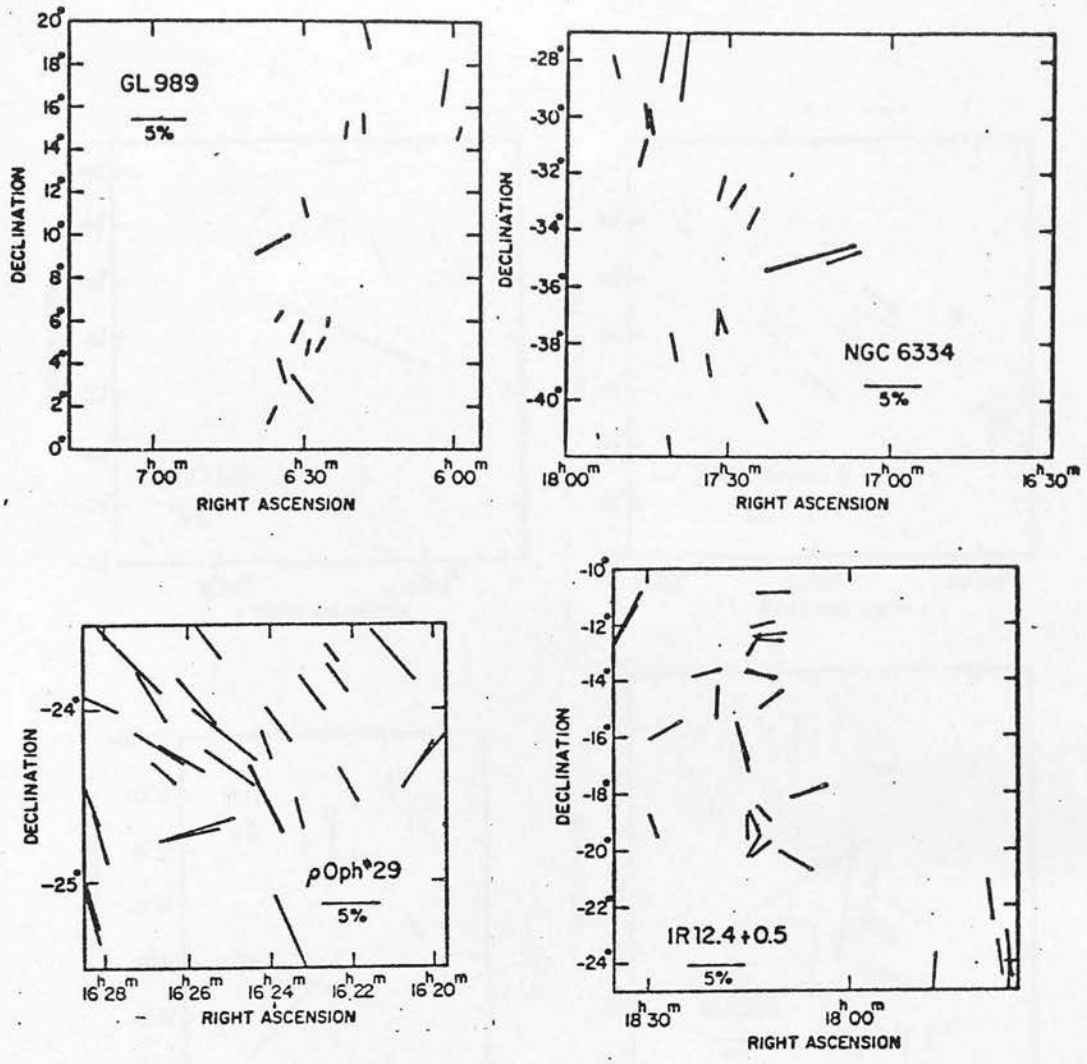

Figure VI.10 Infrared polarization measurements of sources in GL 989, ρ Oph #29, NGC 7334 and IR 12.4 + 0.5 (heavy lines) compared with nearby optical interstellar polarization. The length of the line is proportional to the percent polarization, and the orientation is that of the electric vector on the sky.

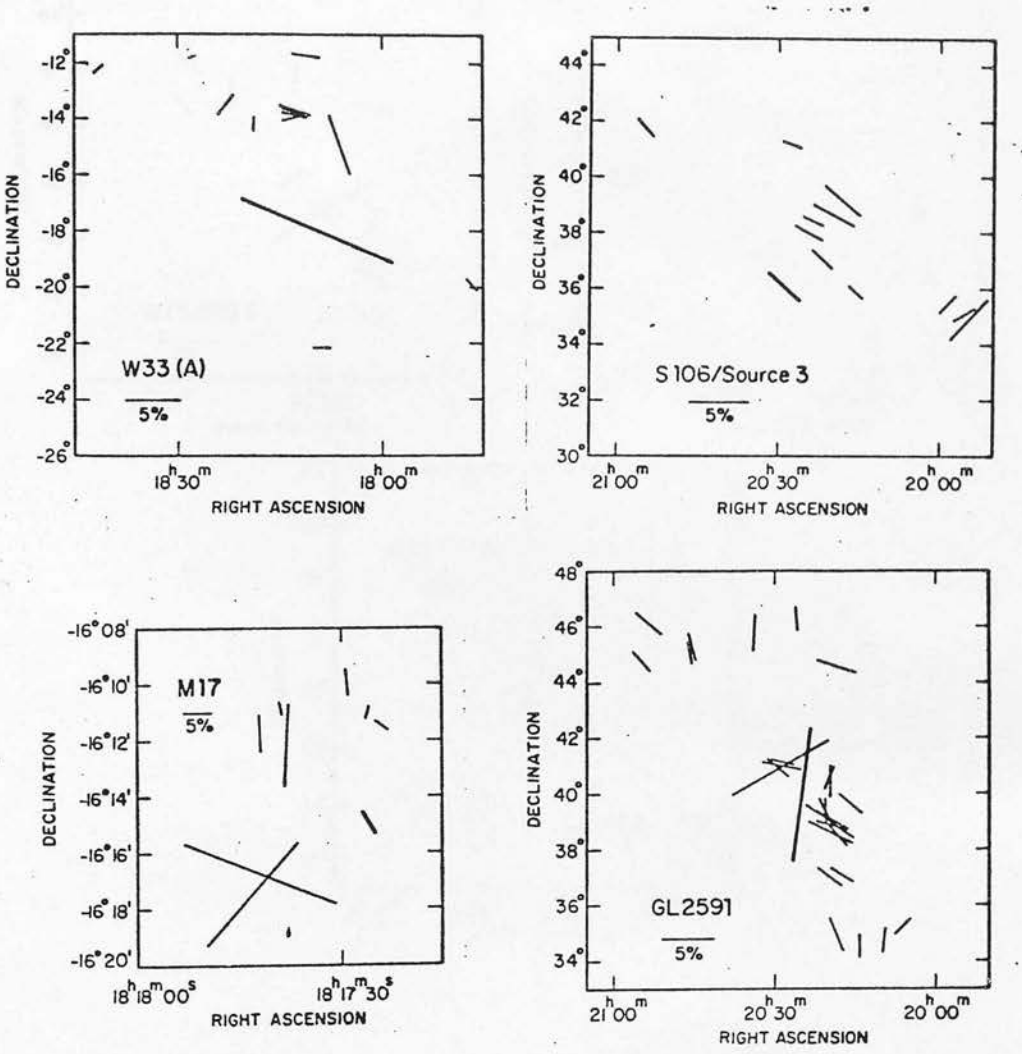

Figure VI.11 Infrared polarization measurements of sources in W33 A, S106, M17 and GL 2591 (heavy lines) compared with nearby optical interstellar polarization. The length of the line is proportional to the percent polarization, and the orientation is that of the electric vector on the sky.

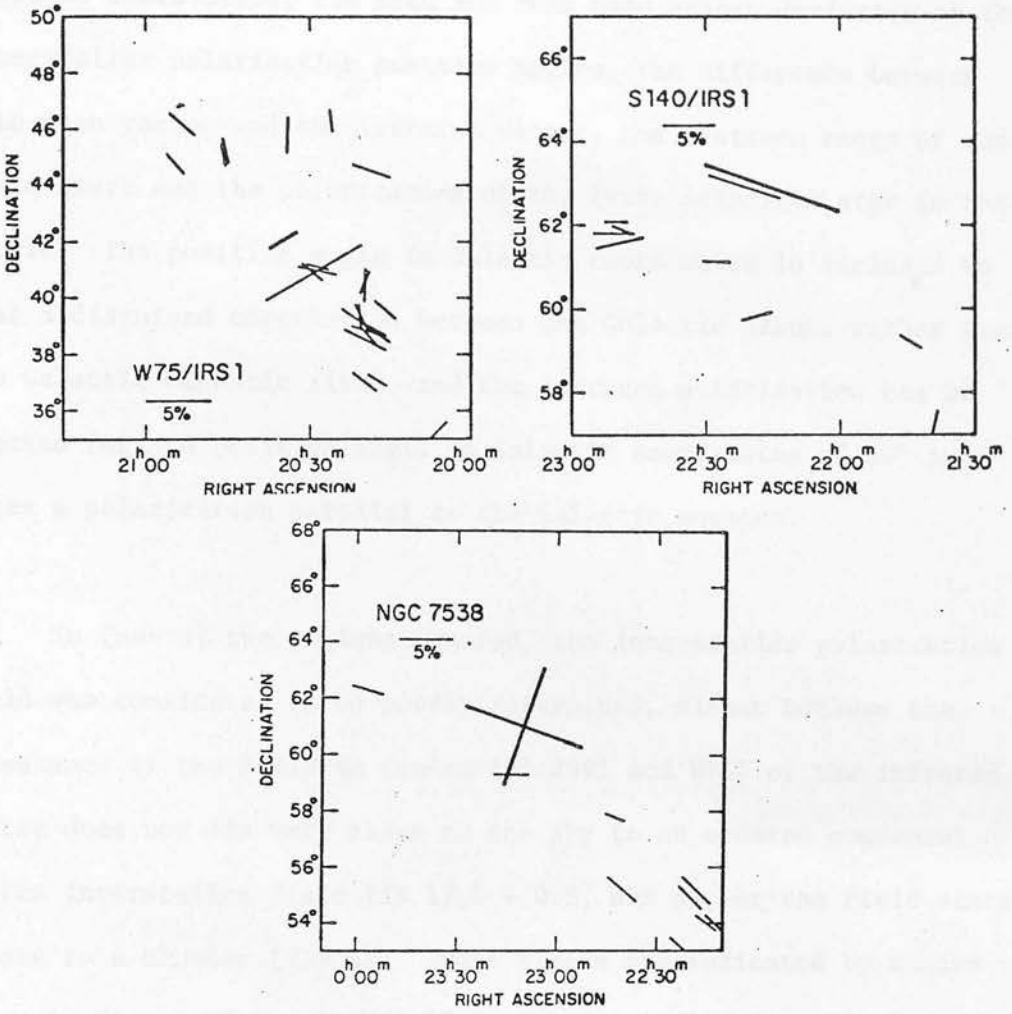

Figure VI.12 Infrared polarization measurements of sources in W75, S140 and NGC 7538 (heavy lines) compared with nearby optical interstellar polarization. The length of the line is proportional to the percent polarization, and the orientation is that of the electric vector on the sky.

Table VI.3 indicates the distance of each source, the degree and orientation of infrared polarization in both equatorial and Galactic coordinates, the mean and root mean square deviation of the interstellar polarization position angles, the difference between this mean vector and the infrared vector, the distance range of the field stars and the polarization of the least polarized star in the sample. The position angle in Galactic coordinates is included so that a disguised correlation between the Galactic plane, rather than the Galactic magnetic field, and the infrared polarization can be checked for. A position angle in Galactic coordinates of 90° indicates a polarization parallel to the Galactic equator.

In four of the regions studied, the interstellar polarization field was considered to be poorly determined, either because the appearance of the field is random (GL 2591 and W75) or the infrared source does not lie very close on the sky to an ordered component of the interstellar field (IR 12.4 + 0.5, W33 A), or the field stars belong to a cluster (W33 A). These fields are indicated by shaded boxes in Figure VI.7. In NGC 7538, IRS 4 coincides so closely with IRS 1 in position angle that only two vectors appear in the figure. Figure VI.13 illustrates the same information as presented in Figures VI.8-12 in histogram form.

It is evident from the appearance of Figures VI.7-13 that there is a strong correlation between the infrared position angle and the mean interstellar position angle. A chi-squared test indicates that there is a probability of less than 10^{-3} that the distribution of

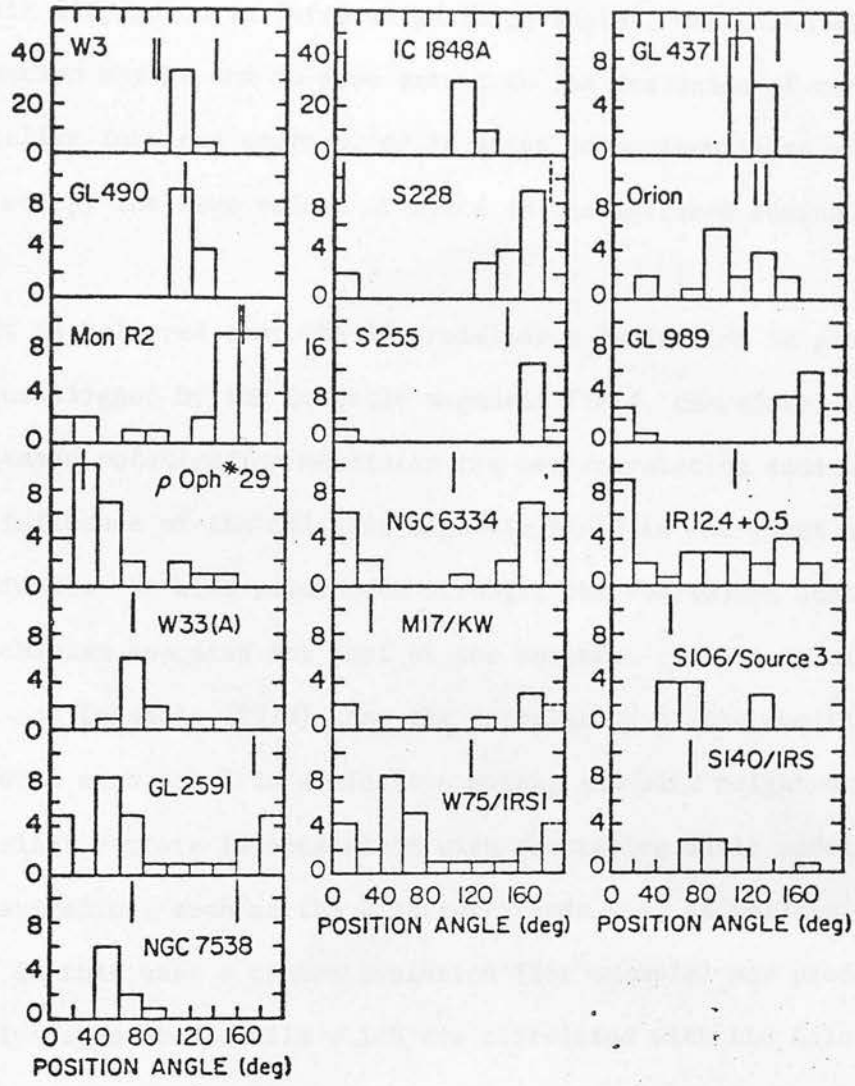

Figure VI.13 Histograms of the distribution of optical interstellar polarization angles compared with the position angle of infrared polarization (shown as vertical lines) for the sources discussed in the text.

position angles illustrated in Figure VI.7 is random. Besides the intrinsic dispersion in infrared position angles, the width of the distribution may be due to some extent to the inclusion of non-protostellar infrared sources, or to using comparison stars which do not occupy the same volume of space as the infrared source.

It is believed that the interstellar polarization is produced by grains aligned by the Galactic magnetic field, therefore, *whatever the infrared polarization mechanism* the new correlation indicates a strong influence of the Galactic magnetic field in the giant molecular clouds. It also reinforces strongly the conclusion that the same mechanism operates for most of the sources. It was pointed out in Dyck and Lonsdale (1979) that the correlation of the position angles with each other in a single complex, and with neighbouring interstellar vectors is consistent with scattering shell models for the polarization, such as the Elsässer-Staude one, as well as an IS model. In this case a common evolution (for example) may produce similarly orientated shells which are correlated with the Galactic magnetic field or the plane of the Galaxy. In light of the observations and interpretation of the circular polarization presented here, these possibilities are no longer as plausible as the interpretation that the correlation suggests a common alignment of grains both within the molecular clouds and in the nearby interstellar medium. An independent test of this hypothesis would be to repeat the analysis described above for the infrared polarization vectors of the molecular cloud sources, for *known* bipolar nebulae which have available polarimetry. Unfortunately the sample is so small that

the analysis is not very meaningful. In addition, the interpretation is seriously prejudiced by the fact that the evolutionary status of several of these objects is in question. Some, e.g. R Mon, are enveloped in cool dust, which is interpreted by Harvey et al (1979) as evidence of their recent formation, while others, e.g. GL 618, are interpreted as preplanetary nebulae. In this case there is less reason to suppose that the nebulae would reflect the magnetic field or the Galactic plane.[1] Of the six nebulae with polarization observations $\theta_{NEB} - \langle\theta*\rangle$ ranges from 7 to 67 with $\Delta < 30°$ and $\Delta > 50°$. There is clearly no support for the ES model from this, though as previously noted there is no especial reason to expect any.

There remains, however, the possibility that the correlation is caused by some other mechanism than the Galactic magnetic field. The most likely alternative is that the correlation arises by some influence of Galactic differential rotation rather than the magnetic field, and that it is in fact a correlation with the Galactic plane. It is important to ask this question, even though it is not obvious how such a correlation between the plane and the infrared polarization, such that the infrared vectors are parallel to the plane, could arise. In regions where the interstellar polarization field is well defined but does not align with the Galactic plane, this hypothesis can be tested, by comparison of the plane, the interstellar polarization and the infrared vector. The infrared vectors lie between the

1 Though note that it has been suggested that there is an alignment of planetary nebulae with the Galactic plane (Melnick and Harwit 1975).

plane and the field in Orion, Mon R2, NGC 6334 and S140. In S255, M17 and GL 989 the vector is closer to the plane than the field and in S106 and S228 it is closer to the field. In seven regions in which the interstellar field is either not well defined or cannot be found because the infrared sources lie beyond the range of the polarization catalogues, the infrared vectors of four lie at greater than 40° to the plane, and two are nearly orthogonal to it. The remaining source lies at 33° to the plane. Thus out of 16 sources with interstellar polarization fields not parallel to the plane, three show a preference for the plane rather than the field. Rotations of the individual clouds can also be looked for as a test of the Galactic plane correlation hypothesis. Of the three sources with a preference for the plane only for GL 989 has evidence been found for rotation of the cloud in which it is embedded, NGC 2264 (Crutcher et al 1978). Radio velocity data is hard to interpret, however rotations have also been inferred in several other clouds. These are GL 437 (Schneps et al 1978), Orion (Kutner et al 1977), Mon R2 (Loren 1977), W3 (Brackman and Scoville 1978) and S106 (Lucas et al 1979). GL 437, W3 and Mon R2 appear to rotate about axes perpendicular to the axis of Galactic differential rotation, and Orion, if the velocity interpretation is correct, rotates in the opposite sense to differential rotation. The rotation axis of S106 lies along the axis of the visible nebula but does not coincide with the infrared vector. Observations of several other clouds have been made but no rotations are apparent.

It thus seems clear that there is no reason to suppose that

the infrared polarization/mean interstellar polarization position angle correlation is a disguised correlation between the infrared vector and the Galactic plane. Therefore it is concluded that the original hypothesis is in fact the most plausible one: the correlation is between the infrared polarization and the interstellar magnetic field.

(4) Some Interesting Sources.

It has been remarked earlier that the linear polarization data is consistent with the IS model developed in Chapter IV, but adds no evidence in support of it. The data has been found to be very informative, however, in the discovery of the correlation with the Galactic magnetic field. The IS model and the correlation then continue to produce a scenario in which the Galactic magnetic field permeates the dense, star forming molecular clouds, aligning the grains in a similar orientation within the clouds as in the interstellar medium. This scenario applies to all the sources for which the correlation exists, not only those for which circular polarization has been observed.

The implications of the picture are returned to in Chapter VII. In the remainder of this chapter some particular individual sources with interesting characteristics are discussed briefly.

Six sources in Table VI.3 show infrared position angles which differ by 40° or more from the mean vector of the field stars. Of

these W75 and GL 2591 lie in a direction in the Galaxy, Cygnus, where the polarization field is very confused, presumably because of, for example, disorder of the magnetic field along the line-of-sight. Little can therefore be said about the discrepant values of $\theta_{IR} - \langle\theta_*\rangle$ of these sources, beyond noting that they are poorly determined.

The distance to IC 1848 A is uncertain (Osterbrock 1956), therefore the field stars may not lie at the same distance as the source. There is also an indication of nebulosity on the Palomar plates at the position of the infrared source (Loren and Wootten 1978) and the two fainter sources nearby (Beichman 1979), but it is unclear whether there is any association of the nebulosity with the infrared source. The depth of the silicate feature and the estimate of the optical extinction would imply that the source is relatively obscured. The appearance of the nebulosity is reminiscent of bipolar or cometary nebulae (Cohen and Lewis 1978), such as the one also found near GL 989, Allen's source in NGC 2264 (Allen 1972). This source is also highly obscured but the infrared position angle, as in the case of IC 1848 A does not correspond to the mean interstellar field. The association of the nebula with GL 989 is clearer than in the case of IC 1848 A, but again the infrared position angle bears no obvious relationship to the apparent geometry. Both of these objects are clearly associated with regions of likely recent star formation (Loren and Wootten 1978, Harvey et al 1977, Crutcher et al 1978) and are quite likely to be pre-main sequence stars (Beichman 1979, Thompson and Tokunaga 1978). It is possible that the infrared

polarization from these objects arises to some extent from scattering in the nebulosity.

For the remaining two objects for which $\theta_{IR} - \langle\theta_*\rangle$ is quite large--NGC 6334/IRS 1 and NGC 7538/IRS 9--such a mechanism seems fairly likely. In the case of these objects, maps of the near vicinity of the compact sources at short infrared wavelengths reveal extended emission which becomes bluer with increasing distance from the compact source, which is strongly suggestive of reflection nebulosity (Becklin and Neugebauer 1974, Werner et al 1979). The position angle of infrared polarization is shown superimposed on these maps in Figure VI.14. It is striking in the case of NGC 7538/IRS 9 that the angle is perpendicular to the ridge of the extended emission. It is well known that reflection nebulae and bipolar nebulae tend to be highly polarized in a radial pattern, such that the position angles at points in the nebula are perpendicular to radius vectors from the star (e.g. Hall 1967, Zellner 1974, Cohen and Kuhi 1977). This is the characteristic that led Elsässer and Staude (1979) to interpret the observations at 11 μm of Dyck and Beichman (1974) in KL as due to a reflection nebula. The angle observed in NGC 7538/IRS 9 may therefore be related to the ridge, reinforcing the interpretation of the extended flux as reflection nebulosity. The obvious way to confirm this suggestion is to observe the polarization of the nebulosity, therefore at 2 μm an observation was made at the point 20" south of IRS 9 marked as position B in Figure VI.14, with a 8" beam. Detection of polarization from this point was marginal, due to the faintness of the source, but a small

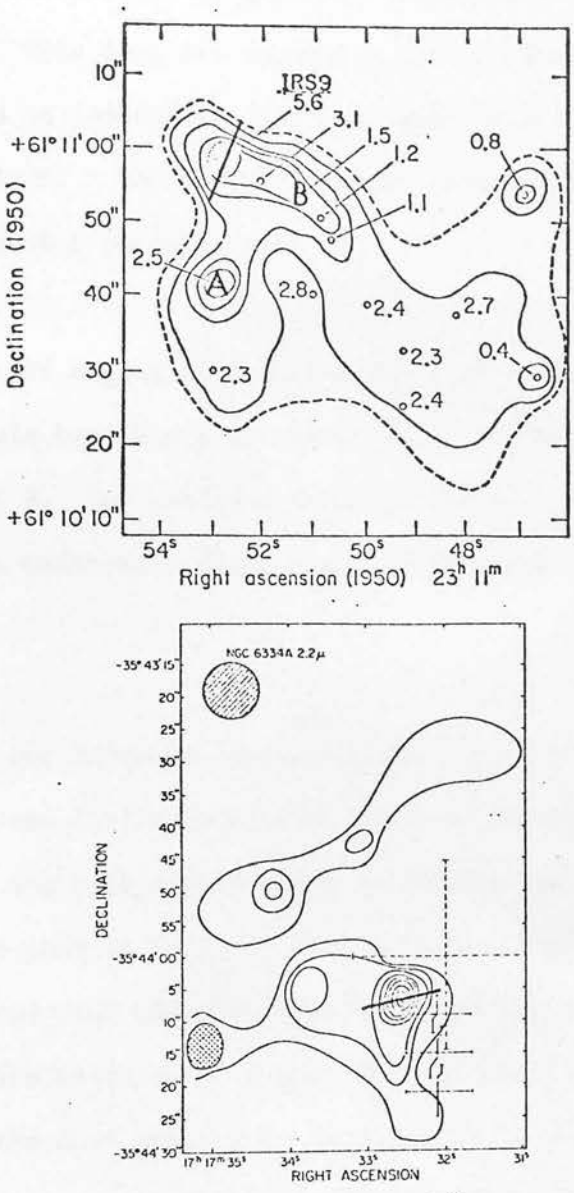

Figure VI.14 Infrared polarization vectors superimposed on the maps of:

a. NGC 7538/IRS 9 (Werner et al 1979, 2.2 μm map), and
b. NGC 6334 (Becklin and Neugebauer 1974).

degree of polarization was observed (3 ± 1.5%) with a position angle of about 100°. This marginal detection has in fact been confirmed, and in addition an observation has been made at point A, by Tokunaga and Lebofsky (1979). The polarization at this point is large (16.5 ± 2.5%) with a position angle of 153°.

The position angles of points A and B are consistent with the reflection nebula hypothesis if the illuminating source is at the position of IRS 9. The position angle of IRS 9 itself, however, is then hard to understand without a very peculiar illuminating geometry.

Evidence for infrared scattering has also been found for S228. Frogel and Persson (1973) found that the flux becomes bluer in larger apertures. No map exists with which to compare the infrared position angle, but note that it lies 28° from the mean interstellar position angle. Scattered flux has also been suggested as the origin of the ridge of emission between IRS 3 and IRS 1 in OMC 2 (Gatley et al 1974) because the dust appears to be too cold to emit at 2 μm. However, in this case the infrared position angle shows no relationship to the ridge and is very close to the interstellar position angle (Figure VI.15). In all the other sources for which there are near infrared maps or plates of the surrounding region there is no direct indication of reflection nebulosity, or that the position angle of infrared polarization bears any relation to extended emission. These include S140 (Dinerstein et al 1979, Beichman et al 1979), W3 (Wynn-Williams et al 1972), GL 437 (Kleinmann et al 1977),

S255 (Beichman et al 1979) and Mon R2 (Beckwith et al 1976). These maps with the infrared vectors superimposed are shown in Figures VI.16-17.

Another object of interest, in particular with regard to the possibility of polarization by the reflection nebula mechanism, is S106/IRS 3. S106 is an optically visible Hα knot which resembles a bipolar nebula strongly. IRS 3 was discovered by Sibille et al (1975) between the two lobes, and has been interpreted as the energy source for the three nearby compact H II regions (Pipher et al 1976) as well as the optical lobes. The infrared position angle is illustrated in Figure VI.17 which shows the nebulosity and the compact H II regions. The rotation axis found by Lucas et al 1978 coincides with the optical axis. The position angle coincides with the nearby interstellar field and bears no precise relation to the source geometry as might be expected if IRS 3 illuminated the lobes. However, the beam used for the IR polarimetry is much smaller than the nebulosity, and it might be expected that if IRS 3 were behind an obscuring disc of a bipolar nebula the infrared polarization may arise by scattering in the disc and therefore show an angle approximately parallel to the optical axis, as is observed.

Studies of infrared reflection nebulosity are important for the understanding of infrared grain properties. However, interpretations of polarization studies of reflection nebulae are complicated by the uncertainty in the albedo and phase function of grains even at optical wavelengths (Nandy and Wickramasinghe 1972), and in the infrared

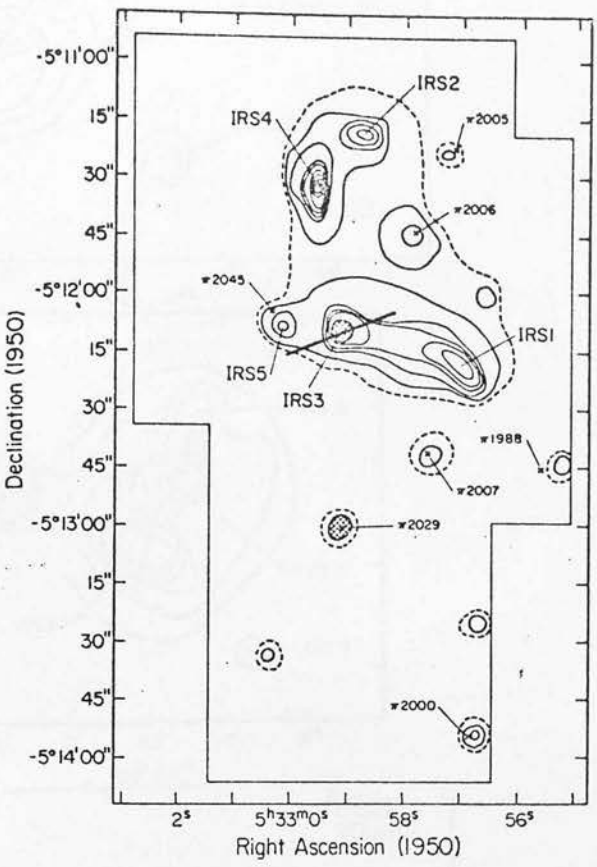

Figure VI.15 Infrared polarization vector of IRS 3 superimposed on the 2.2 μm map of OMC 2 (Gatley et al 1974). The magnitude of the polarization is not indicated.

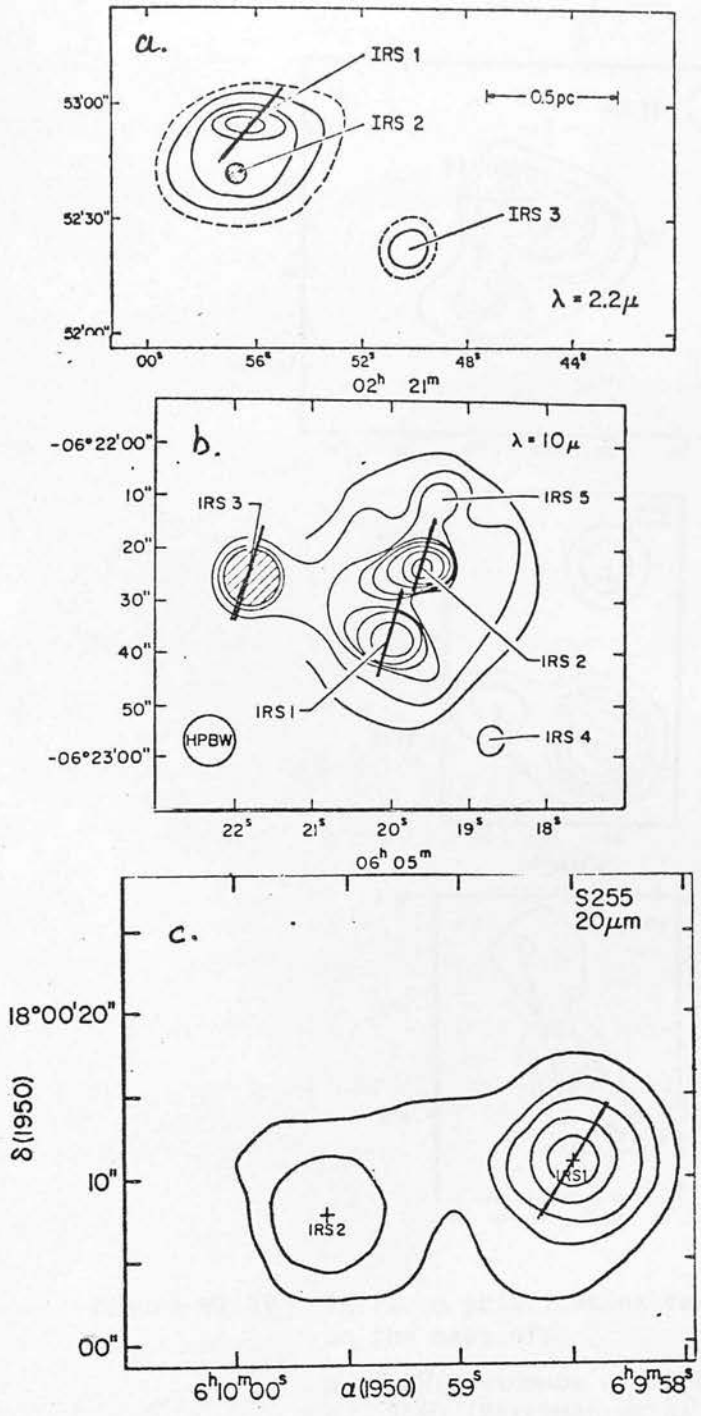

Figure VI.16 Infrared polarization vectors superimposed on the maps of:

a. W3 (Wynn-Williams et al 1972),
b. Mon R2 (Beckwith et al 1976) and
c. S255 (Beichman et al 1979).

The direction of polarization only is marked, not the magnitude.

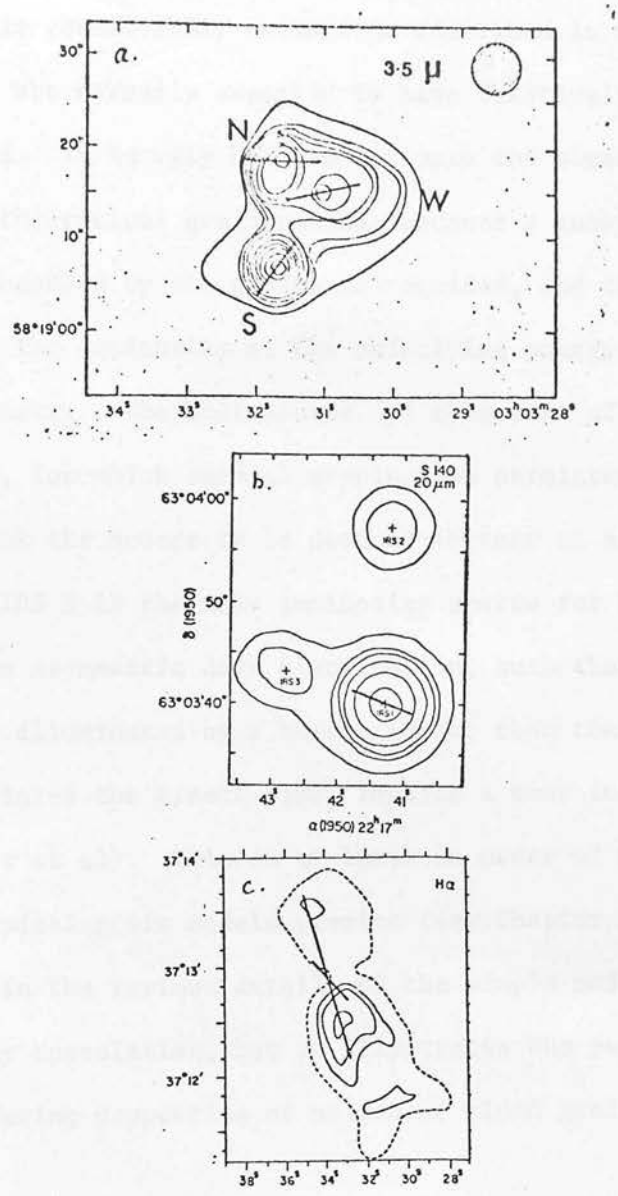

Figure VI.17 Infrared polarization vectors superimposed on the maps of:

a. GL437(Kleinmann et al 1977),
b. S140 (Beichman et al 1979) and
c. S106 (Hα map of Pipher et al 1976).
The rotation axis is also shown (longer of the two lines (Lucas et al 1979)).

The direction of polarization only is marked, not the magnitude.

the situation is considerably worse. As described in Chapter IV, typical grains are normally expected to have relatively low albedos in the infrared. It is very hard to estimate the observed albedo for comparison to theoretical grain models, because a knowledge of the total energy absorbed by the grains is required, and this relies upon a knowledge of the luminosity of the underlying energy source(s) and the source geometry. The best source for this sort of analysis is NGC 7538/IRS 9, for which careful mapping has permitted some details of the nature of the source to be deduced (Werner et al 1979). Assuming that IRS 9 is the sole luminosity source for NGC 7538 E, a model with an asymmetric dust distribution, such that the reflection nebula is illuminated by a hotter object than the foreground dust which radiates the direct flux, implies a near infrared albedo of ~0.1 (Werner et al). This is at least an order of magnitude larger than typical grain models predict (see Chapter IV). Uncertainties in the various details of the simple model make this analysis highly speculative, but it illustrates the possible importance of scattering properties of molecular cloud grains at infrared wavelengths.

The remaining sources listed in Table VI.3 all show position angles which are relatively close to the nearby interstellar polarization field, however two of them, GL 437 N and Mon R2/IRS 1, remain discrepant by possessing degrees of polarization too large for an IS mechanism, as illustrated in Figure VI.5. In GL 437 two of the sources, W and S, are visible optically (Kleinmann et al 1977). N is the reddest source at H and K, and possesses the deepest silicate

extinction (Table VI.1). Kleinmann et al (1977) mapped GL 437 at 3.5 μm (Figure VI.17) but no asymmetry which might be interpreted as evidence of a scattering nebula is visible to their resolution.

While the position angle of GL 437 N is sufficiently dissimilar to those of GL 437 S and W, and the nearby interstellar field, that a contribution from a scattering component similar to those suggested to exist in NGC 7538/IRS 9 and NGC 6334/IRS 1 is plausible, Mon R2 is more curious. In Mon R2 the position angles of all three sources agree exactly with each other, and also very closely with the interstellar field. In addition it is the presumably more evolved source--the extended H II region IRS 1--which has the largest degree of polarization. It is possible that the extinction to IRS 1 has been poorly estimated, or, since IRS 1 does not exceed the upper limit $P_K < 0.6\ A_v$ (Figure VI.5) by a large degree, that the polarization efficiency is particularly enhanced in this source. Alternatively, it may be that a scattering component in Mon R2/IRS 1 coincidently has the same orientation as the interstellar polarization, thereby enhancing it considerably.

It seems most likely that some combination of the first two alternatives is operating, especially in view of the fact that the "polarization efficiency criterion," $P_K < 0.6\ A_v$, is extrapolated to the dense regions of a molecular cloud from the interstellar medium, and in any case an error of only 5 magnitudes in A_v would be sufficient to eliminate the discrepancy. Such an error is within the estimated error in the extinction to Mon R2/IRS 1 (Figure VI.5).

As noted before, there is no empirical justification for extrapolating such a polarization efficiency law into the molecular clouds, where it has already been concluded that the alignment mechanism must operate under different conditions (dense, possibly $T_d \simeq T_g$) than in the interstellar medium (rare, $T_d << T_g$). If this interpretation is correct then the observations of Mon R2 may imply that the polarization efficiency in molecular clouds can be greater than found in the interstellar medium (subject to the uncertainty in A_v).

Perhaps the most interesting complex of sources that has been observed is NGC 7538, an optical H II region with several compact radio sources (Martin 1973) and infrared sources (Wynn-Williams et al 1974, Willner 1977, Werner et al 1979) associated with it. IRS 6, 7, 8 and 10 were not observed for polarization because they are probably reddened stars which may not even be associated with the complex (Wynn-Williams et al, Werner et al). IRS 2 is an extended H II region with no silicate feature, therefore it also was not observed. IRS 3 and 11 are potentially of interest but are too faint to observe for polarization. The remaining sources in the complex, IRS 1, 4, 5 and 9 have all been observed (this work, Dyck and Capps 1978, Dyck 1979). IRS 5 was found to be unpolarized, as noted earlier, and is likely to be at the centre of the optical nebula. IRS 9 has also been discussed above, and is probably a compact protostar surrounded by a reflection nebula.

NGC 7538/IRS 1 is an ultracompact H II region which is probably at a very early stage of evolution. It lies close on the sky to

IRS 2, a more evolved H II region. Downes and Wilson (1974) estimate from an interpretation of H_2CO 4.8 GHz emission line observations that a dense shell ($n_{H_2} > 10^5$ cm^{-3}) surrounds the infrared sources with a size 7×10^{17} cm $\lesssim d \lesssim 4.3 \times 10^{18}$ cm (at a distance of 4.9 kpc). Comparison of the GHz radio and the Brackett line flux shows that IRS 1 is much more obscured than IRS 2, in qualitative agreement with the relative silicate optical depths of the two sources (Willner 1977, Werner et al 1979). This means that much of the obscuration to IRS 1 probably arises within about 7×10^{17} cm of the source, consistent with the lower size limit from the H_2CO observations. The infrared source itself is unresolved on a scale 10 times smaller than this, and the 2 μm continuum flux is probably thermal dust emission, since the upper limit on the width of the Brackett γ line is an order of magnitude less than that expected from the plasma indicated by the radio flux (Werner et al).

The polarization data for IRS 1 is shown in Figure VI.1. The fall in degree of polarization between 1.65 μm and 2.2 μm is most probably due to dilution of the polarized flux of IRS 1 by the relatively unpolarized flux of IRS 2. The suggestion that IRS 2 is unpolarized is consistent with its identification with an optical knot of nebulosity (Habing et al 1972) on the Sky Survey, and with a 0.9 μm star (Beetz et al 1976), and the low obscuration derived from the Brackett lines and radio flux of 8.5 magnitudes (Werner et al).

IRS 4, on the other hand, is found to be quite highly polarized with a position angle very similar to that of IRS 1. It is probably

a compact H II region similar in nature to IRS 1 - 3 (Wynn-Williams et al 1974) although it has not been studied in any detail; in particular its size is unknown.

IRS 4 is of the order of 3 pc or more distant from IRS 1 - 3, therefore within the same complex there is direct evidence that the polarization mechanism operates well within the denser material associated with particular sources and also operates over distances within the molecular cloud an order of magnitude larger.

The same kind of situation is also observed in Orion and W3, although it is not so striking, since the position angles are not as similar to each other as in NGC 7538. The KL nebula is of a very similar absolute size as the implied dust concentration at IRS 1. Due to the relative proximity of Orion, polarization maps at 11.1 and 19.6 μm have shown that the dust is aligned throughout the nebula. OMC 2/IRS 3 is of a similar distance from KL as NGC 7538/IRS 4 is separated from IRS 1, with OMC 1/IRS 2 between the two, and all three are polarized in a similar orientation. In Orion, there is even evidence that one source, OMC 2/IRS 3, lies in a separate density peak to the other sources (Smith et al 1979).

In summary, it is known that the dust density increases towards the molecular cloud peaks where star formation is occurring, and therefore it is most likely that most of the extinction occurs in the central regions. There are also indications that the dust distribution may be clumpy and that some sources, e.g. NGC 7538/IRS 1 have

quite localised extinctions, but the relative amounts of molecular cloud and localised extinction are generally unknown. Other sources, e.g. NGC 7538/IRS 9 require asymmetric dust distributions in interpretation. The new polarization studies tend to reinforce these conclusions. In particular they indicate that the grains must be aligned in a similar orientation in the dense, localised distributions, the more tenuous medium eveloping the whole complex, and the interstellar medium. This alignment appears to persist over large distances and is not destroyed by density gradients in the dust distribution. A particularly important point to note is that in this picture the alignment mechanism must operate in much hotter and denser regions than envisaged by DB.

There are indications that the polarization *efficiency* may vary between members of a single cluster, and may be greater in molecular clouds than in the interstellar medium, though the interpretation of this is complicated by selection effects, projection effects and inaccuracies in the estimated extinctions.

The implications of these results are discussed in Chpater VII.

CHAPTER VII

DISCUSSION

(1) Implications of the Model.

Interpretation of the observations of linear and circular polarization has led to a model in which the polarization is produced by transfer through a medium of aligned grains, with a twist in the direction of grain alignment along the line-of-sight, in some cases at least. The grains are aligned by the Galactic magnetic field, which permeates the molecular clouds. This conclusion poses two obvious questions: how is the alignment effected and what is the cause of the twist?

The Davis-Greenstein mechanism is generally not efficient enough in aligning the interstellar grains to produce the observed optical interstellar polarization, given the magnetic field strengths that are expected to exist in the interstellar medium (Chapter II). This problem extrapolates to the molecular clouds. At the cloud centres it is expected that the gas and dust temperatures are similar because the densities are high enough that the dust will collisionally heat the gas (Goldreich and Kwan 1974). Therefore DG alignment is expected to be inefficient in the central regions (Chapter II). At some distance from the central regions the gas should decouple from the dust, because the dust temperature falls more slowly ($\alpha r^{-0.4}$) with distance r than the dust density ($\alpha r^{-\alpha}$; $1 < \alpha < 2$) (Goldreich and Kwan, Werner et al 1976, Westbrook et al 1976). Authors therefore tend to assume that the polarization is most likely

to arise in the less dense, cooler regions of the clouds, where there may be a large difference between the gas and dust temperatures.

These considerations should not be allowed to over-influence the present interpretation, because there are already suspicions that the DG alignment process may be a considerable over-simplification of the real situation. In fact, the present observations, coupled with other recent investigations which imply clumpiness and irregularity of the dust distribution in star-forming complexes (Beichman et al 1979, Werner et al 1979) and increased dust densities at the location of star formation (Thronson et al 1979, Smith et al 1979) strongly suggest that much of the extinction and polarization is occurring in the relatively dense and warm central regions of the clouds. Support for this conclusion also comes from the observations of Harris et al (1978) that ice absorption is confined to the densest regions, since the ice feature is observed to be polarized in BN. In this case, unless χ'' is large (Chapter II), there is no alternative but to conclude that a more efficient alignment mechanism than Davis-Greenstein alignment is required. Before considering what this might be, it may be helpful to look a little closer at some of the characteristics of the polarized sources.

There has been a suggestion that the polarization efficiency may vary within a complex of sources, which might imply a real inefficiency in the mechanism under certain conditions, such as high density or high dust temperature. Determination of whether this is true, and of the nature of the inefficiency by theoretical

considerations or optical interstellar observations would help in establishing the characteristics of the alignment mechanism.

If one assumes isotropic flux-freezing of the magnetic field to the ionized gas as a molecular cloud collapses (Mestel 1965, Mouschovias 1978; also see later discussion) then the magnetic field strength B will increase with gas density ρ according to

$$B \propto \rho^{2/3}$$

Then, if the other parameters of equations II.5 and 6 remain unaltered, it can be shown that the ratio of the timescales for Davis-Greenstein alignment (τ_{DG}) and collisional disorientation (τ_{gas}) will go as

$$\tau_{DG}/\tau_{gas} \propto \rho^{-1/3}$$

In other words, as the density increases, Davis-Greenstein alignment increases in efficiency.

Unfortunately, this simple reasoning is complicated by various factors, one of the most important being the decrease in efficiency with decreasing difference between gas and dust temperatures, as described above. Also, in the denser regions the grains may well be larger, due to accretion, and large grains are harder to align than small ones. These factors are evident in equations II.5 and 6.

In the interstellar medium there is some indication that the alignment efficiency is *poorer* in denser regions. Serkowski, Mathewson and Ford (1975) suggested that the alignment efficiency is lower when λ_{max} is large. As explained in Chapter II, λ_{max} is usually interpreted as an indicator of grain size, the larger values being associated with larger grains, and denser regions. Wilking et al (1979a) observed a similar effect within the ρ Ophiuchi dark cloud. However, if this interpretation of λ_{max} is correct these observations could just reflect the fact that larger grains are harder to align, and may not be very relevant to the enhanced density peaks of the molecular clouds where the physical conditions are likely to be very different (in particular, as regards the other two major characteristics which affect the alignment: the relative dust and gas temperatures, and the magnetic field strength).

Taking these considerations into account therefore, it must be concluded that neither an increase, nor a decrease in polarization efficiency with increasing temperature or density can be ruled out by theoretical considerations and interstellar polarization observations. The infrared polarization observations themselves can provide little insight into the postulated polarization efficiency variations because they combine selection and projection effects with the theoretical interpretation problems described above. An example is chance projection of a source with little local polarization at the back edge of the cluster with a more locally polarized one at the front edge, combined with a polarization efficiency that is a function of temperature or density. Confusion can also arise by the

inclusion of sources as single objects, which may in fact be double, or unresolved small clusters, e.g. W3/IRS 5.

The question of the polarization efficiency, then, does not constrain the search for an appropriate alignment mechanism, however it has an interesting offshoot. By considerations of this sort the problem of the degree of polarization/size correlation may be understood. By the same chance projection and selection effects, such a correlation could be easily masked. This possibility has already been alluded to when the correlation was introduced. In fact, a strong indication exists that the youngest, most interesting sources tend to be among the most highly polarized. These include BN, W33 A, GL 2591, NGC 7538/IRS 1, S255 and S140. Special attention has been drawn to each of these sources as likely protostars because of their locations, luminosities and spectral energy distributions, not only their compact size. Therefore, turning the argument around, a size/degree of polarization correlation might be *expected* to exist if the youngest and reddest sources are most highly polarized. Then the observed scatter in the correlation may be masking a good, intrinsic correlation, due to projection and selection effects as suggested above. If such a correlation does exist, then it would imply that the polarization efficiency does indeed *increase* with density.

Turning to the question of the origin of the twist in the grain alignment required by the model for the circular polarization, it is pertinent to ask whether there is actually a gentle twist or a fairly

abrupt rotation in alignment, perhaps at the boundary of the localised dust clouds and the more extended components. Unfortunately there is no effective way to distinguish between these alternatives. In the interstellar medium the second is more probable, it being quite likely that different clouds along the line-of-sight have different orientations of grain alignment. If two sources with opposite senses of circular polarization were observed in a single complex it would be strong evidence that the second phenomenon was occurring in the molecular clouds also. In fact the two sources in Orion have the same sense of circular polarization. The fact that five objects in four different complexes have been observed to have similar degrees of ellipticity speaks for the continuous twist interpretation, since such a mechanism is much more likely to produce similar effects in different clouds (because the same laws of physics hold for them all) than an abrupt dislocation.

If the circular polarization is produced by twists in the grain orientation then some of the scatter in the infrared position angles within a complex could be due to sources lying at different distances along the line-of-sight in the twisting medium. This is consistent with the detection of circular polarization in Orion, where there are some differences between the position angles, and the non-detection of circular polarization in NGC 7538, where the position angles are identical. Extrapolating this idea one might expect circular polarization to occur in GL 437 and W3, but not in Mon R2.

A rotation in the position angle of linear polarization might

also be expected in a twisting medium. Then a variation in grain characteristics along the line-of-sight is also required, such that at different wavelengths one is looking at different depths in the twisting medium. Such effects have been observed in the interstellar medium (e.g. Coyne 1974). In the molecular clouds the amounts of twist required by the models developed in Chapter IV are too small for a rotation to be easily observable. The maximum rotation might be expected between the ice and silicate features. If all the ice were at one side of the cloud in a simple 2 slab model, a rotation of only 8° is predicted in BN between 3.1 and 9.7 μm by the models with the largest twist angles (ϕ = 50°). A rotation of 8° is detectable but is not observed. It is not possible from this analysis to deduce whether the twist is smaller than 50°, or that there is no variation in the grain parameters along the line-of-sight. In the other sources with some wavelength information of polarization there is no rotation of position angle to the accuracy of the data (~±5°).

(2) The Alignment Problem.

The problem of the alignment of the interstellar grains has been mentioned briefly in Chapter II.3, and the Davis-Greenstein alignment mechanism has been described. Several other alignment mechanisms have been suggested in the fifties, sixties and early seventies, but all are inadequate. These include weathervaning (Gold 1952), cosmic ray bombardment (Salpeter and Wickramasinghe 1970) and absorption of starlight from a particular direction

(Harwit 1970). Under certain circumstances weathervaning might be the most viable of these alternatives. Gold proposed that grains moving at hypersonic velocities through the gas would become aligned. Purcell (1969) concluded that radiation pressure might provide sufficient driving force in certain conditions but cannot explain the large-scale Galactic polarization. It is possible that within the molecular clouds, weathervaning might be successful if there are sufficient sources of energy, however the radiation pressure would have to be greater than the gas pressure, which is extremely unlikely. Also the fact that the grains are believed to be coupled to the gas in the denser regions (Goldreich and Kwan 1974) argues against significant relative motion between the two. The correlation with the direction of nearby interstellar polarization of the infrared vectors implies that the mechanisms are the same, although Martin (1971) has pointed out that charged grains will naturally precess around the magnetic field, thereby showing a correlation with it whatever the alignment process.

Suggestions have been made whereby DG alignment might be made more efficient. It was suggested that ferromagnetic grains might be considerably easier to align (Jones and Spitzer 1967, Shapiro 1975) or paramagnetic ones could become "super-paramagnetic" with inclusions of clusters of ferromagnetic atoms to act as magnetic moments (Jones and Spitzer), or even be naturally super-paramagnetic (Duley 1978). It has also been anticipated that graphite would be a very efficient polarizer because graphite flakes are anisotropic, presenting metallic properties to radiation polarized parallel to one axis and dielectric ones to radiation polarized parallel to the

orthogonal axis (e.g. Greenberg 1968). However, Aannestad and Purcell (1973) have shown that this effect is much smaller than the anisotropy due to the grain shape.

Because the silicate grains in KL are clearly aligned, and because they felt there was not much evidence for magnetic impurities in the grains, Dyck and Beichman (1974) did not consider ferromagnetic or super-paramagnetic properties, and predicted the grain temperature and magnetic field strength in OMC 1 on the basis of the normal DG alignment. For the grain shapes and sizes used by them, the degree of alignment required by their model fit to the observed silicate band polarization, a gas temperature of 70°K and a molecular hydrogen density of $10^{4.3}$ cm^{-3} suitable for the outer regions of OMC 1 (Zuckerman and Palmer 1975), equations II.5-7 led to a value of ~6°K for the dust temperature and ~7 milligauss for the aligning field. While the dust in the interstellar medium may be as cold as 8°K or less (Spitzer 1978) 6°K for grains in a molecular cloud is unreasonable. Also, as pointed out by Dennison (1977), in regions where the dust temperature is this low, the gas temperature is likely to be lower than 70°K, which would aggravate the dust temperature problem still further. The magnetic field strength implied by the polarimetry is also larger than typical estimates, although the measurements of magnetic field strength in molecular clouds is very ambiguous, as explained in section 3 of Chapter II.

In fact, it is widely believed that in the molecular clouds the dust is heated by the newly formed stars or by the nearby H II

regions (e.g. Gatley et al 1979, Becklin et al 1976) and that the gas is heated collisionally by the dust at sufficiently high densities (Goldreich and Kwan 1974, Zuckerman and Palmer 1975). Such a situation agrees very well with most observations, for example in Orion the central temperature of the dust is about 80°K (Forrest and Soifer 1976, Forrest et al 1976, Pipher et al 1978) while the gas is at about 70°K (Forrest, Houck and Reed 1976, Werner et al 1976). This is not universally true, however: in OMC 2 and NGC 2264 it appears that the dust probably cools rather than heats the gas (Thronson et al 1979, Crutcher et al 1979).

If the gas temperature is close to the dust temperature then the DG mechanism cannot work at all, and if the dust temperature is higher than the gas temperature then *reverse* DG would operate, to produce alignment in the opposite sense to that seen in the interstellar medium, where there is little doubt that $T_g > T_d$. Dennison (1977) assumed that in the outer regions of OMC 1 the gas would decouple from the dust as the density falls off and that T_g would fall sufficiently below T_d for reverse DG alignment to be effective enough to align the grains. Reverse alignment requires a larger magnetic field strength than normal alignment, but Dennison was able to offset this increase over the value required by DB somewhat, by using a larger value for $\tau_{10\ \mu m}$, thereby reducing the degree of alignment required (Chapter IV).

The new observations and their interpretation presented in this work pose some problems for the model proposed by Dennison.

The most obvious one is that the infrared vectors are observed to be *parallel* to the nearby interstellar vectors, not perpendicular as they would be if normal DG alignment operates in the interstellar medium and reverse DG in the molecular clouds. Also, there is evidence that the polarization mechanism operates in the dense central regions, not only in the cooler, outer layers. Finally, Kwan and Scoville (1976) have suggested that the gas may be effectively coupled to the dust even at densities below $n_{H_2} = 10^4$ cm^{-3}. In this case there would not be a significant difference between the gas and the dust temperatures even in the outer layers of the clouds.

There seems to be no alternative but to conclude that an alignment mechanism is required that can align the grains in regions where the density is high and where the gas and dust temperatures are comparable. The Orion observations also indicate that the orientation of alignment must be the same with respect to the magnetic field, irrespective of the relative gas and dust temperatures, if it is true that $T_g > T_d$ in OMC 1 and $T_g < T_d$ in OMC 2 (Thronson et al 1979), because the same orientation of polarization is seen in the OMC 1 infrared sources as in OMC 2/IRS 3. This condition effectively rules out DG alignment, even if the grains are ferromagnetic or super-paramagnetic.

For the specific grain model adopted in Chapter IV it is relevant whether the mechanism aligns prolate and oblate grains with their semi-major axes parallel or not, however the choice of an oblate shape for the graphite grains is fairly arbitrary. It is

usually assumed that graphite particles are flakes but such a condition should not be allowed to influence the search for a suitable alignment mechanism becuase it is not at all clear that the graphite really does exist as flakes, or for that matter that the ice and silicate grains are prolate in shape. As pointed out in Chapter IV the choice of grain shapes is not critical to the model, and in any case is only broadly determined by it. Also, although graphite was chosen as being the most likely composition for the third type of grain, it is not unique, and could be replaced by a material of similar optical properties, such as iron, which might be more likely to exist as prolate grains.

Perhaps the most promising alignment mechanism is "pinwheeling" (Purcell 1975) combined with the classic DG alignment. Purcell proposed that grains can be accelerated to suprathermal rotation speeds by "rocket" torques resulting from inhomogeneities on the grain surface, such as photoelectric emissivity, molecule formation or variation in accommodation coefficient. The grains may not then be subject to the requirement that the gas temperature be significantly different to the grain temperature, and might become easily aligned by the DG mechanism.

Purcell (1979) showed that pinwheeling grains must rotate about their axes of greatest inertia, therefore they would be aligned by the DG mechanism with their long axes perpendicular to the magnetic field, regardless of the gas temperature, as required by the observations in the interstellar medium and the molecular clouds.

In order for the mechanism to be viable, there must be a plausible torque available. Formation of H_2 molecules at active sites on an irregular grain surface, followed by ejection, with an accompanying donation of angular momentum to the grain, is the most efficient torque in the interstellar medium (Purcell 1979). However, in the dense molecular clouds it is not at all clear that such a mechanism can be successful. Processes of interstellar chemistry in molecular clouds most likely differ greatly from those in the diffuse interstellar medium, not least because of the uncertain spatial relationship of H II regions and infrared sources to the grains. Even if it is assumed that there is sufficient atomic hydrogen available to combine on grain surfaces to form H_2 at the high densities involved (10^4-10^5 cm^{-3}), the temperatures of the grains in these dense regions are likely to be too high for H_2 molecule formation. For example, H_2 is not expected to form on ice grains which are warmer than 22 K; even graphite grains should be at 25 K or less to effectively catalyze molecule formation (Willis and Fitton 1975).

Again this difficulty raises the suggestion that perhaps alignment occurs in the outer regions of the cloud where the temperatures are lower. According to the equations of Goldreich and Kwan (1974), in the distance that the dust density has decreased by a factor of 100, the temperature may decrease sufficiently for effective molecule formation. However, this idea would restrict the polarization to arising only at densities of the order of 10^3 cm^{-3} or less, in contradiction to the indications that it arises

in denser regions described earlier. More specifically, it contradicts the observation that the ice probably only exists at significantly higher densities than 10^3 cm^{-3} (Harris et al 1979).

Another possible spin-up torque for the grains in molecular clouds may be collisions with the gas atoms, if the gas and dust temperatures are not identical. It has been assumed that collisions between the grains and the gas result in heating of the gas, the grains themselves being heated by ultraviolet, optical and near infrared flux from the energy sources in the clouds. This scenario is made very plausible by the large energies radiated by the grains at far infrared wavelengths, and the observations that generally indicate that the gas is cooler than the dust. Goldreich and Kwan (1974) assumed that a gas molecule will rebound from a collision with a grain with an average energy of $3kT_d/2$, and derived relationships between the gas and dust temperatures such as the ones illustrated in Figure VII.1. If the accommodation coefficient δ (sticking probability) varies slightly over the surface of the grain some molecules will rebound with an increase in kinetic energy, while others will be more likely to stick, removing energy less quickly and efficiently. This will result in a torque. This idea is illustrated in Figure VII.2 which is adopted from Purcell (1975). In this case the accommodation coefficient is identical over the surface of the grain, but a molecule striking the grain in the concavities is more likely to hit again before returning to the gas.

The increase in rotational energy of the grain over the kinetic

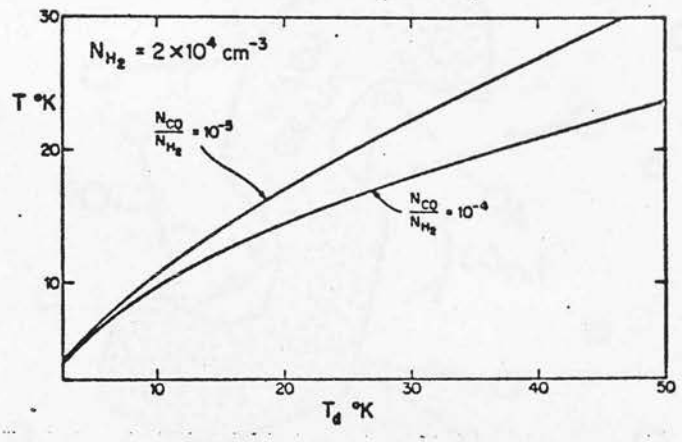

Figure VII.1 Graph of the gas kinetic temperature T versus the dust temperature T_d, from the models of Goldreich and Kwan (1974).

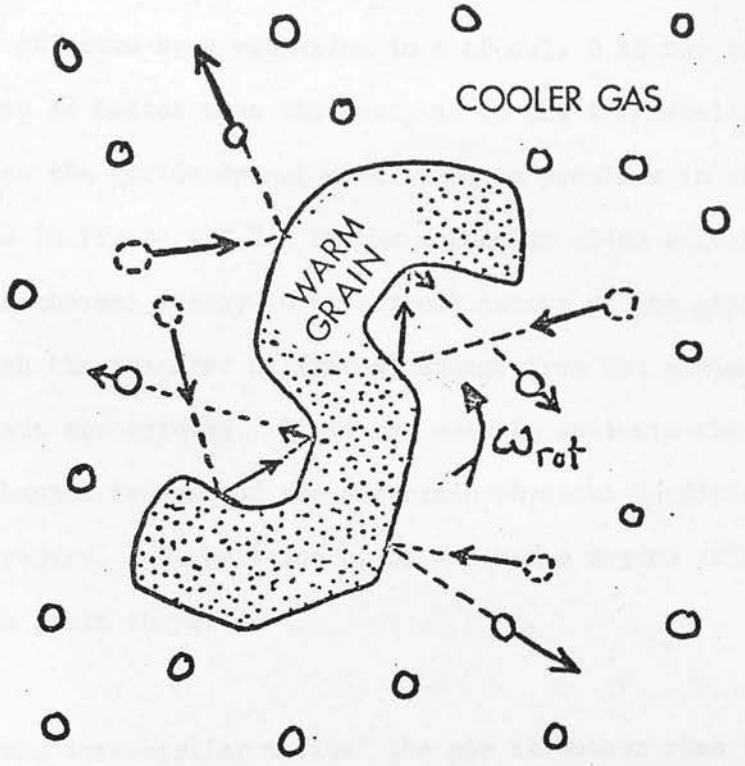

Figure VII.2 A dust grain which may be capable of being spun-up to suprathermal velocities, due to effective variations in the sticking probability of the colliding gas atoms caused by the peculiar grain shape (after Purcell (1975)).

value derived in this fashion depends on the ratio of grain to molecule mass, and the fractional variation in accommodation coefficient. Purcell (1975) calculates that an increase in rotational energy of 10^3 can be effected by a variation in δ of only 0.1% for the case when the gas is hotter than the dust, as in the interstellar medium. In this case the grains do not need to be as peculiar in shape as illustrated in Figure VII.2. In the molecular cloud situation the transfer of thermal energy to rotational energy of the grain must compete with the transfer of thermal energy from the grain to the gas to effect the spin-up. It is not easy to estimate the efficiency of the mechanism because of the uncertain physical conditions in the alignment region, and the value of δ, which can depend critically on the unknown grain shape.

In "the interstellar medium" the gas is hotter than the dust, in which case the grains will rotate in the opposite sense to that in the molecular clouds. This is not inconsistent with the alignment of the grains in the same orientation in the two media because the axis of rotation is the same in each case.

Once the grains have achieved suprathermal rotation, the Davis-Greenstein mechanism can eventually align them, because the randomisation effect of collisions with gas atom has effectively been removed. The particular mechanism postulated here, variation in the accommodation coefficient, essentially replaces the classic assumption that the grain surface is uniform to collisions.

The process may be complicated by the possibility that the grains will accrete a mantle of molecules before alignment is effected, in which case the pattern of variation in accommodation coefficient can be lost, and the grain may not remember its original direction of spin. If many such "crossovers" accompanied by disorientations of the grain's angular momentum occur during the time required to align the grain, then pinwheeling will be inefficient. Disorientation depends upon the time required for spin-up τ_m, the time between crossovers τ_x, and the degree to which the grain is disorientated during a crossover, compared to the paramagnetic relaxation time, τ_{DG} (which is not reduced by the pinwheeling effect from the classic value). Purcell finds that $\tau_x = 1.3(\tau_L + 0.6\tau_m)$ where τ_L is the timescale for a change in the torque. τ_L is unknown, especially in the case of spin-up by collisions, when physical irregularities on the grain surface may need to be covered to destroy the spin orientation. For spin-up by H_2 formation, τ_L might be taken as the time required to accrete a monomolecular layer, which may be calculated with some degree of accuracy given the typical conditions in clouds. In this case, Spitzer (1978) has shown that spin-up will be "short-lived," (*i.e.* $\tau_L < \tau_m$) and that paramagnetic relaxation cannot account for interstellar polarization by an order of magnitude. Spitzer and McGlynn (1979) considered the degree of disorientation between crossovers, and concluded that two or three crossovers would occur before disorientation would be complete. In this case, "long-lived" spin-up ($\tau_L > \tau_{DG}$) may occur, in which case the alignment can be effective.

Alternatively, the timescale for alignment may be shortened by super-paramagnetic properties of the grains; the value of χ'' can then exceed by many orders of magnitude the value normal for paramagnetic grains, $\chi'' = 2 \times 10^{12}\ \omega/T_d$ (Chapter II). Another possibility was suggested by Srnka and De (1978). Electrically charged spinning grains may have internal magnetic fields which can increase by a large amount the effective magnetic field of the background medium, thus reducing the alignment timescale (equation II.5).

There remain unsolved problems associated with the alignment mechanisms, including pinwheeling, but the new polarization observations help to constrain the characteristics required and should inspire further theoretical consideration. Specifically, the molecular cloud polarization observations show that the mechanism must operate at high densities, relatively similar gas and dust temperatures and must align grains in the same orientation with respect to the magnetic field under widely differing temperature and density conditions.

(3) Magnetic Fields in Dense Clouds and the Origin of the Twists.

The role of magnetic fields in star formation is extremely hard to treat theoretically, but is obviously of considerable importance. Magnetic fields have been invoked to play an important part in the solution of the angular momentum problem by magnetic braking, and support of the cloud against free-fall collapse, which would permit

many more stars to form than are observed. These problems are intimately linked.

The Galactic magnetic field can probably not support a cloud adequately against free-fall collapse once it is initiated, even perpendicular to the lines of force; parallel to them collapse can proceed unimpeded, the amount of flattening depending on the critical mass for collapse. Mouschovias (1978) calculates that a cloud of mass 10^5 $M_\odot$ and density $n_H \sim 10^4$ cm^{-3} requires a field of ~0.81 milligauss to prevent collapse and fragmentation. It seems likely that angular momentum can more adequately stabilize the collapse. However, three-dimensional hydrodynamical collapse calculations in the presence of both magnetic fields and angular momentum are extremely complex.

A collapsing cloud must conserve angular momentum, $I\Omega$. Calculations show, however, that the centrifugal force at the surface of star, formed by a cloud collapsing with angular momentum derived from Galactic rotation, would exceed the gravitational force by several orders of magnitude. A solar mass cloud starting with a density of $n_H \sim 20$ cm^{-3} would need to decrease its radius, R, by 10^7 to produce stellar densities. Centrifugal force goes as $1/R^3$, therefore the angular velocity Ω must increase by 10^{14} resulting in a rotation period of about 1 minute. This is the angular momentum problem: not only would collapsing clouds disrupt by the action of centrifugal forces long before stellar densities are reached, but

angular velocities anywhere near those expected for collapsing clouds conserving angular momentum are not observed. Several mechanisms have been proposed to overcome the angular momentum problem. The most realistic are transfer of the angular momentum from rotational into orbital motion of a binary system, or transfer of the momentum into the surrounding interstellar gas. In the first case star clusters would rotate and should therefore flatten, which is not observed.

Mestel and Spitzer (1956) suggested that a magnetic field could transport angular momentum from the cloud into the surrounding medium in a characteristic time τ_J, given by (Mouschovias 1977b)

$$\tau_J = \frac{8}{15} \frac{\rho_{cl} R_{cl}}{\rho_{ext} v_{A,ext}}$$

where ρ_{cl} and ρ_{ext} are the densities of the cloud and external media respectively, and $v_{A,ext}$ is the Alfvén speed in the external medium, $v_{A,ext} = B/(4\pi\rho_{ext})^{1/2}$ (Mouschovias 1977a). This equation applies to a cloud with axis of rotation parallel to the uniform magnetic field. Applying the equation to the dense core of a collapsing cloud using $\rho_{cl} \simeq 10^4$ to 10^5, $\rho_{cl}/\rho_{ext} = 10$, $R_{cl} = 0.5$ pc, and $B \propto \rho^{\kappa}$, $(1/3 \leq \kappa \leq 1/2$, see later), where B in the interstellar medium is 3 microgauss, shows that the core can lose its angular momentum to the surrounding envelope in a timscale of about 2×10^6 years. This is short compared to the collapse and fragmentation time of a cloud not simply in free-fall collapse but stabilized in some way. Therefore magnetic braking would appear to be quite efficient, and

angular velocity rather than angular momentum is conserved. A scenario that evolves is the following (Mouschovias 1978). The outer layers of the cloud are left behind in the collapse, being supported by magnetic tension, and the collapse of the core continues. At some stage characterised by a critical density, the magnetic field will diffuse out of the material by ambipolar diffusion (see below), allowing conservation of angular momentum to continue at that point. This angular momentum is then available for the formation of binary stars. If the critical density at which the field decouples is lower than a certain value (~2.2×10^6 cm^{-3}, Mouschovias 1977b), centrifugal forces will disrupt the core to produce a binary star system.

It therefore seems quite likely that a solution to the problems associated with the theoretical understanding of the process of star formation requires adequate hydrodynamical treatment of collapse in the presence of magnetic fields and angular momentum. Such calculations for magnetic fields oriented at oblique angles to the angular momentum vector have not been attempted. It is clear, however, that skewing of the field lines is a possible outcome of such models. The magnetic field does not vanish in the central core, since it cannot fall below the background envelope value, *therefore it is quite likely that a small twist will occur in the field lines* as the core spins up, or as a result of the angular momentum transfer process. *This is just the kind of situation required by the interpretation of the circular polarization observations.* The similarity of the interstellar medium magnetic field direction and the molecular cloud field direction is a natural consequence of such a scenario.

Further analysis of such a situation is not possible until the theoretical processes associated with star formation are much better understood than they are at present. In spite of the generality of the discussion, the plausibility of the existence of twists in the molecular cloud grain alignment is well illustrated. The new observational results clearly merit consideration in further theoretical models. Additional insight may come from study of circular polarization in the ice feature. The models (Figure IV.6) predict structure in the circular polarization in the ice band, which if detected would clearly indicate that the twist must originate in the central regions where the ice is supposed to exist ($n_H > 10^5$ cm^{-3}, Harris et al 1979). Non-detection of structure could not so easily be interpreted, since it could be due to inadequate sensitivity, or to incorrect choice of model parameters, such as size and shape of the grains, which are not particularly well determined (Chapter IV).

The question of the diffusion of the magnetic field out of the collapsing cloud is an important one for understanding the alignment problem and the field strengths likely to exist in the protostellar vicinities. One would like to know the critical densities at which the field decouples from the gas, and the diffusion timescale. It follows directly from Maxwell's equations that if the conductivity is high the magnetic flux moving with the gas fluid is constant (Mestel 1965). In other words the magnetic field is "frozen" into the fluid and follows the collapsing cloud. For isotropic contraction the enhancement of the field strength as the density increases is expected to go as $B \propto \rho^{\kappa}$, $\kappa = 2/3$. Observations of Zeeman

splitting in OH masers indicates that the field strengths are less than predicted by this relationship at the densities expected to exist in masing regions (e.g. Lo et al 1975). The fields are more compatible with the idea that κ is reduced from 2/3 because collapse can occur faster parallel to the field lines than perpendicular (Mestel 1965), to $1/3 \leq \kappa \leq 1/2$. Mouschovias (1978) has recently shown that the situation is considerably more complex than this simple interpretation, and that the value of κ depends on the stage of contraction as well as the initial conditions. The resultant value of κ at the cloud centre is however unchanged from that assumed by Mestel (1965), $1/3 \leq \kappa \leq 1/2$.

Mouschovias (1977b) calculates that the critical densities for decoupling of the field from the gas for the formation of binary stars are in the range 7.5×10^3 to 2.2×10^6 cm^{-3}. Therefore massive single star formation requires critical densities larger than this. The double or single nature of the protostars studied here is not defined, but it seems reasonable to expect that the field can be still frozen in at the densities observed, for example, in the centre of OMC 1 of 10^5-10^6 cm^{-3} (Zuckerman and Palmer 1975). It is clear that the field does not remain frozen-in throughout collapse however, since analogously to the angular momentum problem, stars would then have magnetic fields of the order of 10^8 gauss. This is not such a ridiculous result as rotation periods of one minute, but it is still unacceptable and implies that diffusion of the field must indeed occur, at sufficiently high densities.

Eventually, flux-freezing breaks down, and the ions and magnetic field may diffuse out through the neutral molecules and atoms. The timescale for ambipolar diffusion, as this is called, is given by

$$\tau_B = \frac{\langle u\sigma_s \rangle}{2\ Gm_H} \frac{n_i}{n_H} \frac{1}{(1 + 4n_{He}/n_H)^2}$$

(Spitzer 1978) where n_i is the ion density, n_H, n_{He} the neutral hydrogen and helium densities, m_H the mass of the hydrogen atom, u the collisional velocity between the atoms and σ_s the cross-section for collisions. G is the gravitational constant. For typical parameters, and an ionization degree $n_i/n_H \sim 10^{-8}$ (Guélin et al 1977) $\tau_B \simeq 5 \times 10^5$ years. Thus it seems that the field remains frozen-in for a considerable time compared to the formation time of a massive star ($\sim 10^6$ years; Larson 1978). Comparison to the free-fall collapse time is not very meaningful since, as discussed above, considerable stabilization against free-fall collapse must occur.

The diffusion timescale can be increased by many orders of magnitude if the ionization degree is higher than estimated by Guélin et al (1977) either by cosmic ray excitation in regions near cloud surfaces, or by recent bursts of star formation in nearby regions. Such ideas are consistent with the model of sequential star formation and the observations that stars form in clusters near cloud surfaces.

Evidence that the fields do indeed remain frozen-in for long timescales comes again from the maser observations. The VLBI observations of H_2O masers indicate that they may be associated with the

envelopes of protostars (Genzel et al 1979). Although the correspondence of OH and H_2O masers is not determined, it seems likely that they are related; therefore the magnetic fields inferred from the Zeeman observations must have remained frozen-in to the dense gas throughout the stellar formation time.

Assuming, therefore, that the fields can remain frozen-in long enough for stars to form, the field strengths can be estimated for the densities expected in the protostellar clusters, $\sim 10^5$ cm^{-3}, using the relation $B \propto \rho^{\kappa}$ where κ is as derived by Mouschovias (1978), $1/3 \leq \kappa \leq 1/2$, and the initial conditions $B \simeq 10^{-6}$ gauss and $\rho \sim 1$ cm^{-3} (Spitzer 1978). This leads to fields of the order of 0.05 milligauss $\leq B \leq$ 0.32 milligauss. These values are considerably lower than those required for the infrared polarimetry, if, neglecting the temperature difficulty described in the last section, the grains are to be aligned by the DG mechanism. Therefore the conclusion is strongly reinforced that a more effective alignment mechanism and/or super-paramagnetic grains are required to interpret the protostellar polarizations.

CHAPTER VIII

CONCLUSIONS

All the polarimetric data that have been presented in Chapter III can be attractively explained by an extension of a well established feature of the interstellar medium, without the need for sophisticated scattering models. For all the sources with measured circular polarization the data can be matched well with an IS model using extinction and phase-lag cross-sections calculated with Rayleigh theory, and a grain model which has been used successfully in the interstellar medium. In BN, the model predicted polarization at $\lambda < 4$ μm still falls below the observed polarization, but the inclusion of graphite grains in the model greatly improves the fit obtained by Dyck and Beichman (1974) using only ices and silicates. The degree of alignment has also been reduced from that required by DB by 40%, and a better fit to the silicate band polarization has been obtained.

Even though the fit of the model to the polarization of BN at short wavelengths is too low, *the degree of circular polarization can be matched by an IS model with a twist in the grain alignment along the line-of-sight of* 47°. In other words, even if the linear polarization fit were considered inadequate the circular polarization is easily produced by conversion of that linear polarization that *is* predicted to arise in the aligned grain medium. In addition, since the presence of some aligned grains is *required* by the 20 μm observations, the ice band polarization can be interpreted in the same

fashion as the silicate band; by transfer through an aligned grain medium. Therefore *the requirement for a specialised asymmetric scattering geometry* with a steep density gradient such as a central, optically thick disc *falls away immediately*. As much as 6% of the flux at 2 μm from BN may be due to a scattering component which could enhance the polarization by aligned grains, but it is more likely that the scattering properties of the aligned grains have been underestimated due to use of grains that are too small, since the orientation of polarization from the scattering shell would have to coincide with that from the aligned grains in order to enhance it.

The shallower slopes of the near infrared polarization spectra of the other sources, compared to BN, imply that they would be well fitted by the IS model, possibly with no requirement for a greater scattering efficiency than provided by the model grains. The relative grain compositions probably vary a little from source to source: in GL 2591 a greater percentage of a material like graphite, compared to silicate, than in BN can explain the non-detection of polarization in the ice band. Alternatively, (or in addition), the larger scattering grains possibly implied by the turnover in the polarization spectrum at 2 μm may mask the ice polarization. In this case, aligned grains approximately four times larger than in the interstellar medium are implied.

In the face of compelling evidence that the long wavelength polarization is produced by aligned grains, the attractiveness of a self-consistent model for both the linear and circular polarization

at all wavelengths, and the quality of observational data presently available, it is very clear that a more sophisticated scattering model to overcome the problems of the ES model is not warranted. A more urgent need is for higher resolution, sensitive photometric and polarimetric mapping of protostellar environments at 1.6 to 3.5 μm, which would elucidate the geometries, and the scattering properties of the grains. Such mapping would also be desirable in the vicinity of NGC 7538/IRS 9, NGC 6334/IRS 1 and OMC 2 which are most likely to be infrared reflection nebulosities, with a larger telescope than available for the research described here.

A comparison of the orientation of infrared polarization in the molecular clouds with the nearby interstellar polarization field shows that the polarization mechanism is the same for most of the protostellar sources, and is closely linked to the Galactic magnetic field, which must permeate the dense clouds where stars have formed, with little tangling or disruption. The precise location of the polarizing dust is uncertain but studies of certain sources, notably those in NGC 7538 and Orion, indicate that it is the same dust as is responsible for most of the extinction, which increases towards the density enhancements of the clouds, in agreement with far infrared, submillimeter and molecular line studies. The size/degree of polarization correlation is not supported by the new data, but it is likely that this is due to selection and projection effects, to some extent. There is an indication that the youngest sources are in fact the most highly polarized, consistent with the idea that the grains are aligned in relatively dense clumps localised to these sources, as

well as the dust which envelops the clusters, and that the polarization efficiency may be enhanced in the denser regions.

The classic Davis-Greenstein alignment mechanism cannot account for the observations because it would produce polarizations in the interstellar sources perpendicular to those of the molecular cloud sources, not parallel as observed, if the dust is hotter than the gas in the molecular clouds, as widely believed. The gas and grain temperatures are also too similar in the clouds for very effective DG alignment, and magnetic fields in the interstellar medium are too weak to account for the optical polarization by DG alignment.

"Pinwheeling" may be able to aid the alignment of the grains, if transfer of thermal to kinetic energy via gas collisions in the presence of variations in the accommodation coefficient on the grain surfaces is efficient enough in dense clouds to spin the grains up to suprathermal velocities so that paramagnetic alignment is effective. The field strength or the imaginary part of the magnetic susceptibility of the grains may still need to be enhanced in this case, to avoid disorientation of the grains as the irregularities are covered up by accretion of molecules onto the grain surfaces, in timescales shorter than the paramagnetic relaxation time. This may be by spin-related magnetism or super-paramagnetic grains.

Collapse of the molecular clouds with frozen-in magnetic fields has probably occurred; calculations and maser observations indicate that the fields have not had time to diffuse out by ambipolar

diffusion by the time a massive star has formed, in some clouds at least. Field strengths calculated for the dense central regions assuming flux-freezing are lower than required by unassisted DG alignment, which confirms the conclusion that a more efficient alignment mechanism is required. The twists in the orientation of grain alignment along the line-of-sight in the cloud may possibly arise in the rotation of a magnetic, collapsing cloud. The correspondence of the molecular cloud magnetic field with the magnetic field in the intercloud medium is a natural result of models of collapsing magnetic clouds.

BIBLIOGRAPHY

Aannestad, P. A., and Purcell, E. M. (1973). Ann. Rev. Astron. Astrophys. 11, 309.

Aitken, D. B., and Jones, B. (1973). Ap. J. 184, 127.

Allen, D. A. (1972). Ap. J. 172, L55.

Asano, S., and Yamamoto, G. (1975). App. Opt. 14, 29.

Axon, D. J., and Ellis, R. S. (1976). Mon. Not. R. Astron. Soc. 177, 499.

Balick, B. (1972). Ap. J. 176, 353.

Becklin, E. E. (1979). Personal communication.

Becklin, E. E., and Neugebauer, G. (1967). Ap. J. 147, 719.

Becklin, E. E., and Neugebauer, G. (1974). In H II Regions and the Galactic Centre, editor A. F. M. Moorwood (Neuilly-Sur-Seine, ESRO). p. 39.

Becklin, E. E., Neugebauer, G., and Wynn-Williams, C. G. (1973). Ap. J. 182, L7.

Becklin, E. E., Beckwith, S., Gatley, I., Matthews, K., Neugebauer, G., Sarazin, C., and Werner, M. W. (1976). Ap. J. 207, 770.

Becklin, E. E., Matthews, K., Neugebauer, G., and Willner, S. P. (1978). Ap. J. 220, 831.

Beckwith, S., Evans, N. J. II, Becklin, E. E., and Neugebauer, G. (1976). Ap. J. 208, 390.

Beichman, C. A. (1979). Thesis, University of Hawaii.

Beichman, C. A., Becklin, E. E., and Wynn-Williams, C. G. (1979). Ap. J. 232, L47.

Beetz, M., Elsässer, H., Poulakos, C., and Weinberger, R. (1976). Astron. Astrophys. 50, 41.

Bergeat, J., Lefevre, J., Kandel, R., Lunel, M., and Sibille, F. (1976). Astron. Astrophys. 52, 245.

Bertout, C., and Yorke, H. W. (1978). In Protostars and Planets, ed. Gehrels, Arizona.

Blair, G. N., Peters, W. L., and Vanden Bout, P. A. (1975). Ap. J. 200, L161.

Blair, G. N., Evans, N. J. II, Vanden Bout, P. A., and Peters, W. L. III (1978). Ap. J. 221, 382.

Brackman, E. J., and Scoville, N. Z. (1978). Preprint.

Breger, M. A. (1976). Ap. J. 204, 789.

Breger, M. A. (1977). Ap. J. 215, 19.

Breger, M., and Hardorp, J. (1973). Ap. J. 183, L77.

Burton, W. B. (1976). Ann. Rev. Astron. Ap. 14, 275/

Capps, R. W. (1976). Thesis, University of Arizona.

Capps, R. W. (1979). Preprint.

Capps, R. W., and Knacke, R. C. (1976). Ap. J. 210, 76.

Capps, R. W., Gillett, F. C., and Knacke, R. C. (1978). Ap. J. 226, 863.

Carrasco, L., Strom, S. E., and Strom, K. M. (1973). Ap. J. 182, 95.

Chandrasekhar, S. (1946). Ap. J. 103, 357.

Churchwell, E., and Walmsley, C. M. (1973). Astron. Astrophys. 23, 117.

Cheung, L., Frogel, J. A., Gezari, D. Y., and Hauser, M. G. (1978). Ap. J. 226, L149.

Cohen, J. G., and Frogel, J. A. (1977). Ap. J. 211, 178.

Cohen, M. (1973). Ap. J. 185, L75.

Cohen, M., and Kuhi, L. V. (1977). P.A.S.P. 89, 829.

Cohen, M., and Lewis, R. R. (1978). Mon. Not. R. Astron. Soc. 184, 801.

Colley, D., and Scott, P. F. (1977). Mon. Not. R. Astron. Sco. 181, 703.

Coyne, G. V. (1974). Astron. J. 79, 568.

Coyne, G. V., Gehrels, T., and Serkowski, K. (1974). Astron. J. 79, 581.

Crutcher, R. M., Hartkopf, W. I., and Giguere, P. T. (1978). Ap. J. 226, 839.

Danielson, R. E., Woolf, N. J., and Gaustad, J. E. (1965). Ap. J. 141, 116.

Davidson, K. M., and Harwit, M. (1967). Ap. J. 148, 443.

Davis, L., Jr., and Greenstein, J. L. (1951). Ap. J. 114, 206.

Day, K. L. (1976a). Ap. J. 203, L99.

Day, K. L., and Donn, B. (1978). Ap. J. 222, L45.

Deharveng and Maucherat (1979). Astron. Astrophys., in press.

Dennison, B. (1977). Ap. J. 215, 529.

Dickel, H. R., Dickel, J. R., and Wilson, W. J. (1977). Ap. J. 217, 56.

Dickel, J. R., Dickel, H. R., and Wilson, W. J. (1978). Ap. J. 223, 840.

Dinerstein, H. L., Lester, D. F., and Rank, D. M. (1979). Ap. J. 227, L39.

Downes, D., and Wilson, T. L. (1974). Ap. J. 191, L77.

Duley, W. W. (1978). Ap. J. 219, L129.

Dyck, H. M. (1979). Personal communication.

Dyck, H. M., Forbes, F. F., and Shawl, S. J. (1971). Astron. J. 76, 901.

Dyck, H. M., Capps, R. W., Forrest, W. J., and Gillett, F. C. (1973). Ap. J. 183, L99.

Dyck, H. M., and Beichman, C. A. (1974). Ap. J. 194.

Dyck, H. M., and Simon, T. (1977). Ap. J. 211, 421.

Dyck, H. M., and Capps, R. W. (1978). Ap. J. 220, L49.

Dyck, H. M., and Jones, T. J. (1978). Astron. J. 83, 594.

Dyck, H. M., and Lonsdale, C. J. (1979). Astron. J. 84, 1339.

Eiroa, C., Elsässer, H., and Lahulla, J. F. (1979). Preprint.

Elias, J. (1978). Ap. J. 224, 453.

Elmegreen, B. G. (1978). In Protostars and Planets, ed. Gehrels, Arizona.

Elmegreen, B. G., and Lada, C. J. (1977). Ap. J. 214, 725.

Elmegreen, B. G., Lada, C. J., and Dickinson, D. F. (1979). Ap. J. 230, 415.

Elsässer, H., and Staude, H. J. (1978). Astron. Astrophys. 70, L3.

Elvius, A., and Hall, J. S. (1965). Astron. J. 70, 138.

Emerson, J. P., Jennings, R. E., and Moorwood, A. F. M. (1973). Ap. J. 184, 401.

Evans, N. J. III (1978). In Protostars and Planets, ed. Gehrels, Arizona.

Evans, N. J. II, Blair, G. N., and Beckwith, S. (1977). Ap. J. 217, 448.

Field, G. B. (1974). Ap. J. 187, 453.

Field, G. B. (1975). In The Dusty Universe, ed. Field, Smithsonian.

Field, G. B. (1978). In Protostars and Planets, ed. Gehrels, Arizona.

Finn, G. D., and Simon, T. (1977). Ap. J. 212, 472.

Forrest, W. J., and Soifer, B. T. (1976). Ap. J. 208, L129.

Forrest, W. J., Houck, J. R., and Reed, R. A. (1976). Ap. J. 208, L133.

Foy, R., Chelli, A., Sibille, F., and Lena, P. (1979). Astron. Ap. 79, L5.

Frogel, J. A., and Persson, S. E. (1973). Ap. J. 186, 207.

Gardner, F., and Whiteoak, J. B. (1972). Ap. Lett. 12, 107.

Gatley, I., Becklin, E. E., Matthews, K., Neugebauer, G., Penston, M. V., and Scoville, N. Z. (1974). Ap. J. 191, L121.

Gatley, I., Werner, M. W., Sellgren, K. W., and Becklin, E. E. (1979). Preprint.

Genzel, R., Downes, D., Moran, J. M., Johnston, K. J., Spencer, J. H., Walker, R. C., Haschick, A., Matveyenko, L. I., Kogan, L. R., Kostenko, V. I., Rönnäng, B., Rydbeck, O. E. H., and Moiseev, I. G. (1978). Astron. Astrophys. 66, 13.

Gehrels, T. (1978). In Protostars and Planets, ed. Gehrels, Arizona.

Gehrels, T. (1974). Astron. J. 79, 590.

Gehrz, R. D., Hackwell, J. A., and Smith, J. R. (1975). Ap. J. 202, L33.

Gillett, F. C., Stein, W. A., and Low, F. J. (1968). Ap. J. 153, L185.

Gillett, F. C., and Forrest, W. F. (1973). Ap. J. 179, 483.

Gillett, F. C., Forrest, W. F., Merrill, K. M., Capps, R. W., and Soifer, B. T. (1975a). Ap. J. 200, 609.

Gillett, F. C., Jones, T. W., Merrill, K. M., and Stein, W. A. (1975b). Astron. Astrophys. 45, 77.

Gillett, F. C., and Soifer, B. T. (1976). Ap. J. 207, 780.

Gilra, D. P. (1971). Nature 220, 237.

Gold, T. (1952). M.N.R.A.S. 112, 215.

Goldreich, P., and Kwan, J. (1974). Ap. J. 189, 441.

Grasdalen, G. L. (1974). Ap. J. 193, 373.

Grasdalen, G. L. (1976). Ap. J. 205, L83.

Greenberg, J. M. (1968). In Nebulae and Interstellar Matter, ed. Middlehurst and Aller, Chicago, Chap. 6.

Guélin, M., Langer, W. D., Snell, R. L., and Wootten, H. A. (1977). Ap. J. 217, L165.

Gull, G. E., Houck, J. R., McCarthy, J. F., Forrest, N. J., and Horwit, M. (1978). Astron. J. 83, 1440.

Habing, H. J., Israel, F. P., and de Jong, T. (1972). Astron. Astrophys. 17, 329.

Habing, H. J., Goss, W. M., Matthews, H. E., and Winnberg, A. (1974). Astron. Astrophys. 35, 1.

Hackwell, J. A., Gehrz, R. D., Smith, J. R., and Briotta, D. A. (1978). Ap. J. 221. 797.

Hall, J. S. (1949). Science 109, 166.
Hall, J. S. (1958). Publ. U.S. Nav. Obs. 17 IV.
Hall, R. C. (1967). P.A.S.P. 77, 158.

Harper, D. A. (1974). Ap. J. 192, 557.

Harper, D. A., Low, F. J., Rieke, G. H., and Thronson, H. A. (1976). Ap. J. 205, 136.

Harris, S. (1976). Mon. Not. R. Astron. Soc. 174, 601.

Harris, S., and Scott, P. F. (1976). Mon. Not. R. Astron. Soc. 175, 371.

Harris, S., and Wynn-Williams, C. G. (1976). Mon. Not. R. Astron. Soc. 174. 644.

Harris, D. H., Woolf, N. J., and Rieke, G. H. (1978). Ap. J. 226, 829.

Harvey, P. M., Campbell, M. F., and Hoffman, W. F. (1977a). Ap. J. 211, 786.

Harvey, P. M., Campbell, M. F., and Hoffman, W. F. (1977b). Ap. J. 215, 151.

Harvey, P. M., Campbell, M. F., and Hoffman, W. F. (1978). Ap. J. 219, 891.

Harvey, P. M., Campbell, M. F., Hoffman, W. F., Thronson, H. A., and Gatley, I. (1979a), Ap. J. 229, 990.

Harvey, P. M., Thronson, H. A., and Gatley, I. (1979b). Ap. J. 231, 115.

Harwit, M. (1970). Nature 261, 61.

Heiles, C. (1976). Ann. Rev. Astron. Ap. 9, 923.

Herbst, E. (1978). In Protostars and Planets, ed. Gehrels, Arizona.

Hiltner, W. A. (1949). Ap. J. 109, 471.

Hoag, A. A., and van P. Smith, E. (1959). P.A.S.P. 71, 32.

Hudson, H. S., and Soifer, B. T. (1976). Ap. J. 206, 100.

Hulst, P. C. van de (1949). Rech. Astron. Obs. Utrecht 11, part 1.

Hulst, P. C. van de (1949). ibid, part 2.

Hulst, P. C. van de (1957). Light Scattering by Small Particles, Wiley, New York.

Irvine, W. W., and Pollack, J. B. (1968). Icarus 8, 324.

Israel, F. P. (1976). Astron. Astrophys. 48, 193; 52, 175.

Israel, F. P. (1978). Astron. Astrophys. 70, 769.

Israel, F. P., Habing, H. J., and de Jong, T. (1973). Astron. Astrophys. 27, 143.

Israel, F. P., and Felli (1978). Astron. Astrophys. 63, 325.

Johnson, H. L. (1968). In Nebulae and Interstellar Matter, ed. Middlehurst and Aller, Chap. 5, Chicago.

Jones, T. J., and Dyck, H. M. (1978). Ap. J. 220, 159.

Jones, R. V., and Spitzer, L. Jr. (1967). Ap. J. 147, 943.

Joyce, R. R., Gezari, D.Y., Scoville, N. Z., and Furenlid, I. (1978). Ap. J. 219, L29.

Kahn, F. D. (1974). Astron. Astrophys. 37, 149.

Kemp, J. C. (1972a). Ap. J. 175, L35.

Kemp. J. C. (1972b). IAU Symp. No. 52, ed. Greenberg and van de Hulst, Dordrecht.

Kemp, J. C., and Wolstencroft, R. D. (1972). Ap. J. 176, L115.

Klare, G., and Neckel, Th. (1977). Astron. Astrophys. Suppl. 27, 215.

Kleinmann, D. E., and Low, F. J. (1967).

Kleinmann, D. E., and Wright, E. L. (1973). Ap. J. 185, L31.

Kleinmann, S. G., Sargent, D. G., Gillett, F. C., Grasdalen, G. L., and Joyce, R. R. (1977). Ap. J. 215, L79.

Knacke, R. F. (1978). In Protostars and Planets, ed. Gehrels, Arizona.

Knacke, R. F., Cudaback, D. D., and Gaustad, J. E. (1969). Ap. J. 158, 151.

Knacke, R. F., and Capps, R. W. (1977). Ap. J. 216, 271.

Knacke, R. F., and Capps, R. W. (1979). Preprint.

Kobayashi, Y., Kawara, K., Maihara, T., Okuda, H., Sato, S., and Noguchi, K. (1978). P.A.S.P. 30, 377.

Kunkle, T. D. (1979). Thesis, University of Hawaii.

Kutner, M. L., Tucker, K. D., Chin, G., and Thaddeus, P. (1977). Ap. J. 215, 521.

Kwan, J., and Scoville, N. Z. (1976). Ap. J. 209, 169.

Lada, C. J. (1978). Ap. J. Suppl. 32, 603.

Lada, C. J., Dickinson, D. F., and Penfield, H. (1974). Ap. J. 189, L35.

Lada, C. J., Oppenheimer, M., and Hartquist, T. W. (1978a). Ap. J. 226, L153.

Larson, R. B. (1978). In Protostars and Planets, ed. Gehrels, Arizona.

Lester, D. F., Dinerstein, H. L., and Rank, D. M. (1979). Ap. J. 229, 981.

Lequeux, J. (1977). In IAU Symp. 75, eds. de Jong and Maeder, Dordrecht.

Liszt, H. S., Wilson, R. W., Penzias, A. A., Jefferts, K. B., Wannier, P. G., and Solomon, P. M. (1974). Ap. J. 190, 557.

Loer, S.J., Allen, D.A., and Dyck, H. M. (1973). Ap. J. 183, L97.

Lonsdale, C. J., Dyck, H. M., Capps, R. W., Wolstencroft, R. D. (1979). Preprint.

Loren, R. B. (1977). Ap. J. 215, 129.

Loren, R. B., and Wootten, H. A. (1978). Ap. J. 225, L81.

Lucas et al (1979). Preprint.

Manchester, R. N. (1974). Ap. J. 188, 637.

Martin, P. G. (1971). Mon. Not. R. Astron. Soc. 153, 279.

Martin, P. G. (1972). Mon. Not. R. Astron. Soc. 159, 179.

Martin, P. G. (1973). Mon. Not. R. Astron. Soc. 163, 141.

Martin, P. G. (1974). Ap. J. 187, 461.

Martin, P. G. (1975). Ap. J. 202, 389.

Martin, A. H. M., and Gull, S. F. (1976). Mon. Not. R. Astron. Soc. 175, 235.

Martin, P. G., Illing, R., and Angel, J. R. P. (1972). Mon. Not. R. Astron. Soc. 159, 191.

Matthews, H. E., Goss, W. M., Winnberg, A., and Habing, H. J. (1977). Astron. Astrophys. 61, 261.

Mathewson, D. S., and Ford, V. L. (1970). Mem. R. Astron. Soc. 74, 139.

Mathewson, D. S., and Nicholls, D. C. (1968). Ap. J. 154, L11.

Mathis, J. S. (1979). Ap. J. 232, 747.

Mathis, J. S., Rumpl, W., and Nordsieck, K. H. (1977). Ap. J. 217, 425.

McBreen, B., Fazio, G. G., Stier, M., and Wright, E. L. (1979). Ap. J. 232, L183.

McMillan, R. S. (1977). Ap. J. 216, L41.

McMillan, R. S. (1978). Ap. J. 225, 417.

McMillan, R.S. (1979). preprint.

Melnick, G., and Harwit, M. (1975). Mon. Not. R. Astron. Soc. 171, 441.

Merrill, K. M., and Soifer, B. T. (1974). Ap. J. 189, L21.

Merrill, K. M., and Stein, W. A. (1976). P.A.S.P. 88, 847.

Merrill, K. M., Russell, R. W., and Soifer, B. T. (1976). Ap. J. 207, 763.

Mestel, L. (1965). Quart. J. R. Astron. Soc. 6, 161 and 265.

Mestel, L., and Spitzer, L. Jr. (1956). Mon. Not. R. Astron. Soc. 116, 583.

Moran, J. M., Reid, M. J., Lada, C. J., Yen, J. L., Johnston, K. J., and Spencer, J. H. (1978). Ap. J. 224, L67.

Morris, M., Palmer, P., Turner, B. E., and Zuckerman, B. (1974). Ap. J. 191, 349.

Morton, D. C. (1975). Ap. J. 197, 85.

Mouschovias, T. Ch. (1977a). In IAU Symp. 75, ed. de Jong and Maeder, Dordrecht.

Mouschovias, T. Ch. (1977b). Ap. J. 211, 147.

Mouschovias, T. Ch. (1978). In Protostars and Planets, ed. Gehrels, Arizona.

Mueller, H. (1948). J. Opt. Soc. Am. 38, 661.

Mufson, S. L., and Liszt, H. S. (1979). Ap. J. 232, 451.

Myers, P. C., Ho, P. T. P., Schneps, M. H., Chin, G., Pankonin, V., and Winnberg, A. (1978). Ap. J. 220, 864.

Nandy, K., and Wickramasinghe, N. C. (1972). Rep. Prog. Phys. 35, 157.

Ney, E. P., Merrill, K. M., Becklin, E. E., Neugebauer, G., and Wynn-Williams, C. G. (1975). Ap. J. 198, L129.

Osterbrock, D. E. (1957). Ap. J. 125, 622.

Penston, M. V., Allen, D. A., and Hyland, H. (1971). Ap. J. 170, L33.

Perry, C. H., Agrawal, D. K., Anastassakis, E., Lowndes, R. P., Rastogi, A., and Tronberg, N. E. (1972). The Moon 4, 315.

Persson, S. E., and Frogel, J. A. (1974). Ap. J. 188, 523.

Pipher, J. L., Sharpless, S., Savedoff, M. P., Krassner, J., Varlese, S., Soifer, B. T., and Zeilik, M. II (1977). Astron. Astrophys. 59, 215.

Pipher, J. L., Sharpless, S., Savedoff, M. P. Kerridge, S. J., Krassner, J., Schurmann, S., Soifer, B. T., and Merrill, K. M. (1976). Astron. Astrophys. 51, 255.

Pipher, J. L., Duthie, G., and Savedoff, M. P. (1978). Ap. J. 219, 494.

Pollack, J. B., Toon, O. B., and Khare, B. N. (1973). Icarus 19, 372.

Puetter, R. C., Russel, R. W., Soifer, B. T., and Willner, S. P. (1979). Ap. J. 228, 118.

Purcell, E. M. (1969). Ap. J. 158, 433.

Purcell, E. M. (1975). In The Dusty Universe, ed. Field, Smithsonian.

Purcell, E. M. (1979). Ap. J. 231, 404.

Purcell, E. M., and Spitzer, L. Jr. (1971). Ap. J. 167, 31.

Rieke, G. H., Low, F. J., and Kleinmann, D. E. (1973). Ap. J. 186, L7.

Rogers, C., and Martin, P. G. (1979). Ap. J. 228, 450.

Salpeter, E. E. (1977). Ann. Rev. Astron. Ap. 15, 267.

Salpeter, E. E., and Wickramasinghe, N. C. (1969). Nature 222, 442.

Savage, B. D., and Mathis, J. S. (1979). Ann. Rev. Astron. Ap. 17, 326.

Schlosser, W., and Schmidt-Kaler, Th. (1974). In Planets, Stars and Nebulae Studied with Photopolarimetry, ed. Gehrels, Arizona.

Schneps, M. H., Martin, R. N., Ho. P. T. P., and Barrett, A. H. (1978). Ap. J. 221, 124.

Serkowski, K. (1962). Adv. Astron. Ap. 1, 289.

Serkowski, K. (1971). In Serkowski et al 1975.

Serkowski, K. (1973). Ap. J. 179, L101.

Serkowski, K., and Rieke, G. H. (1973). Ap. J. 183, L103.

Serkowski, K., Mathewson, D. S., and Ford, V. L. (1975). Ap. J. 196, 261.

Shapiro, P. R. (1975). Ap. J. 201, 151.

Sharpless, S. (1959). Ap. J. 131, 247.

Shurcliff, W. A. (1962). Polarized Light, Harvard.

Sibille, F., Bergeat, J., Lunel, M., and Kandel, R. (1975). Astron. Astrophys. 40, 441.

Simon, T., Simon, M., and Joyce, R. R. (1979). Ap. J. 230, 127.

Smith, J., Lynch, D. K., Cudaback, D., and Werner, M. W. (1979). Preprint.

Snow, T. J. (1976). Ap. J. 204, 759.

Soifer, B. T., and Pipher, J. L. (1975). Ap. J. 199, 663.

Soifer, B. T., Russell, R. W., and Merrill, K. M. (1976). Ap. J. 210, 334.

Soifer, B. T., Puetter, R. C., Russell, R. W., Willner, S. P., Harvey, P. M., and Gillett, F. C. (1979). Ap. J. 232, L53.

Spitzer, L. Jr. (1978). Physical Processes in the Interstellar Medium, Wiley, New York.

Spitzer, L. Jr., and Jenkins, E. B. (1975). Ann. Rev. Astron. Ap. 13, 133.

Spitzer, L. Jr., and McGlynn, T. A. (1979). Ap. J. 231, 417.

Srnka, L. J., and De, Bibhas, R. (1978). Ap. J. 225, 422.

Stark, A. A., and Blitz, L. (1978). Ap. J. 225, L15.

Staude, H. (1979). Private communication.

Stebbins, J., Huffer, C. M., and Whitford, A. (1940). Ap. J. 91, 20.

Stokes, G. G. (1852). Trans. Cambridge Phil. Soc. 9, 399.

Terzian, Y. (1970). Astron. J. 75, 1155.

Thaddeus, P., Kutner, M. L., Penzias, A. A., Wilson, R. W., Jefferts, K. B. (1972). Ap. J. 176, L73.

Thompson, R. I., and Tokunaga, A. T. (1978). Ap. J. 226, 119.

Thompson, R. I., and Tokunaga, A. T. (1979a). Ap. J. 229, 153.

Thompson, R. I., and Tokunaga, A. T. (1979b). Ap. J. 231, 763.

Thompson, R. I., and Tokunaga, A. T. (1979c). Preprint.

Thronson, H. A., and Harper, D. A. (1979). Ap. J. 230, 133.

Thronson, H. A., Harper, D. A., Keene, J., Lowenstein, R. F., Mosely, H., and Telesco, C. M. (1978). Astron. J. 83, 492.

Tokunaga, A. T., and Lebofsky, M. J. (1979). Private communication.

Tokunaga, A. T., and Thompson, R. I. (1979a). Ap. J. 229, 583.

Tokunaga, A. T., and Thompson, R. I. (1979b). Ap. J. 233, 127.

Tokunaga, A. T., Erickson, E. F., Caroff, L. J., and Dana, R. A. (1978). Ap. J. 224, L19.

Turner, B. E., and Thaddeus, P. (1977). Ap. J. 211, 755.

Vrba, F. J., Strom, S. E., and Strom, K. M. (1976). Astron. J. 81, 958.

Walker, (1956). Ap. J. Suppl. 2, 365.

Wendker, H. J., and Baars, J. W. M. (1974). Astron. Astrophys. 33, 157.

Werner, M. W., Gatley, I., Harper, D. A., Becklin, E. E., Lowenstein, R. F., Telesco, C. M., and Thronson, H. A. (1976). Ap. J. 204, 420.

Werner, M. W., Elias, J. H., Gezari, D. V., Hauser, M. G., and Westbrook, W. E. (1975). Ap. J. 199, L185.

Werner, M. W., Becklin, E. E., and Neugebauer, G. (1977). Science 197, 723.

Werner, M. W., Becklin, E. E., Gatley, I., Matthews, K., Neugebauer, G., and Wynn-Williams, C. G. (1979). Mon. Not. R. Astron. Soc. 188, 463.

Westbrook, W. E., Werner, M. W., Elias, J. H., Gezari, D. Y., Hauser, M. G., Lo, K. Y., and Neugebauer, G. (1976). Ap. J. 209, 94.

Whittet, D. C. B. (1977). Mon. Not. R. Astron. Soc. 180, 29.

Whittet, D. C. B., and van Breda, I. G. (1978). Astron. Astrophys. 66, 57.

Wickramasinghe, N. C. (1970). Nature 228, 540.

Wilking, B. A., Lebofsky, M. J., Rieke, P. G., and Kemp, J. C. (1979a). Preprint.

Wilking, B. A., Lebofsky, M. J., Martin, P. G., Rieke, G. H., and Kemp, J. C. (1979b). Preprint.

Willis, R. F., and Fitton, B. (1976). Ap. Sp. Sci. 55, 71.

Willner, S. P. (1976). Ap. J. 206, 728.

Willner, S. P. (1977). Ap. J. 214, 706.

Wilson et al (1979). Astron. Astrophys. 76, 66.

Wright, E. L., DeCampli, W., Fazio, G. G., Kleinmann, D. E., Lada, C. J., and Low, F. J. (1979). Ap. J. 228, 439.

Wynn-Williams, C. G. (1971). Mon. Not. R. Astron. Soc. 151, 357.

Wynn-Williams, C. G. (1976). Observatory 96, 6.

Wynn-Williams, C. G. (1978). Private communication.

Wynn-Williams, C. G., and Becklin, E. E. (1974). P.A.S.P. 86, 5.

Wynn-Williams, C. G., Becklin, E. E., and Neugebauer, G. (1972). Mon. Not. R. Astron. Soc. 160, 1.

Wynn-Williams, C. G., Becklin, E. E., and Neugebauer, G. (1974). Ap. J. 187, 473.

Wynn-Williams, C. G., Becklin, E. E., Forster, J. R., Matthews, K., Neugebauer, G., Welch, W. J., and Wright, M. C. A. (1977a). Ap. J. 211, L89.

Wynn-Williams, C. G., Becklin, E. E., Matthews, K., Neugebauer, G., and Werner, M. W. (1977b). Mon. Not. R. Astron. Soc. 179, 255.

Wynn-Williams, C. G., Becklin, E. E., Matthews, K., and Neugebauer, G. (1978). Mon. Not. R. Astron. Soc. 183, 237.

Yorke, H. W. (1977). Astron. Astrophys. 58, 473.

Yorke, H. W., and Krügel, E. (1977). Astron. Astrophys. 54, 183.

Zaikowski, A., and Knacke, R. F. (1975). Ap. Sp. Sci. 35, 97.

Zeilik, M. II, and Lada, C. J. (1978). Ap. J. 222, 896.

Zeilik, M. II, Kleinmann, D. E., and Wright, E. L. (1975). Ap. J. 199, 401.

Zellner, B. (1974). In Planets, Stars and Nebulae Studied with Photopolarimetry, ed. Gehrels, Arizona.

Zuckerman, B. (1977). In IAU Symp. 75, ed. de Jong and Maeder, Dordrecht, p. 123.

Zuckerman, B., and Palmer, P. (1975). Ap. J. 199, L38.

APPENDIX A

RAYLEIGH EXPRESSION FOR THE PHASE-LAG EFFICIENCY OF GRAINS IN THE INTERSTELLAR MEDIUM

The Rayleigh approximation to the theory of light scattering by small particles involves the assumption that the particle is small enough that the electric field of the incident wave may be thought of as a homogeneous applied field, and that surface effects on the particle can be ignored. This means that the wavelength of radiation both inside and outside the particle must be large compared to the particle. Making these assumptions, the Rayleigh expression for the phase-lag efficiency is derived by analogy to the extinction efficiencies as follows. For an ellipsoid, if $\underset{\sim}{E}_o$ is the applied field of the incident wave, the induced internal field in the particle $\underset{\sim}{E}$ can be expressed in terms of the polarization per unit volume $\underset{\sim}{P}$ and a tensor L which depends on the shape of the grain

$$\underset{\sim}{E} = \underset{\sim}{E}_o - L4\pi\underset{\sim}{P}$$

In terms of the dielectric tensor ε

$$\underset{\sim}{E} = \frac{1}{\varepsilon - 1} 4\pi\underset{\sim}{P}$$

therefore

$$4\pi\underset{\sim}{P} = (\varepsilon - 1)(\underset{\sim}{E}_o - L4\pi\underset{\sim}{P})$$

The dipole moment induced in the particle is given by

$$\underset{\sim}{p} = \underset{\sim}{P}V = \alpha \underset{\sim}{E}_o$$

where V is the volume of the particle and α is the polarizability tensor. Then, assuming that the axes of the dielectric tensor ellipsoid align with the particle axes,

$$\frac{4\pi\alpha}{V} = \frac{\varepsilon - 1}{(\varepsilon - 1)L + 1} \qquad \text{A1}$$

The complex refractive index of the interstellar medium $\tilde{m} = \tilde{n}' - i\tilde{n}''$ has been defined in terms of the complex forward scattering amplitude function of the particles, S(0), in equations IV.2:

$$\tilde{n}_j' - 1 = \mathrm{Im}[S_j(0)]2\pi N k^{-3}$$

$$\tilde{n}_j'' = \mathrm{Re}[S_j(0)]2\pi N k^{-3} \qquad \text{A2}$$

for the jth grain axis. The extinction cross-section is given in terms of the absorption coefficient $\gamma = 4\pi\tilde{n}''/\lambda$ by

$$\gamma = NC_{ext}$$

where N is the number density of particles. Therefore from A2 it follows that

$$C_{ext_j} = \frac{\lambda^2}{\pi} \mathrm{Re}[S_j(0)]$$

The cross-section for phase-lag defined analogously to C_{ext} in

Chapter IV, $C_{p_j} = \frac{4\pi}{N\lambda} (\tilde{n}_j'' - 1)$, is then given by

$$C_{p_j} = \frac{\lambda^2}{\pi} \, \mathrm{Im}[S_j(0)]$$

Now

$$S(0) = ik^3\alpha$$

(van de Hulst 1957), therefore

$$C_{p_j} = \frac{8\pi^2}{\lambda} \, \mathrm{Im}[i\alpha_j] \qquad \text{A3}$$

$\mathrm{Im}[i\alpha_j]$ is found from equation A1 in terms of the complex dielectric constant for the jth axis $\varepsilon_j = \varepsilon_j' - i\varepsilon_j''$ and the corresponding shape factor L_j

$$\mathrm{Im}[i\alpha_j] = \frac{V}{4\pi} \frac{[(\varepsilon_j' - 1)^2 + \varepsilon_j''^2]L_j + \varepsilon_j' - 1}{[(\varepsilon_j' - 1)L_j + 1]^2 + \varepsilon_j''^2 L_j^2} \qquad \text{A4}$$

The efficiency Q is found from the cross-section C

$$Q = C/\sigma$$

σ is the geometrical cross-section, $\sigma = \pi ab$, where a and b are the semi-axes of the ellipsoid of volume $V = \frac{4}{3} \pi ab^2$. Then, from equations A3 and A4,

$$Q_p = \frac{8\pi b}{3\lambda} \frac{[(\varepsilon_j' - 1)^2 + \varepsilon_j''^2]L_j + \varepsilon_j' - 1}{[(\varepsilon_j' - 1)L_j + 1]^2 + \varepsilon_j''^2 L_j^2}$$

APPENDIX B

Reprinted from:
THE ASTRONOMICAL JOURNAL VOLUME 84, NUMBER 9 SEPTEMBER 1979

THE RELATIONSHIP BETWEEN THE INFRARED POLARIZATION OF PROTOSTELLAR SOURCES AND NEARBY INTERSTELLAR POLARIZATION

H. M. Dyck
Institute for Astronomy, University of Hawaii, Honolulu, HI 96822

Carol J. Lonsdale[a)]
Department of Astronomy, University of Edinburgh
Received 26 April 1979

ABSTRACT

We have compared infrared polarization data for 31 protostellar sources buried in compact H II regions and molecular clouds with the interstellar polarization in the immediate vicinity of the sources, as determined from field stars. We find a strong tendency for the infrared and interstellar polarization directions to be parallel. 20 sources (65% of the sample) have measured infrared position angles of polarization lying within 30° of the average local interstellar polarization direction. We conclude that these data provide strong empirical evidence that the galactic magnetic field has played an important role in the evolution of molecular clouds.

I. INTRODUCTION

The role of magnetic fields in the formation of stars in dense molecular clouds is a question which is difficult to treat theoretically, yet, which is of great importance. It has long been thought that the presence of a field in a gravitationally-contracting cloud may affect the luminosity function of the resultant cluster as well as allow transfer of angular momentum back to the galaxy. Spitzer (1968) has argued on the basis of certain simple assumptions that a cloud will contract with the initial field frozen in, owing to a small fractional ionization within the cloud. More detailed calculations carried out by Mouschovias (1976) also indicate that the field will be completely trapped by the evolving cloud. Mouschovias expects that fields of a few milligauss will be present in clouds with gas densities above about 10^6 cm^{-3}. Some empirical evidence for the existence of enhanced fields is provided by infrared polarization and cm OH observations of sources buried in dense clouds (see Chaisson and Vrba 1978 for an overview). For example, the Becklin–Neugebauer (BN) object in the Orion nebula possesses large amounts of linear polarization between 1.6 and 13 μm (Breger and Hardorp 1973, Loer *et al.* 1973, Dyck *et al.* 1973, Capps 1976). This polarization has been interpreted as arising from light scattered and absorbed by grains partially aligned in a several milligauss transverse magnetic field (Dyck and Beichman 1974). Chaisson and Beichman (1974) reported observations of the 1612 and 1665 OH lines in the Orion complex which show an apparent Zeeman pattern characteristic of a longitudinal field of the order of 5 mG strength. A number of sources other than BN which have large infrared polarization may have fields with strengths of the order of 10^{-3}–10^{-2} mG. These include W 51 and NGC 7538(N) (Lo *et al.* 1975) and sources near the Galactic center (Capps and Knacke 1976, Knacke and Capps 1977). Thus the phenomenon of grains partially aligned by an enhanced field could be common in dense molecular clouds.

An alternative to the aligned grain model, in which the infrared polarization is produced by scattering in a geometry similar to that observed for bi-polar nebulae, has recently been proposed by Elsässer and Staude (1978). Their model was developed specifically to account for the large visual polarization seen for young stars in the W3 and M17 complexes; the authors also demonstrate that it can reproduce the gross features of the wavelength dependence of infrared polarization seen for BN. The stars in W3, in particular, all have position angles of polarization which are roughly parallel to the local interstellar polarization in that part of the galaxy (Schulz *et al.* 1978). Elsässer and Staude explain the common orientation of position angles by postulating that evolution of the cloud in the presence of the galactic magnetic field has resulted in common geometrical alignment of the nebular structures.

For either model one might expect a correlation between the ambient galactic field direction and the position angle of polarization observed for infrared sources embedded in H II regions and molecular clouds. This expectation was first tested by Kobayashi *et al.* (1978) who showed that the direction of interstellar polarization was nearly parallel to the direction of infrared polarization for GL 490, GL 2591, and BN. However, the small number of sources does not allow one to generalize

[a)] Guest observer at Mauna Kea Observatory.

 0004-6256/79/091339-10$00.90

about the extent of the phenomenon. The observational sample of 2 μm polarimetry has recently been extended to more than two dozen sources in various parts of the galaxy. In the remainder of this paper we discuss the relationship between infrared and interstellar polarization for 28 of these sources. We demonstrate that there is a strong correlation between the two and conclude that the galactic magnetic field has played a dominant role in the evolution of dense interstellar clouds.

II. SOURCE SELECTION AND DATA

We have tried to restrict our sample to objects believed to be in various stages of protostellar evolution. All sources having recognizable stellar photospheric features in their spectra (e.g., first-overtone bands of CO) have been excluded. Thus objects such as GL 2205 (= OH 26.5 + 0.6) and OH 0739-14 have been excluded. The sources selected were usually discovered first in infrared or radio surveys of regions where other astronomical phenomena indicate recent star formation. They are generally associated either with compact H II regions or with molecular cloud complexes. Many have deep absorption features attributed to silicate and water-ice grains. The infrared data were taken from published observations of Kobayashi *et al.* (1978) and Dyck and Capps (1978) and from previously unpublished observations made at Mauna Kea Observatory. The visual data were derived from the polarimetry of Hall (1958), Breger (1976), Vrba, Strom, and Strom (1976), Mathewson and Ford (1970), Klare and Neckel (1977), and Hoag and van P. Smith (1959). In general we have used three criteria to select field stars with which to compare the infrared sources. These are (1) that the stars bracket the distance to the infrared source, (2) that the visual polarization is greater than about 1–2%, and (3) that the selected stars bracket the position of the infrared source in both right ascension and declination. We feel that these criteria minimize the effects of foreground or multiple clouds upon a determination of the field direction in the vicinity of the infrared source. In some cases, however, it was necessary to relax one or more of the criteria in order to obtain a sufficiently large sample of stars. Once the sample of stars—usually numbering ten to twenty—was defined, we formed the arithmetic mean of the measured position angles and calculated the rms deviation about the mean.

The resultant set of observational and derived data are presented in Table I. We have included the source name, distance, measured amount, and direction of infrared polarization in the first four columns of the table. In the last six columns of the table we have listed, respectively, the direction of infrared polarization in galactic coordinates, the mean and rms deviation of the interstellar polarization, the difference between the interstellar and infrared direction, the distance range encompassed by the stars, the minimum polarization in the sample, and any special comments. A position angle in galactic coordinates of 90° indicates an orientation parallel to the galactic plane. The table includes thirty-one infrared sources with measurable polarization. Included in the table are W 51/IRS 2, K 3-50 IRS and G 45.1 + 0.1 (Dyck and Capps 1978) although these sources lie beyond the distance range covered by existing interstellar polarization measurements, because the orientation of the infrared polarization in galactic coordinates is relevant to the analysis.

III. DISCUSSION

The striking feature about the table is the close agreement between the position angle of infrared polarization and the average direction of interstellar polarization for a large fraction of the sources. Of the thirty-one sources listed in the table, twenty (65% of the sample) show $\leq 30°$ difference between the directions of infrared and interstellar polarization; ten ($\sim 32\%$ of the sample) show $\leq 15°$ difference. Another way of presenting the data is shown in Figs. 1–19. In these figures we have plotted the individual infrared and interstellar polarization vectors for the sources listed in Table I. In these plots the thin lines represent the interstellar polarization and the heavy lines the infrared polarization. The length of the line is proportional to the amount of polarization and the orientation is the same as the orientation of the electric vector projected on the sky. In Fig. 20 we show histograms for each region, which illustrate the number of stars in each 20° interval of position angle. Visual inspection of these figures reveals that the infrared polarization measured for the majority of the sources tends to be parallel to the local interstellar polarization. In each case, all interstellar polarization vectors within the distance and polarization limits stated in Table I which lie in the area of sky covered by the figure, are plotted. Each figure is discussed separately below. Unless otherwise stated, the interstellar polarization data are taken from Hall (1958).

W3: The infrared polarization of three sources in the complex has been measured. The interstellar field is well determined. IRS 5 and IRS 9 show position angles which agree well with each other, while IRS 1, which is a more extended source with an associated H II region has a somewhat different orientation. The infrared vectors are distributed about the interstellar field, and the galactic plane lies close to the direction of interstellar polarization.

IC 1848A/IRS: The interstellar polarization field is also well determined in the vicinity of this source, and agrees well with the galactic plane. The infrared vector is almost orthogonal to the interstellar field.

GL 437: Three infrared sources have been observed in the complex, which also lies in a region of the galaxy where the interstellar polarization field is well defined and parallel to the galactic plane. As in the case of W3 the sources show some scatter and are distributed on either side of the interstellar field direction.

TABLE I. Polarization data for infrared sources and nearby stars. Unless noted P_{IR} and θ_{IR} are 2.2 μm data.

Source	d(kpc)	$P_{IR} \pm \varepsilon$(%)	θ_{IR}(°)	θ^{G}_{IR}(°)	$\theta_* \pm$ rms(°)	$\theta_{IR}-\theta_*$(°)	$d_{min}-d_{max}$	P^{min}_{visual}(%)	Notes	References
W3/IRS 1	3.1	5.0±0.6	140	118	109±8	31	2.5-3.8	2.8		1
W3/IRS 5	3.1	10.1±0.2	84	62	109±8	-25	2.5-3.8	2.8		1
W3/IRS 9	3.1	2.4±0.6	90	66	109±8	-19	2.5-3.8	2.8		1
IC 1848A/IRS 1	1.7	2.9±0.4	11	162	116±5	75	1.2-2.2	2.2	6	2
GL 437 W	3.0	8±1	104	72	118±3	-14	2.3-3.6	3.1		3,4
GL 437 N	3.0	24±1	89	57	118±3	-29	2.3-3.6	3.1		3,4
GL 437 S	3.0	3.2±0.5	141	109	118±3	23	2.3-3.6	3.1		3,4
GL 490	1.4	6.3±0.9	115	80	116±7	- 1	0.9-1.9	3.0	2	5
S 228	1.0	5.6±1.8	6	131	160±17	28	0.5-1.7	1.0	4	6,7
OMC 1/IRS 1	0.5	17.5±0.2	113	51	109±22	4	?	2.1	5	8
OMC 1/IRS 2	0.5	9.1±0.3	133	71	109±22	24	?	2.1		8
OMC 2/IRS 3	0.5	3.8±0.3	124	62	109±22	15	?	2.1		9
Mon R2/IRS 1	0.95	22±2	161	98	170±20	- 9	0.5-1.5	1.0		10,11
Mon R2/IRS 2	0.95	16.0±1	160	97	170±20	-10	0.5-1.5	1.0		10,11
Mon R2/IRS 3	0.95	5.1±0.6	161	98	170±20	- 9	0.5-1.5	1.0	3	10,11
S 255/IRS 1	1.0	14.6±0.9	150	89	171±6	-21	0.5-1.5	2.1	4	17,12
GL 989	0.8	3.7±0.9	117	55	172±19	-55	0.3-1.3	1.0	2	13,5
ρ Oph #29	0.2	6.4±1.6	28	77	37±16	- 9	0.2	2.2		14
NGC 6334/IRS 1	0.7	8.6±1.3	105	160	180±17	-75	0.4-1.2	2.0		15,16
IR 12.4+0.5	1.8	3.6±0.7	106	171	116±31	-10	1.2-2.4	2.0	4	18
W 33(A)	4.4	15.6±0.8	68	129	84±19	-16	3.2-4.9	1.2	4	19,20
M 17/KW IRS	1.8	4.5±0.3	32	93	176±8	36	1.8	2.0	4	21
G 45.1+0.1	5	3.0±0.4	174	54	-	-	-	-		22
W 51/IRS 2	6.5	4.7±0.3	130	10	-	-	-	-		23
K 3-50/IRS	8	1.9±0.2	67	123	-	-	-	-		24
S 106/Source 3	2.3	3.5±0.4	51	103	58±9	- 7	1.8-2.8	1.9		25
GL 2591	1.5	12.1±0.3	172	44	40±31	-48	1.0-2.0	2.0	4	26
W 75/IRS 1	1.5	2.5±0.6	120	170	43±27	77	1.0-2.0	2.0	4	19,23
S 140/IRS 1	0.9	13.4±0.7	70	102	86±17	-16	0.5-1.5	2.0		27
NGC 7538/IRS 1	4.9	11.2±0.1	72	91	60±15	-12	4.2-5.6	1.8		23,28
NGC 7538/IRS 9	4.9	11.2±0.7	160	179	60±15	-80	4.2-5.6	1.8		28

Notes: 1. Infrared P and θ are 3.8μm data. 2. Infrared polarimetry from Kobayashi et al (1978). 3. Infrared P and θ are 1.65μm data. 4. Distance uncertain. 5. P_{IR} differs from value quoted by Dyck and Capps (1978) because it represents more observations. 6. Correct coordinates are RA: $2^h57^m37^s.8$, δ: 60°17'28" (Beichman 1979).

References to Table I.

1. Wynn-Williams, Becklin, and Neugebauer 1972.
2. Loren and Wootten 1978.
3. Kleinmann *et al.* 1977.
4. Wynn-Williams 1978.
5. Merrill and Stein 1976.
6. Frogel and Persson 1973.
7. Harris 1976.
8. Wynn-Williams and Becklin 1974.
9. Gatley *et al.* 1974.
10. Loren 1977.
11. Beckwith *et al.* 1976.
12. Beichman, Becklin, and Wynn-Williams 1979.
13. Allen 1972.
14. Elias 1978.
15. Becklin and Neugebauer 1974.
16. Cheung *et al.* 1978.
17. Evans *et al.* 1977.
18. Wright *et al.* 1979.
19. Dyck and Simon 1977.
20. Capps, Gillett, and Knacke 1978.
21. Kleinmann and Wright 1973.
22. Zeilik *et al.* 1975.
23. Wynn-Williams *et al.* 1974.
24. Wynn-Williams *et al.* 1977b.
25. Pipher *et al.* 1976.
26. Wynn-Williams *et al.* 1977a.
27. Blair *et al.* 1978.
28. Becklin *et al.* 1979.

GL 490: Similarly to the previous three sources, this object lies in the Perseus direction, in which the interstellar polarization field is well ordered and coincident with the galactic plane. The infrared vector matches the field direction precisely. The infrared data are from Kobayashi *et al.* (1978).

S228: The interstellar polarization field is well determined in this region, and the average value of the position angle lies within fifteen degrees of the galactic plane. The infrared source has a position angle within 30° of the interstellar field, but nearly 45° from the plane.

Orion: Two infrared sources in OMC 1 and one in OMC 2 have been observed. The vectors agree with each other quite closely. It has been possible, in this case, to restrict the area observed in the figure to a region closely associated with the infrared sources, by using the interstellar polarization data of Breger (1976). Due to the complex nature of the Orion region one might expect that interstellar polarization field would be disordered; however, a component near 100° is clear in both the figure and the histogram. The infrared vectors lie close to this direction. The line of constant galactic latitude in the Orion region lies at about 40° to the average interstellar polarization direction. The infrared vectors tend to lie between this and the polarization field. The scatter in the interstellar data is too great to determine whether the infrared vectors lie closer to the polarization field or to the plane of the galaxy.

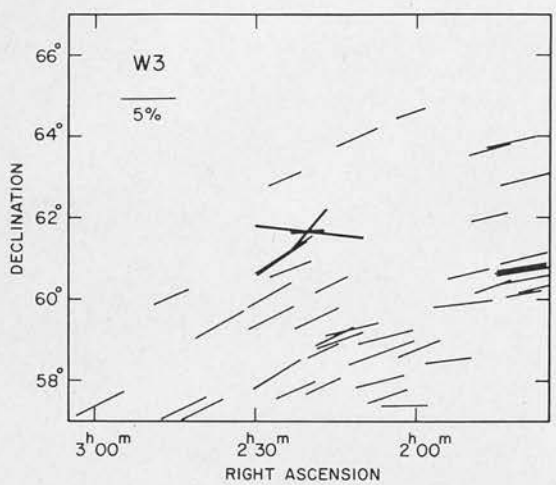

FIG. 1. Infrared polarization measurements of three sources in W3 (heavy lines) compared with nearby optical interstellar polarization (thin lines). The length of the line is proportional to the percent polarization (5% level is indicated) and the orientation is that of the electric vector on the sky.

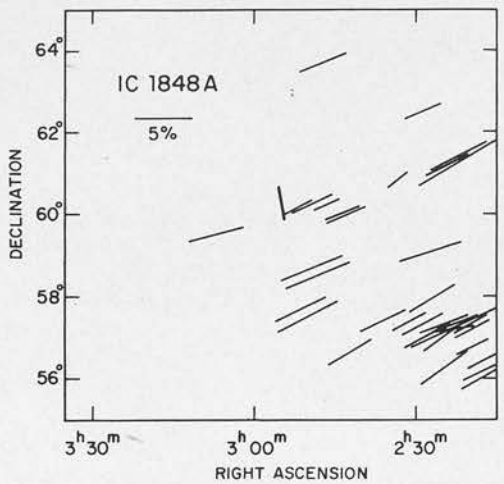

FIG. 2. Same as Fig. 1 except for IC 1848A.

Mon R2: The interstellar data are from Hall (1958), Hoag and van P. Smith (1959), and Mathewson and Ford (1970). The three infrared sources observed in Mon R2 all show virtually the same position angle, which is

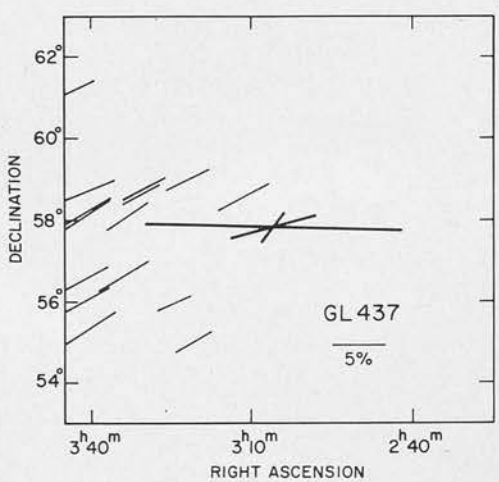

FIG. 3. Same as Fig. 1 except for three sources in GL 437.

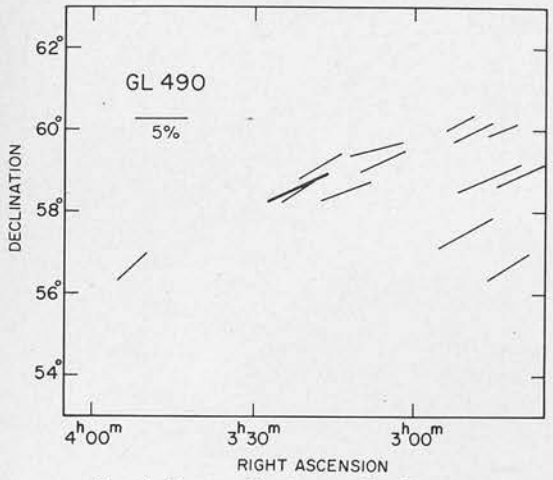

FIG. 4. Same as Fig. 1 except for GL 490.

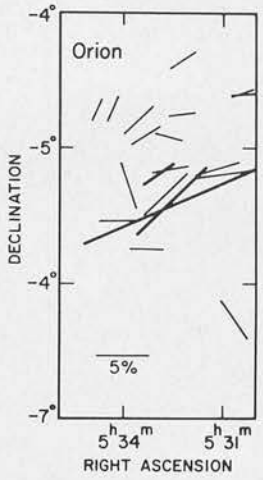

FIG. 6. Same as Fig. 1 except for three sources in OMC 1 and OMC 2.

very close to the average interstellar position angle. The interstellar data do not originate very close to Mon R2 but the orientation parallel to the infrared sources is clearly dominant, therefore the field is considered to be well determined. The two stars to the west of Mon R2 lie in the Orion complex, and were therefore not used in the analysis. The galactic plane is oriented at 20° to the average interstellar field, and the IR vectors lie between the two.

S 255/IRS 1: The interstellar field is unambiguously defined in this region. The galactic plane lies about 20° from the average field, and coincides with the infrared vector.

GL 989: This is Allen's source in NGC 2264. The infrared polarization data are from Kobayashi *et al.* (1978), and the interstellar data from Hall (1958) and Mathewson and Ford (1970). The field is well determined, and is oriented approximately 20° from the galactic plane. The infrared vector lies nearer to the orientation of the plane than to the average interstellar polarization direction, but is not close to either.

ρ Oph #29: The interstellar polarization data for this cloud are taken from Vrba *et al.* (1976), who have already pointed out the strong degree of alignment of the field star vectors. The galactic plane at this longitude lies in the same orientation as the average interstellar position angle, and the infrared vector coincides with this direction.

NGC 6334/IRS 1: The interstellar polarization data are supplemented from Klare and Neckel (1977). The field is well determined and lies about 35° from the galactic plane. The infrared vector does not agree with the average interstellar position angle, and is about equidistant from it and from the plane.

IR 12.4 + 0.5: The interstellar data are taken from Klare and Neckel (1977) and Mathewson and Ford (1970) in addition to Hall (1958). The figure and the histogram indicate interstellar polarization components

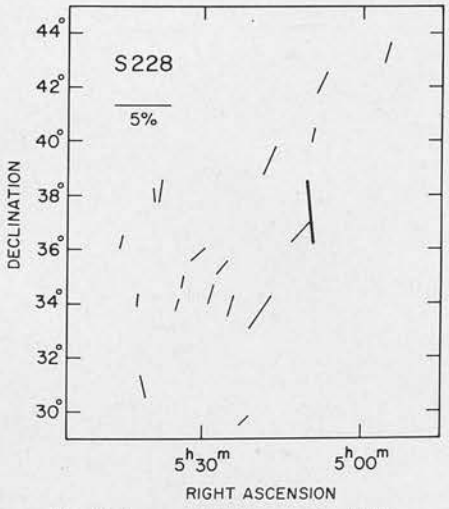

FIG. 5. Same as Fig. 1 except for S228.

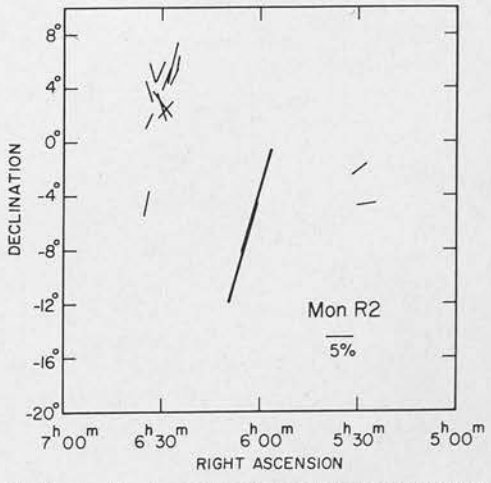

FIG. 7. Same as Fig. 1 except for three sources in Mon R2 (only two vectors show owing to overlap of position on the drawing).

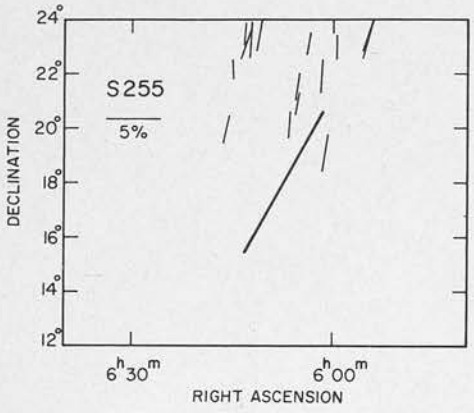

FIG. 8. Same as Fig. 1 except for S255.

near 100° and near 0°, respectively. The appearance of the field is not tidy, therefore, it is considered to be poorly defined. The infrared vector matches the component near 100° rather well but does not lie very close to it on the sky. This component has been used in the analysis. The IR vector is approximately perpendicular to the galactic plane.

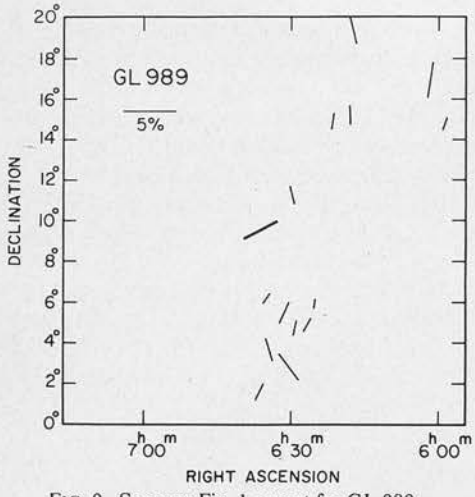

FIG. 9. Same as Fig. 1 except for GL 989.

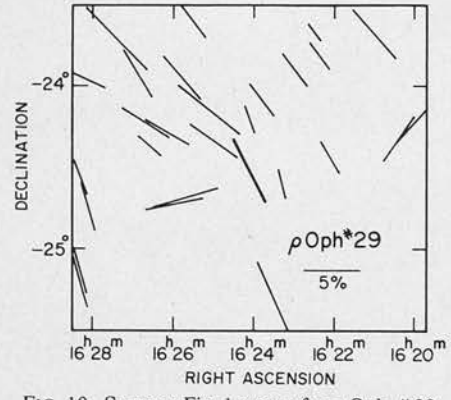

FIG. 10. Same as Fig. 1 except for ρ Oph #29.

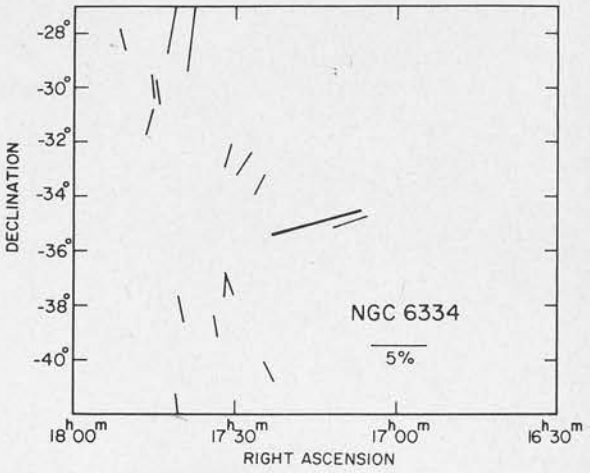

FIG. 11. Same as Fig. 1 except for NGC 6334.

W33(A): The data are supplemented from Klare and Neckel (1977). A strong component at 70° is evident from the histogram, but the figure illustrates that this component is confined to a small area, which is not very close to the infrared source. In fact, most of the stars with this orientation belong to the open cluster NGC 6611. Therefore, this field is also considered to be poorly determined. The infrared vector does not lie close to the galactic plane.

M 17/KW IRS: The interstellar polarization data were taken from the study of Schulz *et al.* (1978). All stars detected at the 3σ level with polarization greater than 2% were used. The distances of these stars are expected to be well within the limits used for other fields, even if they do not lie within the M 17 complex, as claimed by Schulz *et al.* Neglecting the very high polarization of the stars to the south of the figure (which is presumably not of interstellar origin) there is a clear interstellar component at 0°. The infrared vector lies 36° from the interstellar field, and agrees well with the orientation at the galactic plane.

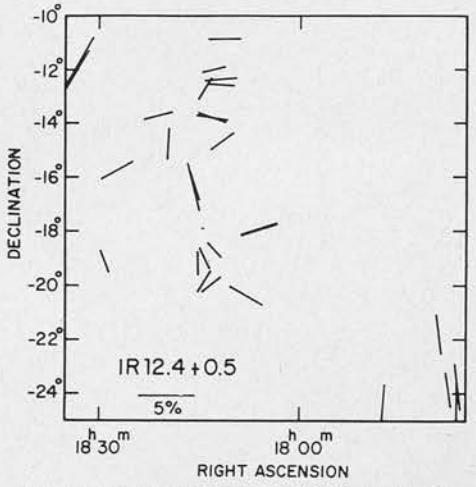

FIG. 12. Same as Fig. 1 except for IR 12.4 + 0.5.

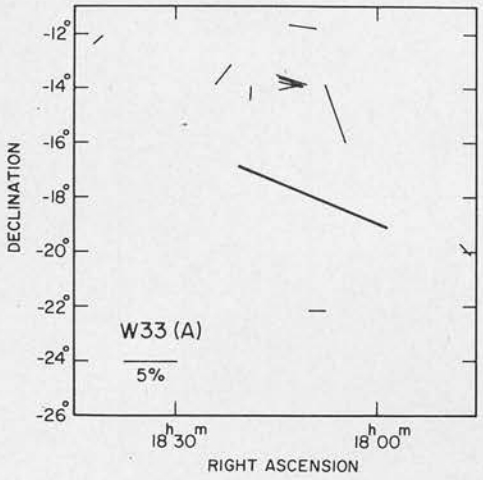

FIG. 13. Same as Fig. 1 except for W 33(A).

G 45.1 + 0.1, W51/IRS 2, and K 3-50/IRS: These sources all lie beyond the distance limit of Hall's catalogue. In each case the infrared vector makes a considerable angle with the galactic plane.

S 106/Source 3: There is a well-defined orientation to the interstellar polarization field in the immediate vicinity of the infrared source, which agrees well with the infrared position angle. The three stars which lie 30 min to the west of S106 are presumably not associated with the S106 region, and the remaining eight stars were therefore averaged to obtain the interstellar position angle. The galactic plane is oriented 20° from the average position angle of the field stars, and the infrared vector lies closer to the field than to the plane. S 106 is a particularly interesting source because it has an optical appearance which resembles a bipolar nebula, with the infrared source situated between the two lobes. If the polarization were caused by scattering in the lobes the position angle would be expected to be perpendicular to the optical axis, but in fact lies only 25° from it. It is possible that the small aperture of the infrared polarization observation excluded any flux from the lobes. The position angle is consistent with polarization produced by scattering in the thick equatorial disk.

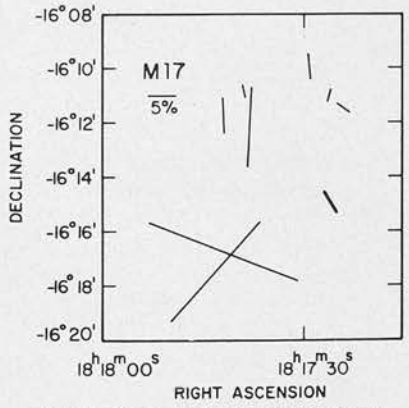

FIG. 14. Same as Fig. 1 except for M17.

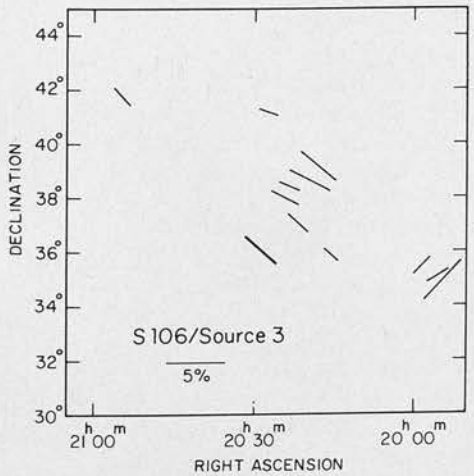

FIG. 15. Same as Fig. 1 except for S 106/Source 3.

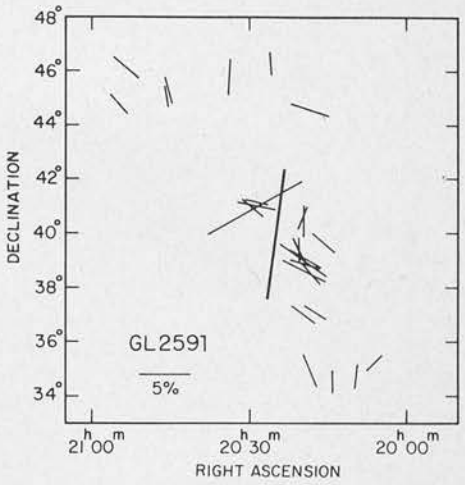

FIG. 16. Same as Fig. 1 except for GL 2591.

GL 2591 and W75/IRS 1: These sources lie close together in the Cygnus region, where the interstellar polarization behavior is very confused. The figures are

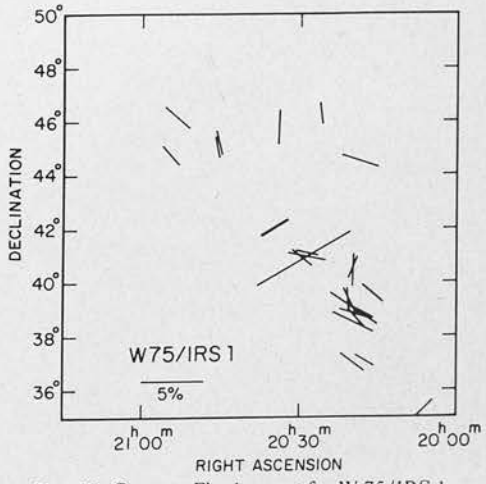

FIG. 17. Same as Fig. 1 except for W 75/IRS 1.

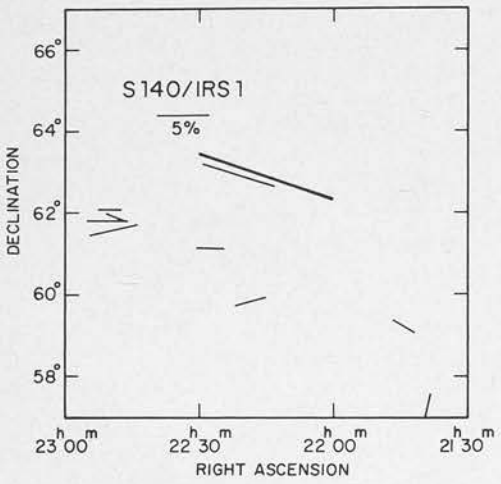

FIG. 18. Same as Fig. 1 except for S 140/IRS 1.

essentially the same, except that they have slightly different centers. There is a tendency for the interstellar position angles to lie near 40°, but there is considerable scatter. The fields are therefore considered to be poorly determined. Neither source lies particularly close to the averaged interstellar field direction, nor to the direction of the galactic plane.

S 140/IRS 1: The interstellar field is well determined and in good agreement with the infrared vector. The galactic plane lies at 30° to the interstellar field, and the infrared vector lies between the two.

NGC 7538: The two infrared sources lie perpendicular to each other. One of them, IRS 1, lies close to both the well-defined interstellar polarization field and the direction of the galactic plane.

In order to illustrate concisely the agreement between the two directions we have plotted in Fig. 21 a histogram of the number of sources versus the absolute value of the difference between the two polarization directions, $\Delta\theta$. The difference interval has been taken to be 15°. The

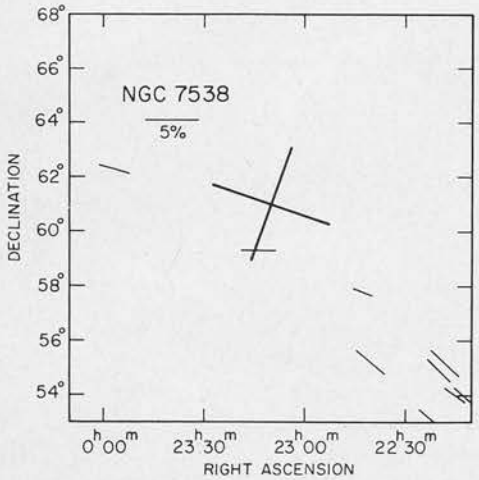

FIG. 19. Same as Fig. 1 except for two sources in NGC 7538.

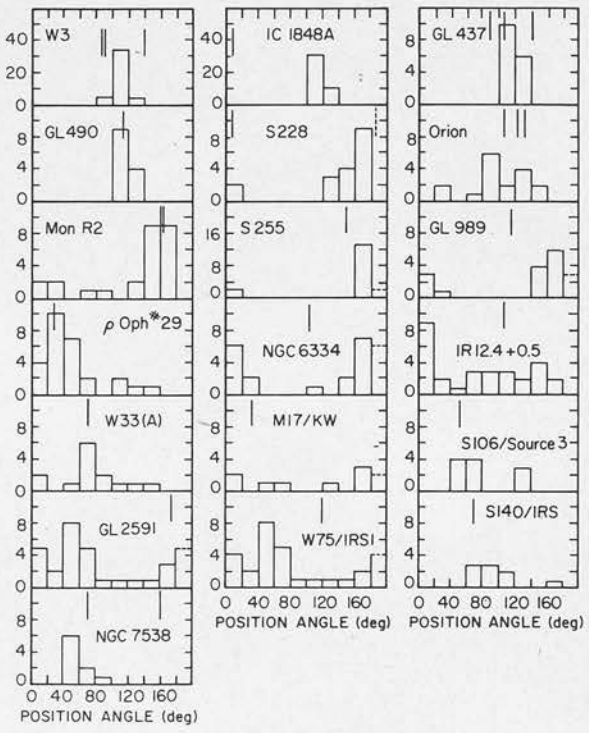

FIG. 20. Histograms of the distribution of optical interstellar polarization angles compared with the position angle of infrared polarization (shown as vertical lines) for the sources discussed in the text.

four poorly-defined fields are indicated by shaded boxes. It is clear that there is a large concentration of sources with small differences. The width of the infrared distribution in Fig. 21 will be the convolution of several distinct contributions: (1) the dispersion introduced because the infrared source may not occupy the same volume of space as the comparison stars; (2) the dispersion introduced by including unrecognized nonprotostellar objects in the sample; and (3) any intrinsic dispersion of the infrared position angles. If the true distribution of differences were random then the probability that a distribution such as that shown in Fig. 21 could occur is almost negligible. Assuming the sample has not been strongly biased by our selection criteria, we conclude that the relationship between the infrared and interstellar polarization directions is not a chance result.

If it is accepted that a correlation exists between the infrared position angle and the average interstellar polarization field then it is necessary to consider how this can be interpreted. The direction of the interstellar polarization is usually interpreted as the direction of the galactic magnetic field (normal Davis-Greenstein alignment). The direction of infrared polarization, therefore, tends to be parallel to the direction of the local galactic field. Thus there is strong observational evidence linking the galactic magnetic field to the mechanism which produces the infrared polarization.

This result implies that the galactic magnetic field

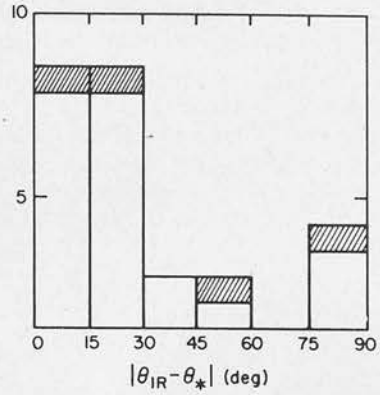

FIG. 21. A histogram of the distribution of differences between infrared and optical interstellar polarization position angles for the sources discussed in the text. The shaded areas represent fields in which the interstellar polarization direction is poorly determined (see text for details).

must play an important role in star formation. If the infrared polarization is produced by aligned grains near the source (Dyck and Beichman 1974) this conclusion is clear. If the infrared polarization is produced by the bipolar nebula mechanism this conclusion is also likely to be valid. A possible scenario is that the contracting cloud will collapse faster along the field lines than across them (Mouschovias 1976) thereby producing a flattened disk perpendicular to the field direction. This geometry and orientation tend to be preserved in the subfragments which evolve to become stars. In the standard picture of bipolar nebulae these flattened disks will become the obscuring, equatorial disks and the visible lobes will lie along the field lines. [We note that this geometry results in polarization electric vectors (for the bipolar nebulae) which are perpendicular to the field lines. If these vectors are to be parallel to the local interstellar polarization then *reverse* Davis–Greenstein alignment must occur for interstellar grains.] It is also possible, however, that the nebular equatorial disks will be aligned by galactic angular momentum and will lie in the plane of the galaxy. The resulting infrared polarization will always be parallel to the galactic plane. It is well known that the interstellar polarization as a large scale phenomenon, is oriented along the plane of the galaxy (e.g., Axon and Ellis 1976). This is evident also, in several of the regions studied here. Therefore, it is possible that the correlation which we have discovered relates not to the galactic magnetic field, but to differential rotation in the plane, which aligns the bipolar nebulae, as described above.

The interstellar polarization field is not uniform everywhere in the galaxy, therefore it is possible to test this hypothesis by studying the relationship between the infrared vector and the galactic plane, in the regions where a well-defined interstellar field does not align perfectly with the galactic plane. The fields of W3, IC 1848A, GL 490, ρ Oph, and NGC 7538 all show close agreement between the galactic plane and the average interstellar field direction, and are therefore not used in this analysis. Of the remaining well-defined fields the infrared vectors lie between the plane and the field in Orion, Mon R2, NGC 6334, and S 140. In S 255, M 17, and GL 989 the IR vector lies closer to the plane than to the field, and in S 106 and S 228 it lies closer to the field than the plane. Of the four poorly defined fields, all the IR vectors lie greater than 40° from the galactic plane, and two are nearly orthogonal to it. The three sources for which no interstellar polarization data exist all show IR vectors inclined at large angles to the plane. Therefore, out of a sample of sixteen regions there are three infrared sources which lie closer to the galactic plane than to the interstellar field and two which lie closer to the field. Seven others cannot be compared to the polarization field but show no alignment to the galactic plane. These statistics illustrate that there is no evidence that another galactic phenomenon, other than the magnetic field, is influencing the infrared sources.

To test further the possibility that another mechanism is responsible for the correlation, we investigated the effect of galactic differential rotation on the clouds. This is the most obvious alternative influencing force to the magnetic field. Velocity gradients in collapsing interstellar clouds induced by galactic differential rotation should be easily observable. However, very few clouds have been found to be rotating. This is often due to the fact that the analysis of radio velocity data can be ambiguous, but it is clear that simple rotations are not obviously present in most clouds. Evidence for rotation has been suggested in GL 437 (Schneps *et al.* 1978), Orion (Kutner *et al.* 1977), Mon R2 (Loren 1977), NGC 2264, which contains GL 989 (Crutcher *et al.* 1978), and W3, (Brackman and Scoville 1978). CO observations of several of the other clouds have been made, with no indication of rotation. Of those clouds for which rotation is suggested, GL 437, W3, and Mon R2 rotate about axes perpendicular to the axis of galactic differential rotation. The interpretation of rotation in Orion has been disputed by Ho and Barrett (1978), but even if it exists it is in the opposite sense to galactic differential rotation. Only in NGC 2264 does the suggested axis of rotation coincide with the axis of the galaxy. The infrared position angle of GL 989 lies closer to the plane than the polarization field but is not close to either.

It is clear from the above discussion that there is no support for the suggestion that the infrared polarization/mean interstellar-polarization field-position angle correlation is in fact a disguised correlation between the infrared vector and the galactic plane. Therefore, the most obvious conclusion to make is that the infrared sources are indeed strongly influenced by the galactic magnetic field, which is responsible for the interstellar polarization.

IV. CONCLUSION

We have demonstrated that there is a good correlation between the direction of infrared polarization shown by

protostellar sources and the direction of nearby interstellar polarization. We conclude that this is evidence for the existence of a strong link between the primitive galactic magnetic field and the field in an evolved molecular cloud. It is not possible, unfortunately, to use this correlation to distinguish between the two most plausible mechanisms which account for the infrared polarization. The important point, however, is that our conclusion is independent of which mechanism operates: In either case the galactic magnetic field must play an important role in the evolution of molecular clouds.

We wish to thank R. W. Capps, E. E. Becklin, C. G. Wynn-Williams, R. B. Loren, and R. D. Wolstencroft for very helpful discussions, and T. J. Lee for discussions and assistance with some of the observations. CJL wishes to acknowledge receipt of an SRC research grant and a scholarship from the Carnegie Trust for the Universities of Scotland.

REFERENCES

Allen, D. A. (1972). Astrophys. J. **172,** L55.
Axon, D. J., and Ellis, R. S. (1976). Mon. Not. R. Astron. Soc. **177,** 499.
Becklin, E. E., Gatley, I., Matthews, K., Neugebauer, G., Werner, M., and Wynn-Williams, C. G. (1979). Preprint.
Becklin, E. E., and Neugebauer, G. (1974). In *H II Regions and the Galactic Center,* edited by A. F. M. Moorwood (Neuilly-Sur-Seine, ESRO), p. 39.
Beckwith, S., Evans, N. J. II, Becklin, E. E., and Neugebauer, G. (1976). Astrophys. J. **208,** 310.
Beichman, C. A., Becklin, E. E., and Wynn-Williams, C. G. (1979). Preprint.
Beichman, C. A. (1979). Thesis, University of Hawaii.
Blair, G. N., Evans, N. J. II, Vanden Bout, P. A., and Peters, W. L. III (1978). Astrophys. J. **219,** 896.
Brackman, E. J., and Scoville, N. Z. (1978). Bull. Am. Astron. Soc. **10,** 405.
Breger, M. (1976). Astrophys. J. **204,** 789.
Breger, M., and Hardorp, J. (1973). Astrophys. J. Lett. **183,** L77.
Capps, R. W., Gillett, F. C., and Knacke, R. F. (1978). Astrophys. J. **226,** 863.
Capps, R. W., and Knacke, R. F. (1976). Astrophys. J. **210,** 76.
Capps, R. W. (1976). Ph.D. thesis, University of Arizona.
Chaisson, E. J., and Beichman, C. A. (1974). Astrophys. J. Lett. **199,** L39.
Chaisson, E. J., and Vrba, F. J. (1978). *Proceedings of the Conference on Protostars and Planets* (to be published).
Cheung, L., Frogel, J. A., Gezari, D. Y., and Hauser, M. G. (1978). Astrophys. J. **226,** L149.
Crutcher, R. M., Hartkopf, W. I., and Giguere, P. T. (1978). Astrophys. J. **226,** 839.
Dyck, H. M., Capps, R. S., Forrest, W. J., and Gillett, F. C. (1973). Astrophys. J. Lett. **183,** L99.
Dyck, H. M., and Beichman, C. A. (1974). Astrophys. J. **194,** 57.
Dyck, H. M., and Capps, R. W. (1978). Astrophys. J. Lett. **220,** L49.
Dyck, H. M., and Simon, T. (1977). Astrophys. J. **211,** 421.
Elias, J. (1978). Astrophys. J. **224,** 453.
Elsasser, H., and Staude, H. J. (1978). Astron. Astrophys. **70,** L3.
Frogel, J. A., and Persson, S. E. (1973). Astrophys. J. **186,** 207.
Gatley, I., Becklin, E. E., Matthews, K., Neugebauer, G., Penston, M. V., and Scoville, N. (1974). Astrophys. J. **191,** L121.
Hall, J. S. (1958). Publ. U. S. Naval Obs. **17,** VI.
Harris, S. (1976). Mon. Not. R. Astron. Soc. **174,** 601.
Ho, P. T. P., and Barrett, A. H. (1978). Astrophys. J. **224,** L23.
Hoag, A. A., and van P. Smith, E. (1959). Publ. Astron. Soc. Pac. **71,** 32.
Klare, G., and Neckel, Th. (1977). Astron. Astrophys. Suppl. **27,** 215.
Kleinmann, D. E., and Wright, E. (1973). Astrophys. J. **185,** L131.
Kleinmann, S. G., Sargent, D. G., Gillett, F. C., Grasdalen, G. L., and Joyce, R. R. (1977). Astrophys. J. **215,** L79.
Knacke, R. F., and Capps, R. W. (1977). Astrophys. J. **216,** 271.
Kobayashi, Y., Kawara, K., Maihara, T., Okuda, H., Sato, S., and Noguchi, K. (1978). Publ. Astron. Soc. Japan **30,** 377.
Kutner, M. L., Tucker, K. D., Chin, G., and Thaddeus, P. (1977). Astrophys. J. **215,** 521.
Lo, K. Y., Walker, R. C., Burke, B. F., Moran, J. M., Johnston, K. J., and Ewing, M. S. (1975). Astrophys. J. **202,** 650.
Loer, S. J., Allen, D. A., and Dyck, H. M. (1973). Astrophys. J. Lett. **183,** L97.
Loren, R. B., and Wootten, H. A. (1978). Astrophys. J. **225,** L81.
Loren, R. B. (1977). Astrophys. J. **215,** 129.
Mathewson, D. S., and Ford, V. L. (1970). Mem. R. Astron. Soc. **74,** 139.
Merrill, K. M., and Stein, W. A. (1976). Publ. Astron. Soc. Pac. **88,** 874.
Mouschovias, T. Ch. (1976). Astrophys. J. **207,** 141.
Pipher, J. L., Sharpless, S., Savedoff, M. P., Kerridge, S. J., Krassner, J., Schurmann, S., Soifer, B. T., and Merrill, K. M. (1976). Astron. Astrophys. **51,** 255.
Schneps, M. H., Martin, R. N., Ho, P. T. P., and Barrett, A. H. (1978). Astrophys. J. **221,** 124.
Schulz, A., Protel, K., and Schmidt, Th. (1978). Astron. Astrophys. **64,** L13.
Spitzer, L. (1968). *Diffuse Matter in Space* (Interscience, New York).
Vrba, F. J., Strom, S. E., and Strom, K. M. (1976). Astron. J. **81,** 958.
Wynn-Williams, C. G., Becklin, E. E., Forster, J. R., Matthews, K., Neugebauer, G., Welch, W. J., and Wright, M. C. A. (1977a). Astrophys. J. **211,** L89.
Wynn-Williams, C. G., Becklin, E. E., Matthews, K., Neugebauer, G., and Werner, M. W. (1977b). Mon. Not. R. Astron. Soc. **179,** 255.
Wynn-Williams, C. G., Becklin, E. E., and Neugebauer, G. (1972). Mon. Not. R. Astron. Soc. **160,** 1.
Wynn-Williams, C. G., Becklin, E. E., and Neugebauer, G. (1974). Astrophys. J. **187,** 473.
Wynn-Williams, C. G., and Becklin, E. E. (1974). Publ. Astron. Soc. Pac. **86,** 5.
Wynn-Williams, C. G. (1978). Private communication.
Zeilik, M., Kleinmann, D. E., and Wright, E. L. (1975). Astrophys. J. **199,** 401.